Zeitschrift: IABSE reports of the working commissions = Rapports des commissions de travail AIPC = IVBH Berichte der Arbeitskommissionen

Band: 34 (1981)

Rubrik: Session I: Modelling of material behaviour

SESSION 1

June 2 nd, 1981

Modelling of Material Behaviour

Modélisation du Comportement des Matériaux

Modellierung des Materialverhaltens

Part 1
Morning Session

Chairman: **Prof. Dr. L. Cedolin, Italy**

Introductory Reporter: **Prof. Z.P. Bazant, USA**
Advances in Deformation and Failure Models for Concrete[1])

Part 2
Afternoon Session

Chairman: **Prof. Dr.-Ing. G. Mehlhorn, F.R.G.**

Introductory Reporter: **Prof. K.H. Gerstle, USA**
Material Modeling of Reinforced Concrete[1])

[1]) Published in Introductory Report IABSE Colloquium, Delft 1981, Volume - Band 33.

Leere Seite
Blank page
Page vide

Structural Concrete as a Plastic Material

Béton armé comme matériau plastique

Stahlbeton als plastisches Material

M.W. BRAESTRUP
Lic. techn.
Department of Structural Engineering, TU
Copenhagen Lyngby, Denmark

SUMMARY

A rigid, perfectly plastic 3-parameter constitutive model for concrete is presented. The modified Coulomb failure criterion is adopted as a yield condition with the associated flow rule. The limited ductility is accounted for by neglecting the tensile strength in practical applications and replacing the compressive strength by a reduced effective strength. The dissipation in kinematical discontinuities is calculated, and the relationship between cracks and yield lines is discussed. References to applications of the model are given.

RÉSUMÉ

Un modèle rigide, parfaitement plastique à 3 paramètres constitutifs est introduit pour le béton. Le critère de rupture de Coulomb modifié est proposé comme critère de plasticité avec la règle d'écoulement associée. La ductilité limitée est prise en compte en négligeant la résistance en tension en applications pratiques et remplaçant la résistance en compression par une résistance effective réduite. La dissipation plastique dans des discontinuités kinématiques est calculée, et la relation entre fissures et lignes d'écoulement est discutée. Des références aux applications du modèle sont indiquées.

ZUSAMMENFASSUNG

Ein starr-ideal plastisches, 3-parametrisches Materialmodell für Beton wird besprochen. Das modifizierte Coulombsche Bruchkriterium ist als Fliessbedingung mit dem zugeordneten Fliessgesetz angenommen. Die begrenzte Duktilität wird durch Vernachlässigung der Zugfestigkeit in praktischen Anwendungen und durch Ersatz der Druckfestigkeit durch eine reduzierte effektive Festigkeit berücksichtigt. Die Dissipationsleistung in kinematischen Diskontinuitäten wird berechnet und die Relation zwischen Rissen und Fliesslinien wird diskutiert. Hinweise auf Anwendungen des Modelles werden gegeben.

1. INTRODUCTION

In order to make realistic predictions about the behaviour of structures under applied loads, it is neccessary to model the response of the materials from first loading to failure. However, if attention is restricted to the strength of the structure, a short-cut can be made by considering the state of collapse only. This is accomplished by using the theory of plasticity and applying the theorems of limit analysis, which are valid under certain idealized constitutive assumptions.

The theory of plasticity is a branch of the strength of materials, which can be traced back to the work of GALILEO [1638], who determined the failure moment of a beam composed of a material with infinite compressive strength (p 115, op.cit.). COULOMB [1776] established a yield (or rather failure) criterion (cf. Section 2 below), and gave an engineering formulation of the upper bound theorem (p 343-344, op. cit.). The plastic potential was introduced by v. MISES [28.1] who, in a generalization of earlier work, proved that the work done by a given plastic strain rate is stationary in the actual state with respect to varying stress states satisfying the yield criterion. Significant work was carried out in the Soviet Union in the thirties and forties, cf. GVOZDEV [49.1].

In fact, the theorems of limit analysis were stated by GVOZDEV [38.1], but his work was not widely known and credited in the West till much later. The commonly cited formulation is due to DRUCKER, PRAGER, & GREENBERG [52.2] and is based upon variational theorems proved by HODGE & PRAGER [48.2] and HILL [50.1]. PRAGER [55.1] and KOITER [53.2] extended the theorems to bodies with singular yield surfaces.

The plasticity theory of Gvozdev was formulated with explicit reference to structural concrete. On the other hand, the school of Prager and Hill was mostly concerned with metallic bodies, and concrete was long regarded as a brittle material, generally unfit for plastic analysis. The implications of applying rigourous limit analysis to reinforced concrete structures were discussed by DRUCKER [61.1].

When plasticity is applied to reinforced concrete structures, a main problem is the formulation of a suitable constitutive description of the concrete. Early investigations of plane elements relied upon the square yield locus for plane stress (cf. below), which may be generalized into the modified Coulomb yield condition, used by CHEN & DRUCKER [69.1] to treat a problem of plain concrete. Within the last decade, this material model has been applied to a number of non-standard cases, mainly shear in plain and reinforced concrete, by a research group at the Technical University of Denmark, NIELSEN & al. [78.7], BRAESTRUP & al. [78.1], JENSEN [77.2]. Similar research has been carried out at various other institutions, notably the Swiss Institute of Technology, MUELLER [78.6], MARTI [80.4]. In May 1979 a Colloquium on Plasticity in Reinforced Concrete was organized in Copenhagen, sponsored by the International Association for Bridge and Structural Engineering. Most of the results obtained so far are collected in the conference reports [78.3],[79.5].

The collapse of a structure is characterized by large irreversible deformations. By comparison, the elastic geometry changes are small, and in the absence of stability problems they may conveniently be neglected. Also work-hardening effects are without great importance for the collapse load. Thus the structure is idealized as a rigid, perfectly plastic body.

The theory of perfect plasticity only involves the rates or increments of plastic strains, and does not predict the magnitude of the total deformations. However, when we describe the structure as rigid-plastic, and only consider the instant of collapse, then the incipient plastic deformations are the first and

only to occur, and it is immaterial whether they are regarded as increments or not. Consequently, the use of superposed dots is avoided, and although the term "rate" is employed, the distinction from conventional "small strains" is merely academical.

The constitutive equations of plasticity and the validity of the limit analysis theorems require unlimited ductility, i.e. the materials shall be able to undergo arbitrarily large deformations at constant stress level. Apparently concrete cannot be considered to satisfy this requirement to any reasonable degree. An abstract discussion of this matter is quite complicated and rather futile. Instead it is proposed to regard the theory of plasticity as a mathematical tool by which it is possible to describe the behaviour of concrete structures at collapse. The merits of the approach will then have to be judged by the correspondence between the theoretical predictions and experimental evidence.

2. MODIFIED COULOMB CRITERION

One of the simplest descriptions of the strength of a material is the frictional hypothesis introduced by COULOMB [1776], stating that in a section subjected to the shear stress τ and the normal stress σ failure occurs for

$$\tau = c - \sigma\tan\varphi \tag{1}$$

Thus the strength is defined by two material parameters, the cohesion c and the angle of internal friction φ. For $\varphi = 0$, the criterion reduces to Tresca's condition of maximum shear stress.

For a material obeying equation (1), the uniaxial tensile strength f_t and compressive strength f_c are:

$$f_t = \frac{2c}{\sqrt{k}} \qquad \text{and} \qquad f_c = 2c\sqrt{k} \tag{2a,b}$$

$$\text{where} \quad k = \frac{1+\sin\varphi}{1-\sin\varphi} \tag{3}$$

The Coulomb criterion is used mainly for soils, but it may also be applied to other granular materials, such as concrete. One drawback of the model is that for reasonable values of the angle of friction, the ratio between tensile and compressive strength, implied by equations (2), is unrealistically high. This can be amended by introducing Rankine's maximum stress criterion, stating that tension failure occurs for

$$\sigma = f_t \tag{4}$$

The combination of equations (1) and (4) is called the modified Coulomb failure criterion, visualized in Fig. 1.

COULOMB [1776], p 348-349, attempted to determine the cohesion of a material by loading a specimen in pure shear, and found that failure occured for a shear load approximately equal to that required to break the specimen in direct tension. This led Coulomb to identify the cohesion c with the tensile strength f_t. As seen from equation (2a), this is in fact correct for a Coulomb material with $k = 4$, corresponding to $\tan\varphi = 0.75$, which is precisely the value adopted by Coulomb in his applications, cf. HEYMAN [72.1], p 120-121. However, if the Coulomb criterion is valid, then failure in pure shear will occur at a shear stress which is less than the tensile strength f_t, cf. Fig. 2. The fact that the same value was obtained shows that the material (a sandstone) obeys a modified Coulomb criterion, where tension failure takes place by separation rather than by sliding. For such materials, the cohesion is substantially higher than

the uniaxial tensile strength, as seen in Fig. 2.

The idea of combining the criteria of maximum shear stress and maximum normal stress appears to be due to DORN [48.1], in the case of cast iron. For concrete, the combination of Coulomb sliding failure and Rankine separation failure was suggested by COWAN [53.1], PAUL [61.2], and SANDBYE [65.1].

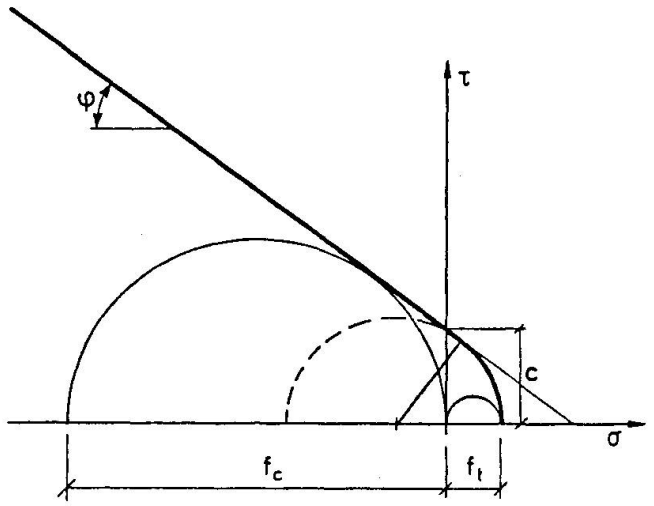

Fig. 1 Modified Coulomb failure criterion

Fig. 1 shows the modified Coulomb criterion as the envelope of the Mohr's circles for the states of stress which can be sustained on a section in the material, and such a failure criterion was proposed by MOHR [1900]. Mohr's failure envelope is also called the intrinsic curve of the material, and COWIN [74.1] has shown that the Mohr-Coulomb criterion follows from a simple constitutive assumption.

Many suggestions have been made for the shape of the failure envelope. One of the earliest is a parabola, cf. LEON [35.1], reflecting the experimental fact that the angle of friction, i.e. the slope of the curve, decreases with increasing compressive stress. On the other hand, the parabola is defined by two parameters only, whereas the modified Coulomb criterion has the attractive feature that the tensile strength may be varied independently of the compressive strength and the angle of friction.

The failure envelope of Fig. 1 is open towards the negative direction of the σ-axis, which means that theoretically the material is able to sustain arbitrarily high hydrostatic compression. It is further characteristic for any Mohr-Coulomb criterion that it does not involve the intermediate principal stress, which does have some influence, according to modern investigations. To take account of these defects, various more sophisticated criteria have been formulated, e.g. MAGNAS & AUDIBERT [71.1], De GARIEL-THORON [77.1], DRAGON & MRÓZ [79.3], OTTOSEN [79.7].

Failure of concrete may also be defined as the onset of unstable internal cracking, depending upon the loading path, KOTSOVOS & NEWMAN [78.4],[79.6], or defined by a limiting volumetric strain, CARINO & SLATE [76.1]. A maximum strain criterion, LOWE [78.5], leads to a model which is very similar to the modified Coulomb condition. Surveys of failure criteria for concrete are also given by CHEN [78.2] and WASTIELS [79.8].

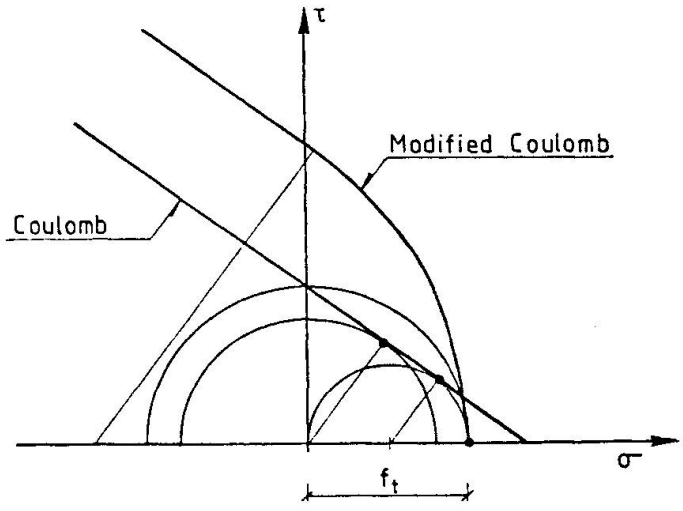

Fig. 2 Modified and unmodified Coulomb criteria with Mohr's circles of stress for pure shear and uniaxial tension

3. CONSTITUTIVE MODEL FOR CONCRETE

To be able to subject structural concrete to plastic analysis, we introduce the assumption:

> Concrete is regarded as a rigid, perfectly plastic material with the modified Coulomb failure criterion as yield condition and with the associated flow rule. The compressive strength is f_c^* , the tensile strength is f_t^* , and the angle of friction is φ .

When the failure criterion of Fig. 1 is adopted as yield condition, the yield surface can be determined in the space of principal stresses $(\sigma_1,\sigma_2,\sigma_3)$. Fig. 3 shows the yield loci in the cases of plane strain and plane stress. They are found from the yield surface by projecting on, respectively intersecting with, the plane $\sigma_3 = 0$. Figure 3 also illustrates the associated flow rule, the generalized strain rates being the principal strain rates $(\varepsilon_1,\varepsilon_2,\varepsilon_3)$. The slope of the yield locus corresponding to sliding failure is determined by the parameter k , given by equation (3).

The validity of the associated flow rule for granular materials like concrete is questionable. It is obvious that concrete dilates at failure, but experimental evidence seems to indicate that it is not nearly as much as predicted by the normality condition. However, tests of this kind are difficult to interpret because they are based upon an assumed uniform state of deformation, and failure of concrete (and rock) tend to be localized in narrow zones, cf. Section 5 below.

The constitutive description of concrete, introduced above, is very crude in the sense that it attempts to define the strength properties and the deformations at failure by means of only three material parameters, viz. f_c^* , f_t^* , and φ . It would have no purpose to pretend that such a primitive model is particularly realistic, and the approach is open to criticism, BAZANT & TSUBAKI [80.2]. On the other hand, surprisingly accurate predictions may be obtained, provided some care is taken in the definition of the strength parameters.

The stress-strain curve of concrete in compression is characterized by the total absence of a yield plateau and by a falling branch. Consequently, the redistribution of stresses, which is a condition for the validity of the limit analysis theorems, can only take place at the expense of losing strength. This is taken into account by assuming f_c^* , called the effective concrete strength, to be a certain fraction of the uniaxial compressive strength f_c , estimated by standard tests (cylinders, prisms, cubes, etc.). The ratio $\nu = f_c^*/f_c$ is called the effectiveness factor, and

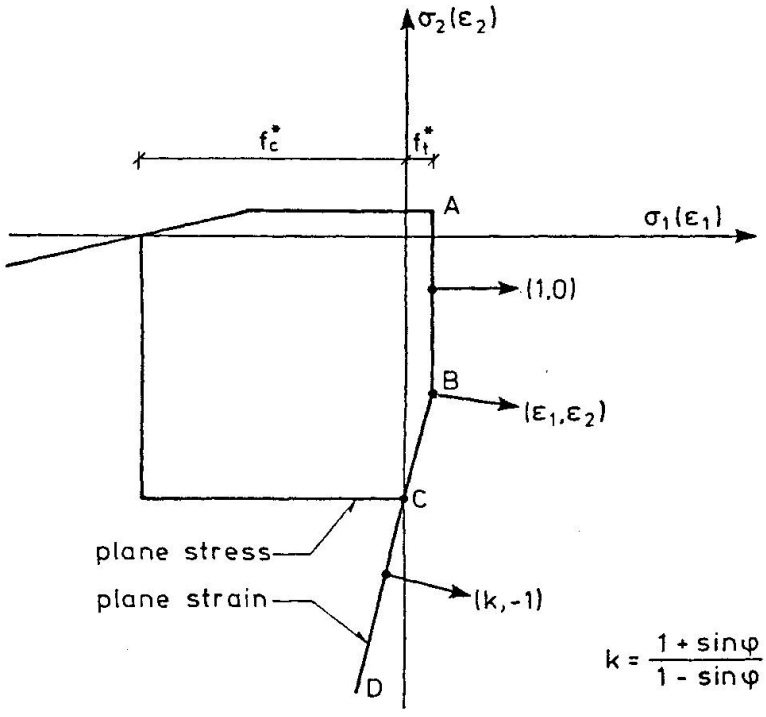

Fig. 3 Yield loci for concrete in plane stress and plain strain

since it is primarily a measure of concrete ductility, it decreases with increasing strength level. Empirical investigations have shown that this trend may be described by assuming the effective strength f_c^* to be proportional to $\sqrt{f_c}$. Incidentally, the same empirical relationship appears to exist between the tensile strength f_t and the compressive strength f_c.

A theoretical estimate of the effective concrete strength may be obtained, EXNER [79.4], by requiring the strain energy (i.e. the area under the stress-strain curve) for a certain limiting strain ε_g to be identical for the actual and the idealized materials. Based upon experimentally determined stress-strain curves, the effectiveness factor is then found as a function of the comcpressive strength f_c, which is very similar to the square root dependency described above. COLLINS [79.2] finds that the effective concrete strength does not only depend upon the value of the corresponding principal compressive strain, but also on the magnitude of the co-existing maximum shear strain.

In addition to reflect the ductility, the effectiveness factor must also incorporate all the effects which are not explicitly accounted for in the theory, e.g. initial state of stress, stiffness of the materials, size effects, etc. Therefore the effectiveness factor for a given type of structure will have to be evaluated by comparing the predictions of plastic analysis with results of tests.

The behaviour of concrete in tension is almost brittle, hence the effective tensile strength f_t^* is very small. If $f_t^* = 0$ is assumed, the lack of ductility in tension becomes immaterial, and the theorems of limit analysis may be applied with confidence. Problems arise if the strain rates change from tensile to compressive, but that is not relevant for simple yield point analysis. Consequently, the tensile concrete strength is prudently neglected for all practical purposes, which means that reinforcement must be provided if tensile stresses cannot be avoided. For $f_t^* = 0$, the yield locus for plane stress (fig. 3) reduces to the socalled square yield locus for concrete, cf. Fig. 4.

The angle of internal friction appears to be fairly independent of the concrete quality, and ample experimental evidence suggests the value $\varphi = 37^o$, corresponding to $\tan\varphi = 0.75$ and $k = 4$. This value corresponds to the slope of the experimental Mohr-Coulomb failure envelope for stress states in the vicinity of $(\sigma_1,\sigma_2,\sigma_3) = (0, 0, -f_c)$. As mentioned in Section 2, the angle of friction is reduced by the superposition of a high hydrostatic compression. Sometimes substantially higher angles of friction are quoted, BAZANT & TSUBAKI [79.1], [80.2], based upon the shear transfer in cracks. However, what is effectively measured by such tests is the slope of the modified Coulomb criterion, Fig. 1, at the intersection with the τ-axis.

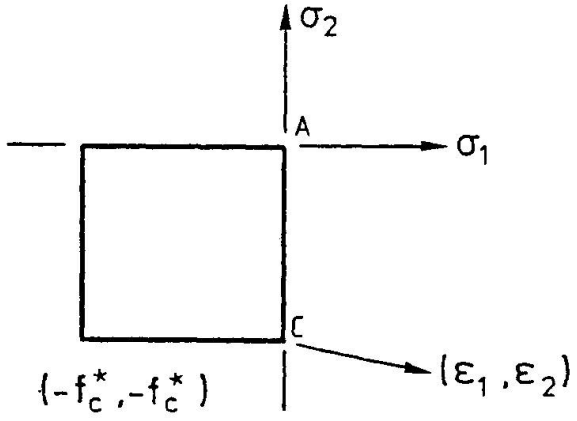

Fig. 4 Square yield locus for concrete in plane stress

The modified Coulomb criterion with a zero tension cut-off was used by DRUCKER & PRAGER [52.1] as a yield condition for soil. For concrete, CHEN & DRUCKER [69.1] introduced a non-zero tensile strength. The yield condition has been discussed by CHEN [70.1] and JENSEN [77.2].

The square yield locus for concrete in plane stress was applied by NIELSEN [64.1] to slabs, and later to walls, NIELSEN [71.2], and shear in beams, NIELSEN [67.1].

In the latter context, NIELSEN [69.2] introduced the concept of effective concrete strength.

4. CONSTITUTIVE MODEL FOR REINFORCEMENT

For the steel reinforcement, we introduce the assumption:

> The reinforcing bars are regarded as rigid, perfectly plastic, and able to resist forces in their axial direction only. The tensile yield stress of the steel is f_y .

It follows that dowel action of the bars is neglected. So is usually the contribution from compressed reinforcement, because it is small in comparison with that of the surrounding concrete. The one-dimensional yield locus for steel subjected to the axial stress σ_s is visualized in Fig. 5. For steel without a definite yield point, the yield stress f_y is defined in a suitable manner, e.g. as the 0.2% offset strength.

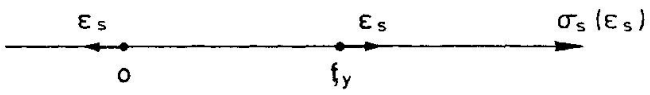

Fig. 5 Yield locus for reinforcing steel

The reinforcement is assumed to be either concentrated in lines (stringers) or continuously distributed over the section (smeared). In the latter case, the bars are assumed to be parallel and sufficiently closely spaced. The tensile strength of a stringer is the yield force $T_y = A_s f_y$, where A_s is the cross-sectional steel area. The strength of smeared reinforcement is characterized by the equivalent yield stress rf_y , where r is the reinforcement ratio, defined as

$$r = \frac{A_s}{A_c} \tag{5}$$

Here A_c is the area of the section of concrete perpendicular to the bars of area A_s .

The actions of reinforcement in different directions are assumed to be independent. Generally, problems with bond and anchorage are neglected. Thus perfect bond is assumed in upper bound solutions. In lower bound solutions, any stress transfer, including complete slip, is possible.

5. DISSIPATION IN YIELD LINES

In the derivation of upper bound solutions, it is very convenient to use failure mechanisms where the deformations are localized in failure surfaces, separating rigid parts of the body. The angle between the relative displacement rate v and the surface is termed α , where $-\pi/2 \leq \alpha \leq \pi/2$, cf. Fig. 6b. The intersection of the failure surface with the normal plane containing the displacement vector is called a yield line. The yield line is a kinematical discontinuity which may be regarded as an idealization of a narrow zone of depth Δ with high strain rates, assumed to be homogeneous, cf. Fig. 6a.

In the normal plane, the local components of the strain rates are

$$\varepsilon_n = \frac{v}{\Delta}\sin\alpha \quad , \quad \varepsilon_t = 0 \quad , \quad \varphi_{nt} = 2\gamma_{nt} = \frac{v}{\Delta}\cos\alpha$$

The transformation formulæ (Mohr's circle) then yield the principal strain rates:

$$\varepsilon_1 = \frac{v}{2\Delta}(1+\sin\alpha) \quad \text{and} \quad \varepsilon_2 = -\frac{v}{2\Delta}(1-\sin\alpha) \tag{6a,b}$$

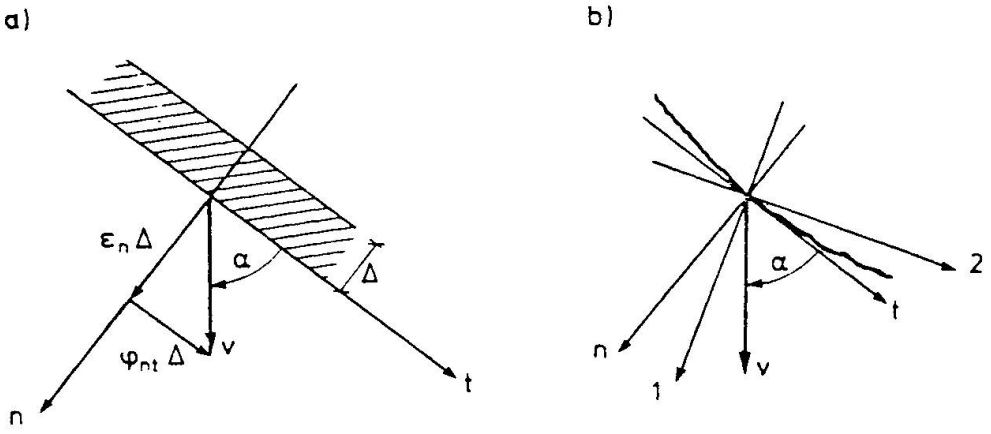

Fig. 6 Yield line in plain concrete
a) Narrow zone with high straining
b) Kinematical discontinuity

The principal directions of strain rate, which coincide with the principal directions of stress, are indicated in Figs. 6. The first principal axis bisects the angle between the deformation vector and the yield line normal.

In the cases of plane stress $(\sigma_3 = 0)$ or plane strain $(\varepsilon_3 = 0)$, the rate of internal work per unit area of the discontinuity is

$$D = (\varepsilon_1 \sigma_1 + \varepsilon_2 \sigma_2) \tag{7}$$

Referring to equations (6), note that the dissipation is independent of the assumed depth Δ of the deforming zone.

The principal stresses (σ_1, σ_2) which are able to produce the principal strain rates $(\varepsilon_1, \varepsilon_2)$ given by equations (6) are determined by the flow rule and the yield condition, Fig. 3. The stress regime on the yield locus depends upon the direction of the strain rate vector, i.e. upon the value of α.

Inserting into equation (7), we find:

$$D = \frac{1}{2} v f_c^* (\ell - m \sin\alpha) \tag{8}$$

for $\varphi \leq \alpha \leq \pi/2$ (plane stress or strain)

$$D = \frac{1}{2} v f_c^* (1 - \sin\alpha) \tag{9}$$

for $-\pi/2 \leq \alpha \leq \varphi$ (plane stress)

Here the parameters ℓ and m are defined as

$$\ell = 1 - (k-1) f_t^*/f_c^* \quad , \quad m = 1 - (k+1) f_t^*/f_c^* \tag{10a,b}$$

Note that equations (8) and (9) are identical for $\alpha = \varphi$. Equation (9) is valid for plane stress only, because the flow rule and the yield condition exclude yield lines with $\alpha < \varphi$ in the case of plane strain. To describe such deformations, it would be necessary to introduce a more sophisticated constitutive model, e.g. by assuming a curved failure envelope (cf. Fig. 1) or a non-associated flow rule.

The derivation of equations (8) and (9) is explained in further detail by JENSEN [75.1], cf. also [78.6]. General formulae for the dissipation in a modified Coulomb material are given by JENSEN [77.2].

Suppose a reinforcement stringer intersects a yield line at the angle β, where $0 \leq \beta \leq \pi$ and $\beta = 0$ corresponds to the same direction as $\alpha = 0$, cf. Fig. 7. The rate of strain ε_s in the stringer is then

$$\varepsilon_s = \frac{v}{\Delta} \sin\beta\cos(\beta - \alpha)$$

The rate of internal work is determined by the flow rule and the yield condition, Fig. 5:

$$W_I = v\, T_y \cos(\beta - \alpha) \quad \text{for} \quad \beta - \alpha \leq \pi/2 \qquad (11)$$

$$W_I = 0 \quad \text{for} \quad \beta - \alpha \geq \pi/2$$

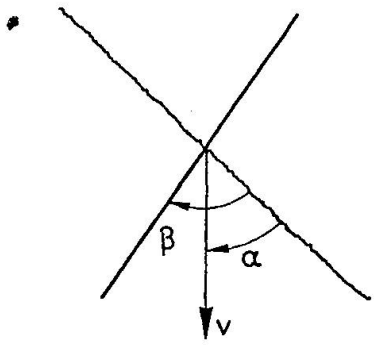

Fig. 7 Yield line with reinforcing bar

If the yield line is crossed by a band of smeared reinforcement, the contribution to the rate of internal work per unit area of the discontinuity is

$$D = v\, r f_y \cos(\beta - \alpha)\sin\beta \quad \text{for} \quad \beta - \alpha \leq \pi/2 \qquad (12)$$

$$D = 0 \quad \text{for} \quad \beta - \alpha \geq \pi/2$$

The factor $\sin\beta$ takes account of the fact that the reinforcement ratio r is defined per unit area perpendicular to the reinforcement, cf. equation (5).

6. CRACKS AND YIELD LINES

Cracks in concrete are damages which are always present at the micro-level, and may occur for a number of reasons, including changes in temperature and humidity. Under load, visible cracks tend to form perpendicular to the direction of first principal stress. Thus from Figs. 6 we conclude that a yield line will only coincide with the crack direction provided that it is perpendicular to the relative displacement rate. In that case, the yield line may be termed a collapse crack, MUELLER [76.2],[78.6].

During a loading history leading to collapse, the principal axes (and the cracks) are likely to change directions, and at failure the latest formed cracks will generally be at an angle to the yield line. This means that shear stresses are transferred across the discontinuity, presumably by aggregate interlock in old cracks and by crushing zones between cracks.

The transfer of shear in yield lines is expressed by the rate of work dissipated, which depends upon the direction α of the deformation, cf. Figs. 6. For $\alpha = \pi/2$, equation (8) reduces to $D = v\, f_t^*$, i.e. the resistance of concrete to cracking is equal to the tensile strength. However, as soon as a tangential deformation is introduced $(\alpha < \pi/2)$, the resistance increases dramatically, and the compressive strength becomes dominant.

If the tensile strength is neglected, the stress state in the yield line is given by the corner C of the yield locus, Fig. 3, for $\varphi < \alpha < \pi/2$ in plane strain and $-\pi/2 < \alpha < \pi/2$ in plane stress $(-\pi/2 < \alpha < \varphi$ in the case of finite tensile strength). Hence the principal stresses are $(\sigma_1, \sigma_2) = (0, -f_c^*)$, corresponding to the local stresses in the yield line (cf. Figs. 6):

$$\sigma_n = -\frac{1}{2} f_c^* (1 - \sin\alpha) \quad , \quad \tau_{nt} = \frac{1}{2} f_c^* \cos\alpha \qquad (13a,b)$$

Note that the shear stress increases to a maximum of half the compressive strength in the case of pure shearing $(\alpha = 0)$.

To minimize the rate of internal work, concrete will tend to fail mainly by cracking, with as little shearing as possible. The efficiency of steel bars as reinforcement is to a large extent due to the restraint they offer against the dilation of cracking concrete. The principal merit of the modified Coulomb condition is that it offers a simple and rational description of this behaviour.

The adoption of a zero tensile strength is equivalent with the assumption that the concrete is potentially cracked in all directions, whether cracks are detected or not. Still, the concrete behaves as an isotropic material, in the sense that the cracks in one direction do not affect the strength in other directions, unless the cracking is associated with significant strains, cf. Section 3. It might be feared that the presence of cracks would reduce the resistance to sliding failure in certain directions. However, experience indicates that the crack width should be very large (several millimeters) before the shear transfer is significantly reduced.

A different approach is that of BAZANT & TSUBAKI [79.1],[80.2]. They regard cracks as unable to transfer shear without the presence of compressive stresses, but rather than describe this behaviour by the modified Coulomb criterion with a zero tensile strength they introduce a so-called slip-free criterion, which is effectively the Coulomb criterion with zero cohesion (cf. BRAESTRUP [80.3]). For isotropic concrete this implies zero compressive strength, but the criterion is intended for concrete under predominantly tensile loading, and with large crack openings. Thus the cracked concrete is assumed to be anisotropic. A constitutive model for cracked concrete valid for small crack displacements has recently been proposed by BAZANT & GAMBAROVA [80.1].

7. APPLICATIONS OF THE MODEL

Early applications of plasticity to structural concrete consists of cases where the strength is mainly governed by the reinforcement, e.g. flexure of beams and slabs, and for such problems, the use of a plastic approach has become standard. Prominent examples are the yield hinge method for beams and frames, BAKER [56.1], and the yield line theory for slabs, JOHANSEN [43.1]. In these cases, the role of the concrete is merely to provide a suitable compression zone.

Plastic analysis of concrete structures subjected primarily to shear loads represents a comparatively new development. Such non-classical applications include in-plane shear in overreinforced (constrained) walls, shear in joints, shear in slender beams with vertical, inclined or no stirrups, shear in deep beams and corbels, punching shear and pull-out, concentrated loading, anchorage and bond. A common feature of these problems is that the strength of the structure is largely dependent upon the concrete properties, which means that the constitutive model for the concrete plays a dominant part.

The predictions of the plastic analysis have been compared with experimental evidence, and in most cases a remarkable qualitative agreement has been found. The quantitative agreement hinges upon the assumed values of the effective strength parameters, cf. Section 3. It appears that reasonable strength predictions are obtained by neglecting the tensile strength f_t^* and adopting an effectiveness factor $\nu = f_c^*/f_c$ of the order of $\nu = 0.5$, f_c being the cylinder strength.

A detailed account of the individual applications is outside the scope of the present paper, and the reader is referred to the papers and reports mentioned in Section 1, as well as to a monograph by NIELSEN and a thesis by BRAESTRUP, both in preparation. A summary of the results will also appear as a chapter of a forthcoming Handbook of Structural Concrete.

8. DISCUSSION

Mathematical models for material response are tools by which engineers may predict the strength and deformations of structures. By introducing a sufficiently large number of constitutive parameters it is possible to describe the behaviour of the most complex material to any desired degree of accuracy. The computational difficulties arising from the application of such complicated models can be overcome by the use of numerical methods adapted for large electronical computers. However, the machine does not give any indications on how to assign realistic values to the various material parameters in any particular application.

In the preceeding sections we have introduced a description of concrete at ultimate which is extremely simple, in the sense that it relies upon only three parameters, which are easily evaluated, the physical significance being straightforward. If the tensile strength f_t^* is neglected, and the standard value $\varphi = 37^o$ is adopted for the angle of friction, then the only parameter left to characterize the material is the effective concrete strength f_c^*, which essentially is a conservative estimate of the uniaxial compressive strength.

It is obvious that such a primitive model cannot furnish any detailed description, even when attention is restricted to strength properties. Nevertheless, experience indicates that surprisingly good predictions are obtained concerning the failure of structures in plain and reinforced concrete.

It appears that the best results are produced for problems involving plane stress. For plane strain, and particularly axisymmetric cases, the solutions tend to significantly overestimate the load-carrying capacity. This is probably due to the fact that the yield condition is unconservative in the presence of high hydrostatic compression. A refinement of the model should address that problem, e.g. by substituting a curved failure envelope for the straight line of the Coulomb criterion, cf. Fig. 1.

A reasonable amendment would be to replace equation (1) by the parabola:

$$\tau^2 = \frac{1}{4} f_c^2 (1 - \sin\varphi)^2 - \sigma f_c \sin\varphi \quad (14)$$

This failure envelope has the property that the inclination is equal to φ for the stress state corresponding to uniaxial compression. The tension cut-off, equation (4), only becomes effective for a tensile strength $f_t < \frac{1}{4} f_c (1 - \sin\varphi)^2 / \sin\varphi$.

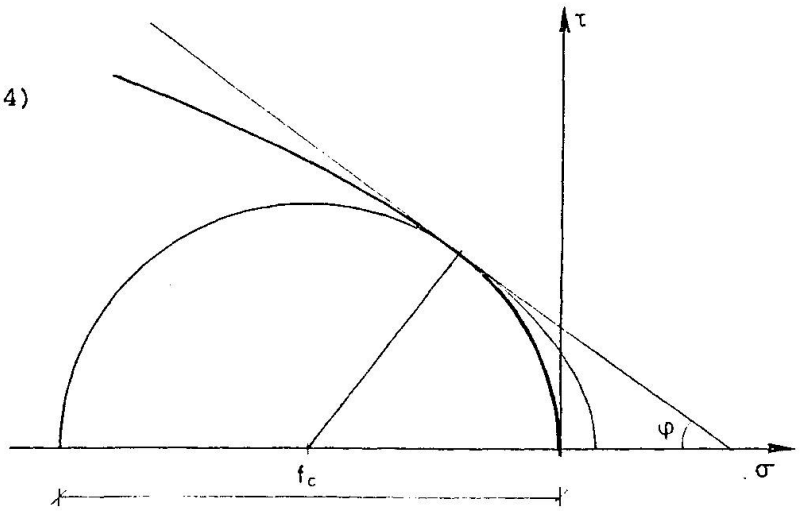

Fig. 8 Parabolic failure envelope with zero tension cut-off.

The modified failure envelope is shown in Fig. 8 for $f_t = 0$. Note that in this case the yield locus for plane stress still is the square yield locus, cf. Fig. 4. For plane strain the lines with slope k (Fig. 3) are replaced by hyperbolas with asymptotes parallel with the hydrostatic axis. Thus plain strain yield lines with deformation inclinations $\alpha < \varphi$ become possible, albeit the resistance against pure shearing ($\alpha = 0$) is infinite. This should lead to a better description of axisymmetric problems without the introduction of additional parameters.

ACKNOWLEDGEMENTS

The research reported has been carried out at the Department of Structural Engineering (ABK) of the Technical University of Denmark under a grant from the Danish Council for Scientific and Technical Research. The material for the present paper is partly extracted from a thesis under preparation.

REFERENCES

[1638] GALILEO: Discorsi e Dimostrazioni Matematiche intorno à due nuone Scienze Attenenti alla Mecanica & i Movimenti Locali. Leyden, Elsevirs, 1638. (English translation: Dialogues concerning Two New Sciences. New York, Dover Publ. 1950, 294 pp.)

[1776] COULOMB, C.A.: Essai sur une application des règles de maximis & minimis à quelques problèmes de statique, relatifs a l'architecture. Mémoires de Mathématique & de Physique Présentés a l'Academie Royale des Sciences, Vol. 7, 1776, pp. 343-382. (English translation: HEYMAN [72.1], pp. 41-74)

[1900] MOHR, O.: Welsche Umstände bedingen die Elastizitätsgrenze und den Bruch eines Materials. Zeitschrift des Vereines deutshcer Ingenieure, Vol. 44II, 1900, pp. 1524-1530, 1572-1577.

[28.1] MISES, R.v.: Mechanik der plastischen Formänderung von Kristallen. Zeitschrift für Angewandte Mathematik und Mechanik, Vol. 8, 1928, pp. 161-185.

[35.1] LEON, A.: Ueber die Scherfestigkeit des Betons. Beton und Eisen, Vol. 34, No. 8, 1935, pp. 130-135.

[38.1] GVOZDEV, A.A.: Opredelenie velichiny razrushayushchei nagruzki dlya staticheski neopredelimykh sistem, preterpevayushchikh plasticheskie deformatsii. Svornik trudov konferentsii po plasticheskim deformatsiyam, Moscow-Leningrad, Akademia Nauk SSSR, 1938, pp. 19-30.
(English translation: The determination of the value of the collapse load for statically indeterminate systems undergoing plastic deformation. International Journal of Mechanical Sciences, Vol. 1, 1960, pp. 322-333.)

[43.1] JOHANSEN, K.W.: Brudlinieteorier. Copenhagen, Gjellerup, 1943, 189 pp. (English translation: Yield-Line Theory. London, Cement and Concrete Association, 1962).

[48.1] DORN, J.E.: The effect of stress state on the fracture strength of metals. Fracturing of Metals, Cleveland, Ohio, American Society of Metals, 1948, pp. 32-50.

[48.2] HODGE, P.G. & PRAGER, W.: A variational principle for plastic materials with strainhardening. Journal of Mathematics and Physics, Vol. 27, No. 1, 1948, pp. 1-10.

[49.1] GVOZDEV, A.: Raschet nesushchei sposobnosti konstruktsii po metodu predelnogo ravnoveiya. (Analysis of the load-carrying capacity of structures by the method of limiting equilibrium). Moscow, Stroiizdat, 1949, 280 pp.

[50.1] HILL, R.: The Mathematical Theory of Plasticity. Oxford, Clarendon Press, 1950, 356 pp.

[52.1] DRUCKER, D.C. & PRAGER, W.: Soil mechanics and plastic analysis or limit design. Quarterly of Applied Mathematics, Vol. 10, 1952, pp. 157-165.

[52.2] DRUCKER, D.C., PRAGER, W. & GREENBERG, H.J.: Extended limit design theorems for continuous media. Quarterly of Applied Mathematics, Vol. 9, 1952, pp. 381-389.

[53.1] COWAN, H.J.: The strength of plain, reinforced and prestressed concrete under the action of combined stresses, with particular reference to the combined bending and torsion of rectangular sections.
Magazine of Concrete Research, Vol. 5, 1953, pp. 75-86.

[53.2] KOITER, W.T.: Stress-strain relations, uniqueness and variational theorems for elastic-plastic materials with singular yield surfaces. Quarterly of Applied Mathematics, Vol. 11, No. 3, 1953, pp. 350-354.

[55.1] PRAGER, W.: The general theory of limit design. 8th International Congress of Theoretical and Applied Mechanics, Proc. Vol. II, 1955, pp. 65-72.
[56.1] BAKER, A.L.L.: The Ultimate-Load Theory Applied to the Design of Reinforced and Prestressed Concrete Frames. London, Concrete Publications Ltd. 1956, 91 pp.
[61.1] DRUCKER, D.C.: On structural concrete and the theorems of limit analysis. International Association for Bridge and Structural Engineering, Memoirs, Vol. 21, 1961, pp. 49-59.
[61.2] PAUL, B.: A modification of the Coulomb-Mohr theory of fracture. Journal of Applied Mechanics, Vol. 28, June 1961, pp. 259-268.
[64.1] NIELSEN, M.P.: Limit analysis of reinforced concrete slabs. Copenhagen, Acta Polytechnica Scandinavica, Civil Engineering and Building Construction Series No. 26, 1964, 167 pp.
[65.1] SANDBYE, P.: A plastic theory for plain concrete. Bygningsstatiske Meddelelser, Vol. 36, No. 2, 1965, pp. 41-62.
[67.1] NIELSEN, M.P.: Om forskydningsarmering i jernbetonbjælker. (On shear reinforcement in reinforced concrete beams). Bygningsstatiske Meddelelser, Vol. 38, No. 2, 1967, pp. 33-58.
[69.1] CHEN, W.-F. & DRUCKER, D.C.: Bearing capacity of concrete blocks or rock. Journal of the Engineering Mechanics Division, Proc. ASCE, Vol. 95, No. EM4, Aug. 1969, pp. 955-978.
[69.2] NIELSEN, M.P.: Discussion on NIELSEN [67.1]. Bygningsstatiske Meddelelser, Vol. 40, No. 1, 1969, pp. 60-63.
[70.1] CHEN, W.-F.: Extensibility of concrete and theorems of limit analysis. Journal of the Engineering Mechanics Division, Proc. ASCE, Vol. 96, No. EM3, June 1970, pp. 341-352.
[71.1] MAGNAS, J.-P. & AUDIBERT, A.: Critères de résistance du béton sous sollicitations multiaxiales. Annales de l'Institut Technique du Bâtiment et des Traveaux Publics, No. 287, Nov. 1971, pp. 22-43.
[71.2] NIELSEN, M.P.: On the strength of reinforced concrete discs. Copenhagen, Acta Polytechnica Scandinavica, Civil Engineering and Building Construction Series No. 70, 1971, 261 pp.
[72.1] HEYMAN, J.: Coulomb's Memoir on Statics: An Essay in the History of Civil Engineering. Cambridge University Press, 1972, 212 pp.
[74.1] COWIN, S.C.: Constitutive relations that imply a generalized Mohr-Coulomb criterion. Acta Mecanica, Vol. 20, 1974, pp. 41-46.
[75.1] JENSEN, B.C.: Lines of discontinuity for displacements in the theory of plasticity of plain and reinforced concrete. Magazine of Concrete Research, Vol. 27, No. 92, Sep. 1975, pp. 143-150.
[76.1] CARINO, N.J. & SLATE, F.O.: Limiting tensile strain criterion for failure of concrete. Journal of the American Concrete Institute, Proc. Vol. 73, No. 3, Mar.1976, pp. 160-165.
[76.2] MUELLER, P.: Failure mechanisms for reinforced concrete beams in torsion and bending. International Association for Bridge and Structural Engineering, Memoirs, Vol. 36 II, 1976, pp. 147-163.
[77.1] GARIEL-THORON, R.de: Un nouveau critère de plasticité: Application a la Mécanique des sols. Annales de l'Institut Technique du Bâtiment et des Traveaux Publics, No. 349, Apr. 1977, pp. 117-152.
[77.2] JENSEN, B.C.: Some applications of plastic analysis to plain and reinforced concrete. Copenhagen, Technical University of Denmark, Institute of Building Design, Report No. 123, 1977, 119 pp.
[78.1] BRAESTRUP, M.W., NIELSEN, M.P. & BACH, F.: Plastic analysis of shear in concrete. Zeitschrift für Angewandte Mathematik und Mechanik, Vol. 58, No. 6, June 1978, pp. 3-14.
[78.2] CHEN, W.-F.: Constitutive equations for concrete. IABSE [78.3], Oct. 1978, pp. 11-34.

[78.3] IABSE. Plasticity in Reinforced Concrete. Introductory Report. Zürich, International Association for Bridge and Structural Engineering, Reports of the Working Commissions, Vol. 28, Oct. 1978, 172 pp.

[78.4] KOTSOVOS, M.D. & NEWMAN, J.B.: Generalized stress-strain relations for concrete. Journal of the Engineering Mechanics Division, Proc. ASCE, Vol. 104, No. EM4, Aug. 1978, pp. 845-856.

[78.5] LOWE, P.G.: Deformation and fracture of plain concrete. Magazine of Concrete Research, Vol. 30, No. 105, Dec. 1978, pp. 200-204.

[78.6] MUELLER, P.: Plastische Berechnung von Stahlbetonscheiben und -Balken. Zürich, Eidgenössische Technische Hochschule, Institut für Baustatik und Konstruktion, Bericht Nr. 83 (ETH Diss. 6083), July 1978, 160 pp.

[78.7] NIELSEN, M.P., BRAESTRUP, M.W., JENSEN, B.C. & BACH, F.: Concrete Plasticity. Beam Shear - Punching Shear - Shear in Joints. Copenhagen, Danish Society for Structural Science and Engineering, Special Publication, Oct. 1978, 129 pp.

[79.1] BAŽANT, Z.P. & TSUBAKI, T.: Concrete reinforcing net: Optimum slip-free limit design. Journal of the Structural Division, Proc. ASCE, Vol. 105, No. ST2, Feb. 1979, pp. 327-346.

[79.2] COLLINS, M.P.: Investigating the stress-strain characteristics of diagonally cracked concrete. IABSE [79.5], Aug. 1979, pp. 27-34.

[79.3] DRAGON, A. & MRÓZ, Z.: A continuum model for plastic-brittle bahaviour of rock and concrete. International Journal of Engineering Science, Vol. 17, No. 2, Feb. 1979, pp. 121-137.

[79.4] EXNER, H.: On the effectiveness factor in plastic analysis of concrete. IABSE [79.5], Aug. 1979, pp. 35-42.

[79.5] IABSE: Plasticity in Reinforced Concrete, Final Report. Zürich, International Association for Bridge and Structural Engineering, Report of the Working Commissions, Vol. 29, Aug. 1979, 360 pp.

[79.6] KOTSOVOS, M.D. & NEWMAN, J.B.: A model of concrete behaviour under generalized stress. IABSE [79.5], Aug. 1979, pp. 19-26.

[79.7] OTTOSEN, N.S.: Constitutive model for short-time loading of concrete. Journal of the Engineering Mechanics Division, Proc. ASCE, Vol. 105, No. EM1, Feb. 1979, pp. 127-141.

[79.8] WASTIELS, J.: Failure criteria for concrete under multiaxial stress states. IABSE [79.5], Aug. 1979, pp. 3-10.

[80.1] BAŽANT, Z.P. & GAMBAROVA, P.: Rough cracks in reinforced concrete. Journal of the Structural Division, Proc. ASCE, Vol. 106, No. ST4, Apr. 1980, pp. 819-842.

[80.2] BAŽANT, Z.P. & TSUBAKI, T.: Discussion on BAŽANT & TSUBAKI [79.1]. Journal of the Structural Division, Proc. ASCE, Vol. 106, No. ST6, June 1980, pp. 1378-1383.

[80.3] BRAESTRUP, M.W.: Discussion on BAŽANT & TSUBAKI [79.1]. Journal of the Structural Division, Proc. ASCE, Vol. 106, No. ST6, June 1980, pp. 1375-1378.

[80.4] MARTI, P.: Zur plastischen Berechnung von Stahlbeton. Zürich, Eidgenössische Technische Hochschule, Institut für Baustatik und Konstruktion, Bericht Nr. 104, Oct. 1980, 176 pp.

A Fracture Mechanics Model for Reinforced Concrete Collapse

Un modèle de mécanique de rupture pour le béton armé.

Ein Bruchmechanikmodell für das Versagen von Stahlbeton.

ALBERTO CARPINTERI
Research Assistant,
University of Bologna,
Bologna, Italy.

SUMMARY
The Limit Analysis of reinforced concrete beams does not take into consideration the cracks which usually develop in concrete, and the consequent stiffness variation and stress concentration. In the present paper such effects will be studied on the basis of Fracture Mechanics concepts. Thus it will be shown how the stability of the process of concrete fracture and steel plastic flow depends on the mechanical and geometrical (scale included) properties of the beam cross-section.

RÉSUMÉ
L'analyse limite de la section d'une poutre en béton armé ne tient pas compte des fissures normalement produites dans le béton et les variations de rigidité et de concentration des contraintes. Dans cette note, on étudie ces effets sur la base des principes de la Mécanique de la Rupture. Par conséquent, on montre que la stabilité du phénomène de formation des fissures dans le béton et de la plasticité de l'acier, dépend des caractéristiques mécaniques et géométriques (y inclus l'échelle) de la section de la poutre examinée.

ZUSAMMENFASSUNG
Die Traglastberechnung eines Trägerquerschnitts aus Stahlbeton trägt keineswegs Rechnung met den Rissen, die in der Regel beim Beton auftreten, sowie den damit zusammenhängenden Steifigkeitsänderungen und Änderungen der Spannungskonzentration. Genannte Wirkungen werden in diesem Beitrag unter Zugrundelegung bruchmechanischer Begriffe untersucht. Es wird sich damit zeigen, inwieweit die stabile Rissausbreitung in Beton und das Fliessen des Stahls von den mechanischen und geometrischen (einschliesslich der Masstabs-) Eigenschaften des Querschnitts abhängig sind.

1. INTRODUCTION.

In the Limit Analysis of the reinforced concrete beam cross-section the stretched part of concrete is conventionally assumed not to be traction bearing, while a perfectly plastic behaviour of the compressed part is hypothesized [1]. Such analysis doesn't take into consideration the cracks, which usually develop in concrete and generally cause that more complex crisis phenomenon which is the collapse of the concrete-steel system. In fact the Limit Analysis approach doesn't consider the stiffness variation and the stress concentration due to the crack's presence at all. On the other hand these two effects can be taken and studied through Fracture Mechanics concepts.

By tradition the problems relating to cracked masonry or concrete constructions are studied on the basis of empirical parameters, such as the crack width, i.e. the distance between the crack free surfaces [2]. Such parameters cannot be considered as absolute indications of the crack stability condition, but only as alarm signals of incipient collapses. In fact the crack width will not be constant, but will generally increase, moving away from the crack tip. It will however depend on the sizes of the cracked structure. In the present treatment scale effects will be emphasized in the collapse phenomena of reinforced concrete beams, as has been already done for plain concrete structures [3] [4] [5] [6].

Four types of potential collapses will be considered:

1) concrete fracture collapse ($K_I \geqslant K_{IC}$);
2) concrete ultimate strength collapse ($\sigma \geqslant f_u$);
3) concrete crushing collapse ($\sigma \geqslant f_c$);
4) steel plastic flow collapse ($\sigma \geqslant f_y$).

The final collapse is generally the definitive and irreversible consequence of the four above mentioned collapses. Such collapses will occur in a well defined sequence, according to the mechanical and geometrical (scale included) properties of the beam cross-section. The only collapse, which, even though very frequent, will not be considered, is the slip between reinforcement and concrete.

Then the stability of the process of concrete fracture and steel plastic flow will be studied, and its dependence on the mechanical and geometrical (scale included) properties of the beam cross-section will be shown. A role of primary importance, besides that of steel percentage A_S/A [2], is played by the non-dimensional number $f_y b^{1/2}/K_{IC}$ (analogous to the Brittleness Number defined in [4]), which includes the mechanical properties of the materials and the sizes of the structure.

2. HYPERSTATIC REACTION OF REINFORCEMENT.

Consider a reinforced concrete beam segment, with a rectangular cross-section of thickness t and width b, subjected to a bending moment M. Let the steel reinforcement be distant h from the external surface, and a through-thickness edge crack of depth $a \geqslant h$ is assumed to exist in the stretched part (Fig. 1). Therefore the cracked concrete beam segment will be in all subjected to the external bending moment M and to an eccentric axial force F, due to the hyperstatic reaction of the reinforcement. It is well-known that a bending moment M* induces a stress-intensity factor K_I at the crack tip equal to:

$$K_I = \frac{M^*}{b^{3/2} t} Y_M(\xi), \tag{1}$$

where $\xi = a/b$ is the relative crack depth and Y_M is the function [7]:

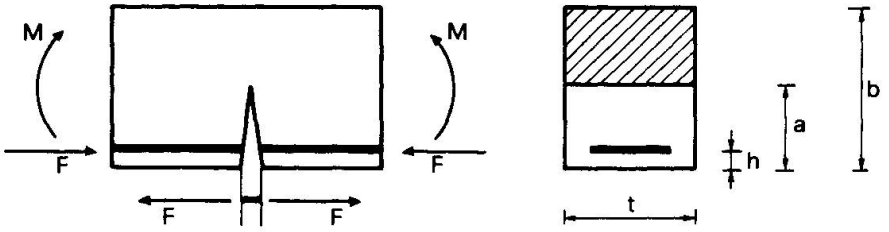

Fig. 1 Cracked reinforced beam segment.

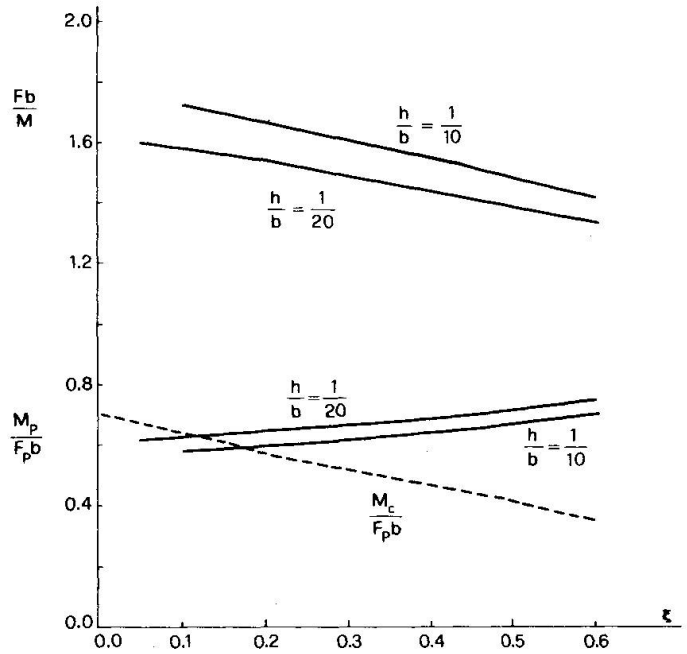

Fig. 2 Hyperstatic reaction of reinforcement and bending moment of reinforcement plastic flow.

$$Y_M(\xi) = 1.99\,\xi^{1/2} - 2.47\,\xi^{3/2} + 12.97\,\xi^{5/2} - 23.17\,\xi^{7/2} + 24.80\,\xi^{9/2}, \tag{2}$$

for $\xi \leqslant 0.6$.

In the same way, an axial tensile force F* induces the stress-intensity factor:

$$K_I = \frac{F^*}{b^{1/2}t}\,Y_F(\xi), \tag{3}$$

with [7]:

$$Y_F(\xi) = 1.99\,\xi^{1/2} - 0.41\,\xi^{3/2} + 18.70\,\xi^{5/2} - 38.48\,\xi^{7/2} + 53.85\,\xi^{9/2}, \quad \text{for } \xi \leqslant 0.6. \tag{4}$$

On the other hand the bending moment M* causes a relative rotation φ equal to [8] [9]:

$$\varphi = \lambda_{MM}\,M^*, \tag{5}$$

with:

$$\lambda_{MM} = \frac{1}{b^2 t E}\int_0^{\xi} Y_M^2(\xi)\,d\xi, \tag{6}$$

while the axial tensile force F* causes the rotation [8] [9]:

$$\varphi = \lambda_{MF} F^*, \tag{7}$$

with:
$$\lambda_{MF} = \frac{1}{btE} \int_0^{\xi} Y_M(\xi)\, Y_F(\xi)\, d\xi. \tag{8}$$

In the case of the considered statically indeterminate system, i.e. the reinforced beam segment (Fig.1), the global moment acting on the cross-section will be:

$$M^* = M - F\left(\frac{b}{2} - h\right), \tag{9}$$

that is, it will be given by the external moment, opening the crack, subtracted by the reinforcement reaction moment, closing the crack. Then the axial force acting on the cross-section will be:

$$F^* = -F. \tag{10}$$

Up to the moment of steel yielding, the global rotation, due to the bending moment M* and to the closing force F*, will be zero:

$$\varphi = \lambda_{MM} M^* + \lambda_{MF} F^* = 0. \tag{11}$$

The equation (11) is the congruence condition able to provide the hyperstatic unknown F. Namely, replacing the expressions (9) and (10) in (11), the result is:

$$\lambda_{MM}\left[M - F\left(\frac{b}{2} - h\right)\right] - \lambda_{MF} F = 0, \tag{12}$$

and finally it is possible to obtain:

$$\frac{Fb}{M} = \frac{1}{\left(\frac{1}{2} - \frac{h}{b}\right) + r(\xi)}, \tag{13}$$

where:

$$r(\xi) = \frac{\int_0^{\xi} Y_M(\xi)\, Y_F(\xi)\, d\xi}{\int_0^{\xi} Y_M^2(\xi)\, d\xi}. \tag{14}$$

The hyperstatic reaction of the reinforcement, against the relative crack depth, for h/b = 1/10, 1/20 , is reported in the diagram of Figure 2. The decrease of the hyperstatic reaction by increasing the crack depth is not intuitive, and indeed it may even surprise the reader. However it can be explained by observing that the compliances λ_{MM} and λ_{MF} both increase by increasing the crack length, but λ_{MF} increases more rapidly than λ_{MM} does. Thus lower and lower axial forces F are needed to annul the rotation due to the external moment M.

3. BENDING MOMENT OF REINFORCEMENT PLASTIC FLOW.

As the expression (13) shows, the force F, transmitted by the reinforcement, increases linearly by increasing the external moment M, until the limit force $F_p = f_y A_s$ is reached, being f_y the steel yield strength and A_s the steel area. From this point onwards a perfectly plastic behaviour of the reinforcement will be considered. It means that the infinitesimal reinforcement segment, which is uncovered, i.e. included between the two crack surfaces, will flow, always transmitting the same force F_p to the cracked concrete segment (Fig. 3).

From (13) it is possible to obtain the moment of plastic flow for the reinforcement:

$$M_p = F_p b \left[\left(\frac{1}{2} - \frac{h}{b}\right) + r(\xi)\right]. \tag{15}$$

Such moment against the relative crack depth, for $h/b = 1/10, 1/20$, is reported in Figure 2. According to the hyperstatic force decrease by increasing the crack depth ξ (Fig. 2), an increase of the moment of reinforcement plastic flow M_p occurs by increasing ξ.

However it is necessary to observe that, if concrete presents a low crushing strength f_c and steel a relatively high yield strength f_y, the concrete crushing collapse can come before the steel plastic flow. If M_c is the external moment of concrete crushing and a hypothesis of linear stress variation through the ligament holds (Fig. 4) [2], it results:

$$\frac{M_c}{F_p b} = \frac{f_c}{f_y \dfrac{A_s}{A}} \cdot \frac{(1-\xi)\left(2+\xi-3\dfrac{h}{b}\right)}{6}. \tag{16}$$

The dashed line of Figure 2 represents the diagram of function (16) for $f_c = 200$ kg cm^{-2}, $f_y = 3600$ kg cm^{-2}, $A_s/A = 0.024$ and $h/b = 1/10$. It can be observed that, although values very favourable to the concrete crushing collapse have been chosen, such collapse in fact comes before the steel plastic flow only for sufficiently high values of the crack depth ($\xi \geqslant 0.175$).

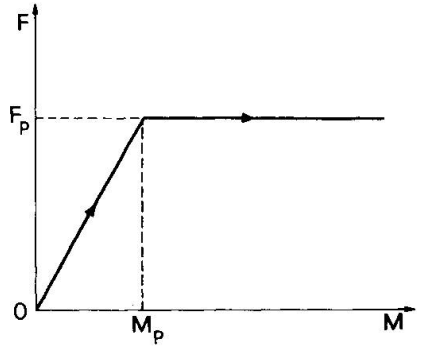

Fig. 3 Hyperstatic force transmitted by the reinforcement against the applied moment.

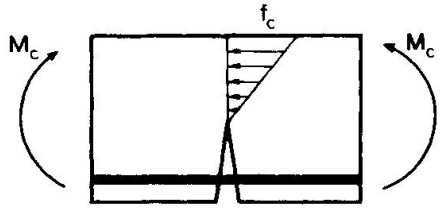

Fig. 4 Hypothesis of linear stress variation through the ligament.

4. RIGID-HARDENING BEHAVIOUR OF THE CRACKED BEAM SEGMENT.

The purpose of the present section is to describe the mechanical behaviour of the cracked reinforced

concrete beam segment, once the bending moment M_p of steel plastic flow has been exceeded. For $M \leqslant M_p$ we have namely $\varphi = 0$, while for $M > M_p$:

$$\varphi = \lambda_{MM}\left[M - F_p\left(\frac{b}{2} - h\right)\right] - \lambda_{MF} F_p. \tag{17}$$

The $M - \varphi$ diagram for the cracked beam segment is represented in Figure 5. This diagram expresses the equivalence of the beam segment with a rigid-linear hardening spring. It is interesting to observe how the hardening line is parallel to the $M - \varphi$ diagram relating to the same cracked beam segment without reinforcement (broken line).

The hardening coefficient λ_{MM}^{-1} against the relative crack depth ξ is reported in Figure 5 again. By increasing the crack depth ξ, the hardening line becomes more and more inclined, until giving rigid--perfectly plastic behaviour. On the other hand, for $\xi \to 0$, the hardening line becomes nearly vertical, until giving a rigid behaviour of the beam segment simulating spring.

Therefore, summarizing, one can conclude that, by increasing ξ, the moment of steel plastic flow increases (Fig. 2), while the slope of the hardening line decreases (Fig. 5). Some $M - \varphi$ diagrams, for $h/b = 1/20$, are reported in Figure 6, varying ξ between 0.05 and 0.50. The moment of steel plastic flow increases very little by increasing ξ; on the other hand the slope of the hardening line decreases sharply.

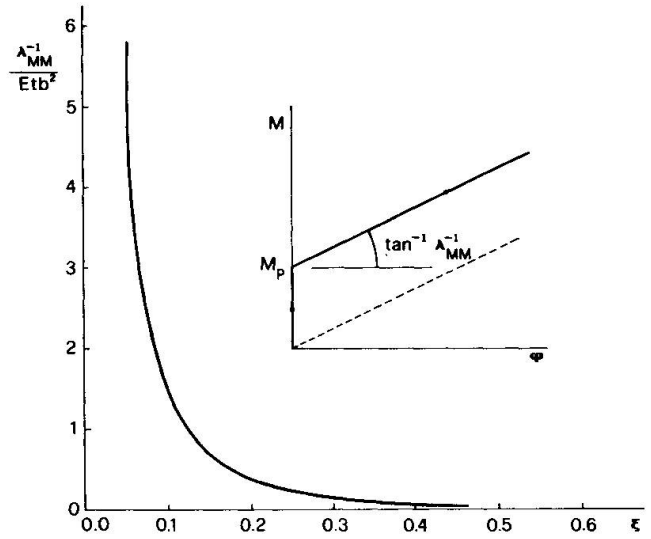

Fig. 5 Hardening coefficient against relative crack depth.

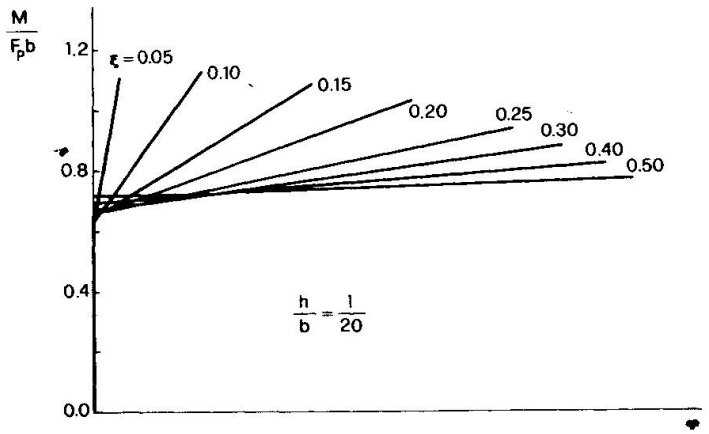

Fig. 6 Moment-rotation diagrams for different crack depths.

5. BENDING MOMENT OF CONCRETE FRACTURE.

In the preceding section the behaviour of the cracked beam segment has been considered, for bending moments higher than the steel plastic flow moment M_p. In the present section the concrete fracture collapse will be examined, which is consequent to the steel plastic flow collapse, i.e. it occurs for a bending moment $M_F \geqslant M_p$.

After the steel plastic flow, the stress-intensity factor acting at the crack tip will be equal to the algebraical addition of the factors (1) and (3), and the actual loadings will be:

$$M^* = M - F_p\left(\frac{b}{2} - h\right), \tag{18}$$

$$F^* = -F_p\,. \tag{19}$$

Thus it will be:

$$K_I = \frac{1}{b^{3/2}t}\,Y_M(\xi)\left[M - F_p\left(\frac{b}{2} - h\right)\right] - \frac{F_p}{b^{1/2}t}\,Y_F(\xi). \tag{20}$$

Presuming the expression (20) to be equal to the concrete fracture toughness K_{IC}, it is possible to obtain the fracture moment M_F:

$$M_F = \frac{K_{IC}b^{3/2}t}{Y_M(\xi)} + \frac{F_p b}{Y_M(\xi)}\left[Y_F(\xi) + Y_M(\xi)\left(\frac{1}{2} - \frac{h}{b}\right)\right]. \tag{21}$$

In non-dimensional form:

$$\frac{M_F}{K_{IC}b^{3/2}t} = \frac{1}{Y_M(\xi)} + N_p\left[\frac{Y_F(\xi)}{Y_M(\xi)} + \frac{1}{2} - \frac{h}{b}\right],$$

where:

$$N_p = \frac{f_y b^{1/2}}{K_{IC}} \cdot \frac{A_s}{A}\,. \tag{22}$$

The concrete fracture moment M_F against the relative crack depth ξ is reported in Figure 7, varying the non-dimensional number N_p (h/b = 1/20).

For N_p values close to zero, that is for low reinforced beams (either, for aggregative materials with high K_{IC}, or for very small cross-sections), the fracture moment decreases while the crack extends, and then a typical phenomenon of unstable fracture occurs.

For higher N_p values, a stable branch follows the unstable one of the curve, which describes the crack extension against the applied load. Already for $N_p = 1$ the minimum of the curve is evident and takes place for $\xi \simeq 0.35$. For higher N_p values, the ξ value, for which the minimum occurs, is lower, while the stable branch becomes steeper and steeper. For $N_p \gtrsim 8.5$ the unstable branch completely disappears and only the stable branch remains.

Analogous behaviour has been underlined in the case of a cracked masonry wall, subjected to an eccentric axial compression force [10]. However in that case the unstable branch and the consequent stable one appear steeper and the existence of the minimum is then more evident.

The locus minimorum is represented by a dashed line in Figure 7. This line divides the quadrant of the diagram into two zones: the upper zone is where the fracturing process is stable, while the lower one is where the process is unstable. Therefore, it is possible to assert that the fracturing process in reinforced concrete becomes stable only when the beam is sufficiently reinforced (either, when the

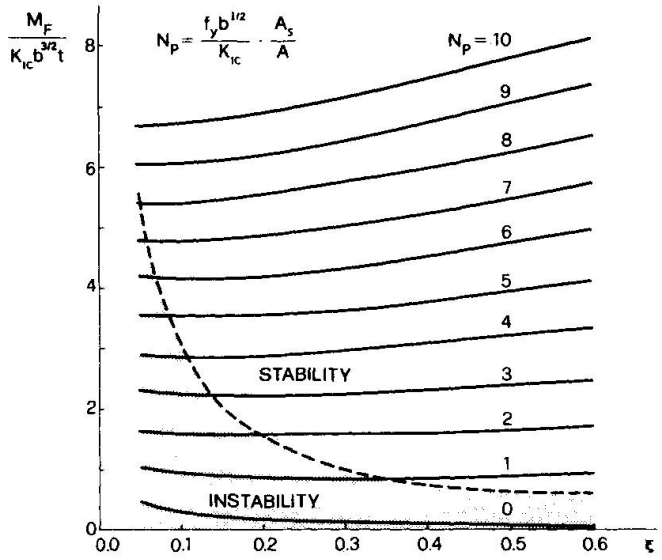

Fig. 7 Bending moment of concrete fracture against relative crack depth (h/b = 1/20).

fracture toughness K_{IC} is sufficiently low, or when the cross-section is sufficiently large), and when the crack is sufficiently deep.

If the curve N_p = constant were perfectly horizontal, a condition of indifferent equilibrium would occur. In fact none of the curves shows such a regularity. However it is important to observe how the curve relating to $N_p = 1$, which could represent the fracturing phenomenon for very common reinforced concrete beams, is only slightly deflected downwards. In fact the minimum is only about 15% lower than the value of the function for $\xi = h/b = 0.05$.

For h/b = 1/10 curves very similar to those of Figure 7 are obtained. Only two slight differences are present:

1) the curves go down, i.e. fracture collapse occurs for lower moments, since the reinforcement, being internal, resists to a lesser extent than in the preceding case;

2) the dashed line goes up, i.e. the stable zone of the diagram shrinks.

Finally it may be interesting to compute the non-dimensional number N_p for three different reinforced concrete beams. As a first example, consider the following set of values:

$$f_y = 2400 \text{ kg cm}^{-2}, \qquad K_{IC} = 80 \text{ kg cm}^{-3/2},$$
$$b = 30 \text{ cm}, \qquad A_s/A = 0.01,$$

from which one obtains:

$$N_P = \frac{f_y b^{1/2}}{K_{IC}} \cdot \frac{A_s}{A} = \frac{2400 \times 30^{1/2}}{80} \times 0.01 = 1.64.$$

Thus, it is possible to verify in the diagram of Figure 7, how, for this very common reinforced concrete beam, the fracturing process is very close to a condition of indifferent equilibrium.

Secondly, examine a low reinforced beam with small cross-section:

$$f_y = 2400 \text{ kg cm}^{-2}, \qquad K_{IC} = 100 \text{ kg cm}^{-3/2},$$
$$b = 20 \text{ cm}, \qquad A_s/A = 0.0024,$$

from which follows:

$$N_P = \frac{f_y b^{1/2}}{K_{Ic}} \cdot \frac{A_s}{A} = \frac{2400 \times 20^{1/2}}{100} \times 0.0024 = 0.26.$$

In this beam the fracturing process occurs in an unstable manner (Fig. 7).
As a third and last case, examine a high reinforced beam with large cross-section:

$$f_y = 3600 \text{ kg cm}^{-2}, \qquad K_{Ic} = 50 \text{ kg cm}^{-3/2},$$
$$b = 150 \text{ cm}, \qquad A_s/A = 0.0240,$$

from which it results:

$$N_P = \frac{f_y b^{1/2}}{K_{Ic}} \cdot \frac{A_s}{A} = \frac{3600 \times 150^{1/2}}{50} \times 0.0240 = 21.16.$$

In this beam the fracturing process occurs in a stable manner (Fig. 7).

6. STABILITY OF THE PROCESS OF CONCRETE FRACTURE AND STEEL PLASTIC FLOW.

In section 5 the stability of reinforced concrete fracturing process has been described on the basis of the curve representing the crack depth against the applied bending moment. In the present section such stability will be studied using energetic considerations.
The stress-intensity factor acting on the crack is:

$$K_I = \frac{1}{b^{3/2} t} Y_M(\xi) \left[M - F\left(\frac{b}{2} - h\right) \right] - \frac{1}{b^{1/2} t} Y_F(\xi) F, \quad \text{for } M \leqslant M_P, \tag{23}$$

$$K_I = \frac{1}{b^{3/2} t} Y_M(\xi) \left[M - F_P\left(\frac{b}{2} - h\right) \right] - \frac{1}{b^{1/2} t} Y_F(\xi) F_P, \quad \text{for } M > M_P. \tag{24}$$

Replacing expression (13) in (23), it results:

$$K_I = \frac{1}{b^{3/2} t} Y_M(\xi) \left[M - \frac{M}{b} \frac{1}{\left(\frac{1}{2} - \frac{h}{b}\right) + r(\xi)} \left(\frac{b}{2} - h\right) \right] -$$

$$- \frac{1}{b^{1/2} t} Y_F(\xi) \frac{M}{b} \frac{1}{\left(\frac{1}{2} - \frac{h}{b}\right) + r(\xi)}, \quad \text{for } M \leqslant M_P. \tag{25}$$

The equations (25) and (24) in non-dimensional form appear as follows:

$$\frac{K_I b^{1/2} t}{F_P} = Y_M(\xi) \frac{M}{F_P b} \left[1 - \frac{1}{1 + \frac{r(\xi)}{\left(\frac{1}{2} - \frac{h}{b}\right)}} \right] - \frac{M}{F_P b} Y_F(\xi) \frac{1}{\left(\frac{1}{2} - \frac{h}{b}\right) + r(\xi)}$$

$$\text{for } M \leqslant M_P, \tag{26}$$

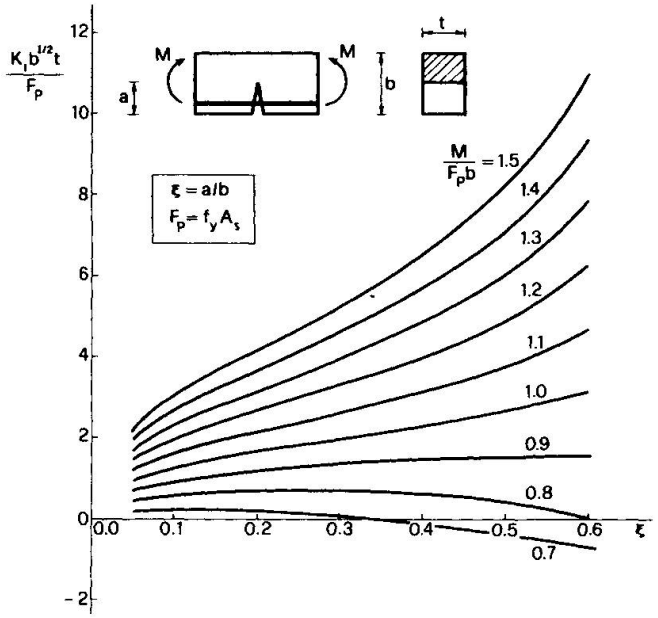

Fig. 8 Stress-intensity factor against relative crack depth, varying the applied moment (h/b = 1/20).

$$\frac{K_I b^{1/2} t}{F_p} = Y_M(\xi)\left[\frac{M}{F_p b} - \left(\frac{1}{2} - \frac{h}{b}\right)\right] - Y_F(\xi), \quad \text{for } M > M_p. \tag{27}$$

The stress-intensity factor K_I against the crack depth ξ is reported in Figure 8, varying the loading parameter $M/F_p b$ (h/b = 1/20). For $M/F_p b$ values lower than about 0.7, the stress-intensity factor is very low for every considered depth $h/b \leq \xi \leq 0.6$. As the curve $M/F_p b = 0.7$ clearly shows, the K_I value is positive for small depths ξ, while it becomes negative for larger depths. This means that, for $0 \leq M/F_p b \leq 0.8$ and sufficiently deep cracks, the assumed model predicts the closing of the crack, as well as the non-plastic state of steel. The plastic limit, as the diagram of Figure 2 suggests, is very near the curve $M/F_p b = 0.7$ reported in Figure 8. . More precisely it is included between the two curves $M/F_p b = 0.60$ and $M/F_p b = 0.75$.

For $M/F_p b > 0.8$ the K_I factor is positive for every investigated depth ξ. For $M/F_p b \gtrsim 0.9$ the K_I factor monotonicly increases as a function of the crack depth ξ. For $M/F_p b \lesssim 0.9$ the function $K_I(\xi)$ presents a positive maximum. This means that, for sufficiently low bending moments and sufficiently deep cracks, the fracturing process is stable. In fact, from an energetic point of view, one can assert that the generalized crack extension force $\mathcal{G}_I = K_I^2/E$ has the same course of K_I, for $M/F_p b > 0.8$. Thus for $0.8 \lesssim M/F_p b \lesssim 0.9$ and for sufficiently high ξ, it results:

$$\frac{\partial \mathcal{G}_I}{\partial \xi} = -\frac{\partial^2 V}{\partial \xi^2} < 0, \tag{28}$$

where V is the total potential energy of the concrete-steel system. That is, for those particular values of the bending moment and the crack depth, the total potential energy V can present, as a stationary point ($K_I = K_{IC}$), only a minimum and therefore a stable equilibrium condition.

7. FRACTURE SENSITIVITY INCREASE DUE TO REINFORCEMENT.

Up to now the only fact that has been clarified is that the concrete fracture collapse follows the reinforcement plastic collapse, and that, between the two mentioned collapses, the mechanical behaviour of the cracked beam segment is linear hardening. However no indication of how much the fracture moment M_F is higher than the plastic flow moment M_P has been given yet.
From (15) and (21) it follows:

$$\frac{M_P}{M_F} = \frac{\left[\frac{1}{2} - \frac{h}{b} + r(\xi)\right] Y_M(\xi)}{\frac{1}{N_P} + Y_F(\xi) + Y_M(\xi)\left(\frac{1}{2} - \frac{h}{b}\right)} \tag{29}$$

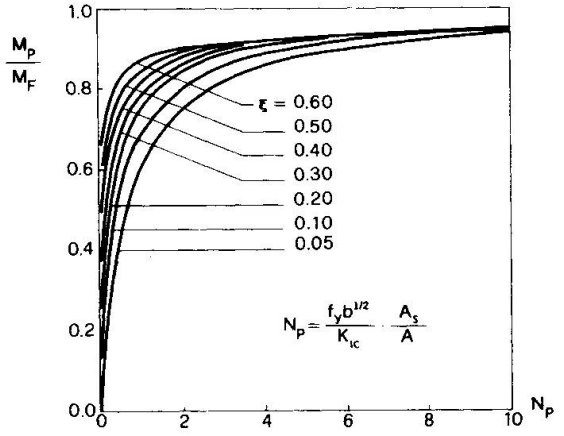

Fig. 9 Ratio between the moment of steel plastic flow and the moment of concrete fracture against the non-dimensional number N_p, varying the relative crack depth ξ (h/b = 1/20).

In Figure 9 the ratio M_P/M_F against the non-dimensional number N_p is represented, varying the crack depth ξ (h/b = 1/20). From this diagram one deduces that, the higher the number N_p and the deeper the crack, the closer the fracture collapse is to the plastic one. It means that the fracture collapse can be obtained immediately after the plastic one, particularly by varying two parameters:
1) by increasing the beam size b;
2) by increasing the steel percentage A_s/A.
Of the four potential collapses mentioned in the Introduction, only three have been explicitly considered up to now. In section 3 it has been said that the concrete crushing collapse tends to precede the others for high steel percentages A_s/A, as equation (16) shows. Once such collapse has been avoided, the other three are to be considered. The steel plastic collapse is certainly the first to be reached, while the ultimate strength collapse and the fracture collapse of concrete follow with a priority which is difficult to estimate.

8. SYNTHESIS AND CONCLUDING REMARKS.

In Figure 10 the diagrams moment-rotation $M(\varphi)$ are reported for h/b = 1/20, $\xi = 0.1$ and for five

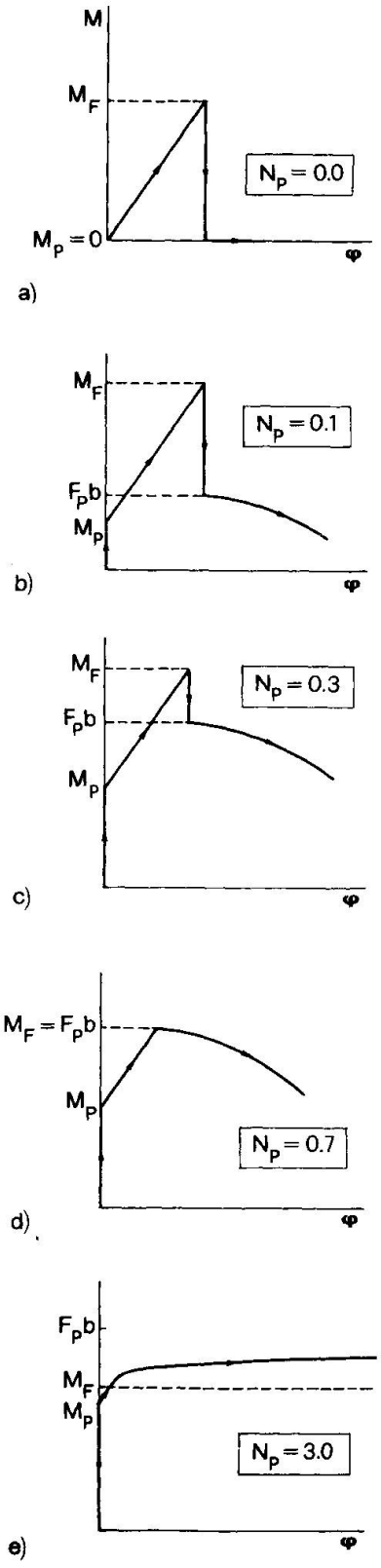

Fig. 10 Mechanical behaviour of the cracked reinforced beam segment, for different non-dimensional numbers N_p ($h/b = 0.05$; $\xi = 0.10$).

different values of number N_p: 0.0, 0.1, 0.3, 0.7, 3.0. Once the cross-section sizes and the mechanical properties of the material have been defined, they represent five different steel areas.

Rigid behaviour ($0 \leqslant M \leqslant M_p$) is followed by linear hardening behaviour ($M_p < M \leqslant M_F$). The latter stops when the concrete fracture collapse occurs. If the fracture phenomenon is unstable (section 5), function $M(\varphi)$ presents a discontinuity and drops from the value M_F to the value F_pb with a negative jump (Figs. 10-a, b, c, d). In fact in this case a complete and instantaneous disconnection of the concrete cross-section occurs. While the rotation φ is constant, the new moment F_pb can be estimated according to the scheme of Figure 11, where each beam segment is subjected to the traction F_p of the reinforcement and to the contact compression F_p, i.e. altogether, to the moment $F_p(b - h) \simeq F_pb$. Then, increasing the rotation φ and lacking any phenomenon of instability, the bending moment decreases with a non-linear law (Fig. 11):

$$M = F_pb \cos\frac{\varphi}{2}. \tag{30}$$

On the other hand, if the fracture phenomenon is stable, function $M(\varphi)$ doesn't present any discontinuity and describes hardening behaviour (Fig. 10-e) analogous to that of Figure 6.

In Figure 10-a the case $N_p = 0$ is considered, i.e. the beam without reinforcement. The plastic flow moment M_p is naturally equal to zero, as well as the moment F_pb, which occurs immediately after the complete disconnection of concrete.

In figure 10-b the case $N_p = 0.1$ is described, i.e. a low reinforced beam. By the diagram of Figure 2 it is possible to obtain the ratio M_p/F_pb, while by the diagram of Figure 9 the ratio M_p/M_F. The slope of the hardening line doesn't vary with respect to the preceding case, since it depends only on the crack length, besides the concrete elastic modulus and the cross-section sizes (Fig. 5).

In Figure 10-c the case $N_p = 0.3$ is considered, which is analogous to the previous one, except for the fact that the ratio M_p/M_F is higher. On the other hand the ratio M_p/F_pb, which is independent of N_p (Fig. 2), remains unchanged.

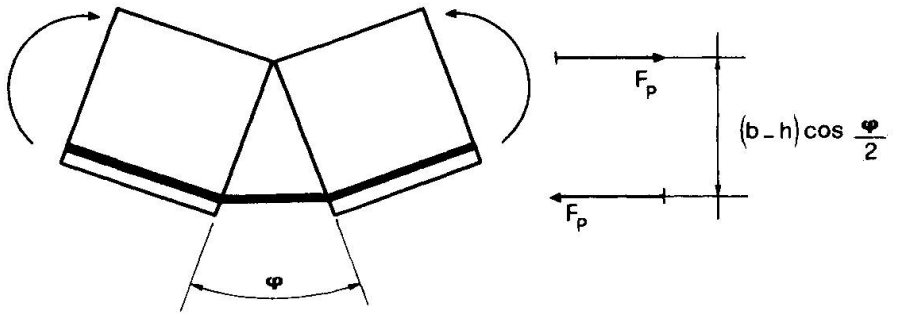

Fig. 11 Statical scheme after the complete disconnection of concrete.

In Figure 10-d the case $N_p = 0.7$ is reported. For this value it is $M_F = F_p b$, and then the discontinuity vanishes.

Finally in Figure 10-e the case $N_p = 3$ is described. In this case the fracture moment M_F is only slightly higher than the plastic moment M_p, and the moment $F_p b$ would be obtainable only with a positive jump of the function. On the other hand, from Figure 7 it is known that the fracturing process, for $N_p = 3$ and $\xi \geqslant 0.14$, is stable, and thus a complete and instantaneous disconnection of concrete can not occur (Fig. 11).

It is observed that, as for $N_p \leqslant 0.7$ it is $F_p b \leqslant M_F$, and then a discontinuity appears in the diagram $M(\varphi)$ (Figs. 10-a, b, c, d), so for $N_p \leqslant 0.7$ the curves of Figure 7 lie completely in the unstable zone.

Therefore it is possible to conclude that, by increasing the steel percentage A_s/A, or, in the same way, by increasing the beam size b, the concrete fracturing process becomes stable. In the meantime, as has been shown in section 7, the fracture sensitivity of the system increases.

ACKNOWLEDGMENTS

The author gratefully acknowledges the research support of the Italian National Research Council (C.N.R.).

REFERENCES.

[1] "Raccomandazioni CEB/FIP per le strutture in cemento armato", Edizione italiana A.I.T.E.C.

[2] AVRAM, C., FILIMON, I., DEUTSCH, I., CLIPII, T.: "Crack control and crack widths in low reinforced concrete members", Corso di Perfezionamento per le Costruzioni in Cemento Armato "Fratelli Pesenti", Politecnico di Milano, 1979, pp. 295 - 319.

[3] CARPINTERI, A. : "Size effect in fracture toughness testing: a Dimensional Analysis approach", Proceedings International Conference on Analytical and Experimental Fracture Mechanics, Ed. G.C. Sih, Roma, 1980.

[4] CARPINTERI, A.: "Notch sensitivity in fracture testing of aggregative materials", Engineering Fracture Mechanics, to appear.

[5] CARPINTERI, A.: "Experimental determination of fracture toughness parameters K_{IC} and J_{IC} for aggregative materials", Proceedings 5th International Conference on Fracture, Cannes, 1981.

[6] CARPINTERI, A.: "Static and energetic fracture parameters for rocks and concretes", Materials and Structures (RILEM), to appear.

[7] OKAMURA, H., WATANABE, K., TAKANO, T.: "Applications of the compliance concept in Fracture Mechanics", ASTM STP 536, 1973, pp. 423 - 438.

[8] OKAMURA, H., WATANABE, K., TAKANO, T.: "Deformation and strength of cracked member under bending moment and axial force", Engineering Fracture Mechanics, 1975, Vol. 7, pp. 531-539.

[9] CARPINTERI, A., DI TOMMASO, A., VIOLA, E.: "Fatigue evolution of multicracked frame--structures", Proceedings International Conference on Analytical and Experimental Fracture Mechanics, Ed. G.C. Sih, Roma, 1980.

[10] CARPINTERI, A., DI TOMMASO, A., VIOLA, E.: "Sulla capacità portante limite di pareti lapidee lesionate", Atti del 5° Congresso AIMETA, Associazione Italiana Meccanica Teorica e Applicata, Palermo, 1980.

Material Modeling of Plain Concrete
Un modèle non-linéaire et tridimensionel pour le béton est proposé
Modellbildung für das Verhalten von Beton

EUGENE Y.-T. CHEN and WILLIAM C. SCHNOBRICH
Research Assistant Professor
Department of Civil Engineering,
University of Illinois at Urbana-Champaign
Illinois, USA

SUMMARY
A nonlinear three dimensional material model for plain concrete is proposed. This model consists of a plasticity-based constitutive relation for the quasiductile behavior of concrete; a principal-stress and a principal-strain-based criterion to monitor the initiation of cracks in tension dominated regions as well as cracking due to the poisson effect; a relative-strain-based concept to gauge the cross-crack stress and stiffness transfer; and a strain-based crushing criterion to indicate the local failure of concrete. Some numerical examples to test the proposed model are also included.

RÉSUMÉ
Ce modèle consiste en une relation constitutive pour le comportement quasiductile du béton qui est basée sur la théorie de la plasticité; à l'aide d'un critère exprimé en fonction des contraintes et dilatations principales on peut contrôler le début de la fissuration dûe à la traction ou aux effets de Poisson; un concept basé sur les dilatations relatives permet d'estimer le transfert de contraintes et de rigidité à travers les fissures tandis que la rupture locale du béton est déterminée en fonction d'un écrasement limite. On vérifie le modèle à l'aide de quelques exemples numériques.

ZUSAMMENFASSUNG
Für den Beton wird ein nichtlineares, dreidimensionales Materialmodell vorgeschlagen, welches auf der Plastizitätstheorie basiert. Mit diesem Stoffgesetz wird das quasiduktile Verhalten von Beton beschrieben; ein Hauptspannungs- und ein Hauptdehnungskriterium wird benützt, um den Rissbeginn in Zugzonen, als auch infolge des Poisson-Effekts zu erfassen; ein Konzept, welches auf Relativdehnungen beruht, erlaubt die Abschätzung der Spannungs- und Steifigkeitsübertragung durch Risse hindurch; und ein auf Stauchungen gegründetes Bruchkriterium beschreibt das örtliche Versagen des Betons. Anhand einiger numerischer Beispiele wird das vorgeschlagene Modell überprüft.

1. INTRODUCTION

Reinforced concrete is by far one of the most commonly used construction materials. This composite material demonstrates a highly nonlinear behavior caused by cracking, crushing, aggregate interlock, bond slip, dowel action, shrinkage and creep, etc. Because reinforced concrete involves so many nonlinear phenomena interacting with one another, the formulation of a "complete" analytical model is very difficult. Consequently, most of the research related to behavior of reinforced concrete structures has been of an experimental nature. Within the past several years there has emerged however an attempt to supplement the experimental effort with numerical analysis. Activity has grown quite rapidly in this endeavor and much progress has been reported [3, 4, 16, 17]. Among the various analytical tools available the computer based finite element method has been accepted as the most powerful one. However, even with the large scale general purpose computer programs accessible today, it is felt that the incompleteness of material models for reinforced concrete is still the biggest limiting factor to the current capacity of structural analysis. The focus of this paper is cast on the three dimensional nonlinear constitutive relations and failure criterion for plain concrete subjected to short term monotonic loading.

2. MATERIAL CHARACTERISTICS AND IDEALIZATION

Concrete exhibits an intrinsic brittleness (low tensile strength) through the formation of cracks. Microcracks exist even before any mechanical load is applied. Both the strength and stiffness of concrete are largely determined by the details of the microcracking process [7, 9]. Concrete, when subjected to multiaxial compression, will exhibit an increasing "pseudo-plastic" behavior as the hydrostatic pressure increases. This "pseudo-plastic" behavior phenomenologically resembles the plastic response experienced by ductile metals. The difference between the two types of materials is that in ductile metals plastic flow is caused by lattice dislocation due to material imperfection, while in concrete it is the result of microcracking.

Based on experimental observations, the general response of concrete can be classified into two stages. A "quasi-ductile" stage characterized by "pseudo-plastic" behavior, followed by a brittle failure herein referred to as "crushing". Microcracking plays an important role in the first stage. The growth and the later bridgement of microcracks into a continuous pattern directly leads to the final crushing of concrete. Depending on the loading, the length of the first, the quasi-ductile, stage will vary. With unreinforced concrete if the loading involves a dominant or significant tension the material is considered failed as soon as cracking occurs.

Because concrete resembles partly the ductile metal behavior and partly the brittle ceramic behavior, an elastic plastic fracture material idealization is adopted in this study to delineate the observed (phenomelogical) time independent behavior of concrete.

3. MATHEMATICAL PRELIMINARIES

In general, the stress tensor defining the state of stress at a point can be depicted as a point in a nine dimensional Eculidean stress space. This stress tensor can be decomposed into two parts; the hydrostatic stress part, σ_m, and the deviatoric stress part, S_{ij}, as follows:

$$\sigma_{ij} = S_{ij} + \sigma_m \cdot \delta_{ij} \tag{1}$$

where $\sigma_m = \frac{1}{3}\sigma_{kk}$; and $S_{ij} = \sigma_{ij} - \sigma_m \cdot \delta_{ij}$ in which δ_{ij} is the Kronecker delta.

Because the stress tensor is real and symmetrical (in the absence of body and surface couples), a set of three orthogonal principal stress directions exist. These directions can be used as a reference frame to describe the same stress point in that space but now involving only three coordinates. A convenient alternative to this principal stress reference is the Haigh-Westergard coordinate system. The geometric representation of these two systems in three dimensional Euclidean stress space is given in Fig. 1 where

$$\xi = |\overline{ON}| = \frac{I_1}{\sqrt{3}}$$

$$\rho = |\overline{NP}| = \sqrt{2J_2}$$

$$\theta_1 = \frac{1}{3}\cos^{-1}(y), \quad 0 \leq \theta_1 \leq 60^o \tag{2}$$

$$\theta_2 = \frac{1}{3}\cos^{-1}(-y), \quad 0 \leq \theta_2 \leq 60^o$$

$$y = \frac{3\sqrt{3}}{2}\,\frac{J_3}{J_2^{3/2}}$$

$$I_1 = \sigma_{kk} = 3\sigma_m$$

$$J_2 = \frac{1}{2} S_{ij} \cdot S_{ij}$$

$$J_3 = \frac{1}{3} S_{ij} \cdot S_{jk} \cdot S_{ki}$$

In these equations is the projection of the stress tensor on the hydrostatic axis, $\underline{n} = 1/\sqrt{3}(1,1,1)$; ρ is the projection of the stress tensor on the deviatoric plane (π-plane); θ_1, and θ_2 are Lode angles (angles of similarity) with $\theta_1 + \theta_2 = 60^o$; I_1 is the first invariant of the stress tensor; and J_2, and J_3 are the second and third invariants of the deviatoric stress tensor. The sign convention used throughout this study is tension (+), compression (-).

4. PLASTICITY IN CONCRETE

In order to apply the traditional incremental theory of plasticity to concrete four things have to be defined apriori: (1) the ultimate strength condition which sets the upper bound of the attainable stresses; (2) the initial yield condition which marks the beginning of plastic flow; (3) the flow rule which relates the plastic strain increments to stress increments; (4) the hardening law which dictates the evaluation of the subsequent yield conditions. Geometrically, the initial and subsequent yield conditions can be represented as different surfaces in stress space analogous to the aforementioned ultimate strength condition (Fig. 2). The initial yield surface is a surface that can only be reached by elastic action. If the straining is continued beyond the current yield surface, a new subsequent yield surface will be developed resulting in some additional plastic flow (microcrack growth in concrete). Upon unloading then reloading, no irrecoverable deformation will occur until this new subsequent yield surface is reached.

Test results indicate that the maximum attainable stresses constitute a convex surface in stress space. The shape of this surface resembles that of a Mohr-Coulomb surface. In the principal stress space this ultimate strength surface follows closely that of a smooth six-fold symmetric conical shape with convexly curved meridians which do not intersect the negative hydrostatic axis. This six-fold symmetry supports the macroscopic isotropy assumption for concrete. Because of the symmetry only a 60^{o} spanned region bounded by the tensile meridian, ρ_t, and the compressive meridian, ρ_c, is essential in defining the ultimate strength surface. If $(\sigma_1, \sigma_2, \sigma_3)$ are principal stresses in descending order, then the tensile meridian, ρ_t, corresponds to the stress condition that $\sigma_1 > \sigma_2 = \sigma_3$; while the compressive meridian, ρ_c, corresponds to that of $\sigma_1 = \sigma_2 > \sigma_3$. Once these two bounding meridians are defined, intermediate meridians, ρ, which correspond to various stress combinations can be interpolated using the Lode angle.

Based on test results [2, 8, 14] and least square fitting [12], the tensile and compressive meridians can be expressed as functions of the hydrostatic parameter, ξ:

$$\frac{\rho_t}{f'_c} = -6.4899 + 2.9458\sqrt{5.0343 - \xi/|f'_c|}$$
$$\frac{\rho_c}{f'_c} = -3.6199 + 2.9458\sqrt{1.6907 - \xi/|f'_c|} \qquad (3)$$

in which f'_c is the uniaxial compressive strength of concrete (Fig. 3). Both the tensile and compressive meridians intersect the positive hydrostatic axis at $\xi/f'_c = -0.18064$. It means that concrete cracks under hydrostatic tension when $\xi/f'_c = -0.18064$.

By fitting hyperbolas to the corners of the Mohr-Coulomb type failure locus on the deviatoric plane (Fig. 4), the ultimate strength surface can be expressed as

$$f(\sigma_{ij}) = \sqrt{2J_2} - [(1-S^2\theta_1^2)\,\rho_1 + S^2\theta_1^2\,\rho_2] = 0 \qquad (4)$$

where

$$S = \frac{1}{60^o} \text{ (or } \frac{3}{\pi})$$

$$\rho_1 = \frac{(1+m) \cdot \rho_t \cdot \cos\theta_1 - \sqrt{(1+2m)\cdot\rho_t^2\cdot\sin^2\theta_1\cdot\cot^2\alpha + m^2\cdot\rho_t^2\cdot\cos^2\theta_1}}{\{\cos^2\theta_1 - \sin^2\theta_1 \cdot \cot^2\alpha\}}$$

$$\rho_2 = \frac{(1+m) \cdot \rho_c \cdot \cos\theta_2 - \sqrt{(1+2m)\cdot\rho_c^2\cdot\sin^2\theta_2\cdot\cot^2\beta + m^2\cdot\rho_c^2\cdot\cos^2\theta_2}}{\{\cos^2\theta_2 - \sin^2\theta_2 \cdot \cot^2\beta\}}$$

in which

$$R_\rho = \frac{\rho_t}{\rho_c}$$

$$\cot\alpha = \frac{2}{\sqrt{3}} (R_\rho - 0.5)$$

$$\cot\beta = \frac{2}{\sqrt{3}} (\frac{1}{R_\rho} - 0.5)$$

When applied to the biaxial case, the proposed ultimate strength criterion in Eq. 4 correlates well with the standard test results of Kupfer et al. [8] (Fig. 5).

It is convenient to assume that the initial and subsequent yield conditions have the same functional form as the ultimate strength criterion defined in Eq. 4

$$f(\sigma_{ij},\omega) = \sqrt{2J_2} - \omega[(1-S^2\theta_1^2)\ \rho_1 + S^2\theta_1^2\ \rho_2] = 0 \qquad (5)$$

where w is now added as the hardening parameter to monitor the change of the yield condition. For concrete the initial value for w, which corresponds to the initial yielding, varies in the range of 0.3 to 0.5. The ultimate value for w which corresponds to the ultimate strength is 1. The values in between the initial and the ultimate cases correspond to various intermediate yield conditions.

In this study it was found that with the selected surface an associated flow rule (Fig. 6) does not hold for the whole spectrum of the response of concrete. An equivalent nonassociated flow rule is thus gradually mobilized as the stress level increases. The equivalent nonassociated flow rule is proposed through the use of a piecewise continuous yield surface together with its associated flow rule (Fig. 7). By properly adjusting the angle as yielding progresses, in other words tuning the inclination of each infinitesimal piece on the yield surface, an overstiffening effect can be assuaged while maintaining symmetry in the elastic-plastic constitutive relations. The modified ϕ angle designated by ϕ^* is defined as

$$\phi^* = \phi \cdot [(1-S^2\theta_1^2) + (S^2\theta_1^2) \cdot \phi_\xi] \qquad (6)$$

in which

$$\phi = \tan^{-1}\left(\frac{\partial f}{\partial \xi}\right) \qquad \text{and} \qquad \phi_\xi = \phi_w \cdot \left[1 - \frac{1}{1 + \frac{1}{\sigma_h}}\right]$$

with

$$\sigma_h = \frac{\xi}{f'_c} + 0.18064$$

and

$$\phi_w = 1, \text{ when } 0 \leq w \leq w_c$$

$$= 1 - \frac{w - w_c}{1 - w_c}, \text{ when } w_c \leq w \leq 1$$

where w_c is the hardening parameter at which an overstiffening effect becomes significant. Generally this corresponds to the onset of mortar cracking at $w_c = 0.7$ to 0.8.

Based on the modified ϕ angle, the outward normals of the hypothesized piecewise continuous yield surface can be written as

$$a_{ij} = (\tan \phi^*) \cdot \left(\frac{d\xi}{d\sigma_{ij}}\right) + \frac{\partial f}{\partial J_2} \cdot \left(\frac{dJ_2}{d\sigma_{ij}}\right) + \frac{\partial f}{\partial J_3} \cdot \left(\frac{dJ_3}{d\sigma_{ij}}\right) \tag{7}$$

Because this paper is concerned only with short-term monotonic loading, an isotropic hardening law is used.

If we assume elastic unloading behavior of concrete together with the associated flow rule and the consistency condition (neglecting the viscosity effect) [10], the incremental elastic plastic constitutive relation can be expressed as

$$d\sigma_{ij} = \left[D_{ijkl} - \frac{D_{ijmn} \cdot a_{mn} \cdot a_{rs} \cdot D_{rskl}}{Y + a_{mn} \cdot D_{mnrs} \cdot a_{rs}}\right] \cdot d\varepsilon_{kl}$$

$$= D^{ep}_{ijkl} \cdot d\varepsilon_{kl} \tag{8}$$

where D_{ijkl}, D_{ijmn}, D_{rskl}, D_{mnrs} are elastic constitutive coefficients; D^{ep}_{ijkl} are elastic-plastic constitutive coefficients; a_{mn}, a_{rs} are the outward normals to the yield surface; and $Y = -\frac{\partial f}{\partial \omega}\frac{d\omega}{d\lambda}$ with $d\lambda$ the instantaneous constant of proportionality used in the flow rule.

5. CRACK MODELING IN CONCRETE

In this study the smeared crack approach is adopted. The advantage of using this approach lies in the fact that it avoids the constant changing of structure topology. The smeared crack representation, which corresponds to an averaging (smoothing) procedure of local discontinuities, allows an equivalent continuum treatment with localized material anisotropy. It simplifies the solution algorithms substantially. Also, it fits well into the approximate nature of the finite element method with C_o-continuity of displacement and bounded nonsingular strain and stress fields. However, it should be noted

that the smeared crack representation tends to diffuse the cracking system. Consequently, no single crack can dominate the behavior.

Experimental observation from different sources all indicate that maximum tensile deformation measured by the maximum tensile strain component is a dominant parameter in predicting brittle fracture of concrete [1]. The Poisson effect may cause some inconsistency when this so called "principal strain criterion" is subjected to multiaxial stress conditions [13]. Nevertheless, the simplicity of this criterion and the fact that it is used only for crack initiation in completely intact concrete make its use feasible. Consequently, it is assumed that the plane of cracking in concrete is normal to the direction of maximum tensile strain component.

Because an orthogonal set of opening cracks is enforced in this study, the direction for any subsequent crack formed in the uncracked subspace following an initial crack is thus fixed. A stress-based new crack initiation criterion is used. This stress-based criterion is very similar to the commonly used "principal stress criterion", except that the direction of this potential crack is pre-defined.

6. RELATIVE STRAIN ACROSS THE CRACK

In the framework of continuum mechanics, a crack may be looked upon as a separation of two neighboring material particles. Upon cracking certain components of displacements will become discontinuous, which implies "relative movement" between the two sides of the crack surface. Because displacements and strains are related through kinematic equations, it is conceivable within a continuum treatment to assume that a set of relative strains exist which represents the relative movement across the crack. As a matter of fact, these "relative strain" quantities are what have been measured across a crack in the experiments through the use of mechanical strain gauges.

In the equivalent continuum treatment of cracked concrete (smeared crack approach), the "relative strain" can be defined as the elastic portion of the corresponding total strain. Before cracking occurs a complete bonding exists between two neighboring particles. It is this bonding that allows them to deform or to be strained together. Once cracking starts, a separation which implies relative movements between these two neighboring particles will occur. These relative movements can be interpreted as a relaxation of the deformation (straining) of one particle with respect to the other. Since the plastic portion of deformation (straining) is nonrecoverable, it is logical to assume that the elastic portion must account for the relaxation and hence the corresponding relative movements. This "relative strain" is more a mathematical than physical parameter. It is used to gauge the local cross-crack stress and stiffness transfer [5].

7. CROSS-CRACK CONSTITUTIVE RELATIONS

Let n, s and t be a set of righthanded orthogonal coordinate directions with n normal and s, t tangential to the cracked surface.

The 3-D cross-crack constitutive relations in terms of stress and relative strain components across the crack, can be described in a matrix form as follows

$$\begin{Bmatrix} \sigma_n \\ \sigma_s \\ \sigma_t \end{Bmatrix} = \begin{bmatrix} k_{nn} & k_{ns} & k_{nt} \\ k_{sn} & k_{ss} & k_{st} \\ k_{tn} & k_{ts} & k_{tt} \end{bmatrix} \begin{Bmatrix} \tilde{\varepsilon}_n \\ \tilde{\varepsilon}_s \\ \tilde{\varepsilon}_t \end{Bmatrix} \tag{9}$$

in which K_{nn} is the cross-crack normal stiffness coefficient; K_{ss}, K_{tt} are the cross-crack shear stiffness coefficients; K_{sn}, K_{tn} are the cross-crack coupled shear stiffness coefficients; K_{ns}, K_{nt} are the cross-crack dilatant-contractant stiffness coefficients; and K_{st}, K_{ts} are the cross-crack cross-shear stiffness coefficients.

Upon replacing the stress and relative strain components in Eq. 9 by the corresponding stress and relative strain increments a set of incremental cross-crack constitutive relations are thus obtained. The assumption in doing so is that the interface stiffness coefficients are path independent in the sense that they are functions only of the current total stresses and the accumulated relative strains.

The stiffness coefficients in Eq. 9 are generally unsymmetrical. Because a symmetric matrix is always desirable from a programming point of view, Eq. 9 is modified so that a symmetric constitutive matrix is achieved as shown in Eq. 10.

$$\begin{Bmatrix} \Delta\sigma_n \\ \Delta\sigma_s \\ \Delta\sigma_t \end{Bmatrix} = \begin{bmatrix} k_{nn} & \frac{1}{2}(k_{ns}+k_{sn}) & \frac{1}{2}(k_{nt}+k_{tn}) \\ \frac{1}{2}(k_{ns}+k_{sn}) & k_{ss} & \frac{1}{2}(k_{st}+k_{ts}) \\ \frac{1}{2}(k_{nt}+k_{tn}) & \frac{1}{2}(k_{st}+k_{ts}) & k_{tt} \end{bmatrix} \begin{Bmatrix} \Delta\tilde{\varepsilon} \\ \Delta\tilde{\varepsilon} \\ \Delta\tilde{\varepsilon} \end{Bmatrix} \tag{10}$$

In the following section, the cross-crack constitutive relations defined here are referred to as the "CSST Model."

8. POST-CRACKING MODEL FOR CONCRETE

Once cracking occurs, the material coordinate system is locally fixed due to the crack introduced anisotropy. Cracks in orthogonal directions can occur simultaneously or subsequently whenever the crack initiation criterion is met in an intact subspace of concrete. This allows concrete to have multi-directional cracking. Upon cracking, Eq. 8 written in the current

principal strain directions (material coordinate directions) needs to be modified to account for the existence of cracks and to simulate the post-cracking behavior of concrete. For this purpose, the CSST model is used, while the constitutive relations for the intact concrete are still enforced in the unracked subspace of concrete.

In this study a gradual stress releasing is implemented through the gradual activation of the CSST model after cracking occurs. This is done by using stress-level-dependent activating factors for the CSST stiffness coefficients when averaging them with those coefficients in Eq. 8 to obtain the final elastic-plastic-fracture stiffness. Letting the numbers 1, 2, 3 represent the current material coordinate directions, the fracture constitutive relations can be written as follows

$$\begin{Bmatrix} \sigma_{11} \\ \sigma_{12} \\ \sigma_{13} \\ \sigma_{21} \\ \sigma_{22} \\ \sigma_{23} \\ \sigma_{31} \\ \sigma_{32} \\ \sigma_{33} \end{Bmatrix} = \begin{bmatrix} W_1 \cdot (^{CSST}_{Model}) & 0 & 0 \\ 0 & W_2 \cdot (^{CSST}_{Model}) & 0 \\ 0 & 0 & W_3 \cdot (^{CSST}_{Model}) \end{bmatrix} \begin{Bmatrix} \tilde{\varepsilon}_{11} \\ \tilde{\varepsilon}_{12} \\ \tilde{\varepsilon}_{13} \\ \tilde{\varepsilon}_{21} \\ \tilde{\varepsilon}_{22} \\ \tilde{\varepsilon}_{23} \\ \tilde{\varepsilon}_{31} \\ \varepsilon_{32} \\ \varepsilon_{33} \end{Bmatrix} \qquad (11)$$

The activating factors, W_i, i=1,2,3, are defined as follows: $W_i = 0$ if there is no active crack normal to the i^{th} direction; otherwise

$$W_i = \frac{1}{(1-\omega)^n} \qquad (12)$$

where w is the current hardening parameter; and n is a curve fitting parameter. Multiplying the stiffness coefficients in the CSST model with a factor of $(\tilde{\varepsilon}_{ij} / \varepsilon_{ij})$ where $\tilde{\varepsilon}_{ij}$ and ε_{ij} are accumulated relative strains and total strains respectively. Equation 11 can be written in tensor notation as

$$\sigma_{ij} = W \cdot D^f_{ijkl} \cdot \varepsilon_{kl} \qquad (13)$$

From Eq. 13 the "path independent" incremental fracture constitutive relations can be written as

$$\Delta\sigma_{ij} = W \cdot D^f_{ijkl} \cdot \Delta\varepsilon_{kl} \qquad (14)$$

Combining Eqs. 8 and 14 under the current local material coordinate system, we

get

$$\Delta\sigma_{ij} = \frac{1}{1+W} \cdot [D^{ep}_{ijkl} + W \cdot D^{f}_{ijkl}] \cdot \Delta\varepsilon_{kl} = D^{epf}_{ijkl} \cdot \Delta\varepsilon_{kl} \tag{15}$$

where D^{epf}_{ijkl} are the current elastic-plastic-fracture stiffness coefficients.

In general the D^{epf}_{ijkl} are not symmetric, because the fracture destroys the continuity originally existing in the intact material. However, in this study an equivalent continuum mechanics approach is used which approximates the fracture effect by changing the material properties. Hence it is proposed to symmetrize the elastic-plastic-fracture stiffness coefficients by letting

$$D^{epf}_{ijkl} = D^{epf}_{jikl} = D^{epf}_{ijlk} = D^{epf}_{klij} = (D^{epf}_{ijkl} + D^{epf}_{jikl} + D^{epf}_{ijlk} + D^{epf}_{klij})/4 \tag{16}$$

In order to be consistent with other parts of the structure, D^{epf}_{ijkl} have to be transformed from their local material coordinate system into the predetermined structural coordinate system.

9. STRAIN-BASED FAILURE CRITERION

The failure criterion prescribes the stress and/or strain condition at which the concrete loses all of its stiffness as well as load carrying capacity. In this study a strain-based failure criterion is adopted. Concrete is considered crushed when

$$\frac{\varepsilon_{eq.}}{\varepsilon_0} \geq R_\varepsilon \tag{17}$$

in which $\varepsilon_{eq.}$ is the equivalent uniaxial strain defined in Eq. 18; ε_o is defined in Eq. 22; and R_ε is defined in Eq. 21 (Fig. 8).

10. EQUIVALENT UNIAXIAL STRESS AND STRAIN

In order to evaluate the parameter Y in Eq. 8 as plastification occurs, the plastic hardening modulus, H, has to be calibrated apriori. A commonly used approach in calculating H is to deduce from the multidimensional condition a pair of quantities, the equivalent uniaxial stress, $\sigma_{eq.}$, and the strain $\varepsilon_{eq.}$. By doing so the well documented uniaxial test results can be generalized and extrapolated. In this study it was found that concrete behavior is very sensitive to the use of an equivalent uniaxial strain once cracks have occurred. This is because the fracture introduced softening effect damages the consistency and integrity of the equivalent uniaxial stress-strain approach used in the plasticity theory. With this drawback in mind, the following definition for the equivalent uniaxial strain is used in this study. It is made up of an elastic part, $\varepsilon^e_{eq.}$, and a plastic part, $\varepsilon^p_{eq.}$.

$$\varepsilon_{eq.} = \varepsilon^e_{eq.} + \varepsilon^p_{eq.} = \frac{\omega . |f'_c|}{E} + \varepsilon^p_{eq.} \tag{18}$$

where w is the current hardening parameter defined as $w = \sigma_{eq.} / |\sigma_o|$; f'_c and

E are the uniaxial compressive strength and the initial modulus of elasticity respectively; and $\varepsilon^{p}_{eq.}$ is the accumulated equivalent uniaxial plastic strain defined in Eq. 23.

In this study the generalized uniaxial compressive stress-strain relationship of Saenz is used [15], Fig. 8.

$$\sigma_{eq.} = \frac{E \cdot \varepsilon_{eq.}}{1 + (R+R_E-2)\left(\frac{\varepsilon_{eq.}}{\varepsilon_0}\right) - (2R-1)\left(\frac{\varepsilon_{eq.}}{\varepsilon_0}\right)^2 + R\left(\frac{\varepsilon_{eq.}}{\varepsilon_0}\right)^3} \tag{19}$$

The equivalent uniaxial tangent modulus is

$$E_t = \frac{d\sigma_{eq.}}{d\varepsilon_{eq.}} = \frac{E \cdot \left[1+(2R-1)\left(\frac{\varepsilon_{eq.}}{\varepsilon_0}\right)^2 - 2R\left(\frac{\varepsilon_{eq.}}{\varepsilon_0}\right)^3\right]}{\left[1+(R+R_E-2)\left(\frac{\varepsilon_{eq.}}{\varepsilon_0}\right) - (2R-1)\left(\frac{\varepsilon_{eq.}}{\varepsilon_0}\right)^2 + R\left(\frac{\varepsilon_{eq.}}{\varepsilon_0}\right)^3\right]^2} \tag{20}$$

in which σ_o and ε_o are the peak strength and corresponding strain under the current stress combination, and ε_f and σ_f are the maximum strain and corresponding stress under the current stress combination. The remaining terms in Eqs. 19 and 20 are defined by the following equations:

$$\begin{aligned} E_S &= \frac{\sigma_0}{\varepsilon_0} \\ R_E &= \frac{E}{E_S} \\ R_\sigma &= \frac{\sigma_0}{\sigma_f} \\ R_\varepsilon &= \frac{\varepsilon_f}{\varepsilon_0} \\ R &= \frac{R_E(R_\sigma-1)}{(R_\varepsilon-1)^2} - \frac{1}{R_\varepsilon} \end{aligned} \tag{21}$$

In order to find σ_o, ε_o, σ_f and ε_f under the current stress combination, the following algorithm is used.

1) Extend a line from the origin in the stress space through the current stress point until it penetrates the ultimate strength surface. Then calculate its length.

2) Find the ratio, r, between the length just calculated and the length corresponding to the uniaxial compression case.

3) $\sigma_0 = r \cdot f'_c$

4) $\varepsilon_0 = \varepsilon_c \cdot [r \cdot T-(T-1)]$, if $r \geq 1$;

$\varepsilon_0 = \varepsilon_c \cdot [-1.6\, r^3 + 2.25 r^2 + 0.35 r]$, if $r < 1$ (22)

where T is taken to be three in this study; and ε_c is the measured uniaxial compressive strain at f_c.

5) $\sigma_f = \sigma_0 / R_\sigma$

6) $\varepsilon_f = R_\varepsilon \cdot \varepsilon_0$

Due to the lack of strain data the empirical formula proposed by Darwin and Pecknold is used to find ε_o. [Darwin, Pecknold, 1974]. Because it is impossible to define σ_f and ε_f on any rigorous experimental basis. it is assumed that $R_\sigma = 4$ and $R_\varepsilon = 4$ realizing that R_σ and R_ε do not have to be the same. Since σ_o and ε_o are calculated differently, the secant modulus, E_s, is not a constant value but a function of the current stress combination.

If the strain hardening hypothesis is used then $w = w(\varepsilon^P_{eq.})$, where $\varepsilon^P_{eq.}$ is the accumulated equivalent uniaxial plastic strain defined as

$$\varepsilon^P_{eq.} = \int d\varepsilon^P_{eq.} = \int m_p \cdot (d\varepsilon^P_{ij} \cdot d\varepsilon^P_{ij})^{1/2} = \int m_p \cdot d\lambda \cdot (a_{ij} \cdot a_{ij})^{1/2} \tag{23}$$

where $d\varepsilon^P_{ij}$ are the incremental plastic strain; and m_p is the equivalent uniaxial plastic strain scaling factor.

$$m_p = \frac{s_f}{\sqrt{s_f^2+2}} \tag{24}$$

in which

$$s_f = \frac{\sqrt{2}}{\tan(\theta+\phi^*)}$$

$$\theta = \cos^{-1}(\sqrt{2/3})$$

It is noted that for hydrostatic insensitive materials $\phi = \phi^* = 0$ and $m_p = \sqrt{2/3}$

If elastic unloading is assumed, then the plastic hardening modulus, H, can be related to the initial and tangent moduli as follows

$$H = \frac{d\sigma_{eq.}}{d\varepsilon^P_{eq.}} = \frac{E_t}{1-\frac{E_t}{E}} \tag{25}$$

From Eqs. 18, 23 and 25 the parameter Y in Eq. 8 can be determined as

$$Y = -\frac{\partial f}{\partial \omega} \cdot \frac{d\omega}{d\lambda} = -\frac{\partial f}{\partial \omega} \cdot \frac{H}{|\sigma_0|} \cdot m_p \cdot (a_{ij} \cdot a_{ij})^{1/2} \qquad (26)$$

11. NUMERICAL STUDY

The proposed constitutive relations are used to simulate the responses of concrete subjected to uniaxial, biaxial, and triaxial compressive loadings. The test and simulated results are shown in Figs. 9-17.

It was found during the study of triaxial loadings, that the phenomenon which is termed yielding in this study existed even under pure hydrostatic stress. This is due to the inelastic compaction of concrete. In order to obtain reasonable results therefore this presence of "yielding" under hydrostatic stress had to be considered. "Classical" plasticity theory, however, does not allow such nonlinear behavior when the material is in a pure hydrostatic stress state. This finding suggests then that a more general approach when using a plasticity theory for concrete in the future may be one that possesses two yield functions, one for volumetric and one for deviatoric response. These two analytical models should be able to interact with each other, so that the shear dilatation and compaction phenomena observed in experiments can be considered.

12. CONCLUSIONS

The smeared crack representation with material sampling points at the integration points proves to be reliable. This statement is valid if the sampling points are not too far away from each other. Consequently, local irregularities will not be overlooked due to the inherent averaging process. Based on this argument, reduced integration should be used with care. Depending on the real stress distribution, sometimes more integration points are needed simply to describe the crack pattern and hence to monitor the nonlinearized material properties with higher precision.

Having been verified on many occasions, the equivalent uniaxial stress-strain approach in a plasticity theory works well with ductile materials. As for concrete, this approach requires further tuning and generalization in order to better reflect the cracking effect.

The equivalent nonassociated flow rule, using a piecewise continuous yield surface to maintain a symmetrical elastic-plastic constitutive matrix, gives a better uniaxial compressive response of concrete than the associated flow rule would.

The "relative strain" parametrization in handling the cross-crack stress and stiffness transfers is a reasonable approach within the realm of continuum mechanics. Besides being a mathematical quantity the "relative strain" also has its practical implication in the mechanical strain gauge measurement across a crack.

REFERENCES

1. Atan, Y., and Slate, F.O., "Structural Lightweight Concrete Under Biaxial Compression," American Concrete Institute Journal, Proceedings, Vol. 70, No. 3, March, 1973, pp. 182-186.

2. Balmer, G.G., "Shearing Strength of Concrete Under High Triaxial Stress-Computation of Mohrs Envelope as a Curve," Structural Research Laboratory Report No. SP-23, U.S. Dept. of the Interior, Bureau of Reclamation, Washington, D.C., 1949.

3. Bazant, Z.P., Schnobrich, W.C., and Scordelis, A.C., Analisi Delle Strutture in Cemento Armato Mediante Il Metodo Degli Elementi Finiti, Carso di Perfezionamento per Le Costruzioni in Cemento Armato "Fratelli Pesenti," Politecnico Di Milano, Italy, 1978.

4. Bergan, P.G., and Holand, I., "Nonlinear Finite Element Analysis of Concrete Structures," International Conf. on Finite Elements in Nonlinear Mechanics, Stuttgart, Germany, (FRG), Aug.-Sept., 1978.

5. Chen, E.Y-T., and Schnobrich, W.C., "Models for the Post-Cracking Behavior of Plain Concrete under Short Term Monotonic Loading," Symposium on Computational Methods in Nonlinear Structural and Solid Mechanics, Oct. 6-8, 1980, Washington D.C.

6. Darwin, 6.D., and Pecknold, D.A.W., "Inelastic Model for Cyclic Biax Loading of Reinforced Concrete," Civil Engineering Studies, SRS No. 409, University of Illinois, Urbana, Illinois, July, 1974.

7. Hsu, 7.T.T.C., Slate, F.O., Sturman, G.M., and Winter, G., "Microcracking of Plain Concrete and the Shape of the Stress-Strain Curve," American Concrete Institute Journal, Proceedings, Vol. 60, No. 2, Feb., 1963, pp. 219-223.

8. Kupfer, H., Hilsdorf, H.K., and Rusch, H., "Behavior of Concrete Under Biaxial Stresses," American Concrete Institute Journal, Proceedings, Vol. 66, No. 8, Aug., 1966, pp. 656-666.

9. Mindess, S., and Diamond, S., "The Cracking and Fracture of Mortar," ASCE Fall Convention, Hollywood, Florida, Oct., 1980.

10. Nayak, G.C., and Zienkiewicz, O.C., "Elasto-Plastic Stress Analysis A Generalization for Various Constitutive Relations Including Strain Softening," International Journal for Numerical Methods in Engineering, Vol. 5, 1972, pp. 113-135.

11. Nelissen, L.J.M., "Biaxial Testing of Normal Concrete," Heron, the Netherlands, Vol. 18, No. 1, 1972.

12. Ottosen, N.S., "A Failure Criterion for Concrete," Journal of the Engineering Mechanics Division, ASCE, Vol. 103, No. EM4, Aug., 1977, pp. 527-535.

13. Pandit, G.S., discussion of "Structural Lightweight Concrete under Biaxial Compression," by Y. Atan and F.O. Slate, American Concrete Institute Journal, Proceedings, Vol. 70, No. 9, Sept., 1973, pp. 660-661.

14. Richart, F.E., Brandtzaeg, A., and Brown, R.L., "A Study of the Failure of Concrete under Combined Compressive Stresses," Bulletin No. 185, University of Illinois, Engineering

15. Saenz, I.P., discussion of "Equation for the Stress-Strain Curve of Concrete," by P. Desayi and S. Krishnan, American Concrete Institute Journal, Proceeding, Vol. 61, No. 9, Sept., 1964, pp. 1229-1235.

16. Schnobrich, W.C., "Behavior of Reinforced Concrete Structures, Predicted by the Finite Element Method," Computers and Structures, Vol. 7, 1977, pp. 365-376.

17. Scordelis, A.C., "General Report-Basic Problems," IASS Symposium on Nonlinear Behavior of Reinforced Concrete Structures, Darmstadt, Germany (FRG), July, 1978.

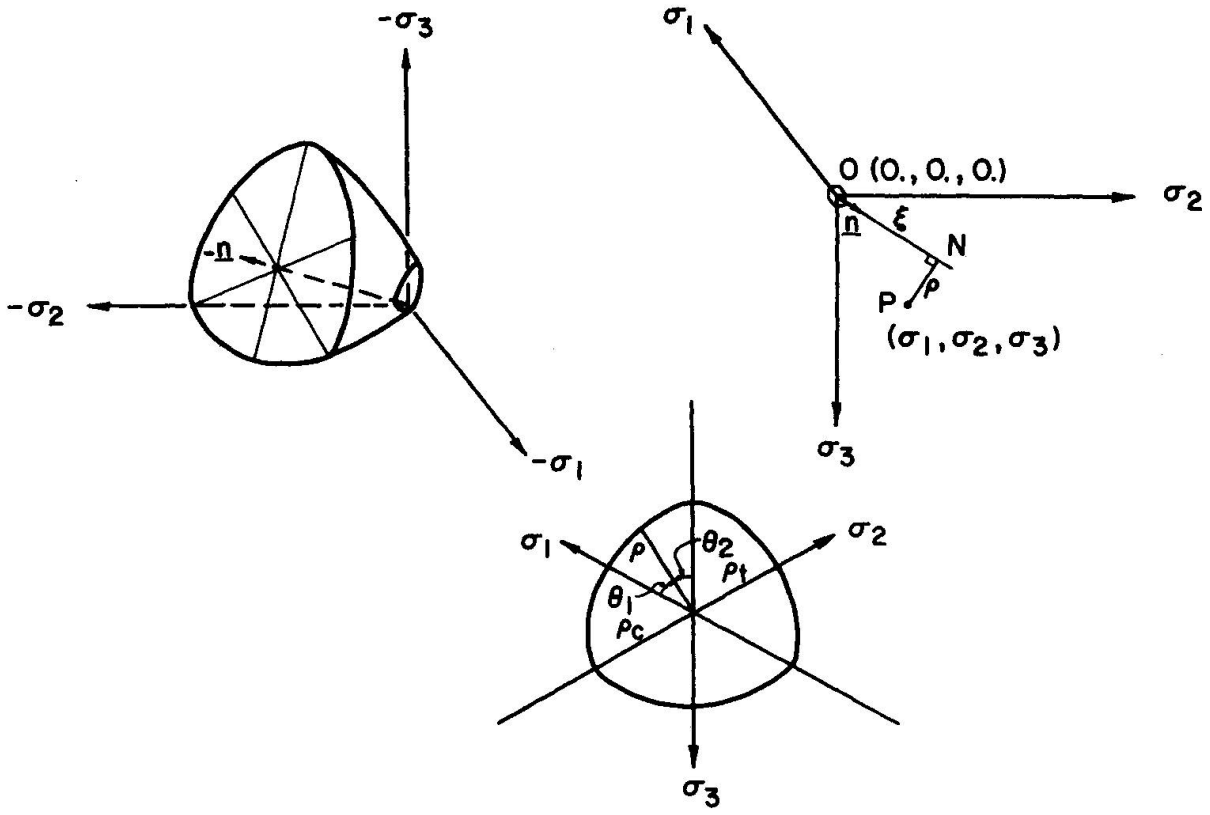

Fig. 1 Haigh-Westergard Coordinate System

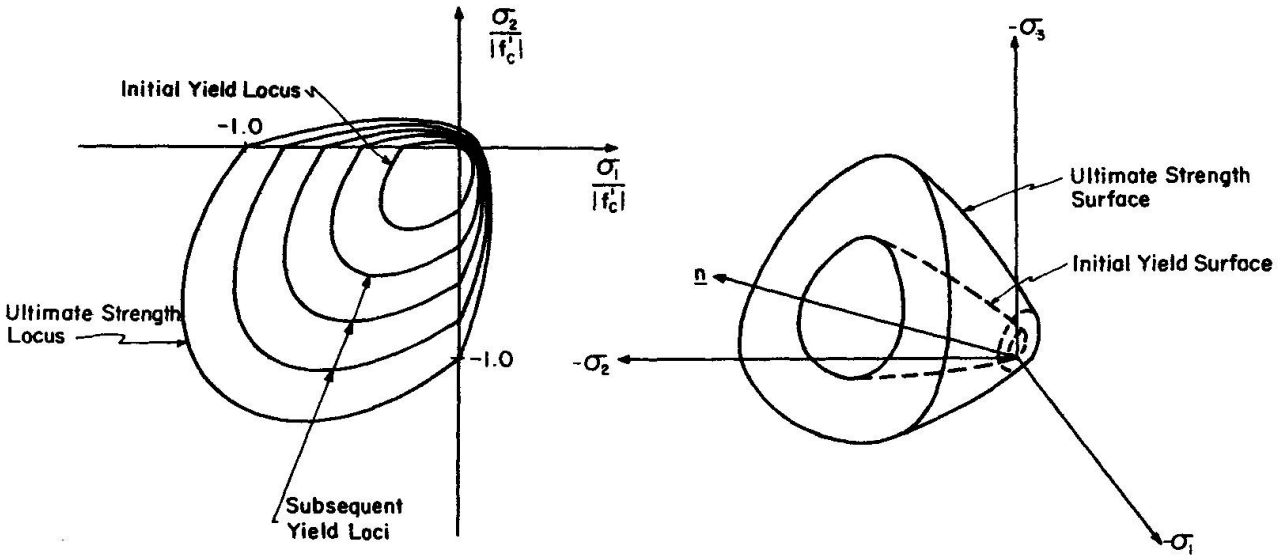

Fig. 2 Yield and Ultimate Strength Surfaces

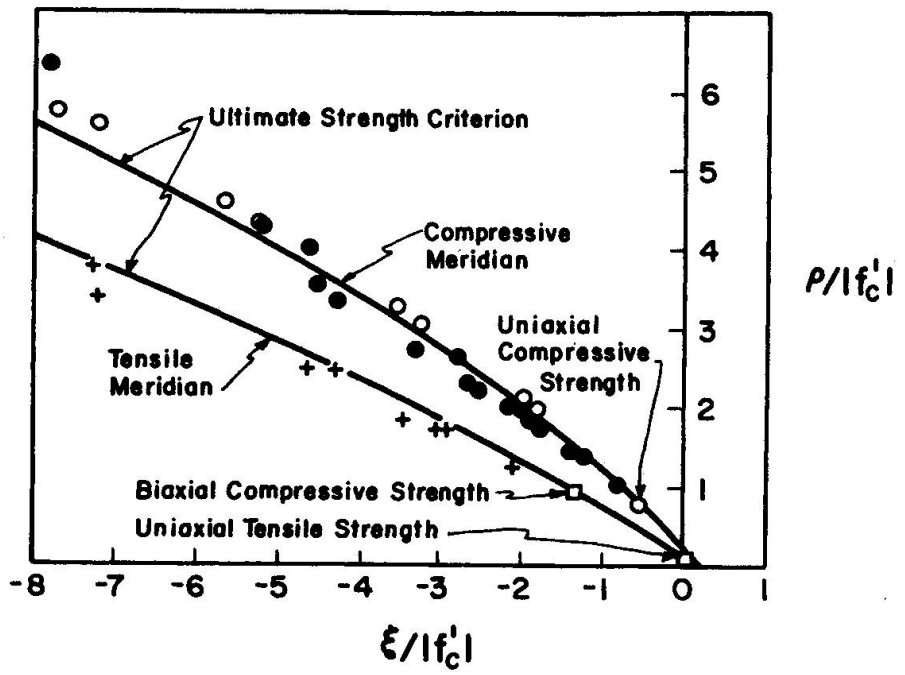

Fig. 3 Tensile and Compressive Meridians

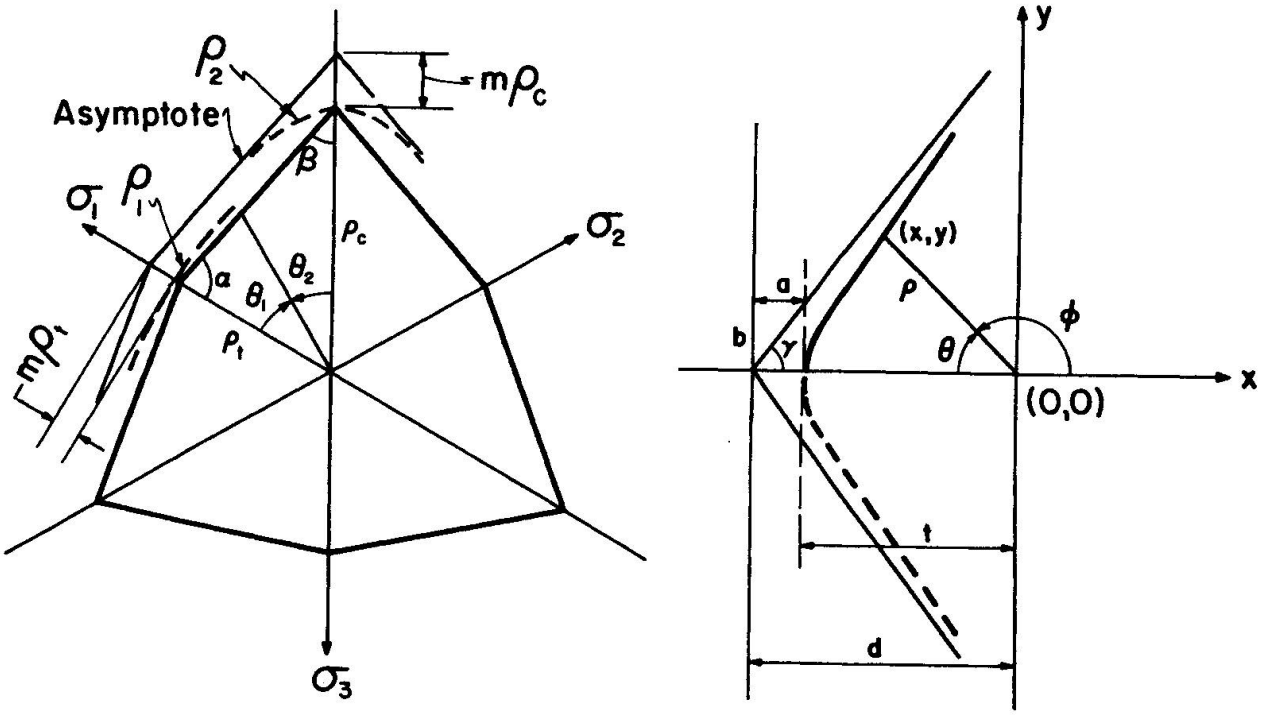

Fig. 4 Hyperbola Fitting

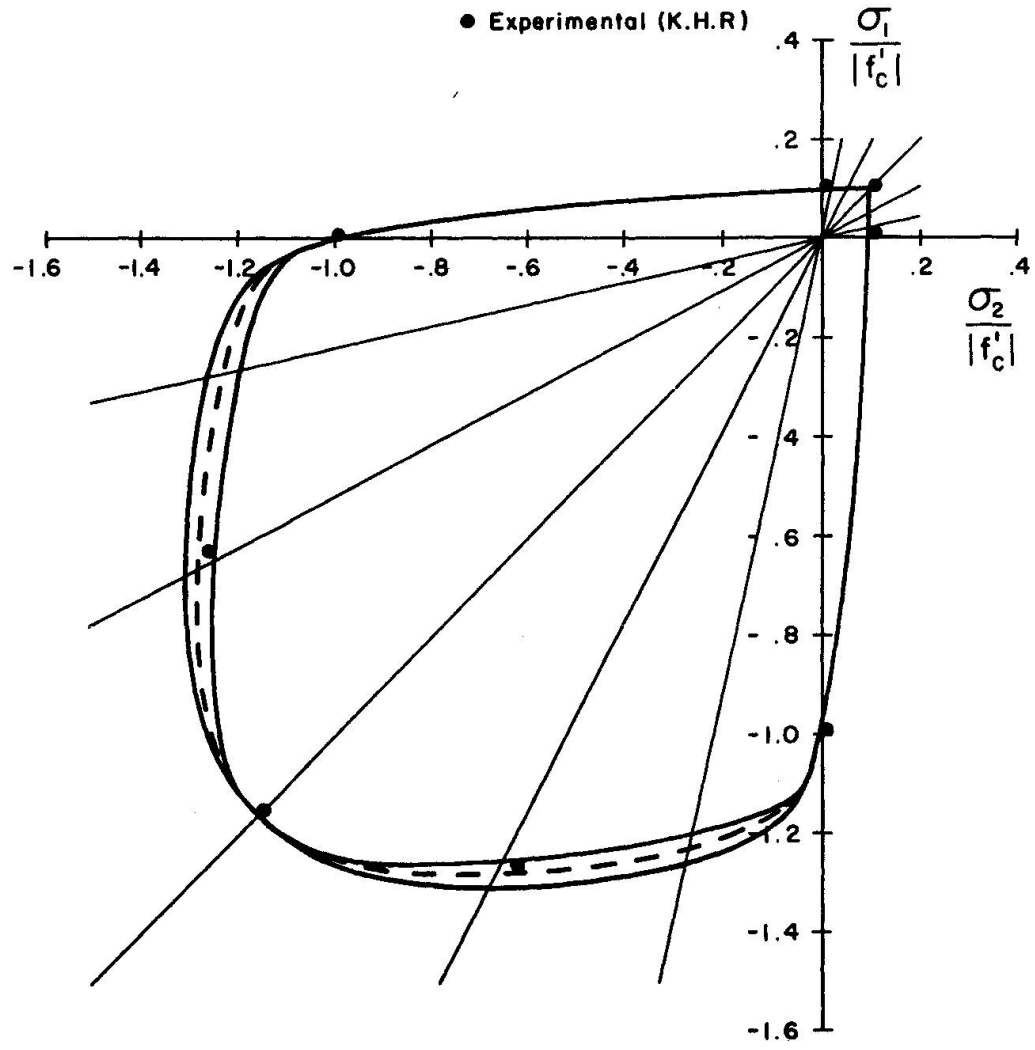

Fig. 5 Biaxial Tests of Kupfer et al

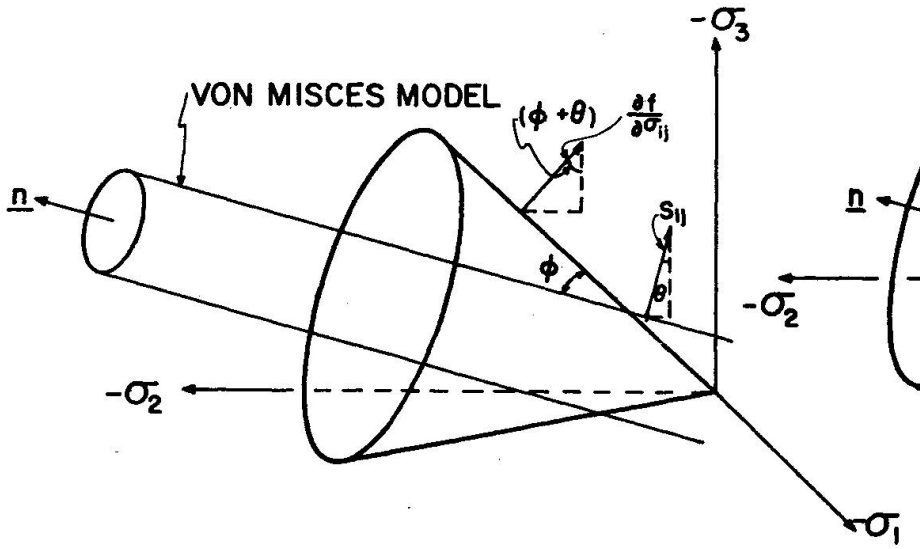

Fig. 6 Normals to the Yield Surfaces

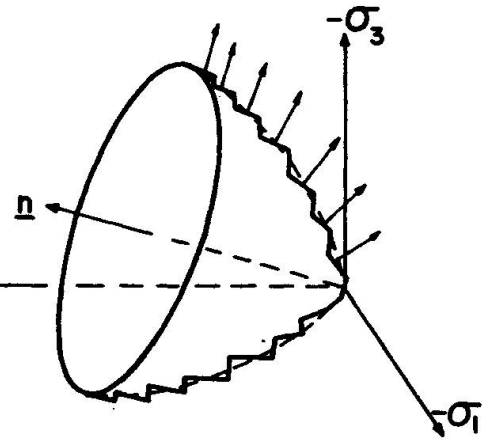

Fig. 7 Piecewise Continuous Yield Surface

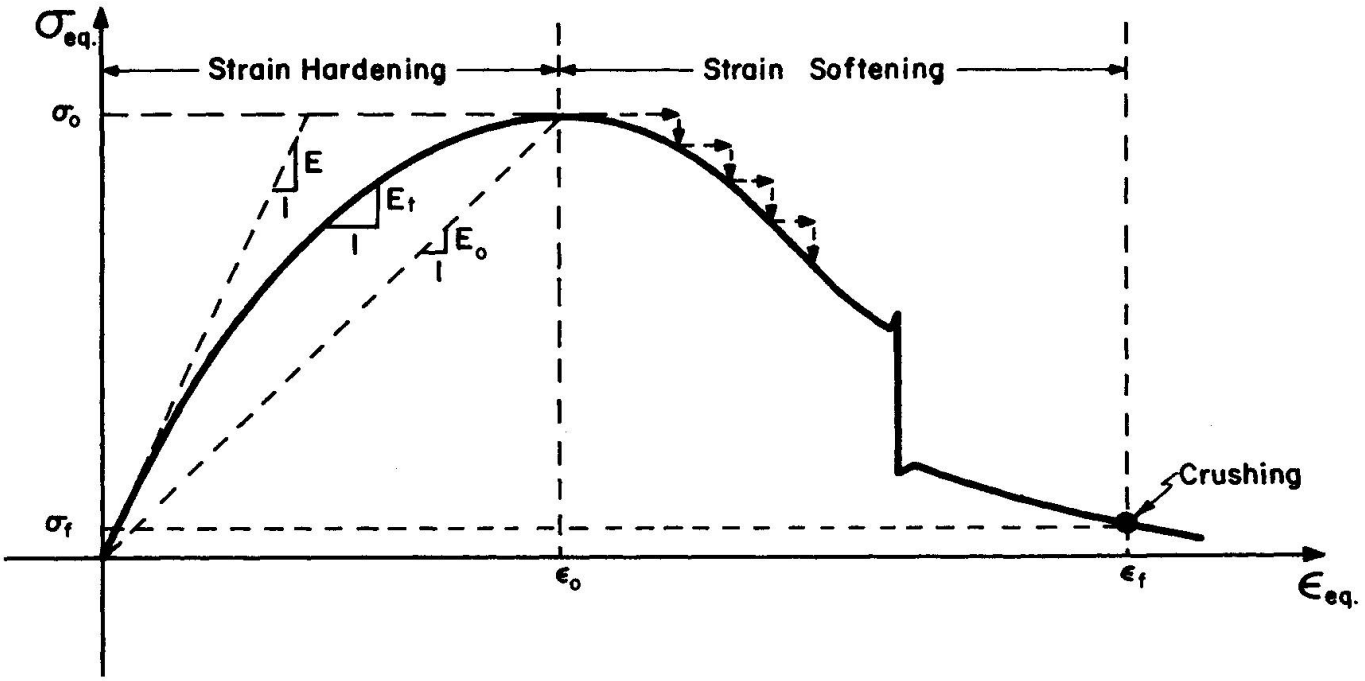

Fig. 8 Uniaxial Stress-Strain Curve of Concrete

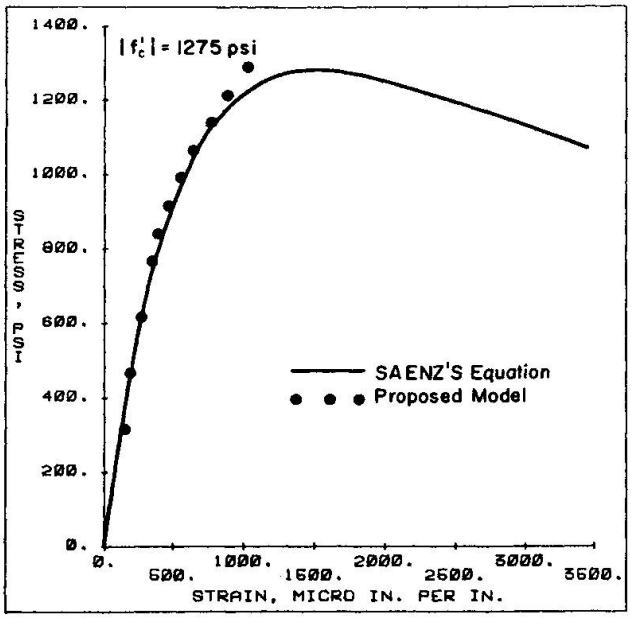

Fig. 9 Uniaxial Compression of Plain Concrete, $|f'_c|$ = 1275 psi

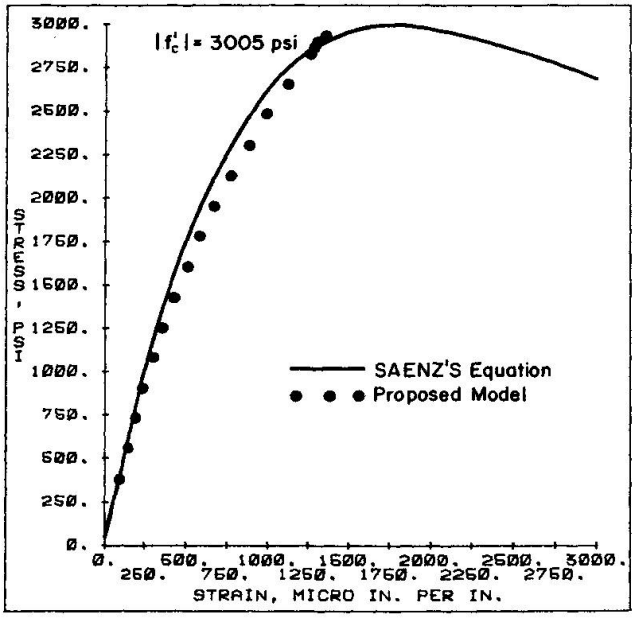

Fig. 10 Uniaxial Compression of Plain Concrete, $|f'_c|$ = 3005 psi

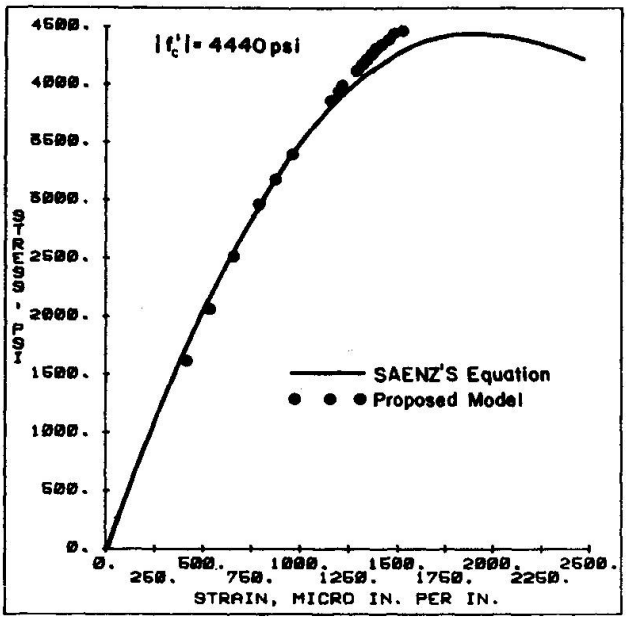

Fig. 11 Uniaxial Compression of Plain Concrete, $|f'_c| = 4440$ psi

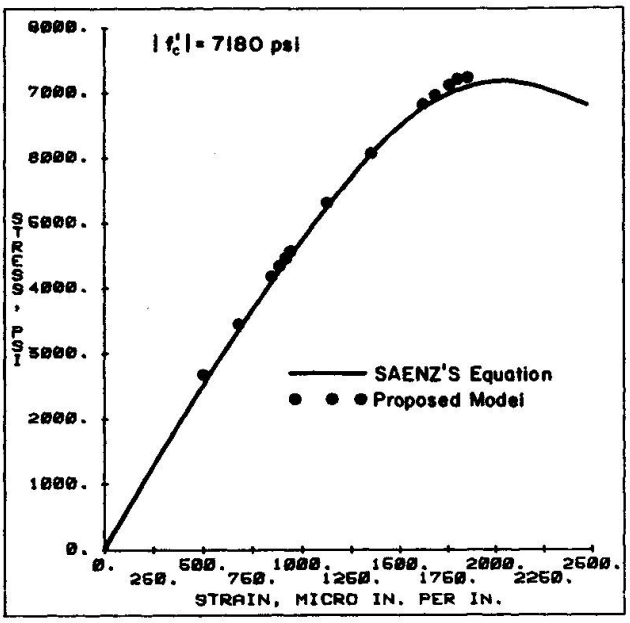

Fig. 12 Uniaxial Compression of Plain Concrete, $|f'_c| = 7180$ psi

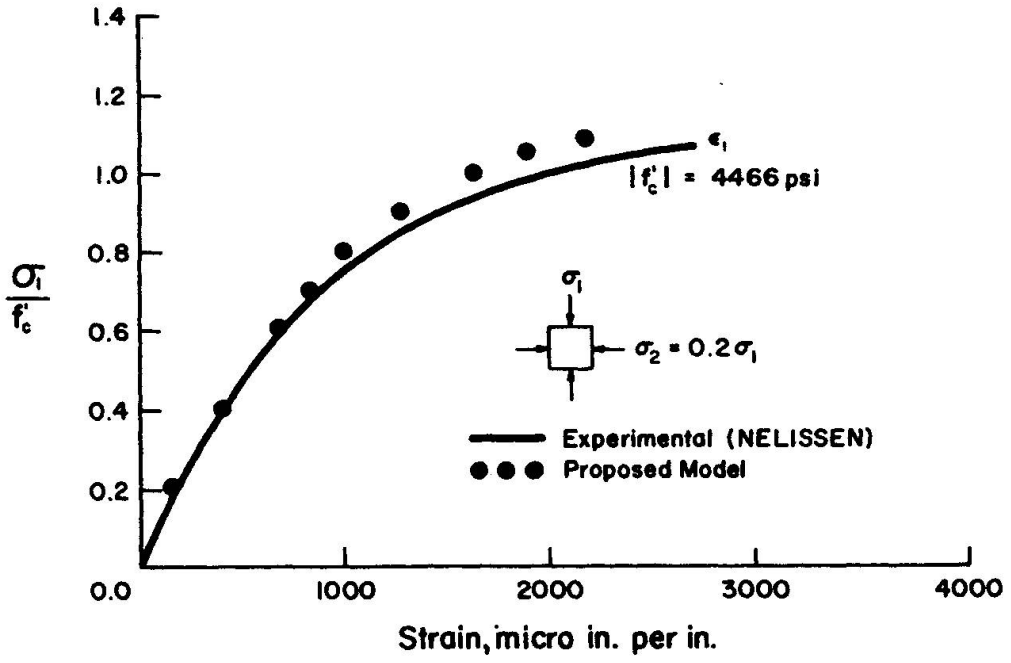

Fig. 13 Biaxial Compression of Plain Concrete, $\sigma_2 = 0.2\sigma_1$

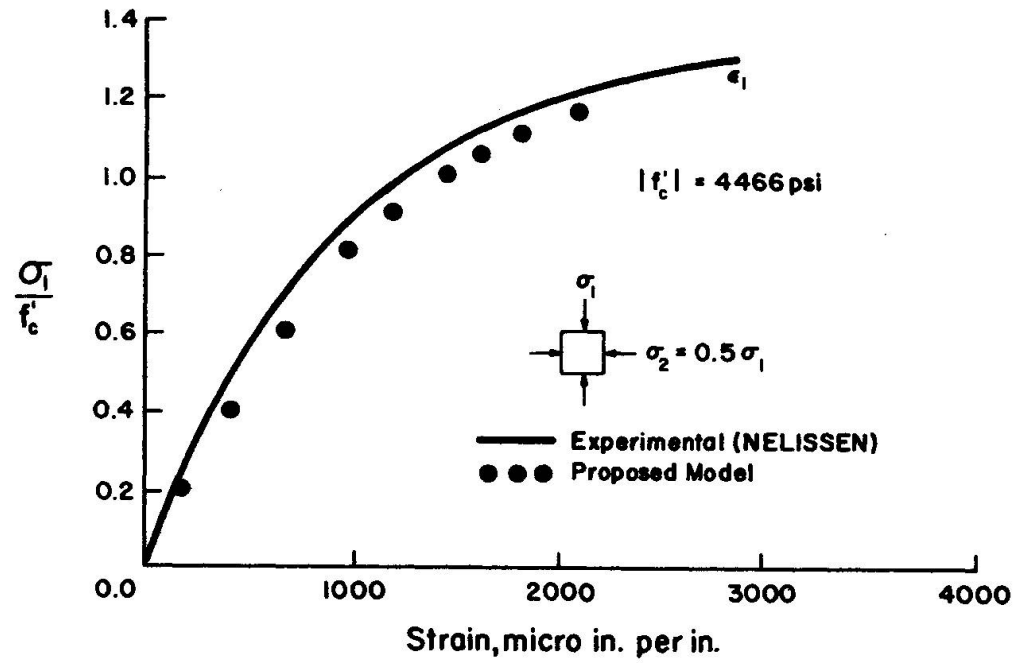

Fig. 14 Biaxial Compression of Plain Concrete, $\sigma_2 = 0.5\sigma_1$

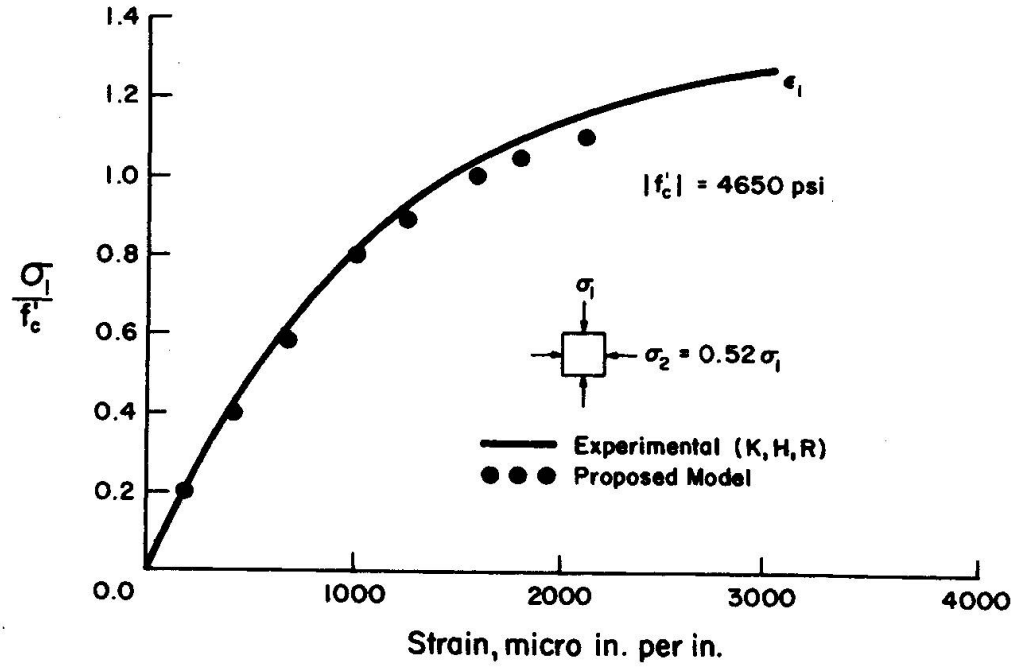

Fig. 15 Biaxial Compression of Plain Concrete, $\sigma_2 = 0.52\sigma_1$

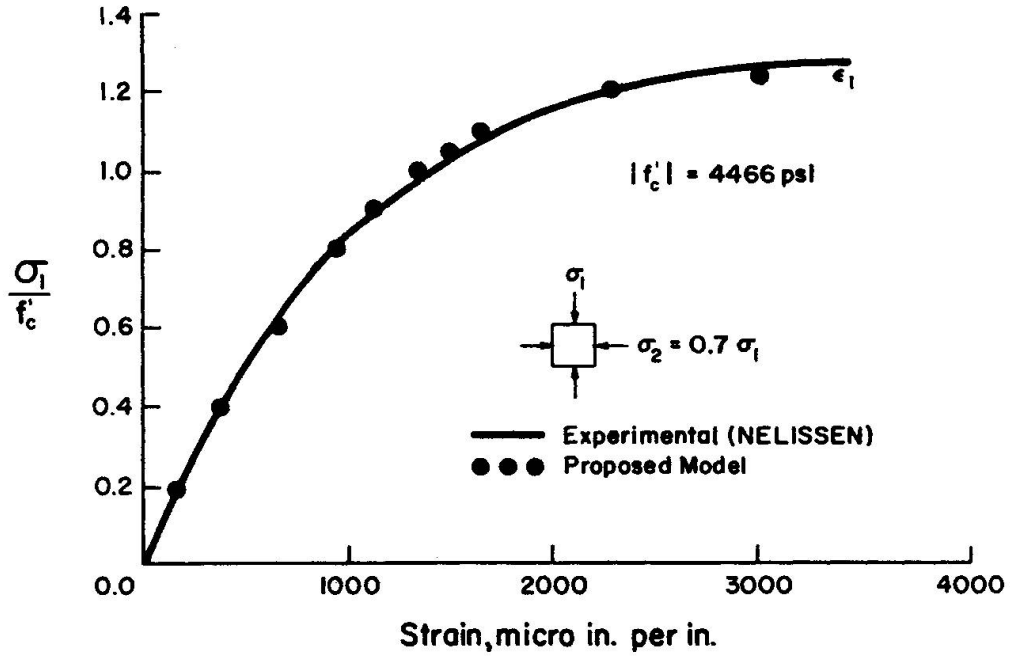

Fig. 16 Biaxial Compression of Plain Concrete, $\sigma_2 = 0.7\sigma_1$

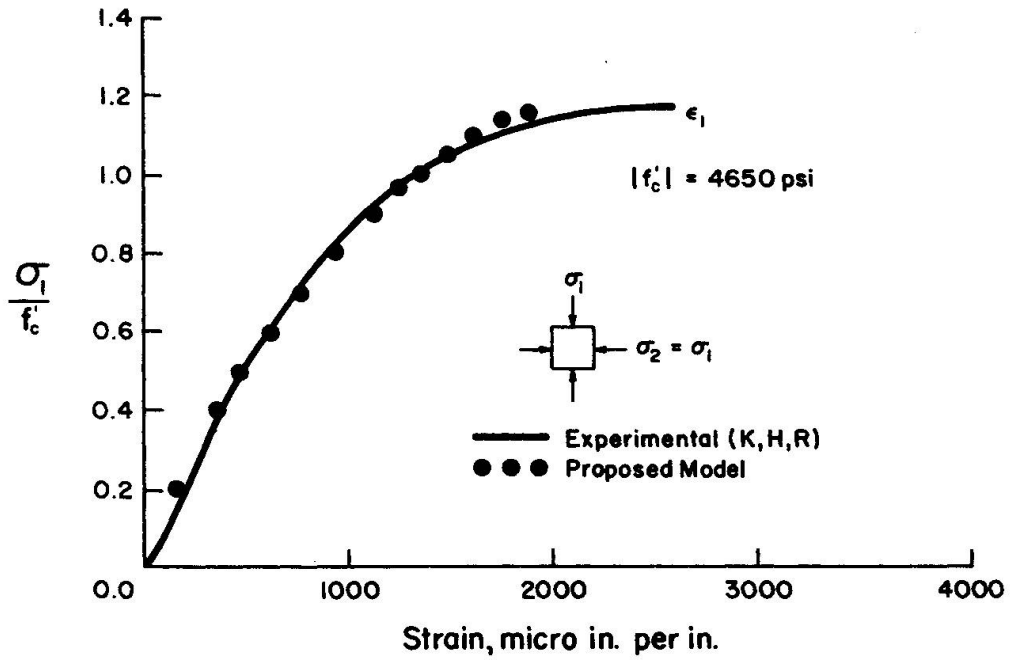

Fig. 17 Biaxial Compression of Plain Concrete, $\sigma_1 = \sigma_2$

Analytical Model for Deformed Bar Bond under Generalized Excitations

Modèle analytique pour l'adhérence de barres nervurées sous sollicitations répétées

Analytisches Modell für den Verbund von Rippenstählen unter beliebigen Beanspruchungen

V. CIAMPI, R. ELIGEHAUSEN
Visiting scholars
University of California
Berkeley, USA

V. BERTERO, E. POPOV
Professor
University of California
Berkeley, USA

SUMMARY

A mathematical model is presented to predict the behavior of a deformed bar, embedded in well-confined concrete, and subjected to generalized cyclic excitations in the range of the low cycle fatigue. It includes the formulation of a simplified model for the local bond stress-slip relationship, based on the elaboration of the result of an extensive experimental study carried out recently at Berkeley; use of a simple but sufficiently accurate model for the stress-strain relationship of reinforcing steel and the numerical solution of the differential equation of bond. An example is presented and commented.

RÉSUMÉ

Un modèle mathématique décrivant le comportement d'une barre crénelée dans un béton bien confiné et soumis à un chargement cyclique quelconque de haute intensité est présenté. Il comprend: 1) la formulation d'un modèle simplifié pour décrire la relation contrainte-glissement en adhérence basé sur les résultats d'un vaste programme expérimental mené récemment à Berkeley, 2) l'utilisation d'un modèle simple mais suffisamment exact pour décrire la relation contrainte-déformation dans la barre d'armature et 3) une solution numérique de l'équation différentielle décrivant l'adhérence. Un exemple est présenté et commenté.

ZUSAMMENFASSUNG

Ein mathematisches Modell zur Berechnung des Verhaltens eines Rippenstabes, verankert in eng verbügeltem Beton und beansprucht durch beliebige zyklische Belastungen hoher Intensität, wird erläutert. Es umfasst die Formulierung eines vereinfachten Modells für die Beziehung zwischen örtlicher Verbundspannung und örtlichem Schlupf, das aus umfangreichen, in Berkeley durchgeführten Versuchen abgeleitet wurde; die Benutzung eines einfachen, jedoch ausreichend genauen Modells für das Spannungs-Dehnungs Gesetz des Bewehrungsstahles und die numerische Lösung der Differentialgleichung des Verbundes. Ein Beispiel ist dargestellt und erläutert.

1. INTRODUCTION

Under severe seismic excitations, the hysteretic behavior of reinforced concrete structures is highly dependent on the interaction between steel and concrete (bond stress-slip relationship) [1]. Tests show that developing displacement ductility ratios of four or more, fixed end rotations caused by slip of the main steel bars along their embedment length in beam-column joints, may contribute up to 50 percent of the total beam deflections [2-4]. These effects must be included in the analyses. However, in spite of recent integrated experimental and analytical studies devoted to finding such a relationship [5], no reliable bond stress-slip laws for generalized excitations are available [6].

In this paper a mathematical model is presented to predict the behavior of a deformed bar, embedded in well-confined concrete, and subjected to generalized cyclic excitations. The local bond stress-slip model, the model for the stress-strain relationship of reinforcing steel, and the technique for solving the differential equation of bond, are discussed and an example is presented.

2. LOCAL BOND STRESS-SLIP MODEL

2.1 Tests

The constitutive relations for bond between deformed bars and normal weight concrete were derived from results of an extensive experimental study carried out at Berkeley during the last year [7]. Altogether some 120 specimens were tested; only those results which are relevant to the formulation of the proposed analytical model are briefly discussed herein.

The test specimens (Fig. 1) represented the confined region of a beam-column joint. Only a short length ($5d_b$) of a grade 60 deformed bar (#8 , $d_b \sim 25$ mm) was embedded in concrete ($f'_c = 30$ N/mm^2). Because cracking might influence the bond stress-slip behavior, the resistance against splitting was simulated as closely as possible to that which might exist in a real structure. Therefore a thin plastic sheet was placed in the plane of the longitudinal axis of the bar (Fig. 1) which limited the concrete splitting area to the desired value. In

Fig. 1 Test Specimen

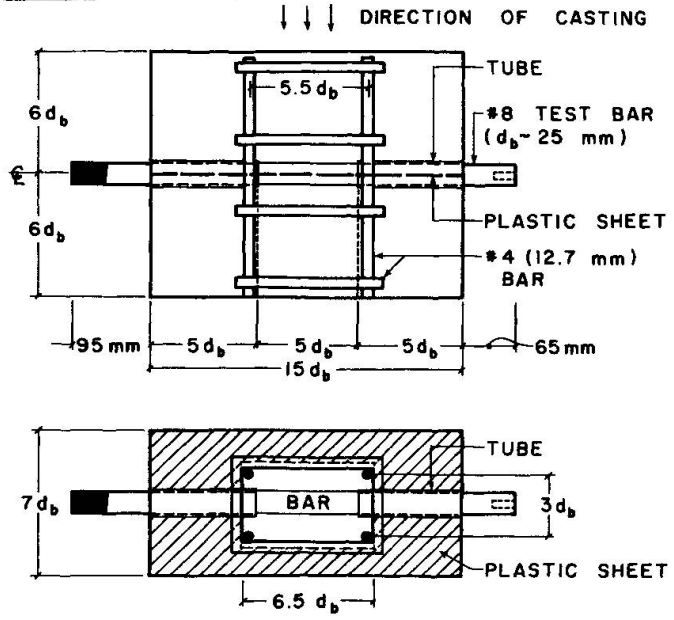

Fig. 2 Foto illustrating test setup

this way the influence of different bar spacings could be modeled as well. In the tests described here, the assumed spacing was 4 d_b. The test specimen was installed in a specially designed testing frame (Fig. 2) and was loaded by a hydraulic servo controlled universal testing machine having a capacity ± 1350 kN, which allowed the application of prescribed tension and compression forces, or displacements, to the embedded bars. The tests were run under displacement control by subjecting the threaded loading end of the bar to the required force needed to induce the desired slip, which was measured at the unloaded bar end (using a linear variable differential transformer, (Fig. 2) and was controlled at a rate of 1.7 mm/min.

The influence of various slip histories on the bond stress-slip behavior was examined. The main parameters were: the peak value of the slip (0.1 mm $\leq s_{max} \leq$ 15 mm); the difference between the peak values of slip ($\Delta s = s_{max} - s_{min}$, see Fig. 3a) between which the specimen was cyclically loaded (Δs = 0.05 mm, 1 s_{max} and 2 s_{max}); and the number of cycles (1 to 10). In the majority of tests, after the specimens were subjected either to 1 or alternatively to 10 cycles up to the selected peak values of slip, the slip was increased monotonically to failure. In a few tests the bar was subjected to a series of cycles at different values of slip. Usually 2 or 3 identical tests were carried out.

In all tests conducted the failures were caused by pulling out of the bars at steel stresses well below yield stress. Prior to failure, splitting cracks developed in the plane of the longitudinal axis of the bars but their growth was controlled by the confining reinforcement (see Fig. 1).

Typical test results are shown in Fig. 3 and summarized below:

(a) The bond stress-slip relationship for monotonic loading in tension was almost identical to that in compression. This could be expected [8] since the specimens were cast with the bars in a horizontal position. The descending branch of the bond stress-slip curve levelled off at a slip approximately equal to the clear distance between protruding lugs of the bar.

(b) If the peak bond stress in tension and compression during cycling did not exceed 70-80 percent of the monotonic τ_{max}, the ensuing bond stress-slip relationship, at slip values larger than the one at which the specimen was cycled, was not significantly affected by up to 10 cycles (Fig. 3a). The bond stress at peak slip deteriorated moderately with increasing number of cycles. These results agree well with earlier findings [9-12]. Although many factors related to early concrete damage (microcracking and microcrushing due to high local stresses at the protruding lugs) may be involved in this bond-resistance deterioration it is believed that the main cause is a relaxation of the concrete between the lugs [12].

(c) When the bar was loaded monotonically to an arbitrary slip value and then cycled up to 10 times between this slip value and a slip value corresponding to a load equal to zero (Δs = 0.05 mm), the monotonic envelope was, for all practical purposes, reached again. From then on the behavior was the same as that obtained in a monotonic test. This agrees well with earlier results [8,11].

(d) Loading to slip values inducing a τ larger than 80 percent of the monotonically obtained τ_{max} in either direction led to a degradation in the bond stress-slip behavior in the reversed direction (Figs. 3b and 3c). The bond stress-slip relationship at slip values larger than the peak value during previous cycles, with $\Delta s = s_{max}$ or $\Delta s = 2\ s_{max}$, was significantly different from the virgin monotonic envelope. There was a deterioration of the bond resistance and the degree of deterioration increased with increasing peak slip s_{max}, increasing Δs, and increasing number of cycles (Fig. 3b and 3c). The largest deterioration was observed for full reversals of slip ($\Delta s = 2\ s_{max}$).

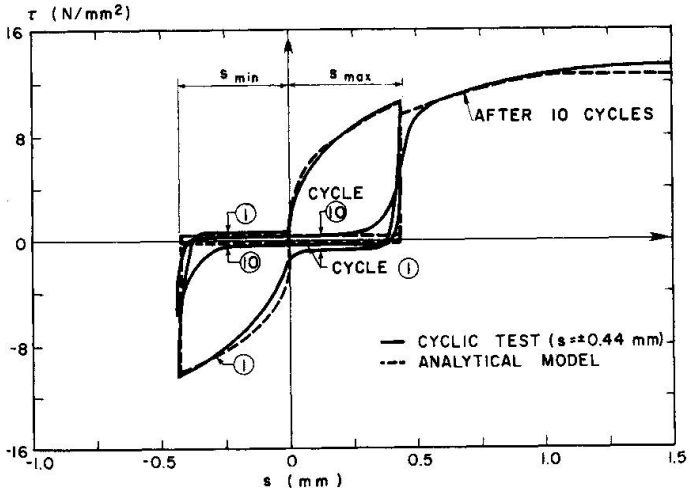

Fig. 3a Cycling between s = ± 0.44 mm

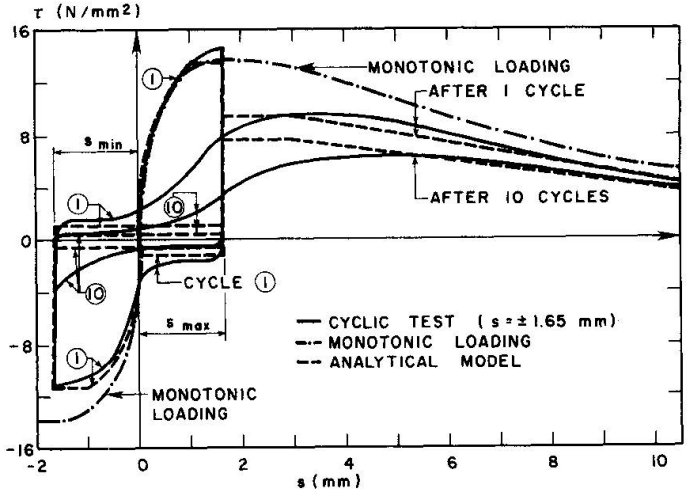

Fig. 3b Cycling between s = ± 1.65 mm

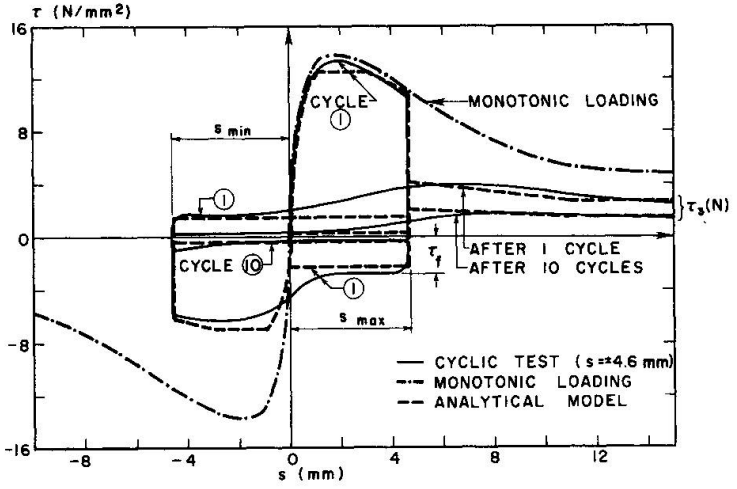

Fig. 3c Cycling between s = ± 4.6 mm

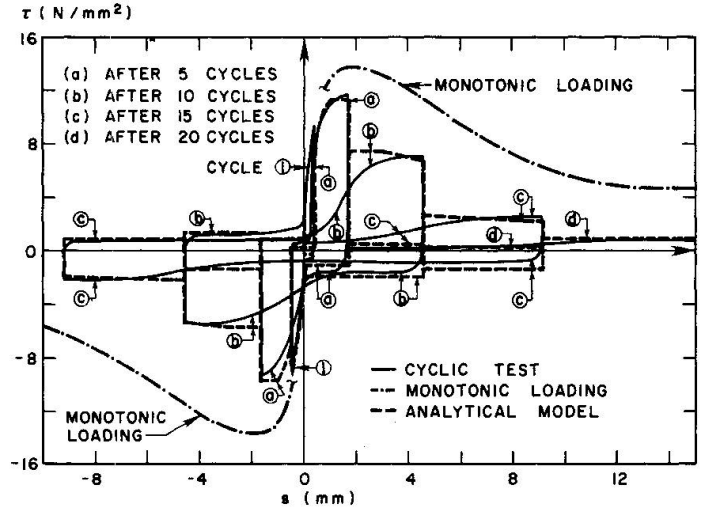

Fig. 3d Cycling under different increasing s_{max}

Fig 3 Comparison of Experimental and Analytical Results on Local Bond Stress-Slip Relationship.

The observed behavior can be explained by assuming that in a well-confined reinforced concrete the maximum bond resistance is controlled by the initiation of a shear failure in a part of the concrete between the protruding lugs of the bar. The larger is the value of the slip with respect to $s_{\tau max}$, i.e. slip at τ_{max}, the larger is the area of concrete between the lugs that is affected by the shear failure, and the smaller is the bond resistance. If the bar is cycled between constant peak values of s_{max} and s_{min}, the main damage is done in the first cycle. During successive cycles, the concrete at the cylindrical surface where shear failure occurred, is mainly grounded off, decreasing its interlocking and frictional resistance.

(e) The frictional bond resistance, τ_f, during cycling was dependent upon the value of the peak slip s_{max}. With repeated cycles τ_f deteriorated rapidly (see Figs. 3a-d), approximately at the same rate as the bond resistance at the peak slip value s_{max}, but at a faster rate than the ultimate frictional bond resistance $\tau_3(N)$ (see Fig. 3c) of the corresponding reduced envelope curve. The mechanism and value of frictional bond resistance are not well described and predicted by existing proposals [6].

2.2 Analytical Local Bond Stress-Slip Model

The assumed bond model is illustrated in Fig. 4. Although it simplifies the observed real behavior, it takes into account the significant parameters that appear to control the behavior observed in the experiments. This model, in spite of being simpler than the one proposed in [5], is believed to be more general. The model's main characteristics, illustrated by following a typical cycle (Fig. 4), are described below.

When loading the first time, the assumed bond stress-slip relationship follows a curve valid for monotonically increasing slip, which is called herein "monotonic envelope" (paths OABCD or $OA_1B_1C_1D_1$). Imposing a slip reversal at an

Fig. 4 Proposed Analytical Model for Local Bond Stress-Slip Relationship.

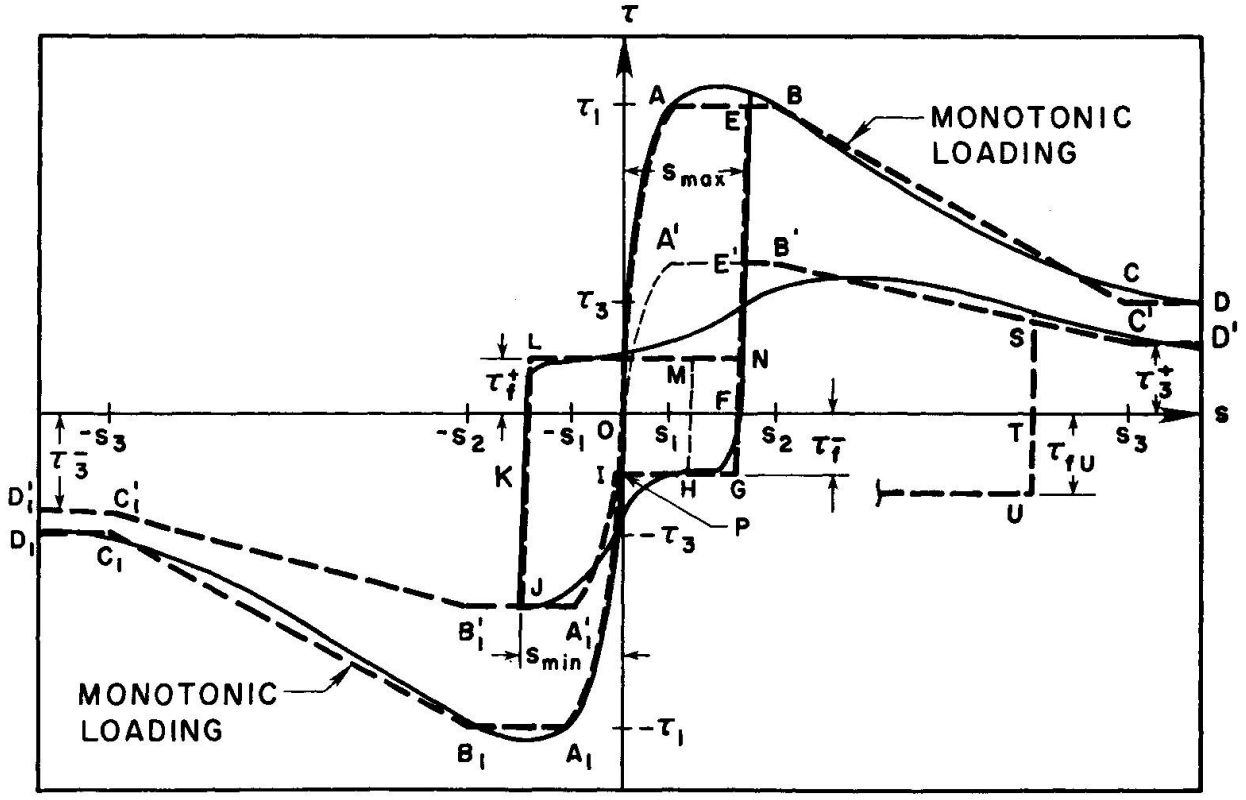

arbitrary slip value, a stiff "unloading branch" is followed up to the point where the frictional bond resistance τ_f is reached (path EFG). Further slippage in negative direction takes place without increase in τ up to the intersection of the "friction branch" with the curve OA_1' (path GHI). If more slip in negative direction is imposed a bond stress-slip relationship similar to the virgin monotonic curve is followed, but with values of τ reduced as illustrated by the paths $IA_1'J$. This curve ($O\ A_1'\ B_1'\ C_1'\ D_1'$) is called "reduced envelope". When reversing the slip again at J, first the unloading branch and then the frictional branch with $\tau = \tau_f^+$ are followed up to point N, which lies on the unloading branch EFG (path JLN). At N the "reloading branch" (same stiffness as the unloading branch) is followed up to the intersection with the reduced envelope O A'B'C'D' (path NE'), which is followed thereafter (path E'B'S). If instead of increasing the slip beyond point N more cycles between the slip values corresponding to the points N and K are imposed, the bond stress-slip relationship is like that of a rigid plastic model, the only difference being that frictional bond resistance decreases with increasing number of cycles. A similar behavior as described is followed if the slip is reversed again at point S (path STU). To complete the illustration of the model details about the different branches referred to in the above overall description are given in the following.

a) Monotonic Envelope

The simplified monotonic envelope simulates the experimentally obtained curve under monotonically increasing slip. It consists of an initial nonlinear relationship $\tau = \tau_1\ (s/s_1)^\alpha$ valid for $s \leq s_1$, followed by a plateau $\tau = \tau_1$ for $s_1 \leq s \leq s_2$. For $s \geq s_2$, τ decreases linearly to the value of the ultimate frictional bond resistance τ_3 at a slip value of s_3. This value s_3 is assumed to be equal to the clear distance between the lugs of the deformed bars. The same bond stress-slip law is assumed regardless of whether the bar is pulled or pushed.

At present, the values s_1, s_2, τ_1, τ_3 and α are choosen to match the experimentally obtained monotonic envelope curve. Studies are in progress to formulate reliable rules to predict such a curve for conditions different from those in the tests.

b) Reduced envelopes

Reduced envelopes are obtained from the monotonic envelope by reducing the characteristic bond stresses τ_1 and τ_3 through reduction factors, which are formulated as a function of one parameter, called herein the "damage parameter d". For no damage, d=0, the reloading branch reaches the monotonic envelope. For full damage, d=1, bond is completly destroyed ($\tau = 0$).

The rationale for this assumption is given by Fig. 5, which shows that reloading curves for similar specimens, subjected to different loading histories, appear to form a parametric family of curves.

The deterioration of the monotonic envelope seems to depend on the damage experienced by the concrete, particularly the length of the concrete between the lugs of the bar that has sheared off. This in turn is a function of the magnitude of the slip induced in the bar in both directions, the larger the s_{max} and the difference between peak slip values, the larger the damage. Another influence factor is the number of cycles. These parameters can be related to the energy dissipated during the loading and unloading processes. Therefore it was assumed that the damage parameter d is a function of the total dissipated energy only. However, it has also been taken into account that only a fraction of the energy

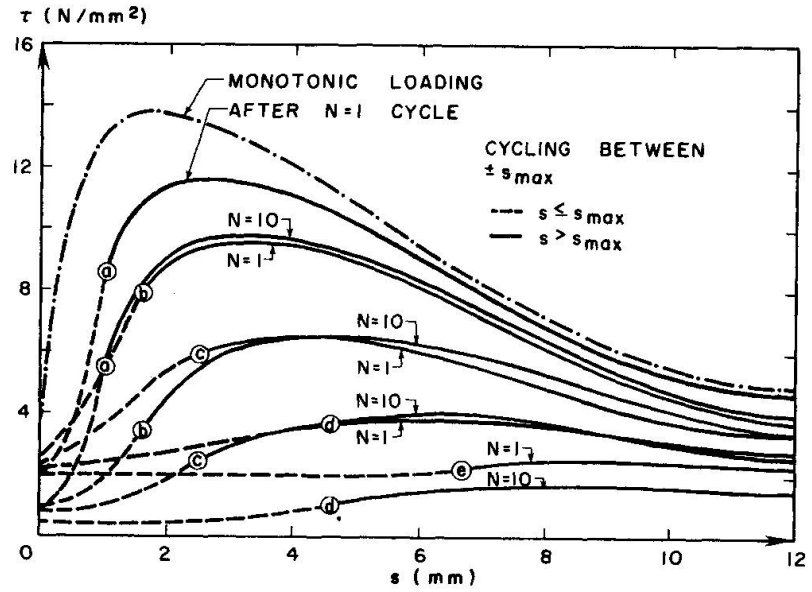

Fig. 5 Effects of number of cycles and of the peak values of slip s_{max} at which the cycling is performed on the ensuing bond stress-slip relationship for $s > s_{max}$.

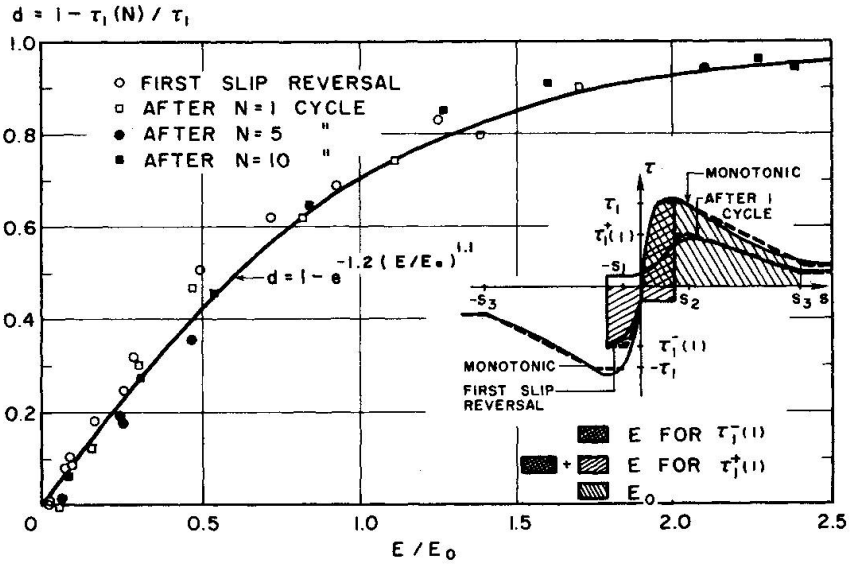

Fig. 6 Damage parameter d as a function of the dimensionless energy dissipation.

dissipated during subsequent cycles between fixed peak slip values appear to cause damage, while the other part appears to be used to overcome the frictional resistance and is transformed into heat.

Fig. 6 illustrates the correlation between the measured damage factor d, for tests with full reversal of slip as a function of the computed dimensionless dissipated energy factor E/E_o. The proposed function for d is shown as well. In the computation of E only 50% of the energy dissipated by friction is taken into account. The normalizing energy E_o corresponds to the absorbed energy under monotonically increasing slip up to the value s_3. Although there is some scatter, the agreement between the analytical and experimental results seems acceptable.

No reduction of the current envelope (monotonic or reduced) is assumed for unloading and reloading only (e.g., paths EGE or JLJ in Fig. 4). If a cycle is not completed to the current values of s_{max} or s_{min} (e.g., path GHM) the damage parameter is interpolated between the values valid for the last slip reversal and for the completed cycle (point E and point P in this example).

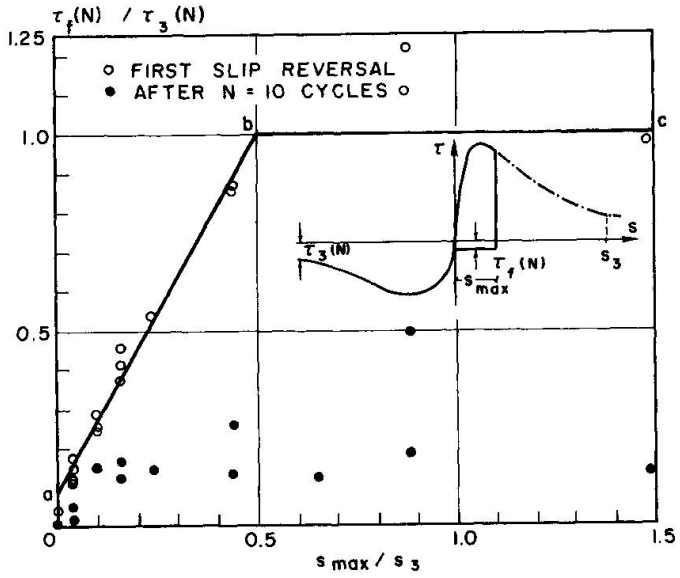

Fig. 7 Relationship between the frictional bond resistance $\tau_f(N)$ and the corresponding ultimate frictional bond resistance $\tau_3(N)$.

It should be observed that the proposal for calculating the damage parameter as a function of the total dissipated energy is theoretically correct only in the range of the low cycle fatigue, that is when a small number of cycles at relatively large slip values is carried out. In fact if a high number of cycles at small slip values is performed, the energy dissipated can be relatively large but no significant damage is produced and the reloading branch reaches the monotonic envelope again [12]. On the other hand, when limiting our attention to a small number of cycles ($\lesssim$ 30), as in the present study, the energy dissipated for cycles between small slip values is rather small and the calculated damage, as a consequence, insignificant.

c) Frictional resistance

The frictional bond resistance after first unloading (τ_f^- in Fig. 4) depends upon the peak value of slip, s_{max}, and is related to the value of the ultimate frictional bond resistance of the corresponding reduced envelope (τ_3^- in Fig. 4). The relationship found in the tests is shown in Fig. 7. However, if cycling is done between fixed values of slip (e.g., between s_{max} and s_{min} in Fig. 4), τ_f is reduced more rapidly than the ultimate τ_3 of the corresponding reduced envelope (see Figs. 3 and 7). Therefore the analytical function oabc in Fig. 7 is used only for the calculation of the frictional resistance for the first slip reversal. For subsequent cycles τ_f (e.g., τ_f^+ in Fig. 4) is deduced from this initial value by multiplying it with an additional reduction factor which depends on the energy dissipated by friction alone.
If unloading is done from a larger slip value than the peak slip in the previous cycle (path STU) the new frictional bond resistance (τ_{fU}^-) is interpolated between two values. The first value is related to τ_3^- of the corresponding new reduced envelope using the analytical function given in Fig. 7 and the second value is the τ_f reached in the last cycle (τ_f^+ in Fig. 4). This interpolation is done in order to have a smooth transition in the values of τ_f.

Note that the concept of relating damage to one scalar quantity, like the normalized dissipated energy, has provided a basis for the relatively easy generalization of the bond behavior for random excitations. The bond model selected can easily be extended to cover bond of bars under conditions different from those reported herein, such as different bar diameter, pattern of deformation (lugs), concrete strength, degree of confinement, effect of transverse pressure, etc. This requires that the pertinent experimental data necessary for computing the different parameters, in particular the monotonic envelope, be obtained.

2.3 Comparison of Analytical Predictions of Local Bond Stress-Slip Relationships with Experimental Results

The local bond stress-slip relationships, obtained using the model described above, are compared in Fig. 3 with the experimental results obtained in some of the Berkeley tests. As can be seen, except for the reloading curves near the values of the peak slip between which the specimen was cycled, the agreement is quite good. In general the model was successful in reproducing most of the experimental results.

3. APPLICATION OF LOCAL BOND STRESS-SLIP MODEL IN PREDICTING BOND BEHAVIOR OF REINFORCING BARS

As noted in the introduction, prediction of response of concrete structures to severe seismic excitations requires the prediction of the slippage of the main longitudinal reinforcing bars in their joints. The above formulation of the local bond stress-slip relationship for well-confined concrete allows determination of slippage of the bar in the part of concrete that is well-confined. This is discussed in Chapter 3.2. Since, in general, the anchorage offered to the bars is sufficient to develop the yield strength of the reinforcing steel, it is necessary to have a reliable mechanical model for reinforcing steel covering its inelastic behavior.

3.1 Reinforcing Steel Model

For the uniaxial σ-ε relationship of the reinforcing steel, the expression proposed in [13] and generalized in [14] was used because of its advantages in the present application with respect to the classic Ramberg-Osgood formulation, that has been used in [4,5]. The equation

$$\frac{\sigma}{\sigma_o} = b\,\frac{\varepsilon}{\varepsilon_o} + \frac{(1-b)\,\varepsilon/\varepsilon_o}{[1 + (\varepsilon/\varepsilon_o)\,R]^{1/R}}$$

where σ_o , ε_o are the stress and strain at first yielding respectively, expresses stress σ as a function of strain ε and accounts for strain hardening through the slope parameter b. It also allows an accurate representation of the reversal curves through the parameter R, which varies depending on the magnitude of the maximum excursion ε_{max} into the plastic range (see Fig. 8).

The simple set of additional rules proposed in [15] was used to avoid the storage of parameters of all reversal curves in the case of a general strain history. Using a proper set of numerical values for the parameters describing the model, the calculated response of a reinforcing bar subjected to a

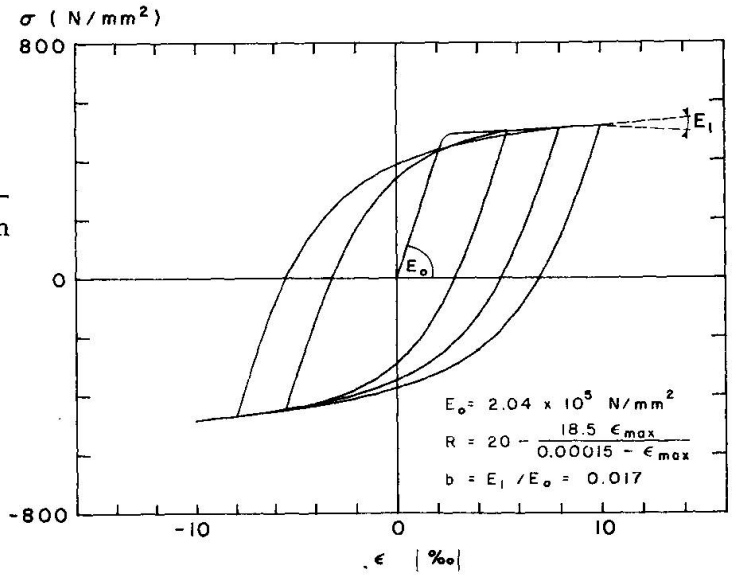

Fig. 8 Analytically predicted uniaxial stress-strain relationship for a #8 Grade 60 reinforcing steel bar.

particular history of strains, Fig. 8, agrees sufficiently well with test results published in [5].

3.2 Technique for Solving the Differential Equation of Bond

The actual behavior of a bar of finite length embedded in a concrete block can be idealized as a one-dimensional problem and modeled using the ordinary non-linear differential equation

$$dN(x)/dx + q(x) = 0 \quad \text{where } q(x) = \pi d_b \, \tau(x) \text{ and } N(x) = A \, \sigma(x)$$

which connects the axial force in the bar, N, to the resultant per unit length of the bond stresses on the perimeter of the bar, q. This equation has to be coupled with the constitutive laws for steel and bond, which can be expressed as

$$\sigma = \bar{\sigma} \, (\varepsilon(x)) = \bar{\sigma} \, (\frac{ds}{dx}) \quad \text{and} \quad \tau = \bar{\tau} \, (s(x)).$$

Note that here the influence of the deformation of concrete on slip has been considered negligible, as commonly assumed, and, as a consequence, the strain in the steel ε has been put equal to ds/dx.

Boundary values are specified at the two end points of the bar. Typically, for a pull-push displacement controlled test, the two displacements at the two ends are assigned; for a pull only test the boundary conditions are the value of the displacement at the pulled end and a null value of the axial force at the other end.

Different techniques can be used in principle for solving this nonlinear, two points boundary value problem: finite differences, finite elements, and shooting techniques. A finite element approach has been tried, for example, with some success in [5], using constant stress elements for the steel and concentrating bond forces (nonlinear springs)at the joints.

In this study a shooting technique has been preferred. It consists of transforming the boundary value problem into an initial value problem, in which the unknown boundary condition at one end has to be guessed, in order to produce, through integration along the length, the values of the normal force and the displacement at the other end. The given boundary condition at that end has now to be matched and this defines a nonlinear equation in the unknown boundary condition at the first end. This nonlinear equation is solved in this case using a modified secant method while the integration along the length is carried out using the trapezoidal scheme. The method has proved itself efficient and suitable for the problem at hand.

3.3 Behavior of Anchorages

Fig. 9 shows the calculated response of a main reinforcing bar (#8, $d_b \sim 25$ mm) passing through a well-confined concrete ($f'_c = 30$ N/mm^2) of a column-beam joint having an anchorage length of 15 d_b. It is loaded at one end only and subjected to reversed slip with increasing amplitude (Fig. 9a). The main aspects of this response, which are summarized below, agree well with those obtained in the experiments reported in [5].

(a) The reduction in stiffness, characterized by pinched hysteretic loops, with increasing amplitude of displacement and number of cycles (Fig. 9c).

(b) The reduction of strength at fixed amplitude of displacement as a function of the number of cycles (Fig. 9c).

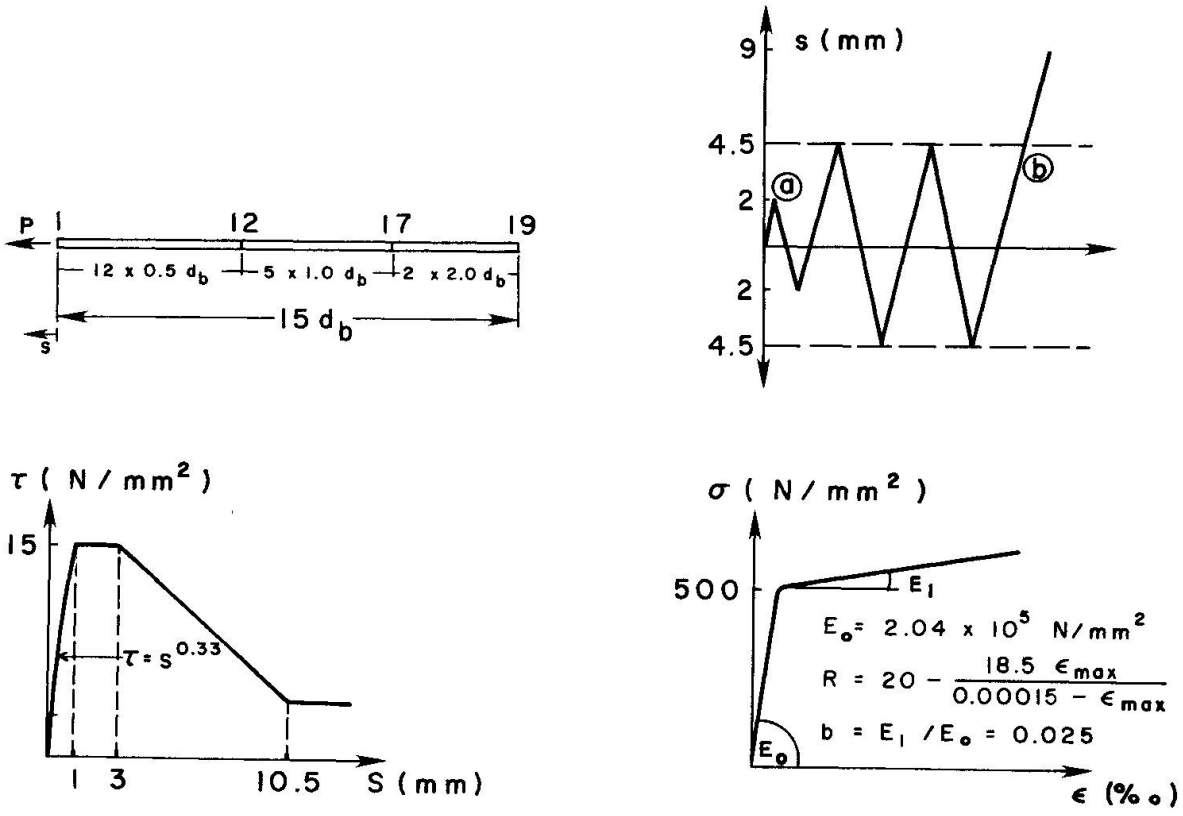

Fig. 9a Bar subdivisions, load history, local bond law and steel law.

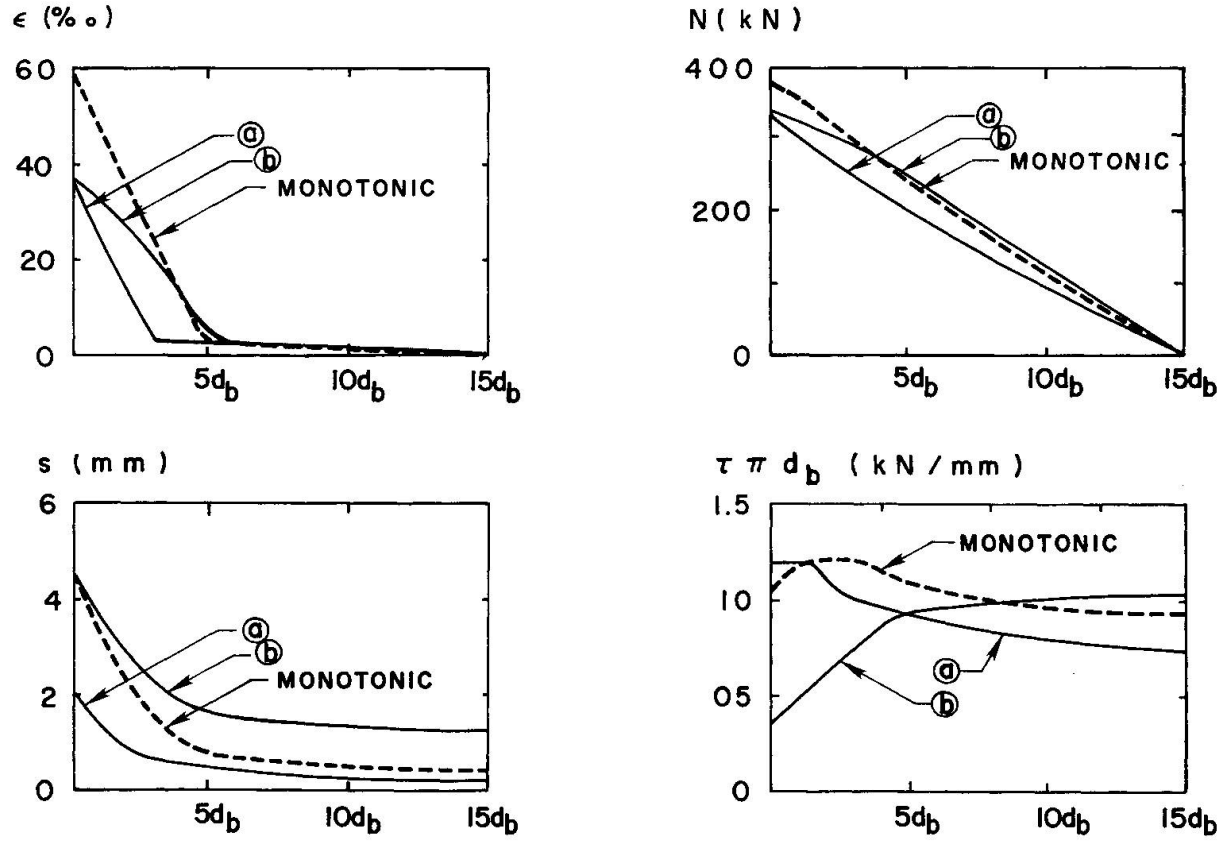

Fig. 9b Distribution of steel strain, slip, normal force and bond force along the bar at s = 2 mm and s = 4.5 mm for monotonic and cycling loading.

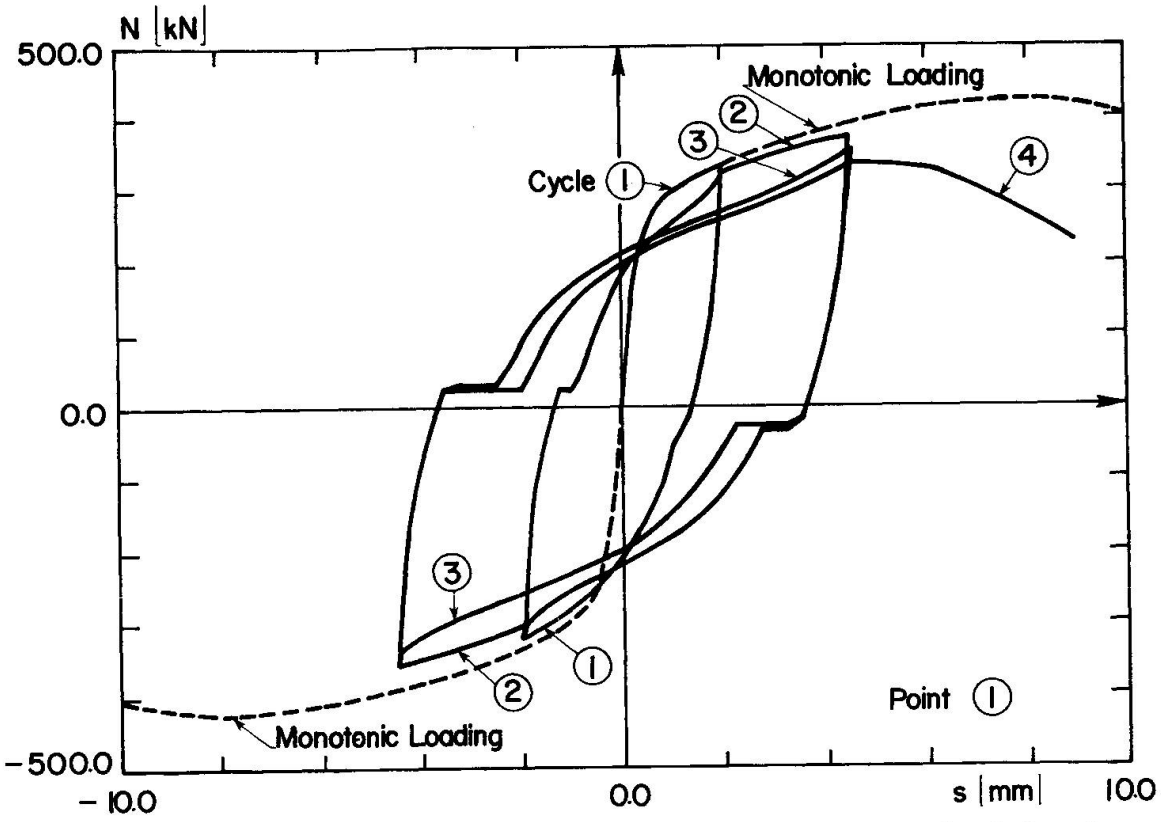

Fig. 9c Normal-force total slip relationship at loaded end.

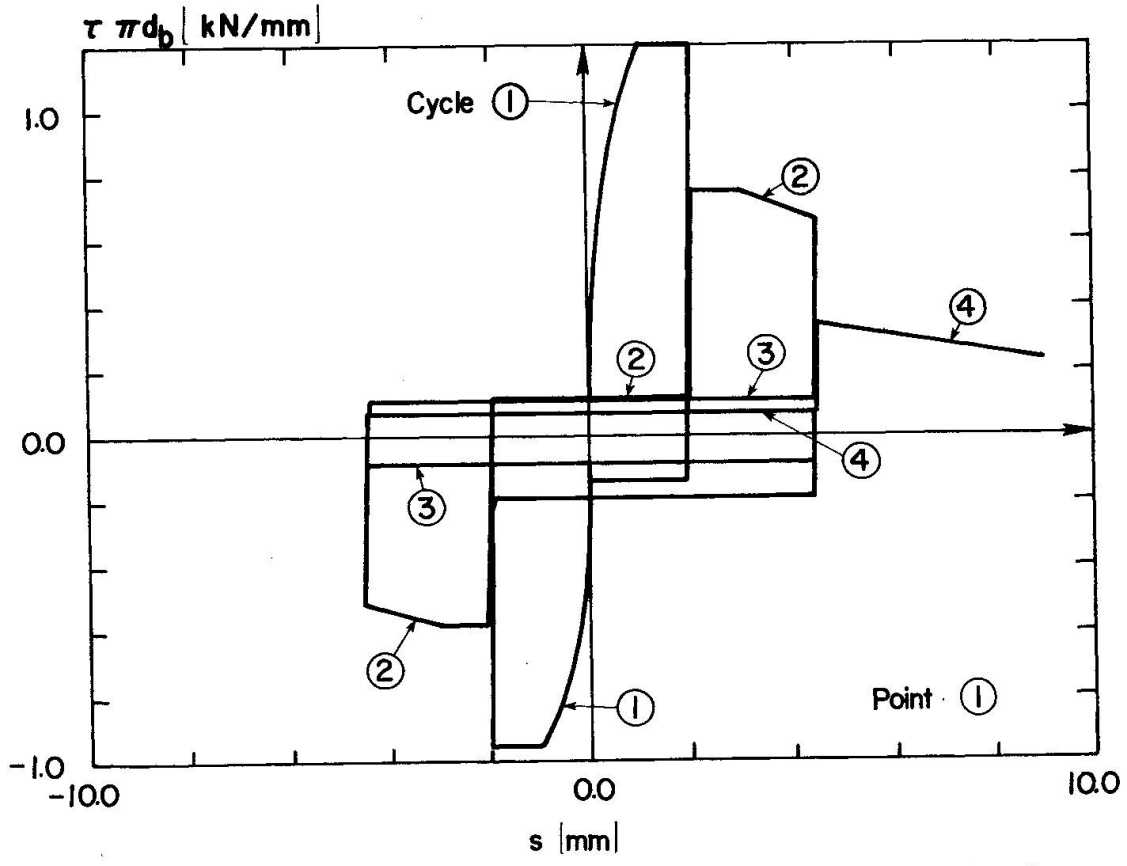

Fig. 9d Bond force-total slip relationship at loaded end.

Fig. 9 Analytically predicted behavior of the anchorage of a #8 deformed bar.

(c) The reduction of maximum strength and of deformability at maximum strength (ductility) compared to monotonic loading (Fig. 9b,c).

(d) The penetration of yield and the corresponding degradation of bond into the anchorage length with increasing peak displacement(see Figs. 9b,d).

However, the quantitative agreement between observed and calculated response needs improvement. Possible reasons for this discrepancy are given below:

(a) In the present study it is assumed that the local bond stress-slip laws for tension and compression loading are equal and do not vary along the anchorage length. However, three different regions with significantly different bond stress-slip behaviors can be identified in a joint [5]: unconfined concrete in tension, confined concrete, and unconfined concrete in compression.

(b) After yielding, the diameter of a bar in tension is significantly reduced due to the Poisson effect. This may reduce the bond resistance. The opposite is true for a bar yielding in compression. These effects were not taken into account.

(c) The presented local bond stress-slip model might be over simplified in modeling the envelope curves (virgin and reduced) and particularly the ascending branches of the reloading curves near the peak slip, during and after cycling.

It is expected that after completing the next step of this current study in which the above mentioned effects will be taken into account, it should be possible to reproduce the experimental results with sufficient accuracy for practical applications.

4. CONCLUSIONS

From the results obtained in this study the following main observations can be made:

(1) During cycling loading the degradation of bond strength and bond stiffness depends primarily on the maximum value of peak slip in either direction reached previously. Other significant parameters are the number of cycles and the difference between the peak values of the slip between which the bar is cyclically loaded, i.e., $\Delta s = s_{max} - s_{min}$.

(2) Cycling up to 10 times between slip values corresponding to bond stresses smaller than approximately 80 percent of the maximum bond resistance, τ_{max}, attained under monotonically increasing slip, reduces moderately the bond resistance at the peak slip value as the number of cycles increase, but does not significantly affect the bond stress-slip behavior at larger slip values.

(3) Cycling between slip limits larger than that corresponding to a bond stress of 80 percent of τ_{max} produces a pronounced deterioration of the bond stiffness at slip values smaller than the peak slip value and has a distinct effect on the bond stress-slip behavior at larger slip values.

(4) The proposed model for the local bond stress-slip law is very simple compared with the real behavior but provides a satisfactory agreement with experimental results under various slip histories.

(5) While the calculated response of long anchorages of reinforcing bars agrees qualitatively well with experimental results, the quantification of the main parameters needs improvement. Reasons for the quantitative disagreement are given and are under study. It is expected that after introducing different local bond stress-slip relationships along the anchorage length, it will be possible to reproduce the experimental results with sufficient accuracy for practical applications.

ACKNOWLEDGEMENTS

The work reported herein was sponsored by the National Science Foundation, under grant PFR79-08984 with the University of California, Berkeley. The support of Dr. Ciampi by the Italian Research Council and of Dr. Eligehausen by the Deutsche Forschungsgemeinschaft are gratefully acknowledged.

REFERENCES

[1] Popov, E. P., "Mechanical Characteristics and Bond of Reinforcing Steel under Seismic Conditions", Proceedings, Workshop on Earthquake-Resistant Reinforced Concrete Building Construction, University of California, Berkeley, July 11-15, Vol. II, pp. 658-682.

[2] Takeda, T., Sozen, M., and Nielsen, N. N., "Reinforced Concrete Response to Simulated Earthquakes", Journal of the Structural Division, ASCE, Vol. 96, No. 12, Dec. 1970.

[3] Ismail, M. A., and Jirsa, J. O., "Behavior of Enclosed Bars under Low Cycle Overloads Producing Inelastic Strains", Journal of the American Concrete Institute, Vol. 69, No. 7, July 1972.

[4] Ma, S. Y., Bertero, V. V., and Popov, E. P., "Experimental and Analytical Studies on the Hysteretic Behavior of Reinforced Concrete Rectangular and T-Beams", Report No. EERC 76-2, Earthquake Engineering Research Center, University of California, Berkeley, 1976.

[5] Viwathanatepa, S., Popov, E. P., and Bertero, V. V., "Effects of Generalized Loadings on Bond of Reinforcing Bars Embedded in Confined Concrete Blocks", Report No. EERC 79-22, Earthquake Engineering Research Center, University of California, Berkeley, 1979.

[6] Tassios, T. P., "Properties of Bond between Concrete and Steel under Load Cycles Idealizing Seismic Actions", Bulletin D'Information No. 131 of the Comité Euro-International du Béton, Paris, April 1979.

[7] Eligehausen, R., Bertero, V. V. and Popov, E. P., "Local Bond Stress-Slip Relationships of Deformed Bars under General Excitations", Report in preparation - UCB.

[8] Rehm, G., "Über die Grundlagen des Verbundes zwischen Stahl und Beton", (About the Basic Laws of Bond between Steel and Concrete), Schriftenreihe des Deutschen Ausschusses fur Stahlbeton, Berlin, 1961.

[9] Bresler, B. and Bertero, V. V., "Behavior of Reinforced Concrete Under Repeated Loads", Journal of the Structural Division, ASCE, Vol. 24, No. 6, June 1968.

[10] Ismail, M. A. and Jirsa, J. O., "Bond Deterioration in Reinforced Concrete Subject to Low Cycle Loads", Journal of the American Concrete Institute, June 1972.

[11] Morita, S., and Kaku, T., "Local Bond Stress-Slip Relationship and Repeated Loading", IABSE Symposium, Resistance and Ultimate Deformability of Structures Acted on by Well-Defined Repeated Loads, Lisbon, 1973.

[12] Rehm, G., and Eligehausen, R., "Einfluss einer nicht ruhenden Belastung auf das Verbundverhalten von Rippenstählen", (Influence of High Cycle Repeated Loads on the Bond Behavior of Ribbed Reinforcing Bars), Betonwerk und Fertigteil-Technik, Heft 6, 1977, in German.

[13] Giuffré, A. and Pinto, P. E., "Reinforced Concrete Behavior under Strong Repeated Loading", G. Genio Civile, No. 5, 1970, in Italian.

[14] Capecchi, D., Ciampi, V., and Vestroni, "Numerical Studies on the Behavior of a Reinforced Concrete Beam Element under Repeated Loadings", Bulletin D'Information No. 132 of the Comité Euro-International du Béton, Paris, April 1979.

[15] Jennings, P. C., "Response of Simply Yielding Structures to Earthquake Excitation", California Institute of Technology, Pasadena, Californiam Report No. 6360, June 1963.

Leere Seite
Blank page
Page vide

Experiments and Models for the Damping Behavior of Vibrating Reinforced Concrete Beams in the Uncracked and Cracked Condition

Essais et modèles pour l'amortissement de poutres en béton armé dans l'état non-fissuré

Versuche und Modelle für das Dämpfungsverhalten schwingerder Stahlbetonträger im ungerissenen und gerissenen Zustand

R. DIETERLE
Research Associate
Swiss Federal Institute of Technology
Zurich, Switzerland

H. BACHMAN
Prof. Dr.
Swiss Federal Institute of Technology
Zurich, Switzerland,

SUMMARY
Different models for the damping behavior of normally reinforced, uncracked and cracked concrete beams and constructions under dominating bending stress are presented. By comparison with experimental results it can be shown that the results of the theoretical damping models are in good agreement with those of the experiments.

RÉSUMÉ
On présente des modèles qui permettent de concevoir l'amortissement de poutres et constructions en béton non-fissurés et fissurés, soumis surtout à des sollicitations de flexion. Par comparaison avec des résultats déterminés à l'aide d'essais on montre, que l'emploi des modèles présentés donne des résultats concordants avec ceux des essais.

ZUSAMMENFASSUNG
Es werden verschiedene Modelle für das Dämfungsverhalten von schwingenden Stahlbetonträgern und -konstruktionen im ungerissenen und gerissenen Zustand, welche vorwiegend auf Biegung beansprucht werden, dargestellt. Anhand von Vergleichen mit experimentellen Resultaten wird die Anwendbarkeit der präsentierten Modelle aufgezeigt.

1. INTRODUCTION

Recently, the dynamic analysis of reinforced concrete structures has greatly increased in significance. Yet important knowledge in several areas is still lacking especially information concerning damping, which can decidedly influence a dynamic calculation.

The damping of reinforced concrete structures is based upon various and at times little-known physical causes, and depends upon numerous influencing perameters. It is therefore not surprising that in experiments the fixed values for the damping scatter within a broad range. The two chief causes for this scatter are as follows:

- The material damping of reinforced concrete building components and reinforced concrete constructions is influenced not only by the damping properties of the material used, but also strongly by the crack condition. For uncracked structures, especially fully prestressed uncracked structures, the damping properties in many cases can be described with closely agreeing values. For normally-reinforced and partly-prestressed structures, however, there exists in the literature a large variation both qualitatively and quantitatively with regard to the influence of the crack condition. Normally it is accepted that reinforced concrete structures in the cracked condition show in addition to low eigenfrequencies a considerable increase in damping in comparison to those in the uncracked condition.
- In general, the damping of an entire reinforced concrete construction is influenced not only by the material damping but also by the system damping, that is by the damping properties of the surroundings (building site, development of statical system, etc.). Since the fraction of the system damping on the total damping can be considerable, it is possible that analogous structures in different surroundings will show very different damping behaviors.

In order to check this behavior and to determine the influence of important construction parameters on the material damping properties of reinforced concrete, systematic experiments on seven normally-reinforced concrete and light-weight concrete beams were conducted at the Institute of Structural Engineering at the Swiss Federal Institute of Technology Zurich. These experiments and the achieved results are described in [1] and [2]. They provide the experimental groundwork for the theoretical work performed in [3]. The most important results of this work are put forth in the following report.

2. OBJECTIVES

The objectives of the described research project are as follows:

1. The determination of the influence of the crack condition, of the stress level and of the amount of reinforcement on the damping properties of normally-reinforced concrete and light-weight concrete beams.
2. The development of physically plausible and mathematically simple models which can not only explain the experimentally recorded damping phenomena on the test beams, but also can predict the material damping properties of more complex concrete and light-weight concrete constructions.

3. TESTS ON NORMALLY-REINFORCED CONCRETE BEAMS

In the experiments mentioned in the introduction, vibration and resonance tests were performed on seven concrete and light-weight concrete beams of varying longitudinal reinforcement. All beams had identical dimensions (length L = 8.40 m, width B = 0.40 m, depth H = 0.24 m), and after cracking all had their first eigenfrequency in the range from 2 to 7 Hz. Briefly repeated here will be several results which give information on the established damping properties and which

are necessary for the disposition and understanding of the following report.

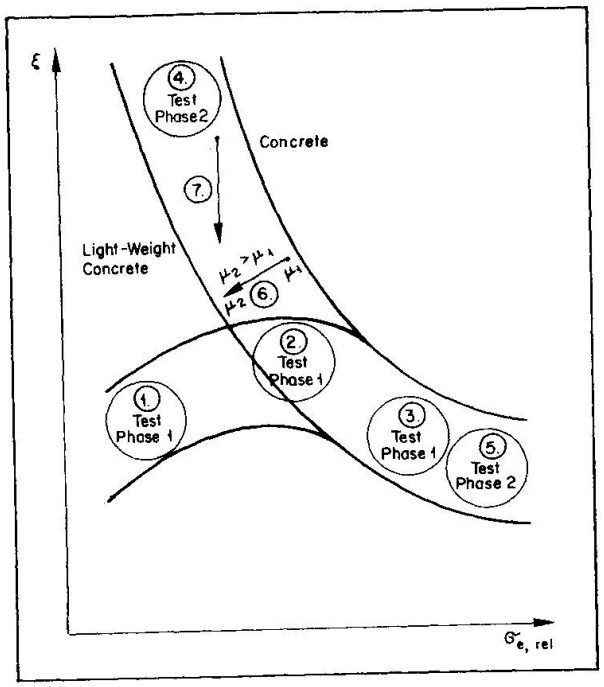

Fig. 1 Damping Ratio ξ as a Function of the Steel Stress $\sigma_{e,rel}$ (schematic)

In Fig. 1, the established curve of the damping ratio as a function of the relative steel stress $\sigma_{e,rel}$ in the middle of the beam is schematically shown for all test beams.

The index "rel" (= relative) signifies that the stress refers to the difference between the values measured in the dynamic test and in the at-rest state.

The established damping properties can be described as follows, with the numbering scheme referring to the numbering scheme of Fig. 1:

Initial Stressing and Cracking Phase

(test phase 1)

1. The damping for all beams increased during cracking (crack formation and spreading) following the increasing steel stress.
2. Approximately as soon as all bending cracks had formed, a condition was reached for which the damping ceased to increase further.
3. With the further increase in stress, respectively steel stress, the damping decreased. As the steel stresses neared the yield point, very small damping values were measured ($\xi < 1\%$), especially for heavily-reinforced beams.

After Conclusion of Cracking and with Repeat of Testing

(test phase 2)

During the repeated execution of the total test program the following damping behavior for each of the beams could be observed:

4. A very high damping was established for small steel stresses, in contrast to test phase 1. For increasing steel stress, however, the damping again decreased.
5. Somewhat smaller values for the damping than in test phase 1 were measured for large steel stresses.
6. A lower damping was found for increasing amounts of reinforcement.
7. The light-weight concrete beams showed a lower damping ability over the entire stress range as the corresponding concrete beams.

The described results show that, contrary to the usual assumptions, the damping ratio as a result of cracking can sink to a very small value after an initial growth. Although this phenomenon appears surprising, it can nevertheless be explained in a physically plausible manner by the still-to-be-described damping models.

4. EXPERIMENTS ON UNREINFORCED CONCRETE TEST BODIES

Numerous experiments for the determination of damping of unreinforced concrete test bodies are described in the literature ([4], [5], [6], [7], [8]). The following influence factors with regard to the damping of unreinforced concrete are considered:

- Water content of the concrete
- Age of the concrete
- Cement content of the concrete
- Frequency
- Level of stress

Many experimental investigations have shown that the cement content and the frequency have an insignificant influence on the damping. In addition it can be established that for small stresses ($\sigma_b < \beta_w/2$), the stress level has practically no influence on the damping properties. However, the water content and, coupled with it, the age of the concrete play a major role in the damping. Greater water contents lead in general to larger damping. In [9], a damping ratio for water saturated specimen of $\xi = 0.6$ to 2.0%, for partially saturated specimen of $\xi = 0.9$ to 1.8%, and for dry specimen of $\xi = 0.2$ to 0.4% are indicated. With increasing age of the concrete the damping in general initially decreases, possibly due to progressive drying. After three to four weeks drying time, however, the influence of the age of the concrete ceases to be significant.

5. THEORETICAL FOUNDATIONS

For the description of the damping properties of a material respectively a construction, two characteristic values can be appropriately defined ([10], [11]):

- The damping energy dissipated per vibration cycle.
- The relationship between the damping energy and the maximal strain energy.

The total damping energy D_o is the energy which is dissipated in the entire test body respectively the entire construction during one vibration cycle [Nm/cycle]. The total damping energy D_o can be calculated from the specific damping energy D by integration over the volume V of the test body

$$D_o = \int_V D \cdot dV \quad . \tag{1}$$

The specific damping energy D is that energy which is dissipated within a volume element respectively a volume at a definite point in the test body during a vibration cycle [Nm/cycle]. Under a linear (uniaxial) stress condition, D can in general be determined from the equation

$$D = d \cdot \left(\frac{\sigma}{\beta_p}\right)^n \tag{2}$$

where d = specific damping coefficient [N/mm^2]
σ = the maximal stress upon the volume element during the vibration
β_p = cylinder strength of the concrete
n = damping exponent.

Empirically, the value of n for low stresses lies between 1.0 and 3.0. For high stresses, however, n can be substantially greater than 3.0. It can be shown that the familiar models for the representation of the damping behavior are contained in this equation. For example, the value $n = 2$ corresponds to viscous damping and the value $n = 1$ corresponds to friction damping with constant frictional force (see [3]).

The specific damping energy D is the most fundamental of all the known used damping values since it is dependent only on the material studied and is not in-

fluenced by the form and the volume of the body or the existing stress distribution.

The maximal strain energy W respectively W_o of a volume element respectively of an elastic body under a linear (uniaxial) stress condition can be calculated from the equation

$$W = \frac{1}{2} \cdot \frac{\sigma^2}{E} \cdot dV \quad , \quad \text{respectively} \quad W_o = \frac{1}{2} \cdot \int_V \frac{\sigma^2}{E} \cdot dV \tag{3}$$

where σ = maximum stress upon the volume element during the vibration
E = modulus of elasticity.

From the relationship of the damping energy D respectively D_o to the maximum strain energy W respectively W_o, the damping ratio ξ of the material respectively of a volume element and the damping ratio ξ_o of the entire test body can be calculated from

$$\xi = \frac{D}{4 \cdot \pi \cdot W} \quad , \quad \text{respectively} \quad \xi_o = \frac{D_o}{4 \cdot \pi \cdot W_o} \quad . \tag{4}$$

The damping ratio corresponds to the percent total of the maximum strain energy respectively vibration energy which is dissipated through damping during every vibration period. In general the relationship

$$\xi^{el} \neq \xi$$

is true because the damping energy D_o is determined not only by the material properties but also by the form of the test body and the stress condition.

For the calculation of a vibrator with one degree of freedom and nonlinear damping properties (no viscous damping), the so-called equivalent viscous damping is very frequently introduced. This makes it possible to simplify for calculation the damping properties of such a vibrator by a linear vibrator with viscous damping. The energy dissipation of the nonlinear vibrator is replaced by the equivalent viscous damping of the linear vibrator, with the equivalent viscous damping ratio ξ_{eq} of the linear vibrator so chosen that both vibrators dissipate the same energy D_o per vibrator period. For known damping energy D_o and strain energy W_o, the equivalent viscous damping ratio ξ_{eq} can be calculated from Equation (4).

The use of the damping ratio ξ for dynamic calculations has the following advantages:

- ξ can be quickly established by simple tests.
- The damping is not dependent on the frequency of vibration (experimentally confirmed).
- The solution of the differential equation of vibration becomes especially simple.

6. PROCEDURE FOR THE DEVELOPMENT OF A DAMPING MODEL FOR A REINFORCED CONCRETE BEAM

Most uncracked and cracked zones for a reinforced concrete beam can appear during service condition. Therefore, since the crack condition of the beam has a very strong influence on its damping properties, the procedure for the development of a damping model was chosen according to the following basic ideas:

- First only small pieces of the beam, each consisting of either a cracked or an uncracked bending element, were considered. A damping model for each of these bending elements was defined.

- A complete reinforced concrete beam is built-up from a number of both cracked and uncracked bending elements, the exact number of each depending on the crack condition (see Fig. 5). Thus, the damping model for the complete beam can be found through suitable superposition of the damping properties of the separate bending elements.

This procedure has the following advantages:

- The influence of the different stresses along the length of the beam can be considered.
- The bond properties, which are important for the damping, can be included.
- By summation of the damping energy for the single bending elements, the damping energy for a totally uncracked, partially cracked or totally cracked beam can be determined.

Using the damping model for a bending beam, the experimentally determined results of [1] must be able to be explained. As a foundation for the damping model for an entire beam, the damping models for a bending element must be able to show the causes of the influence of

- crack growing
- amplitude respectively stress level
- reinforcement content

on the damping of normally-reinforced and also, if possible, prestressed concrete and light-weight concrete beams.

7. DAMPING MODEL FOR AN UNCRACKED BENDING ELEMENT

Fig. 2 shows the damping model for an uncracked bending element. It consists of one damping element with linear viscous damping, which contains the energy dissipated in the concrete bending compression zone as well as in the concrete bending tension zone. The energy dissipated in the reinforcement through stress under the yield level is comparatively small and is there neglected. The main reason for the use of the viscous damping model was that, in agreement with the conducted tests on the unreinforced concrete test bodies as well as those on fully-prestressed uncracked concrete beams, a damping ratio independent of the height of the stress can be obtained (n = 2, ξ = const.; see Eq. (4)).

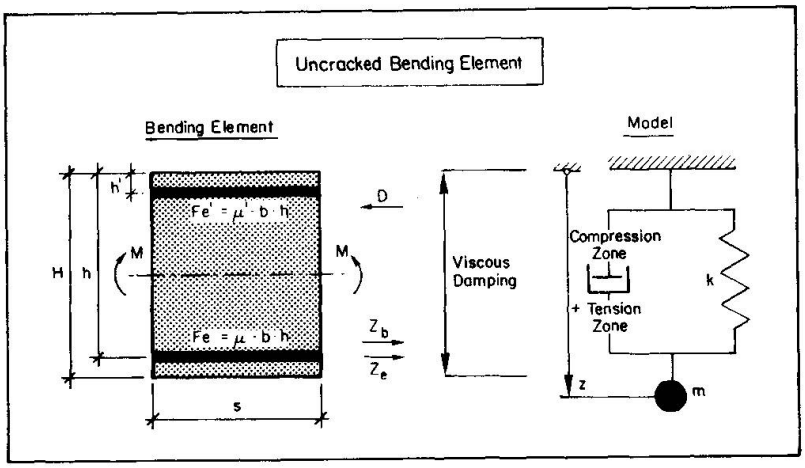

Fig. 2 Damping Model for an Uncracked Bending Element

It is accepted in the following that an equal amount of energy is dissipated by equal-sized tension and compression stresses, so that both tension zone and compression zone contribute the same amount to the energy dissipated in a symmetrically reinforced beam. From Eqs. (1) and (2) with n = 2, the energy $D^{el}_{o,VD}$ dissipated in an uncracked bending element (length s, width B, height H) through viscous damping (VD) can be calculated by integration over the entire volume of the bending element. After the calculation of the maximum strain energy W^{el}_{o} collected

in the bending element, the damping ratio ξ_{VD}^{el} of the uncracked bending element corresponding to Eq. (4) can be calculated from

$$\xi_{VD}^{el} = \frac{d \cdot E_b}{2 \cdot \pi \cdot C_o \cdot \beta_p^2} \qquad (5)$$

with $$C_o = 1 + 3 \cdot n \cdot \frac{h}{H} \cdot (\mu + \mu') \cdot \left(\frac{\frac{H}{2} - h'}{\frac{H}{2}} \right)^2$$

$$n = \frac{E_e}{E_b} \quad .$$

The damping ratio ξ_{VD}^{el} is independent from the level of the stress and is determined besides the modulus of elasticity E_b and the cylinder strength β_p of the concrete mainly through the specific damping coefficient d. This coefficient depends on the material and must therefore be experimentally determinded. The reinforcement ratio μ respectively μ' is considered in the coefficient C_o. Its influence on the damping ratio ξ_{VD}^{el} is relatively negligible.

8. DAMPING MODEL FOR A CRACKED BENDING ELEMENT

Fig. 3 shows the damping model for a cracked bending element. It is a combined damping mechanism, consisting of two damping elements connected in parallel to a spring element. With the linear viscous damping of the first damping element, the portion of the damping which was established in all tests to be independent of the level of stress can be considered (see Fig. 1). The friction damping of the second element carries that portion established to be dependent on the level of the amplitude respectively the stress and the reinforcement ratio. Of the current models used for the consideration of damping, only the friction damping model is capable of explaining the reduction of the damping ratio for growing stress (n = 1, $\xi \sim 1/\sigma$, see Eq. (4)).

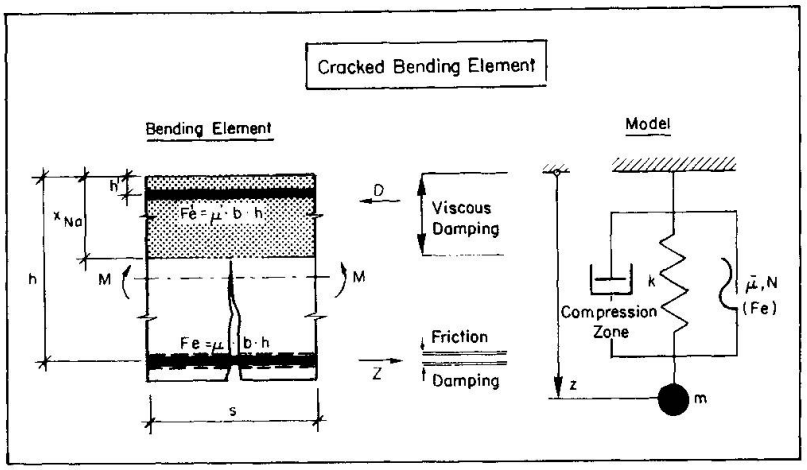

Fig. 3 Damping Model for a Cracked Bending Element

In the following it shall be shown that the assumptions of energy dissipation through friction damping for a cracked beam are fulfilled, in particular the existence of a normal force respectively a friction force and a corresponding displacement.

In the literature, a supposed friction damping is frequently explained by friction between the edges of the cracks. This statement is, however, too superficial. As long as the edges of the crack move in a direction perpendicular to the crack (opening and closing of the crack), no friction force can exist in the crack. The friction damping can exist, however, at the bond respectively the contact area between the concrete of the tension zone and the tension reinforcement.

8.1 Bond Between Reinforcement and Concrete

The bond relationship for ribbed reinforcement has been thoroughly described,

exemples being [12], [13] and [14]. It has been successfully established that the transfer of the tension forces from the reinforcement to the concrete has two results. First, there are radial stresses σ_r working perpendicular to the reinforcement axis and causing a tension ring stress σ_{rz} in the concrete. Second, the reinforcement experiences a displacement v relative to the concrete.

Fig. 4 shows how the rib force P_R of the reinforcement is taken up by the concrete through compression and tension forces (corresponding to σ_r and σ_{rz}).

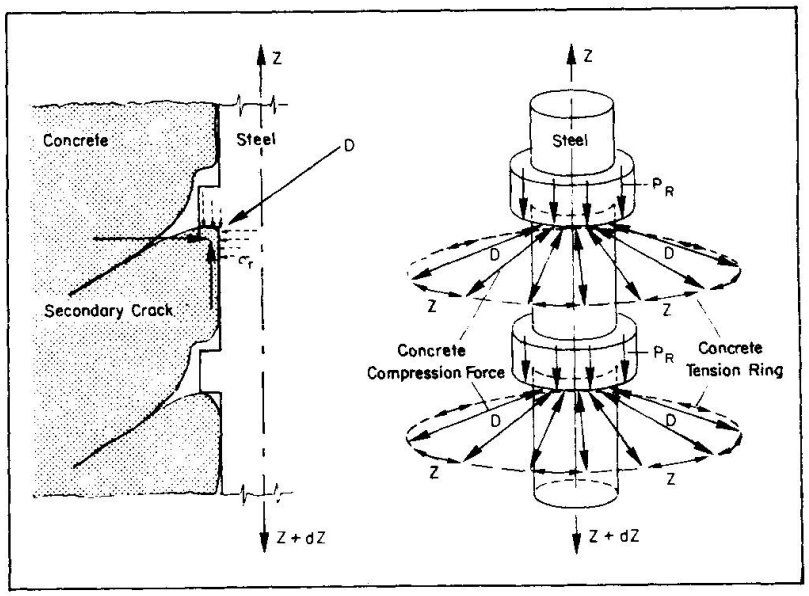

Fig. 4 Spreading of the Bond Stresses τ_v, resp. Ribbing Forces P_R

As a result of the load by the rib force P_R, cracks (secondary cracks) are developed in the surrounding concrete near to every rib. These cracks determine the inclination of the compression force D and consequently the size of the radial stress σ_r. The cracks are in general not visible on the surface of the concrete.

The bond stress τ_v is a hypothetical value with which the effective existing forces between the reinforcement rib and the concrete as well as the friction forces between the steel and the covering concrete can be simplified and included. In [12] are given theoretical relationships as well as a relationship experimentally determined for small bodies concerning the bond stress τ_v and the displacement v of the reinforcement relative to the concrete (bond law). Using these relationships, the distribution of the bond stress τ_v can be calculated, and therefore also the radial stress σ_r and the relative displacement v along the reinforcement axis. Using the now assumed-to-be-known distribution of the bond stress τ_v respectively the radial stress σ_r and the relative displacement v along the reinforcement axis, the friction force F_{FD} on the bending element and the corresponding relative displacement v and from these the energy dissipated through friction damping can be calculated.

8.2 Energy Dissipation through Viscous Damping

In contrast to the uncracked bending element (see Fig. 2), only the bending compression zone shall dissipate energy appropriate to the viscous damping model. The energy dissipated through viscous damping in the bending tension zone and the reinforcement shall be neglected, since the contribution of the bending tension zone to the damping energy, due to its comparatively smaller stresses, is significantly smaller than the contribution of the bending compression zone (see Eq. (2)). The damping energy $D^{el}_{o,VD}$ can now be calculated from Eq. (1) by integration over the volume of the bending compression zone. After determination of the strain energy W^{el}_o, the damping ratio ξ^{el}_{VD} as a result of viscous damping becomes

$$\xi^{el}_{VD} = \frac{6 \cdot E_b}{3 \cdot 4 \cdot \pi} \cdot \frac{d \cdot B \cdot x_{Na} \cdot s \cdot \sigma_b^2}{c_1 \cdot B \cdot x_{Na} \cdot s \cdot \sigma_b^2 \cdot \beta_p^2} = \frac{d \cdot E_b}{2 \cdot \pi \cdot c_1 \cdot \beta_p^2} \qquad (6)$$

with $$C_1 = 1+3\cdot n\cdot\mu\cdot h\cdot\frac{(h-x_{Na})^2}{x_{Na}^3} + 3\cdot n\cdot\mu'\cdot h\cdot\frac{(x_{Na}-h')^2}{x_{Na}^3} \quad .$$

A comparison of Eqs. (5) and (6) shows that the expressions for viscous damping for an uncracked and a cracked bending element differ only in regard to C_o and C_1.

8.3 Energy Dissipation through Friction Damping

In order to be able to calculate the energy $D^{el}_{o,FD}$ dissipated by friction damping in a cracked bending element,

- the coefficient of sliding friction $\bar{\mu}(x,t)$,
- the normal force $N(x,t)$ respectively the radial stress $\sigma_r(x,t)$,
- the relative displacement $v(x,t)$

between the concrete and the reinforcing steel must be known for all times and locations. However, by using the following assumptions and simplifications, the damping energy $D^{el}_{o,FD}$ can be easily calculated.

- Coefficient of sliding friction $\bar{\mu}$ constant over time and location.
- Linear relationship between bond stress $\tau_v(x,t)$ and radial stress $\sigma_r(x,t)$:

$$\sigma_r(x,t) = A\cdot\tau_v(x,t) \qquad (7)$$

  with A = proportionality factor

- Linear relationship in the cracked cross section between the relative displacement $v_{max}(t)$ (between the reinforcement and the concrete) and the steel stress $\sigma_{e,max}(t)$.
- Independence of the bond stress τ_v respectively the radial stress σ_r from the level of the steel stress respectively the stress (τ_v = const.).

With these simplifications, whose justification is thoroughly discusses in [3], the friction force F^{el}_{FD} for a cracked bending element with j reinforcement bars of diameter ϕ becomes

$$F^{el} = \pi\cdot\phi\cdot j\cdot\bar{\mu}\cdot A\cdot\tau_v\cdot s \qquad (8)$$

The damping energy $D^{el}_{o,FD}$ dissipated through friction damping for a harmonically vibrating bending element can be calculated from

$$D^{el}_{o,FD} = 4\cdot F^{el}_{FD}\cdot v_m \quad . \qquad (9)$$

where v_m = the average relative displacement over the length of the bending element.

Using this equation, the damping ratio ξ^{el}_{FD} as a result of friction damping becomes

$$\xi^{el}_{FD} = \frac{4\cdot F^{el}_{FD}\cdot v_m}{4\cdot\pi\cdot W_o} = \text{constant}\cdot\frac{\sigma_{e,max}}{\sigma^2_{e,max}} \quad . \qquad (10)$$

Since the average relative displacement corresponding to the stated simplification increases linearly with the steel stress, the damping ratio ξ^{el}_{FD} is inversely proportional to the steel stress. It can be shown that the crack interval s (that is the length of the bending element) has only a small influence on the damping ratio ξ^{el}_{FD}

8.4 Combination of Viscous Damping and Friction Damping

The damping ratio for a cracked bending element corresponds to the sum of the damping energies for viscous damping and friction damping, and is composed of the sum of the damping ratio for viscous damping and friction damping:

$$\xi^{el} = \xi^{el}_{VD} + \xi^{el}_{FD} \tag{11}$$

$$\xi^{el} = \frac{d \cdot E_b}{2 \cdot \pi \cdot C_1 \cdot \beta_p^2} + \frac{6 \cdot n^2 \cdot E_b \cdot \bar{\mu} \cdot A \cdot j \cdot \phi \cdot \tau_v}{C_2 \cdot B \cdot h} \cdot \frac{v_m(\sigma_{e,max})}{\sigma^2_{e,max}}$$

with $$C_2 = \frac{x_{Na}^3}{3 \cdot h \cdot (h - x_{Na})^2} + n \cdot \mu + n \cdot \mu' \cdot \left(\frac{x_{Na} - h'}{h - x_{Na}}\right)^2 .$$

9. DAMPING MODEL FOR A REINFORCED CONCRETE BEAM

Fig. 5 shows a partially cracked, simply-supported reinforced concrete beam.

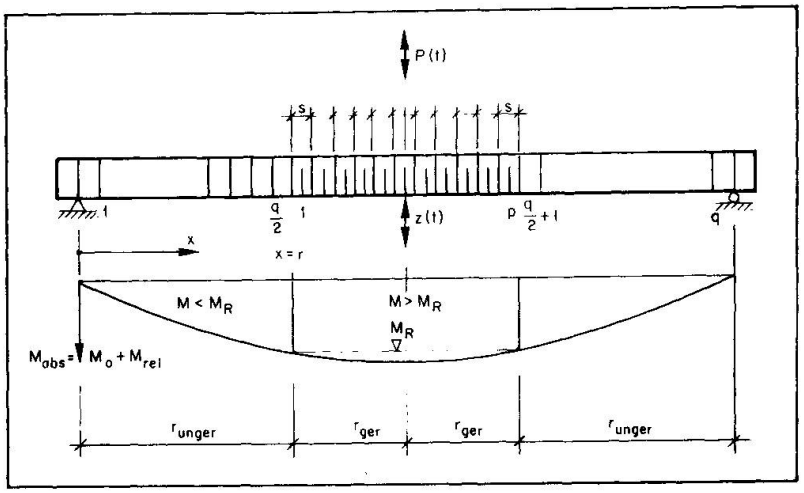

Fig. 5 Partially-Cracked Reinforced Concrete Beam

With the shown bending moment, the cracks due to bending will appear first in the center of the beam. These cracks can be represented by a corresponding number of uncracked (q) and cracked (p) bending elements which depend upon the crack condition of the beam. The damping properties of each uncracked and cracked bending element can be determined with help of the previous section. The damping model for the entire beam is then obtained by a suitable summation of the damping properties of each bending element. Following as an example the damping properties of a simply-supported beam (see Fig. 5) are calculated.

The damping ratio ξ for a perfectly cracked beam ($r = \ell/2$) can be calculated from

$$\xi = \xi_{VD} + \xi_{FD}$$

$$\xi = \frac{d \cdot E_b}{2 \cdot \pi \cdot C_1 \cdot \beta_p^2} + \frac{24 \cdot n^2 \cdot \bar{\mu} \cdot A \cdot j \cdot \phi \cdot E_b \cdot \tau_v}{\pi \cdot h \cdot B \cdot C_2} \cdot \frac{v_m(\sigma_{e,d})}{\sigma^2_{e,d}} \tag{12}$$

where $\sigma_{e,d}$ = maximum steel stress in the middle of the beam.

Fig. 6 shows the damping ratio ξ as a function of the amplitude z respectively the steel stress $\sigma_{e,d}$. The first term is independent of the level of the steel stress respectively stress. The second term is inversely proportional to this steel stress due to the linear relationship between the relative displacement v and the steel stress σ_e. For small dynamic amplitudes respectively stresses, the damping ratio will be relatively large. For growing amlitudes respectively stresses, the damping ratio ξ will approach the damping ratio ξ_{VD} due to the viscous damping.

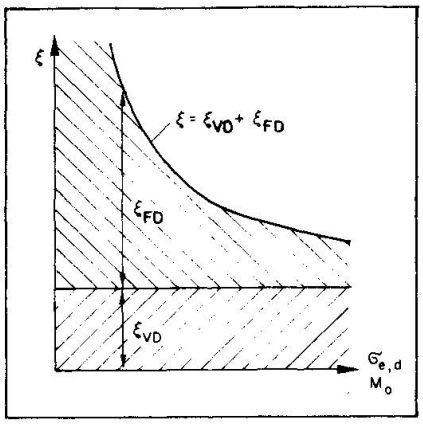

Fig. 6 Damping Ratio ξ as a Function of the Stress for a Fully-Cracked Reinforced Concrete Beam

An uncracked beam (r = 0) dissipates energy only through viscous damping, which makes the damping ratio ξ_{VD} relatively small. Raising the bending stress over the crack moment M_R results in a very quick formation of numerous cracks, beginning in the beam middle. Every increase in the number of cracked bending elements results in a increase in the number of elements with friction damping. This effect causes initially a sharp increase in the damping ratio $\xi = \xi_{VD} + \xi_{FD}$. The growth of the cracked zone slows with further increasing stresses. If the friction force F_{FD} for increasing stress continues to slowly increase, the damping ratio ξ_{FD} will fall after reaching a maximum value. This effect appears since the influence of the amplitude-dependent friction damping (see Eq. 10)) overweighs the influence of the growing friction force.

10. NUMERICAL VALUES AND COMPARISON WITH EXPERIMENTAL RESULTS

It shall now be shown that the described damping model for uncracked and cracked bending elements respectively an entire reinforced concrete beam can be correctly applied to show the real relationships in experimentally tested beams.

10.1 Basic Parameters

a) Viscous Damping

The analysis of numerous reinforced concrete beams and concrete specimens brought the result that the damping ratio ξ_{VD}^{el} for concrete and light-weight concrete can be established in practically all cases as follows:

$$\begin{aligned} &\text{Normal concrete} && : && \xi_{VD} = 0.006 \\ &\text{Light-weight concrete with aggregates of expanded clays} && : && \xi_{VD} = 0.005 \end{aligned} \qquad (13)$$

In these statements, the influence factors for the damping relationships of unreinforced concrete respectively light-weight concrete, namely
- the water content
- the age

although described as important, are not taken into account. This simplification may be made in designed construction, which includes nearly all structures for which a dynamic analysis must be made, for the following two reasons. First, most concretes respectively light-weight concretes used have similar water-cement ratios (0.45 to 0.50). Second, the age of the concrete noticably influences the damping properties only in the first weeks following placement.

b) Friction Damping

A large degree of uncertainty exists concerning the size of the coefficient of sliding friction $\bar{\mu}$ and the proportionality coefficient A (see Eq. (7)). The product $\bar{\mu} \cdot A$ for the test beams described in [10] can be determined with help of Eq. (8). The value for the product $\bar{\mu} \cdot A$ varies for all test beams within the small range of

$$0.01 \leq \bar{\mu} \cdot A \leq 0.03 \quad . \qquad (14)$$

This means that the friction force F_{FD} produced by the steel used in these experiments (Torstahl) amounts to between 1% and 3% of the average force transferred from the steel to the concrete due to the bond stress. Additionally it can be established that the product $\bar{\mu}\cdot A$ would become smaller for increasing test duration. It appears that the coefficient of sliding friction $\bar{\mu}$ decreases with time due to the large number of load changes and the high stress changes.

10.2 Comparison of the Results of the Damping Model with the Experimental Results

As an example, the damping properties of beam B3 (see [1]) due to the described damping model will be compared to the corresponding test results. The detailed procedure and the derivation of the theoretical results are described in [3].

For $\xi_{VD} = 0.006$ and $\bar{\mu}\cdot A = 0.015$, the amplitude-dependent damping ratio ξ becomes

$$\xi = \xi_{VD} + \xi_{FD} = 0.006 + 0.0572\cdot\frac{1}{z_o} \quad . \tag{15}$$

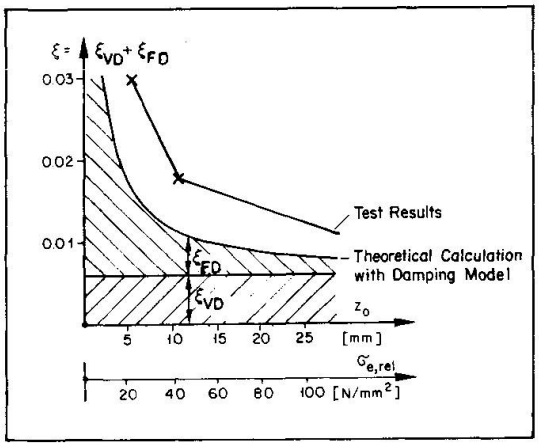

Fig. 7 Test Beam B3, Damping Ratio ξ as a Function of Amplitude z_o

The resulting course of ξ as a function of the amplitude z_o obtained from Eq. (15) is shown in Fig. 7.

The comparison of these results with the experimental results (also shown in Fig.7) shows a good agreement between experiment and theory.

Fig. 8 shows in solid lines the resonance curves developed during a stress level with rising and falling applied frequencies.

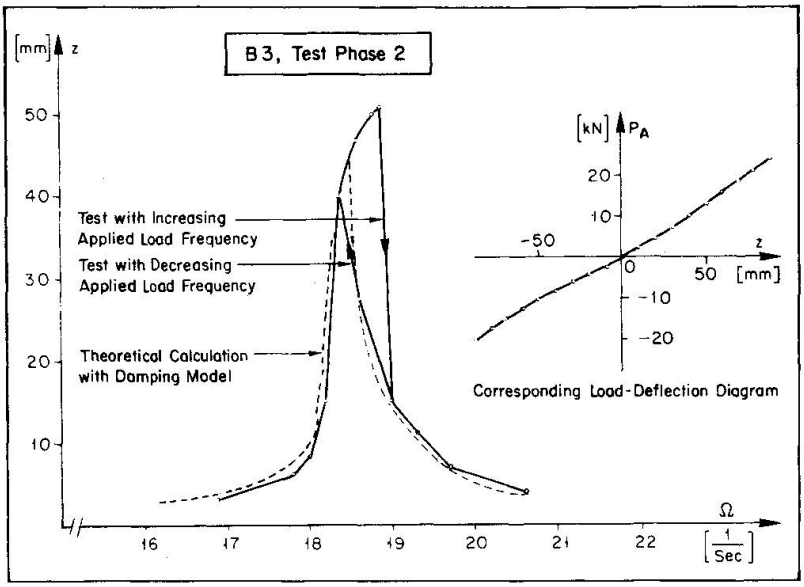

Fig. 8 Test Beam B3, Comparison of a Theoretically Calculated Resonance Curve (F_{FD} = const., indicated Load-Deflection Diagram) with Test Results

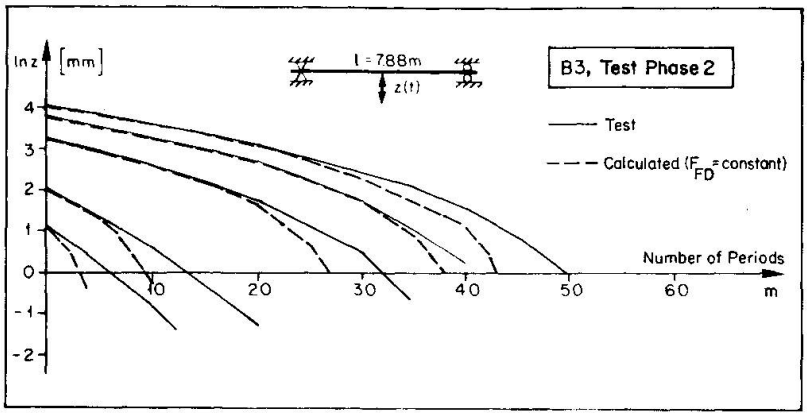

Fig. 9 Test Beam B3, Amplitudes for various Free Vibration Tests, Test Results and Theoretically Calculated Results (F_{FD} = constant)

Fig. 9 shows through solid lines the amplitudes established by numerous tests. On the abscissa is the number of vibration periods m, and on the ordinate is the logarithm of the maximum amplitude z achieved by free vibration test after m periods.

Also shown in Figs. 8 and 9 through dashed lines are the amplitudes calculated for a constant friction force F_{FD} (see Eq. (8)).

A comparison of the corresponding lines shows that the calculated amplitudes agree very well with the experimental results.

It is shown in [3] that by using the effective course of the bond stress τ_v calculated due to the differential equation of bond, that is by using $F_{FD} \neq$ const., a still better agreement between the experimental and the theoretical results can be achieved.

11. LIMITS OF APPLICATION

The previously described damping model may not be used in the dynamic analysis of the following cases without further testing:

a) For very high stresses of the concrete (i.e. $\sigma_b > \beta_w/2$) and the reinforcement steel (i.e. $\sigma_e > 0.7 \cdot \sigma_{e,2.0}$), an important portion of the total damping energy is dissipated by hysteretical damping (energy dissipation through nonlinear material relationships) which is not considered by the damping model. The damping can amount to a multiple of the damping for small stresses.

b) The damping model was developed for use with normally reinforced concrete beams, but is also persumed allowable for use with partially-prestressed and cracked concrete beams. The experimental justification is not considerable, however.

c) Depending on the statical system, the type of supports and the building site, the not included system damping can have an important or even a dominating effect on the total damping of a structure. Most significantly, very stiff structures with fixed supports can have a very large system damping. On the contrary, it appears that thin structures with hinged supports and low-friction rollers or sliding supports show almost no material damping.

d) For a concrete structure which is predominately stressed by shear and torsion, a damping relationship analogous to that for bending stress is expected. It is also supposed for the case that the total material damping will be composed partly of viscous damping and partly from friction damping. The friction damp-

ing can again be limited mainly to the friction between the stirrups respectively the longitudinal reinforcement and the surrounding concrete. However, a displacement in the direction of the shear crack appears in addition to the movement perpendicular to the crack edges. Due to the interlocking of the crack edges, the shear resistance can on the one hand be increased. On the other hand, it is also now possible that due to the relative displacement of the interlocked and no longer stress-free crack edges, energy can be dissipated by friction damping.

REFERENCES

1 Dieterle R., Bachmann H.: "Versuche über den Einfluss der Rissbildung auf die dynamischen Eigenschaften von Leichtbeton- und Betonbalken", Institut für Baustatik und Konstruktion, ETH Zürich, Versuchsbericht Nr. 7501-1, Birkhäuser Verlag Basel und Stuttgart, Dezember 1979.

2 Dieterle R., Bachmann H.: "Einfluss der Rissbildung auf die dynamischen Eigenschaften von Leichtbeton- und Betonbalken", Schweizer Ingenieur + Architekt, 98. Jahrgang, Heft 32/80, 7.8.1980.

3 Dieterle R.: "Modelle für das Dämpfungsverhalten schwingender Stahlbetonträger im gerissenen und ungerissenen Zustand", ETH Zürich, Dissertation Nr. 6768, Institut für Baustatik und Konstruktion, Zürich 1981.

4 Swamy R.N.: "Damping Mechanisms of Cementitious Systems", Chapter 30 in 'Dynamic Waves in Civil Engineering', Wiley Interscience, 1974.

5 Girgrah M., Kesler C.E.: "A Study of the Rheological and Damping Properties of Concrete", Theoretical and Applied Mechanics, Report No. 173, University of Illinois, Urbana, Ill., 1960, p 53 ff.

6 Jones R.: "The Effect of Frequency on the Dynamic Modulus and Damping Coefficient of Concrete", Zement-Kalk-Gips, Nr. 7, 1958, p. 321-322.

7 Ehlers G.: "Das Elastizitätsmass des Betons bei Schwingungen", Beton und Eisen, Heft 20, 1941.

8 Kesler C.E., Higuchi Y.: "Determination of Compressive Strength of Concrete by Using its Sonic Properties", Proceedings of ASTM, Vol. 53, 1953, p. 1044.

9 Richards C.W., Radjy F.: "A New Application of Internal Friction to Concrete Research", Materials Research and Standards, Vol. 6, No. 8, August 1966, p. 386-392.

10 Goodman L.E.: "Material Damping and Slip Damping", Chapter 36 in 'Shock and Vibration Handbook', MacGraw-Hill Book Company, Inc., New York, 1961.

11 Lazan B.J.: "Internal Friction, Damping and Cyclic Plasticity", ASTM Special Technical Publication No. 378, 1965.

12 Rehm G.: "Ueber die Grundlagen des Verbundes zwischen Stahl und Beton", Deutscher Ausschuss für Stahlbeton, Heft 138, Berlin, 1961.

13 Martin H.: "Zusammenhang zwischen Oberflächenbeschaffenheit, Verbund und Sprengwirkung von Bewehrungsstählen unter Kurzzeitbelastung", Deutscher Ausschuss für Stahlbeton, Heft 228, Berlin, 1973.

14 Goto Y.: "Experimental Studies on Cracks Formed in Concrete around Deformed Tension Bars", Technology Reports, Tohoku University, Vol. 44, N.1, 1979.

The Damping Behaviour of R/C Cantilever Elements

Le comportement d'amortissement des éléments en porte à faux en béton armé

Das Dämpfungsverhalten von Stahlbeton-Kragträgerelementen

R. FLESCH
Dipl. Ing. Dr. techn.
Bundesversuchs- u. Forschungsanstalt Arsenal
Vienna, Austria

SUMMARY
Based on recent works of the author mathematical models for the calculation of the energy dissipated during one cycle of loading by SDOF-systems, consisting of elasto-dissipative R/C members and a mass, are presented. Material damping as well as hysteretic slip damping between steel and concrete is taken into account. The energy dissipated during one cycle of vibration is calculated and equated to that of an equivalent viscous damping mechanism in order to evaluate an equivalent damping ratio.

RÉSUMÉ
Basé sur des travaux antérieurs l'auteur présente des modèles mathématiques pour la détermination de l'énergie d'amortissement pour une période de vibration. Ce cas est traité en utilisant un modèle très simple composé d'une masse concentrée et une poutre en encorbellement en béton armé. On tient compte non seulement de l'amortissement interne mais aussi du frottement entre béton et acier. A l'aide du bilan d'énergie on obtient des formules de coefficient d'amortissement visqueux equivalent.

ZUSAMMENFASSUNG
Basierend auf vorangegangenen Arbeiten des Autors werden mathematische Modelle zur Berechnung der Dämfungsarbeit pro Schwingungsperiode für Einmassenschwinger, die aus einem Stahlbeton-Kragträger und einer Masse bestehen, aufgestellt. Es werden hierbei die Materialdämpfung sowie die Dämpfung zufolge Reibung zwischen Stahl und Beton berücksichtigt. Nach Aufstellung der Energiebilanz erhält man Gleichungen für äquivalente viskose Dämpfungszahlen.

1. INTRODUCTION

During the last years from a lot of dynamic insitu tests equivalent viscous damping ratios of R/C structures were obtained. Moreover, R/C members were tested by cyclic loading tests or resonance tests e.g. [7,8,12]; giving in some cases empirical formulas for the energy dissipated e.g. [7, 8] . In the author's opinion too less attempts have been made to model damping mechanism. The stresses in a member (magnitude and distribution) are important parameters of damping, which was mentioned earlier by Lazan [5] and Newmark [9]. Recently several damping mechanism active in R/C members (mainly in R/C tension-compression members) were considered in [10,11].

In the case of uncracked members material damping and hysteretic damping due to slip and counterslip in the lead-in areas at the ends of the member were taken into account. For cracked members an additional hysteretic damping mechanism due to slipping in the lead-in areas at both sides of each main crack (total concrete area cracked) was considered. Material damping was modelled by the formulas of Lazan [5]. For the hysteretic damping four different slip models were developed by the author. The basic idea is, that at least a great part of bond is due to slip, which was found by several authors [1,2,3,4], therefore during reloading counterslip must take place, resulting in hysteretic damping. Formulas for two of these slip mechanism are given in capter 2.

In the case of smooth bars bond is nearly completely due to slip, therefore the mathematical slip models work very well. In practice only deformed steels are used, arising the question how far the models can be still used. In the authors opinion the models can be adapted by some additional coefficients. Some estimations about this problem can be found in [10,11]. Dynamic tests are planned by the author to improve the models. The problems are discussed in capter 3 together with restrictions resulting from differences prototype - mathematical model.

In capter 4 the concept is applied to SDOF-systems consisting of an elasto-dissipative R/C cantilever member and a mass. The bending stiffness is assumed to be linear. For any nonlinear bending stiffness the problem could be linearized by the use of the secant stiffness as it was done for the R/C tension-compression members in [10,11]. The system is excited by sinusoidal forces with the maximum force amplitude $\overline{p_o}$ at resonance frequency (for a nonlinear system at the resonance frequency of the equivalent linear system). The energydissipated during one cycle of vibration is calculated and equated to that of an equivalent viscous damping mechanism in order to evaluate an equivalent damping ratio (fraction of critical damping). Formulas for ξ are given for uncracked as well as cracked members. In the second case a simple cracking mechanism is used giving the number of cracks as a function of the maximum force amplitude $\overline{p_o}$.

In capter 5 the results of calculations are discussed.

2. SLIP MECHANISM

Model 4 and Model 3 [10,11] are shortly discussed in what follows. For each of them the energy dissipated during one load cycle with $F_{max} = F$ and $F_{min} = r.F$ (for $1 > r \geq -1$) is evaluated where F is the total spring force . These models are used to simulate the damping in the lead-in areas at the ends of the member as well as at every main crack.

2.1 Model 1, used for R/C tension-compression members

The configuration of the model is similar to that of Panovko, Golzev and Strakhov [6]. The bond stress τ is assumed to be constant over the lead-in length and independent of the load amplitude over the whole load cycle. The steel force after the lead-in length is given by $\bar{k}F\alpha$ and the concrete force by $(1-\bar{k})F\alpha$, where α is the loading parameter $(1 \geq \alpha \geq r)$. The energy dissipated during one cycle of loading is given by

$$D_v = \frac{(1-\bar{k})^2 (1-r)^3}{6\pi d\tau E_s f_s} F^3 = h_1 F^3 \qquad (1)$$

where d is the sum of all steel diameters, f_s the sum of all steel areas and E_s the E-modulus of steel.

2.2. Model 3, used for R/C tension-compression members

Based on an investigation of the test results of Kuuskoski [1] model 3 was developed. The bond stress τ is assumed to be uniformly distributed over the lead-in length and to depend on the load parameter α. Depending on the parameter c of the bondstress - load relationship one can obtain closed as well as open hysteresis loops. Open hysteresis loops will be used in a forthcoming paper. The expression for the energy dissipated during one cycle of loading for arbitrary values of c and r is quite lengthy and can be found in [10]. For closed loops and r = -1 D_v is of the form

$$D_v = \frac{(1-\bar{k})^2 \; 0{,}9096}{\pi d E_s f_s (a+\bar{b}F)} F^3 = h_3^* \frac{F^3}{(a+\bar{b}F)} \qquad (2)$$

and for r = 0

$$D_v = \frac{(1-\bar{k})^2 \; 0{,}1792}{\pi d E_s f_s (a+\bar{b}F)} F^3 = h_3^{*\prime} \frac{F^3}{(a+\bar{b}F)} \qquad (3)$$

where a and b are coefficients of the bond stress - load relationship.

3. APPLICABILITY OF THE SLIP MODELS TO DEFORMED BARS

In the case of deformed bars only a part of the force is transmitted by slip. Thus, the question arises, whether it is possible to separate the two force transmission mechanism slip and normal stresses at the ribs especially during unloading and reloading. Counterslipping could be largely influenced by the ribs. Furthermore local separation of steel and concrete surfaces due to the action of the ribs (mainly at the ends of the bars) take place, which was reported e.g. by Hahn [3] and Lutz [4]. Moreover, local shear cracking of concrete at a cylinder surface with a diameter corresponding to the maximum diameter of the bar (inlcuding the rib height) will produce slipping or sliding between concrete surfaces. The influence of these facts on the damping mechanism must be studied more detailed.

A first investigation of theapplicability of the models to deformed bars was presented in [11], using the test results of Kuuskoski [1]. From two tension-tension loaded samples with the same E-modulus of concrete and smooth steel in the first and deformed steel in the second case the maximum concrete force in the second case is found to be about twice as much as in the first case. Assuming that about half of the force is transmitted by slipping in the case of the deformed bars, it was found that the

permanent steel stresses at the end of each load cycle ($\alpha = 0$) reported in [1] fit the results obtained with model 3 very well. Later, a more detailed investigation of the available data was carried out by the author and was presented in [10]. It is concluded that bond due to slip lies within 30 - 40 % of the total bond. As a first approximation it is assumed that the models can be used for deformed bars. The coefficient $1-\bar{k}$ as well as the bond stress τ is reduced by the factor r_d $(0{,}3 \leq r_d \leq 0{,}4)$. It seems that r_d will be lower for ribbed bars and higher for torsteel bars.
When using the formulas derived in capter 4 the following facts should be considered for smooth bars as well as for deformed bars:
- the equations for τ give probably too high values. In the slip model a free front end of the bar is assumed. In practise there are hooks, bent up's or at least embedments. This fact tends to reduce the hysteretic loops coefficient r from r = -1 to r = 0.

- the coefficient $(1-\bar{k})$ as well as the bond stress τ decreases with increasing number of load cycles. If the decrease ratio of $(1-\bar{k})$ squared is less than the decrease ratio of τ then the energy dissipated will decrease with increasing number of load cycles. A decrease of τ was considered in model 4 [10,11]. Results of calculations with an improved model will be shown in a forthcoming paper.
- the influence of stirrups on slip and counterslip must be investigated.
- it seems probable that the contribution of slip mechanism to the total damping will decrease if the yield point of steel is approached.

4. DAMPING OF R/C CANTILVER MEMBERS

The concept of [10,11] is now applied to the system shown in Fig. 1. Possible influences of curvature on slip and counterslip are neglected. The equations are derived for symmetrical longitudinal reinforcement. It is assumed that no slip will occur at the fixed end.

4.1. Damping without cracks

The total force in the compression- and the tension area of cross section E-E is given by

$$\alpha F = \frac{p_o \, l \left[\frac{1}{4} + \frac{2\left(\frac{h}{2} - h^{x}\right)\bar{n}\mu^{*}}{h} \right] \alpha}{\left[\frac{1}{6} + \frac{4\left(\frac{h}{2} - h^{x}\right)^{2}\bar{n}\mu^{*}}{h} \right]} = \alpha \frac{p_o \, l \, c_1}{c_2} \qquad (4)$$

The steel force is of the form

$$\alpha F_s = \frac{2\left(\frac{h}{2} - h^{x}\right)\bar{n}\,\mu^{*} p_o \, l \, \alpha}{h c_2} \qquad (5)$$

The parameters h^{x}, $\bar{n}$, h and μ^{*} are defined in Fig. 1.
It is assumed that F_s is transmitted from concrete to steel by bond stress acting over the length l and that bond due to slip is within 30 - 40 % of the total bond $(0{,}3 \leq r_d \leq 0{,}4)$. The bond stress τ now follows as

$$\tau = \frac{2\left(\frac{h}{2} - h^{x}\right)\bar{n}\mu^{*}p_{o}\,r_{d}\,\alpha}{hc_{2}\,d\,\pi} = \bar{b}F\alpha \qquad (6)$$

For model 3 in [11] τ was of the form

$$\tau = a + \bar{b}F\alpha \qquad (7)$$

Therefore now model 3 is used with $a=0$. As force is transmitted from concrete to steel, $(1-\bar{k})$ is given by

$$(1-\bar{k}) = \frac{F_{s}\,\alpha}{F\,\alpha} = \frac{2\left(\frac{h}{2} - h^{x}\right)\bar{n}\,\mu^{*}r_{d}}{hc_{1}} \qquad (8)$$

From equ. (4) and equ. (6) $\bar{b}$ now follows as

$$\bar{b} = \frac{2\left(\frac{h}{2} - h^{x}\right)\bar{n}\,\mu^{*}r_{d}}{hdlc_{1}\pi} \qquad (9)$$

In equ. (2) E_s is now replaced by the E-modulus of concrete, E_c, and f_s by $bh/2$. Then equ. (4), equ. (8) and equ. (9) are inserted in equ. (2). Two mechanism, each equivalent to the half of the slip damping of R/C tension-compression members take place simultaneously (in the compression and the tension area of the member). Thus, the energy dissipated during one cycle of load by slip damping is given by

$$D_{v} = \frac{3{,}6384\left(\frac{h}{2} - h^{x}\right)\bar{n}\,\mu^{*}c_{1}\,p_{o}^{2}\,l^{3}\,r_{d}}{c_{2}^{2}\,h^{2}\,bE_{c}} = h_{o}\frac{\bar{p}_{o}^{2}}{4\xi^{2}} = h_{o}^{*}M^{2} \qquad (10)$$

where M is the bending moment $p_o l$. In another approach the total force in cross section E-E is obtained using the net section of concrete. αF is given by

$$\alpha F = \frac{3p_{o}\,l}{2h}\alpha \qquad (11)$$

It is assumed that a part of this force is transmitted to steel by slip resulting in the same expression for $(1-\bar{k})$ than given by equ. (8). Assuming a linear bending stiffness $K = 3E_c I/l^3$ with $I = bh^3/12$, without material damping the equivalent damping ration is given by

$$\xi = \frac{0{,}4548\left(\frac{h}{2} - h^{x}\right)\bar{n}\,\mu^{*}c_{1}\,hr_{d}}{\pi\,c_{2}^{2}} \qquad (12)$$

Material damping of concrete is modelled by the formulas of Lazan [5]. It is assumed that material damping of steel can be neglected below the yield point. The energy dissipated during one cycle of load is of the form

$$D_{s} = \frac{I\alpha_{1}J'\,\bar{k}^{n}F^{n}}{[bh\,(1-\mu)]^{n-1}} = h_{5}F^{n} \qquad (13)$$

where J and n are material constants which must be evaluated from tests. In this paper only rough estimations of these parameters can be used. The coefficient α_L ($\alpha_L \leq 1$) depends on the stress distribution in the member and is defined by Lazan [5]. Due to the uncertainties of J and n $\alpha_L = 1$ is assumed. The total energy dissipated during one cycle of loading is given by

$$D_T = D_V + D_S \tag{14}$$

The total energy dissipated is equated to that of an equivalent viscous damping mechanism. Thus, the damping ratio is given by

$$\xi^{n-2} - \frac{8\pi l^3}{h_6 E_c b h^3}\xi^{n-1} + \frac{4h_s}{h_6}\left(\frac{c_1 l}{2c_2}\right)^n \bar{p}_o^{n-2} = 0 \tag{15}$$

The coefficient n will be within $2 \leq n < 3$. For $2 < n < 3$ equ. (15) has to be solved by an iterative procedure.

4.2. Damping with cracks

The situation is more complex than in the case of R/C tension - compression members [10,11]. Therefore some simplifications are necessary. To show the contribution of cracks to total damping only this mechanism is taken into account in what follows. In Fig. 2 a simple cracking mechanism and the coefficients used are shown. When the concrete force $F_{c,e}$ in cross section E-E has the value

$$F_{c,e} = \frac{p_o l}{4c_2} = F_{c,c}^{\times} \tag{16}$$

in E-E the first crack will occur. $F_{c,c}^{\times}$ is the cracking tensile force of concrete which is given by

$$F_{c,c}^{\times} = \frac{\beta_{c,c}\, bh}{4} \tag{17}$$

where $\beta_{c,c}$ is the bending tension strength of concrete. Using slip model 3 at the instant of cracking the bond stress is of the form

$$\tau = \bar{b}F\alpha = \bar{b}\frac{p_o l c_1 \alpha}{c_2} = 4\bar{b}F_{c,c}^{\times}\, c_1 \alpha \tag{18}$$

Thus, tgß is given by

$$tg\beta = 4\bar{b}F_{c,c}^{\times} d\pi c_1 \alpha \tag{19}$$

tgδ is of the form

$$tg\delta = \frac{F_{c,c}^{\times}}{l} \tag{20}$$

The locations of the following cracks are now obtained under the simplifying assumption, that on one hand τ is constant and is given by equ. (18) with $\alpha = 1$ and on the other hand the lead-in length is constant. The lead in length is given by

$$l_{e,1} = \frac{l}{4\pi d\bar{b}c_1 l + 1} \tag{21}$$

The length l_e^* is of the form

$$l_e^* = \frac{1}{4\pi d\bar{b}c_1} \tag{22}$$

The i-th crack will occur at the location x_i if the concrete force approaches the value $F_{c,c}^{\times}$ in x_i. x_i is given by

$$x_i = l - (i-1)l_e^* \tag{23}$$

The fictive concrete force in cross-section E-E is given by

$$F_{c,i} = \frac{F_{c,c}^{\times} \cdot l}{l-(i-1)l_e^*} \tag{24}$$

The lead-in length is of the form

$$l_{e,i} = \frac{l_i}{4l_i\pi d\bar{b}c_1 + 1} \tag{25}$$

where l_i is given by

$$l_i = l-(i-1)l_e^* \tag{26}$$

The maximum concrete strain for a cracked section is given by

$$\varepsilon_c = \left[2f_s' \bar{n}(\bar{y}-h^{\times})(h-2h^{\times}) + b\bar{y}^2(h-h^{\times}-\frac{\bar{y}}{3})\right]^{-1} \frac{2M(x)\bar{y}}{E_c} \tag{27}$$

The steel tension force of the cracked section is given by

$$F_s^{(II)} = \frac{\varepsilon_c(h-\bar{y}-h^{\times})}{\bar{y}} E_s f_s = u_1 M(x) \tag{28}$$

For the i-th crack the steel force is obtained from

$$F_{s,i}^{(II)} = u_1\left[l-(i-1)l_e^*\right] p_o = u_{2,i}\, p_o \tag{29}$$

where i is an integer number within $0<i\leq n_r$. n_r is the actual number of cracks. The uncracked region starts at the location x_u

$$x_u = l-(n_r-1)l_e^* - l_{e,n_r} \tag{30}$$

At this point the steel force is of the form

$$F_{s,n_r}^{(I)} = \frac{2(\frac{h}{2} - h^{\times})\bar{n}\mu^*}{hc_2}\left[l-(n_r-1)l_e^* - l_{e,n_r}\right] p_o = u_3 p_o \tag{31}$$

The concrete force transmitted by slip is obtained from

$$F_{c,n_r}^{(I)} = \frac{r_d}{4c_2}\left[l-(n_r-1)l_e^* - l_{e,n_r}\right] p_o = u_4 p_o \tag{32}$$

Further, for the region between two cracks the steel force is given by

$$\bar{F}_{s,i}^{(I)} = \frac{2(\frac{h}{2} - h^{\times})\bar{n}\mu^*}{hc_2}\left[l-(i-1)l_e^* - \frac{l_e^*}{2}\right] p_o = u_{5,i}\, p_o \tag{33}$$

and the concrete force transmitted by slip

$$\bar{F}_{c,i}^{(I)} = \frac{r_d}{4c_2}\left[l-(i-1)l_e^* - \frac{l_e^*}{2}\right] p_o = u_{6,i}\; p_o < \frac{F_{c,c}^{\times}}{2} \tag{34}$$

with $0<i\leq(n_r-1)$. Equ. (33) and (34) are only valid for $F_{c,i}^{(I)} < F_{c,c}^{x}/2$. The energy dissipated during one cycle of load at each crack is now calculated by equ. (3) with a = 0. It is assumed that all cracks will close exactly at the instant $\alpha = 0$. Thus, the energy dissipated due to slip at the i-th crack is of the form

$$D_V = \frac{(1-\bar{k}_i)^2 \cdot 0,1792\ F_{s,i}^{(II)2}}{dE_s f_s\ br_a} = \bar{k}_i^{*2}\ h_3 F_{s,i}^{(II)2} \tag{35}$$

For the point $x_u = 1-(n_r-1)l_e^* - l_{e,n_r}$ the coefficient $\bar{k}_{n_r}^*$ is given by

$$\bar{k}_{n_r}^* = \frac{F_{c,n_r}^{(I)} r_a}{F_{s,n_r}^{(II)}} = \frac{u_u}{u_{2,n_r}} \tag{36}$$

For the region between two cracks the coefficient $\bar{k}^*$ is obtained from

$$\bar{k}_i^* = \frac{\bar{F}_{c,i}^{(I)}}{F_{s,i}^{(II)}} = \frac{u_{6,i}}{u_{2,i}} \quad \text{for } F_{c,i}^{(I)} < \frac{F_{c,c}^{x}}{2} \tag{37}$$

and from

$$\bar{k}_i^* = \frac{F_{c,c}^{x}}{2F_{s,i}^{(II)}} = \frac{F_{c,c}^{x}}{2u_{2,i}P_0} \quad \text{for } F_{c,i}^{(I)} > \frac{F_{c,c}^{x}}{2} \tag{38}$$

During a step by step analysis one could check for each point whether equ. (37) or (38) has to be used. To simplify the procedure the following mean values are used:

$$\bar{k}_i^x = \frac{2u_{6,i}\ p_0 + F_{c,c}^{x}}{4u_{2,i}\ p_0} \tag{39}$$

and

$$\bar{k}_i^o = \frac{2u_{6,i}\ p_0 + F_{c,c}^{x}}{4u_{2,i+1}\ p_0} \tag{40}$$

The total energy dissipated during one cycle of loading is given by

$$\sum_i D_{V,i} = 2\left[\left(\frac{u_u}{u_{2,n_r}}\right)^2 h_3 F_{s,n_r}^{(II)2} + \sum_{i=1}^{n_r-1} \bar{k}_i^{x2}\ h_3 F_{s,i}^{(II)2} + \sum_{i=1}^{n_r-1} \bar{k}_i^{o2} h_3 F_{s,i+1}^{(II)2}\right] \tag{41}$$

From the equations (29), (39), (40) and (41) the following equation is obtained

$$\sum_i D_{V,i} = p_0^2\left[(2u_4^2 + \sum_{i=1}^{n_r-1} u_{6,i}^2)h_3\right] + p_0 F_{c,c}^{x}\ h_3 \sum_{i=1}^{n_r-1} u_{6,i} +$$

$$+\frac{(n_r-1)F_{c,c}^{x2}\ h_3}{4} = p_0^2\ v_1 + p_0 v_2 + v_3 = \frac{\bar{p}_0^2}{4\xi^2} v_1 + \frac{\bar{p}_0 v_2}{2\xi} + v_3 \tag{42}$$

Thus, from the energy balance the following equation for the equivalent damping ratio ξ is obtained

$$\xi = \frac{\bar{p}_0}{4v_3}\left(\frac{\bar{p}_0\Pi}{K} - v_2\right) - \sqrt{\left[\frac{\bar{p}_0}{4v_3}\left(\frac{\bar{p}_0\Pi}{K} - v_2\right)\right]^2 - \bar{p}_0^2\ v_1/v_3} \tag{43}$$

where K is the stiffness, $K = 3\ EI/l^3$, and $I = bh^3/12$.
Equation (43) is now solved for increasing n_r starting with $n_r = 0$ until the following equation is valid

$$\frac{\bar{p}_0 \cdot l}{8\xi c_2} < F_{c,i+1} \tag{44}$$

where $F_{c,i+1}$ is given by equ. (24).

5. RESULTS

Results of calculations for cracked as well as uncracked members with deformed bars are given in what follows. First a set of basic dimensions is chosen. The single parameters are varied in Fig. 3-8 for uncracked members and in Fig. 9-17 for cracked members. In some cases ξ is given as a function of two parameters. As in the case of uncracked members it is assumed that force is transmitted from concrete to steel and vice versa in the case of cracked members, the tendencies are different.

uncracked members:

-damping decreases slightly with increasing dimensions h and b of the cross section. The decrease is less when also mat. damping is considered.
-damping increases slightly with increasing steel area
-thus, combining the first two statements, damping increases slightly with increasing percentage of reinforcement
-damping decreases slightly with increasing E-modulus of concrete
-ξ is a linear function of the coefficient r_d
-the coefficient J was evaluated from Lazan [5] and means only a rough assumption
-the coefficient n has a strong influence on damping. In the case of uncracked members it seems that n will be within $2 \leq n \leq 2.2$
-the influence of h^x on damping can be neglected
-$\bar{p}_o$ and l have only an influence on material damping (small for $2 \leq n \leq 2.2$)

It is concluded that ξ is within $0.01 \leq \xi \leq 0.02$ for uncracked members.

cracked members: (slip damping only)

-damping increases strongly with increasing h and b
-damping decreases strongly with increasing steel area
-thus, damping decreases strongly with increasing perc. of reinforcement

The same tendency was observed by Dieterle [12]

-damping increases with increasing E-modulus of concrete
-r_d within $0.3 \leq r_d \leq 0.4$ has only a small influence on the results
-the influence of $\beta_{c,c}$, $\bar{b}$, h^x and l on damping can be neglected
-the influence of $\bar{p}_o$ is shown in Fig. 13. The results show a max. ξ for low force levels which was also observed by Dieterle [12]. In [12] also a strong decrease of for increasing displacement is reported. This could be due to the decrease of $\bar{k}^*_i$ with the number of load cycles. In a fothcoming paper an attempt will be made to simulate this behaviour.

It seems that the values for obtained by equ. (43) are too high in some cases but that Fig. 9-17 show very well the tendencies.

6. CONCLUSIONS

In this paper the concept of [10,11] is applied to SDOF-systems consisting of a R/C cantilever element and a mass. As the situation is more complex than in the case of R/C tension-compression members, additional simplifications are necessary. In the author's opinion the slip models can be adapted for ribbed bars and torsteel bars. First estimations are discussed in capter 3. The author plans tests to improve the modelling for deformed bars as well as to get the parameters of material damping. In capter 4 equations for equivalent viscous damping ratios ξ are derived. If these equations are used, the limitations discussed in capter 3 should be considered. In a forthcoming paper the decrease of bond and of the coefficient $(1-\bar{k})$ will be taken into account as a function of the number of load cycles.

7. REFERENCES

1. KUUSKOSKI, V.: Über die Haftung zwischen Beton und Stahl. Dissertation Technische Hochschule Helsinki, 1950

2. REHM, G.: Über die Grundlage des Verbundes zwischen Stahl und Beton. Deutscher Ausschuß für Stahlbeton, Heft 138, 1961

3. HAHN, V.: Über die Verbundwirkung des Querrippenstahls. Dissertation Technische Hochschule Stuttgart, 1952

4. LUTZ, L.A.: The Mechanics of Bond and Slip of Deformed Reinforcing Bars in Concrete. Dep. of Struct.Eng., Cornell University Report no. 324, 1966

5. LAZAN, B.J.: Damping of Materials and Members in Structural Mechanics. Pergamon Press, New York, 1968

6. GOODMAN, L.E.: A Review of Progress in Analysis of Interfacial Slip Damping. Coll. on Struct. Damping, ASME, 1959

7. HAWKINS, N.M.(editor): Reinforced Concrete Structures in Seismic Zones. ACI Publication SP-53, 1977

8. BERTERO, V.V. (editor): Proceedings of a Workshop on Earthquake Resistant Reinforced Concrete Building Construction. The University of California, Berkeley, 1977

9. NEWMARK, N.M., HALL, W.J.: Seismic Design Criteria for Nuclear Reactor Facilities. Proc. of the 4th WCEE, Santiago, Chile, 1969

10. FLESCH, R.: Das Dämpfungsverhalten schwingender Stahlbetontragwerke. Dissertation TU-Wien, 1980

11. FLESCH, R.: Estimating Damping of Reinforced Concrete Members and Structures. Int. Conf. on Recent Advances in Structural Dynamics, ISVR-Southampton, 1980

12. DIETERLE, R., BACHMANN, H.: Einfluß der Rissbildung auf die dynamischen Eigenschaften von Leichtbeton- und Betonbalken. Schweizer Ingenieur und Architekt, Heft 32/1980

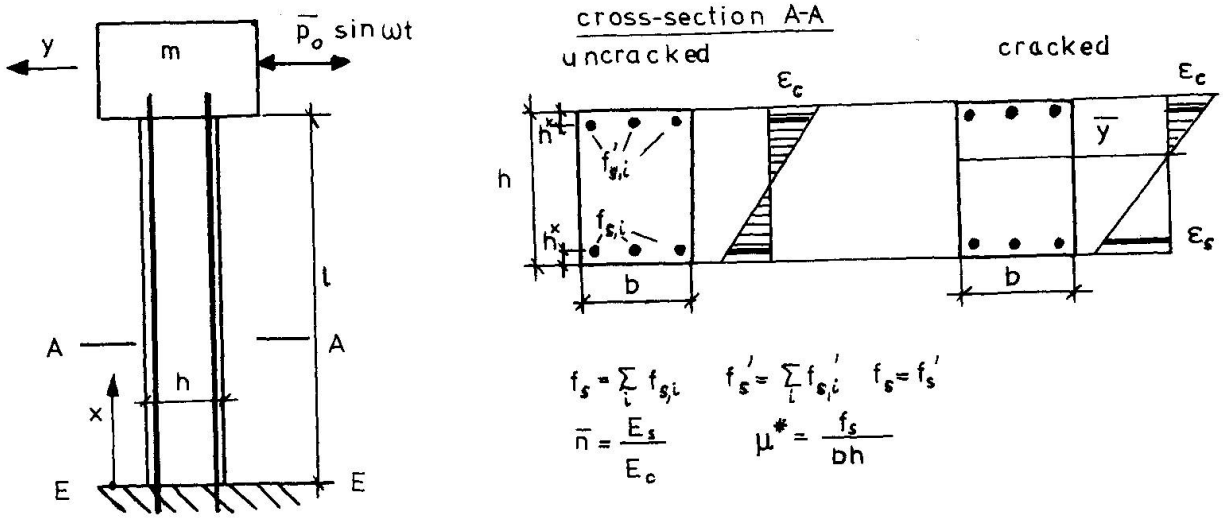
y
m
$\bar{p}_o \sin \omega t$
l
A
A
h
x
E
E
cross-section A-A
uncracked
cracked
ε_c
ε_c
ε_s
h
b
b
$\bar{y}$
$f_s = \sum_i f_{s,i}$
$f_s' = \sum_i f_{s,i}'$
$f_s = f_s'$
$\bar{n} = \frac{E_s}{E_c}$
$\mu^* = \frac{f_s}{bh}$

Fig. 1

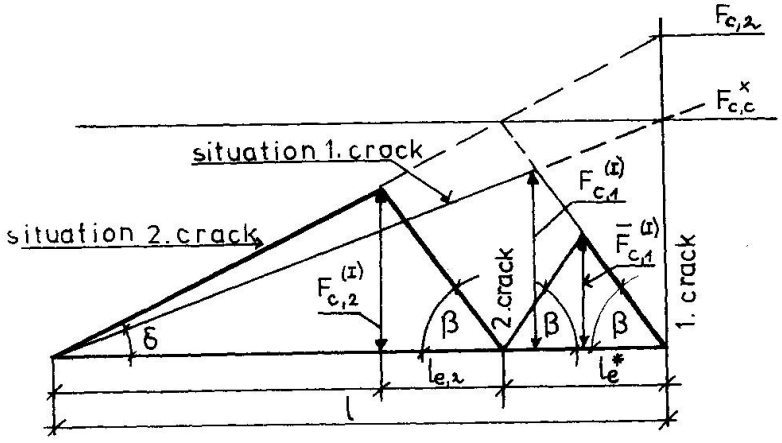
$F_{c,2}$
$F_{c,c}^x$
situation 1. crack
situation 2. crack
$F_{c,1}^{(I)}$
$\bar{F}_{c,1}^{(I)}$
$F_{c,2}^{(I)}$
2. crack
1. crack
β
β
β
δ
$l_{e,2}$
l_e^*
l

Fig. 2

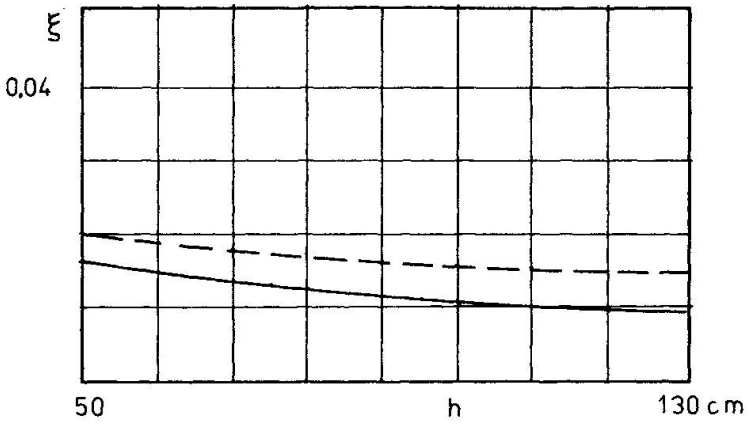

Fig.3
variation of h

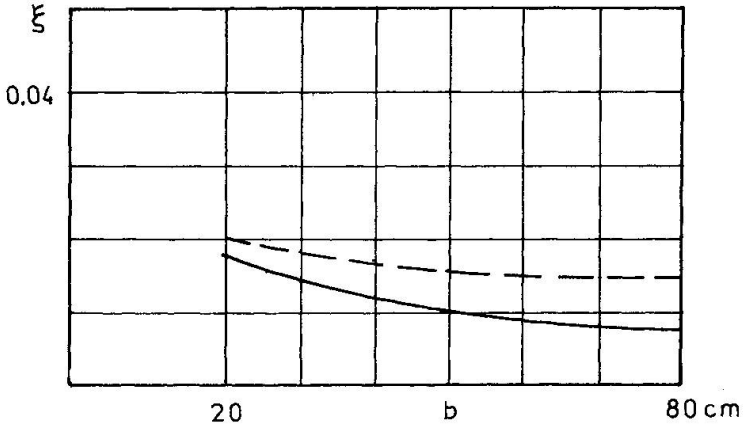

Fig.4
variation of b

<u>uncracked member</u>
basic dimensions:

h =o.9 m
b =0.4 m
E_c=3000 kN/cm^2
5xØ 0.03 m
r_a=0.4
J =3.351 .10^{-9}
n=2
h^x=0.03 m
l= 2.5 m
$\overline{p_o}$=10 kN

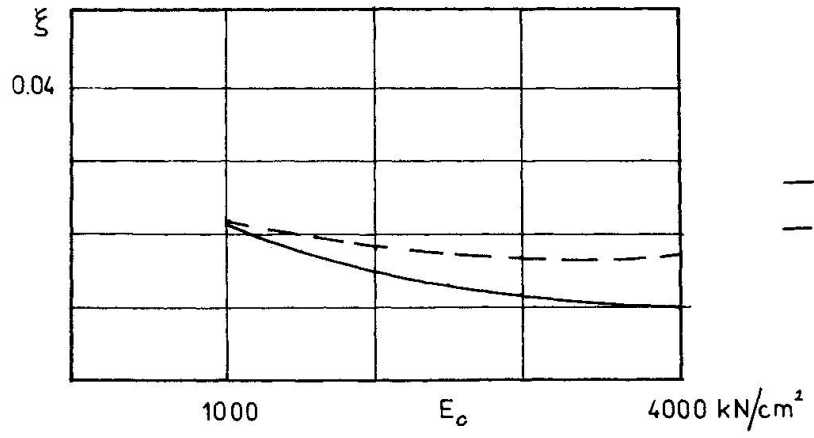

Fig.5
variation of E_c

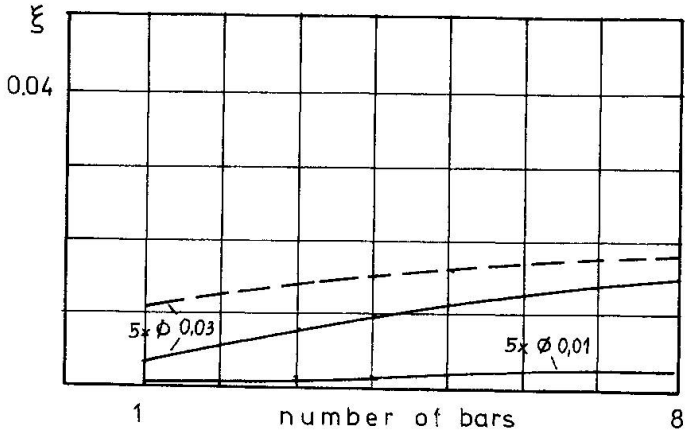

Fig.6
variation of number of bars

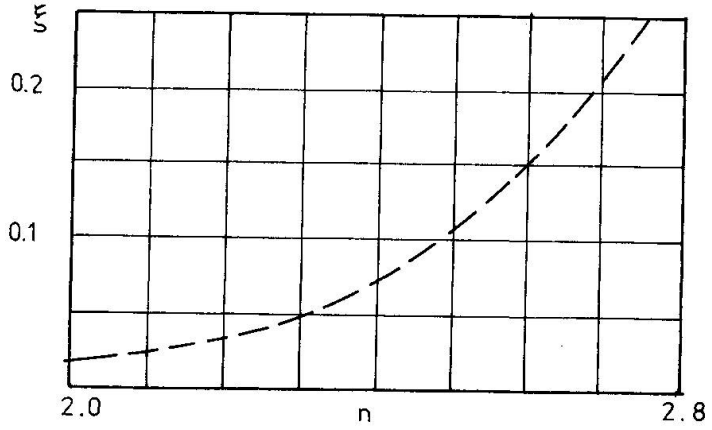

Fig.7
variation of coefficient n

<u>uncracked member</u>

basic dimensions:

h =0.9 m
b =0.4 m
E_c =3000 kN/cm^2
5xØ 0.03 m
r_d =0.4
J =3.351.10^{-9}
n=2
h^x =0.03 m
l =2.5 m
$\overline{p_o}$ =10 kN

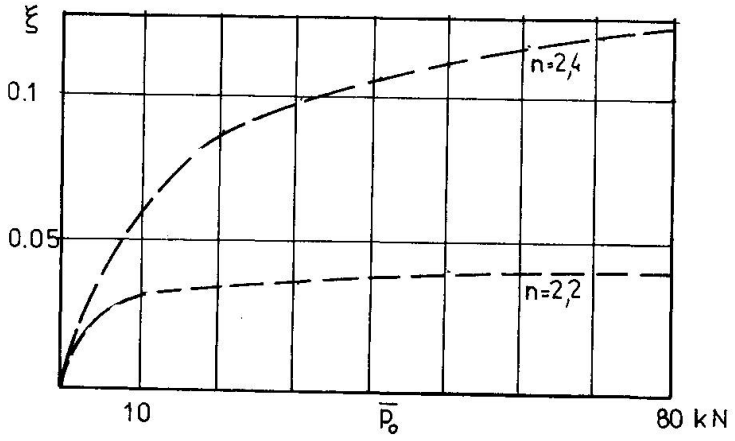

—— slip damping
– – slip +material damping

Fig.8
variation of max.force amplitude

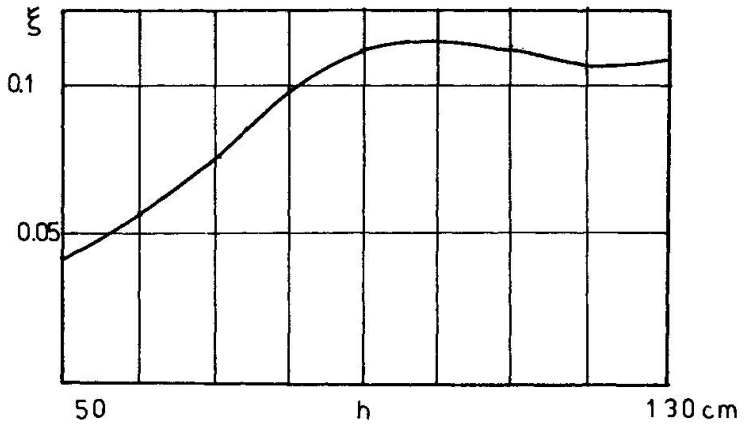

Fig.9
variation of h

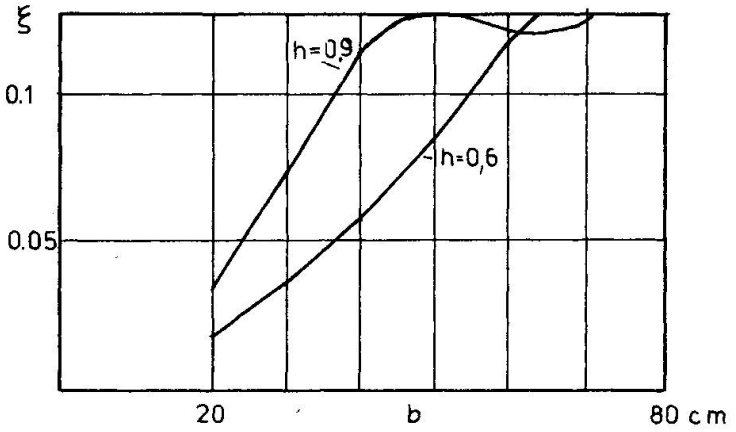

Fig.10
variation of b

<u>cracked member</u>
basic dimensions:

h =0.6 m
b =0.4 m
l =2.5 m
h^{x} =0.03 m
E_c =3000 kN/cm²
5x0 0.03
r_d =0.4
$\beta_{c,c}$=87.5 N/cm²
$\overline{b}$ =60/m²
$\overline{p_o}$ =10 kN

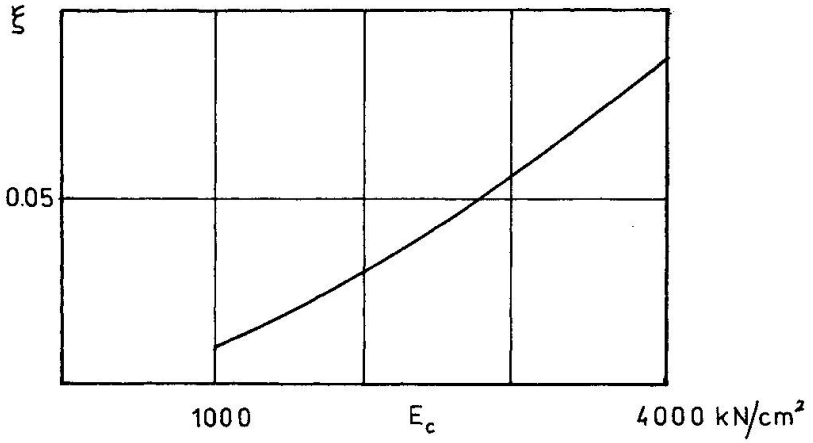

Fig.11
variation of E_c

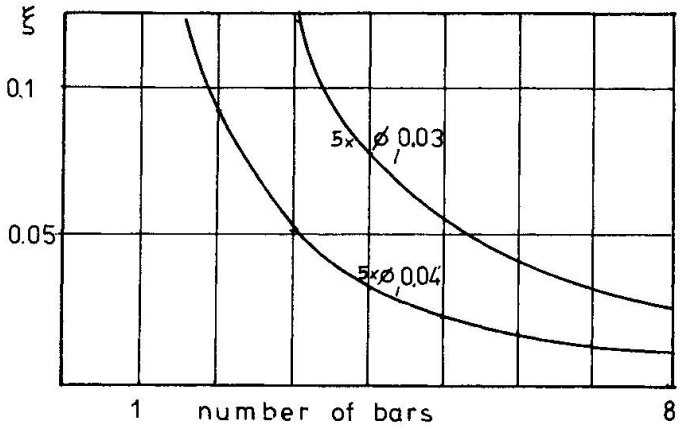

Fig. 12
variation of the number of bars

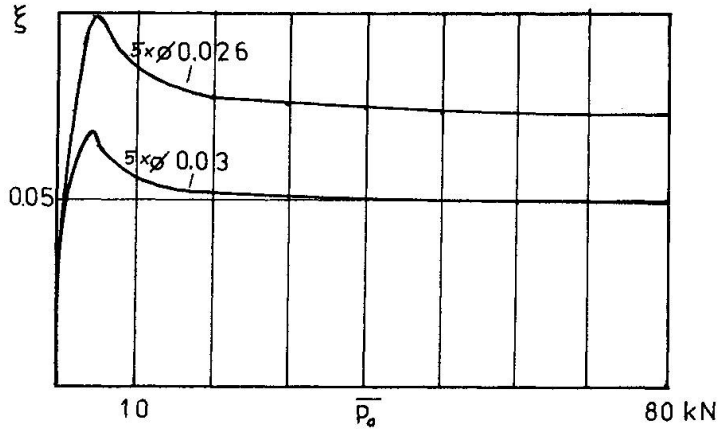

Fig. 13
variation of max. force amplitude

cracked member
basic dimensions:
h =0.6 m
b =0.4 m
l =2.5 m
h^{x} =0.03 m
E_c =3000 kN/cm²
5xØ 0.03
r_d =0.4
$\beta_{c,c}$=87.5 N/cm²
$\overline{b}$ =60/m²
$\overline{p_o}$ =10 kN

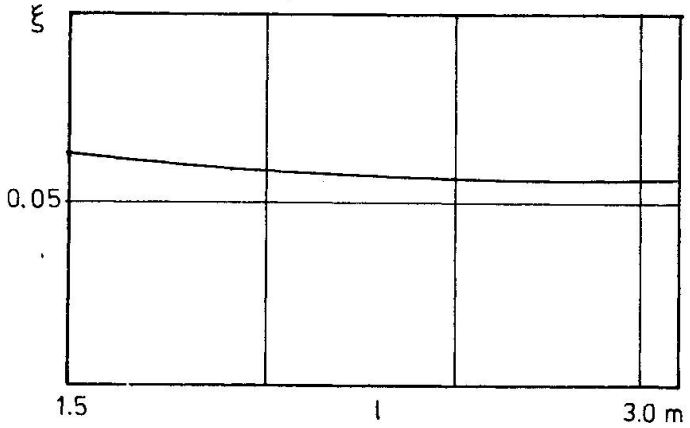

Fig. 14
variation of l

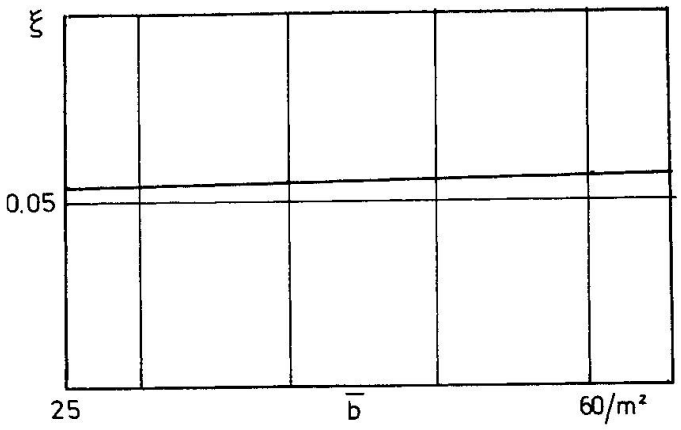

Fig. 15
variation of coefficient $\bar{b}$

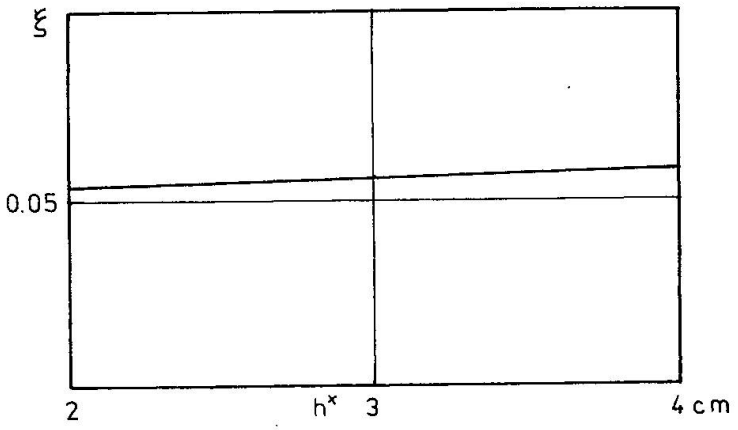

Fig. 16
variation of h^x

<u>cracked member</u>
basic dimensions:
h =0.6 m
b =0.4 m
l =2.5 m
h^x =0.03 m
E_c =3000 kN/cm²
5x0 0.03
r_d =0.4
$\beta_{c,c}$=87.5 N/cm²
$\bar{b}$ =60/m²
$\bar{p_o}$ =10 kN

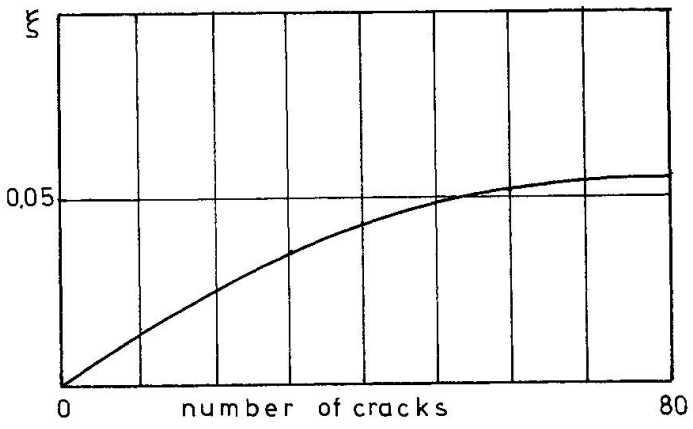

Fig. 17
increase of ξ with number of cracks

On Aggregate Interlock Mechanism in Reinforced Concrete Plates with Extensive Cracking

Sur la transmission des contraintes au moyen de l'engrènement des faces des fissures dans les plaques en béton armé

Über die Querkraftübertragung durch Verzahnung der Rissufer in ebenen gerissenen Stahlbetonscheiben

PIETRO G. GAMBAROVA
Professor
Institute of Structural Engineering (ISTC), Politecnico di Milano
Milan, Italy

SUMMARY
After a review of the characteristics of the so-called Rough Crack Model (recently introduced by Bazant and by the author /13/) for the analysis of stress transmission via aggregate interlock across cracks in reinforced contrete planar elements, the paper deals with two basic aspects of cracks: how cracks (already formed) start opening and slip when the first load is applied, and to what extent the crack shear stiffness is increased because of the apparent extra stiffness of the reinforcement, caused by the bar-to-concrete adhesion (tension stiffening of the reinforcement).

RÉSUMÉ
Après une illustration des caractéristiques du modèle appelé "Modèle des Fissures Rugueuses" (Rough Crack Model) pour l'analyse de la transmission des contraintes au moyen de l'engrènement des faces des fissures dans une plaque en béton armé (Aggregate Interlock), cette étude considère deux aspects basiques du comportement des fissures, c'est à dire la loi selon laquelle les faces des fissures (déjà développées dans la plaque) se déplacent (ouverture et glissement des fissures) au moment où les charges sont appliquées, et l'accroissement de la rigidité au cisaillement des fissures, déterminé par l'adhérence des aciers d'armature au béton (en effect cette adhérence augmente la rigidité "efficace" des barres, parce que le béton limite la déformation moyenne de l'acier).

ZUSAMMENFASSUNG
Es werden zunächst die Eigenschaften des sogenannten "Modells mit rauhen Rissufern" zur Untersuchung der Schubspannungsübertragung (über die Verzahnung der Rissufer durch grobe Zuschläge) in gerissenen Stahlbetonscheiben beschrieben; die Arbeit behandelt dann zwei grundlegende Aspekte des Rissverhaltens: an erster Stelle das Gesetz, wonach sich die als schon entwickelt gedachten Risse öffnen und bei Erstbelastung gleiten, an zweiter Stelle die Bedeutung der Rissschersteifigkeit, die dem versteifenden Effekt zuzuschreiben ist, den der Beton dank dem Stahlbetonverbund auf die Bewehrung ausübt (Mitwirkung des Betons).

1. NATURE OF THE PROBLEM

It is generally recognized that aggregate interlock along the cracked surfaces of a reinforced concrete element is a viable means to resist shear stresses. As a consequence, aggregate interlock mechanism is particularly relevant in reinforced-concrete bidimensional elements (such as plates and shells), which are very often subjected to large in-plane shear forces, being at the same time more or less extensively cracked due to poor tensile strength of the concrete.

A particularly demanding case is represented by the secondary containment structures of nuclear reactors, for which the actual trend is to adopt reinforced concrete, with or without prestressing. In the first case a high level of cracking must be expected, as a result of the internal overpressure due to a possible explosion; as a consequence, if an earthquake occurs when the overpressure is still present, the earthquake-induced shear must be carried by an already cracked structure, with open cracks, which certainly give to the concrete markedly different strength and stiffness characteristics from those of the "solid" concrete.

As a matter of fact, each crack is a discontinuity in the reinforced concrete element under examination (either plate or shell) so that many local contact problems arise at the crack interface such as stress concentrations in both reinforcement and concrete, finite displacements (crack slip and opening), nonlinear behaviour of the contiguous "solid" concrete. For the above-mentioned reasons the analysis of stress transmission via aggregate interlock in cracked, reinforced concrete is a challenging problem, which is still open to new contributions both in the experimental field and in the theoretical formulation.

Traditionally, shear transfer in cracked reinforced concrete has been studied without resorting to concepts of Fracture Mechanics on the assumption that the cracks are already formed, spanning across the stress field.

Speaking of shear or stress transmission in cracked reinforced concrete, one must bear in mind that there are at least three different transfer mechanisms: aggregate interlock (called also interface shear transfer) due to the mutual engagement of the crack faces, which are rough; dowel action due to the flexural stiffness of the bars crossing the cracks, and to the local bar reorientation - kinking - when the cracks undergo major displacements (opening and slip); internal (axial) forces of the bars related to bar axial stiffness, these forces having a shear component in the crack plane and a normal (tensile or compressive) component at right angles to the crack plane.

In what follows most attention will be devoted to stress transfer via aggregate interlock, with particular emphasis on the "allowable paths" in the displacement field (δ_t, δ_n) when the crack starts opening. Three combinations of internal forces across the cracks are analysed: shear and normal tensile force (which tends to open the cracks), shear, shear and normal compressive force (which tends to keep the cracks closed), the allowable paths resulting in second or third order parabolas.

Then the effects of steel-to-concrete bond (which tends to limit steel deformations) are analyzed in order to modify the reinforcement stiffness ma-

trix, by introducing tension stiffening, which makes the embedded reinforcement apparently much more stiff than the external reinforcement. Stress/strain relations for the embedded steel are worked out, should bond be partially due to chemical adhesion and to friction and interlock, or to friction and interlock only. The theoretical results compare favourably with the latest test results.

2. EXPERIMENTAL EVIDENCE AND THEORETICAL FORMULATIONS

Many tests carried out mostly in the last fifteen years definitely show that aggregate interlock mechanism is characterized by four main parameters (Fig. 1): crack opening δ_n, crack slip δ_t, interface shear stress σ^c_{nt}, interface confinement stress σ^c_{nn} (always compressive). Under the applied loads, the crack tends to open and to slip, making it possible to transmit stress through interface engagement. However, this engagement actually occurs only if the confinement action, due to the reinforcement crossing the crack or to the boundary constraints, limits the crack tendency to open (crack dilatancy due to the overriding of the aggregate particles at the crack interface).

The strict connection between shear transmission by aggregate interlock and concrete dilatancy has not become fully understood until recently, so that too much experimental work gives no information about the interaction between confinement and interface shear.

Other physical parameters contribute to shear transfer via aggregate interlock, but their effects are mostly quantitative, and do not modify the nature of the mechanism. Among these parameters, the following must be remembered: average size of aggregate particles, cement matrix strength and aggregate strength, aggregate type (natural or crushed), concrete compressive strength, nature of the loads (monotonic, cyclic-either pulsating or alternate). Also the strength of the steel-to-concrete bond is important, but its effects regard mostly the reinforcement and to a lesser extent the crack interface, so that bond may be better related to steel than to cracks.

As a reminder of the large amount of experimental work done in this field, the following select bibliography can be quoted: Fenwick /1/, Paulay and Loeber /2/, Taylor /3/, Houde and Mirza /4/ (tests on plain concrete specimens with preformed cracks, for different values of aggregate size and type, concrete strength, crack opening); Laible White and Gergely /5/, White and others /6/ (tests on reinforced concrete precracked specimens, subjected to alternate loads, with either external or embedded rebars); Mattock and others /7/ /8/ (tests on the ultimate shear strength of cracked reinforced concrete specimens under either monotonic or cyclic loads); Walraven and Reinhardt /9/ (tests for different values of: steel ratios, bar diameter and orientation, concrete strength, aggregate type and size, steel-to-concrete bond length, monotonic or pulsating loads), Hamadi and Regan /10/ (push-off tests, with either external or embedded rebars, with natural aggregates or expanded clay). In Fig. 2 some experimental curves of Paulay and Loeber are shown.

The relatively large amount of experimental data made it possible (very recently) to formulate analytical models, which are useful for a better understanding of the experimental behaviour, as well as for the implementation of

the computer programs aimed at the analysis of reinforced concrete structures.

According to Fardis and Buyukozturk /11/ the crack faces behave like two rigid surfaces having at least two contact points (if the problem is plane) and from this assumption the relations between interface stresses and crack displacements can be worked out.

According to Walraven /12/ concrete may be considered as a biphase material (perfectly plastic cement matrix and perfectly rigid aggregate particles) with perfectly spherical inclusions (aggregate particles). Through the evaluation of the contact surfaces between the two phases, the stress-to-displacement relations can be worked out.

A different approach has been adopted by Bazant and by the present author /13, 14,15/: the relations between the interface stresses and the crack displacements are mostly empirical, but agree with some general properties which must be satisfied because of the very nature of aggregate interlock. This analytical formulation is called the Rough Crack Model, and is based on the assumption that crack properties may be considered as a material property, in the case of densely cracked plates.

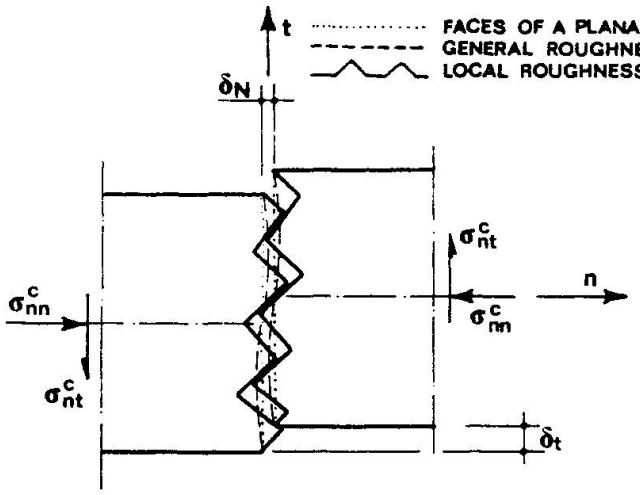

Fig.1 - Crack morphology.

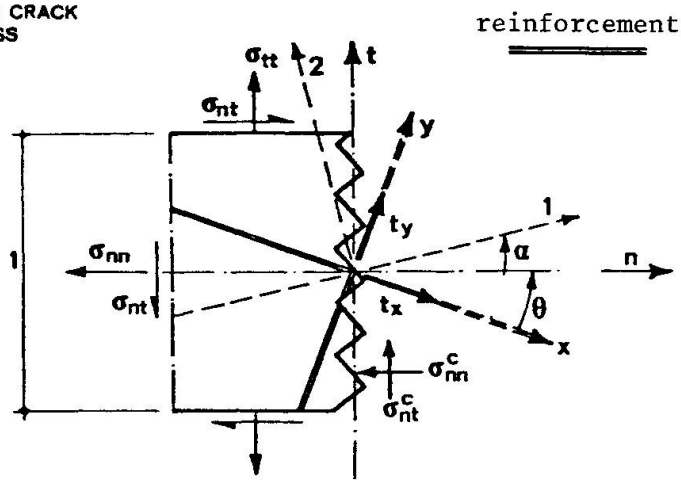

Fig.3 - Sign conventions for a crack crossed by reinforcing bars.

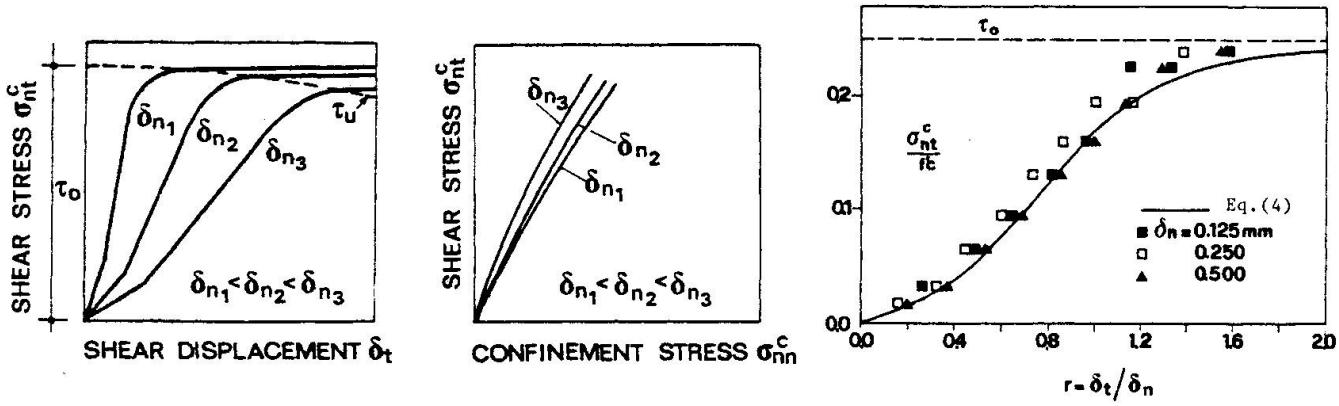

Fig.2 - Paulay and Loeber'test results.

3. ROUGH CRACK MODEL

With reference to Figs. 1 and 3, a crack may be considered planar but locally rough. As an average, over a large area with many parallel and close cracks, the relations among σ^c_{nn}, σ^c_{nt}, δ_n, δ_t may be considered to be a material property, similar to stress-strain relations for solid concrete, and may be generally assumed in the form:

$$\begin{Bmatrix} d\sigma^c_{nn} \\ d\sigma^c_{nt} \end{Bmatrix} = \begin{bmatrix} B_{nn} & B_{nt} \\ B_{tn} & B_{tt} \end{bmatrix} \cdot \begin{Bmatrix} d\delta_n \\ d\delta_t \end{Bmatrix} \qquad (1)$$

where the matrix $\underline{B}$ is the crack stiffness matrix and the stiffness coefficients B_{nn}, B_{nt}, B_{tn}, B_{tt} depend on δ_n δ_t σ^c_{nn} σ^c_{nt} and possibly on other state parameters.

Due to the scarcity of test data, only a path-independent, total stress-total displacement formulation seems possible:

$$\sigma^c_{nn} = f_n(\delta_n,\delta_t) \ , \quad \sigma^c_{nt} = f_t(\delta_n,\delta_t) \qquad (2)$$

so that $B_{nn} = \partial f_n/\partial\delta_n$, $B_{nt} = \partial f_n/\partial\delta_t$, $B_{tn} = \partial f_t/\partial\delta_n$, $B_{tt} = \partial f_t/\partial\delta_t$.

Certain properties of eqs. (2) may be defined by mere speculation on the physical behaviour of a crack: these properties /13/ are mainly based on the fact that interface engagement (i.e. aggregate interlock) increases with crack slip, and decreases with crack opening, so that in the first case the absolute values of the interface stresses increase, and in the second case these values decrease (this is no longer true for very large values of the slip-to-opening ratio, when crack strain softening occurs).

Based on the previous properties and on the available experimental test data (mostly those of Paulay and Loeber /2/) - Fig. 2 - it is possible to give an empirical formulation to the relations (2), which turns out to be primarily dependent on the ratio $r = \delta_t/\delta_n$:

- confinement stress $$\sigma^c_{nn} = -\frac{a_1}{\delta_n}(a_2|\sigma^c_{nt}|)^p \qquad (3)$$

- interface shear stress $$\sigma^c_{nt} = \tau_u r \frac{a_3 + a_4|r|^3}{1 + a_4 r^4} \qquad (4)$$

where $r = \delta_t/\delta_n$, $\tau_u = \tau_o \dfrac{a_o}{a_o+(\delta_n/D_a)^2}$, $p = 1.30\left(1 - \dfrac{0.231}{1+0.185\,\delta_n+5.63\delta_n^2}\right)$

with $a_o = 0.1111$ $\quad a_1 = 0.534 \cdot 10^{-3}$ N/mm

$a_2 = 145\ mm^2/N \quad a_3 = (2.45/\tau_o)\ N/mm^2$

$a_4 = 2.44\ (1-4/\tau_o\ N/mm^2) \quad \tau_o = (1/3 - 1/4)f'_c\ (°)$

D_a = maximum size of aggregate particles

These expressions do not include crack strain softening, because of lack of experimental test data.

A tentative introduction of strain softening could be performed by multiplying σ^c_{nt} - eq.(4) - by a function like $a_5/(a_5 + r^q)$ with $q > 0$, so that for r tending to infinite, the stresses σ^c_{nn} and σ^c_{nt} tend to zero.

In eq. (4), τ_u represents the maximum shear stress which can be transferred at constant δ_n: of course, τ_u must vanish when δ_n tends to infinite, because crack opening exceeds the height of the face humps and the contact between the crack faces is lost (the maximum height of the humps has the same magnitude as the maximum aggregate size D_a).

The crack stiffness matrix $\underline{B}$ can be inverted: $\underline{F} = \underline{B}^{-1}$ is the crack flexibility matrix.

By assuming that the plate is sufficiently large compared to crack spacing and bar spacing, and that the internal forces vary gradually and smoothly (so that they are almost uniform over a distance of several bar and crack spacings), the crack displacements may be "smeared" over a length equal to crack spacing:

$$\begin{Bmatrix} d\varepsilon^{CR}_{nn} \\ d\varepsilon^{CR}_{tt} \\ d\gamma^{CR}_{nt} \end{Bmatrix} = \begin{bmatrix} F_{nn}/s & 0 & F_{nt}/s \\ 0 & 0 & 0 \\ F_{tn}/s & 0 & F_{tt}/s \end{bmatrix} \cdot \begin{Bmatrix} d\sigma^{C}_{nn} \\ d\sigma^{C}_{tt} \\ d\sigma^{C}_{nt} \end{Bmatrix} \quad \text{or} \quad d\underset{\sim}{\varepsilon}^{CR} = \underline{D}^{CR}\ d\underset{\sim}{\sigma}^{C}$$

The matrix $\underline{D}^{CR}$ is the cracked concrete flexibility matrix.

By adding the solid concrete flexibility matrix $\underline{D}^{SC}$ to the cracked concrete flexibility matrix $\underline{D}^{CR}$, the concrete flexibility matrix $\underline{D}^{C}$ is obtained:

$$\underline{D}^{C} = \underline{D}^{SC} + \underline{D}^{CR} \quad \text{where} \quad \underline{D}^{SC} = \begin{bmatrix} E_c^{-1} & -\nu E_c^{-1} & 0 \\ -\nu E_c^{-1} & E_c^{-1} & 0 \\ 0 & 0 & G_c^{-1} \end{bmatrix}$$

The moduli E_c and G_c may be given the values of the elastic behaviour as a first approximation. Otherwise, the values given by any approach based on isotropic non linearly elastic behaviour could be introduced.

(°) The numerical results shown in this paper were obtained with $\tau_o/f'_c = 0.31$.

By adding the reinforcement stiffness matrix $\underline{C}^S$ to the concrete stiffness matrix $\underline{C}^C = \underline{D}^{C-1}$, the equations relating the applied stresses to the strains can be written as follows: $d\underset{\sim}{\sigma} = \underline{C}\, d\underset{\sim}{\varepsilon}$

where $d\underset{\sim}{\sigma} = d\underset{\sim}{\sigma}^C + d\underset{\sim}{\sigma}^S \qquad d\underset{\sim}{\varepsilon} = d\underset{\sim}{\varepsilon}^S = d\underset{\sim}{\varepsilon}^{SC} + d\underset{\sim}{\varepsilon}^{CR} \qquad \underline{C} = \underline{C}^S + \underline{C}^C \qquad (5)$

The matrix $\underline{C}^S$ (see /13/) takes into consideration the steel ratios, the bar orientation, the stress-strain curve of the steel and also (see Sec. 5) the tension stiffening of the reinforcement due to steel-to-concrete bond.

Formulation (5) makes possible the incremental evaluation of the static response of a (cracked + solid) reinforced concrete element of unit length in the direction parallel to the cracks, when the strains are imposed. If the load history is imposed through the orientation α of the principal direction 1 and the ratio $m = \sigma_1/\sigma_2$ of the principal stresses, system (5) has to be rearranged - see system (6) -:

$$\begin{Bmatrix} d\sigma_{nn} \\ d\varepsilon_{tt} \\ d\gamma_{nt} \end{Bmatrix} = \left[C^*\right] \cdot \left\{D_o^*\right\} \, d\varepsilon_{nn} \qquad (6)$$

where:

$$\left\{D_o^*\right\} = \begin{Bmatrix} C_{11} \\ \dfrac{C_{11}+C_{21}+C_{31}}{1+k_1+k_2} \\ \dfrac{C_{11}+C_{21}-C_{31}}{1+k_1-k_2} \end{Bmatrix}$$

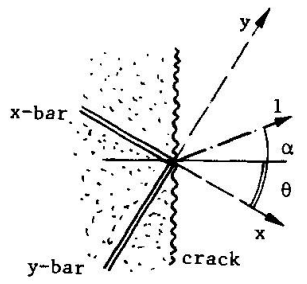

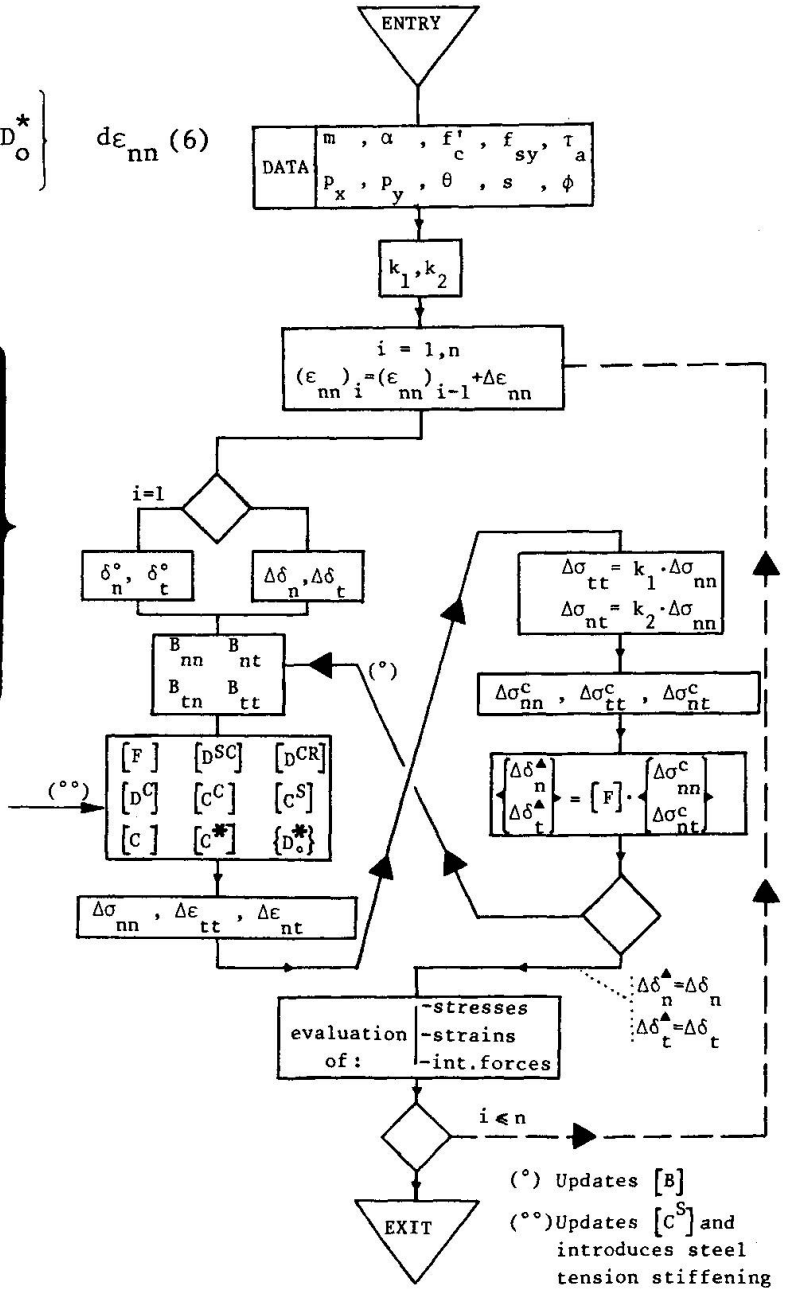

Fig. 4 - Flow chart of the computer program for the evaluation of response curves.

and

$$\left[C^*\right] = \begin{bmatrix} 1 & -C_{12} & -C_{13} \\ 1 & -\dfrac{C_{12}+C_{22}+C_{32}}{1+k_1+k_2} & -\dfrac{C_{13}+C_{23}+C_{33}}{1+k_1+k_2} \\ 1 & -\dfrac{C_{12}+C_{22}-C_{32}}{1+k_1-k_2} & -\dfrac{C_{13}+C_{23}-C_{33}}{1+k_1-k_2} \end{bmatrix}^{-1} ; \quad k_1 = \frac{(1+m) - (1-m)\cos 2\alpha}{(1+m) + (1-m)\cos 2\alpha}$$

$$k_2 = \frac{(1-m)\,\mathrm{sen}\ 2\alpha}{(1+m)+(1-m)\cos 2\alpha}$$

At each load step (i.e. at each increment of the strain ε_{nn}) the matrix $\underline{C}^*$ and the vector $\underset{\sim}{D}_o$ must be updated according to the values of δ_n and δ_t obtained in the previous step. In the flow chart of Fig. 4 the numerical procedure adopted for the evaluation of response curves is shown.

4. KINEMATICS OF THE CRACK AT VERY SMALL VALUES OF CRACK OPENING

When the crack opening is zero there is full continuity in the concrete and no slip is possible along the crack. However, the state $\delta_t = 0$, $\delta_n = 0$ represents a singularity for relations (3) and (4) and this singularity may be overcome through the analysis of the "allowable paths" in the displacement field (Fig. 5), near the origin (δ_n , $\delta_t \to 0$). The knowledge of the relation $\delta_t\ (\delta_n)$ at the origin of the displacement field makes it possible to work out the initial values for δ_t and δ_n, which are to be introduced into the first step of the numerical procedure shown in Fig. 4.

Let us consider again the eqs.(2), that may be turned into the following form:

$$\sigma^c_{nt} = \sigma^c_{nt}(\delta_n, \sigma^c_{nn}) \ , \quad \delta_t = \delta_t(\delta_n, \sigma^c_{nn}) \tag{2'}$$

In order to achieve a given final state (δ_n, δ_t), the work done by the interface stresses for the crack displacements is as follows:

$$L = \int_0^{\delta_n} \sigma^c_{nn}\, d\delta_n + \int_0^{\delta_t} \sigma^c_{nt}\, d\delta_t \tag{2"}$$

and, by differentiating the eqs.(2') :

$$L = \int_0^{\delta_n} \sigma^c_{nn}\, d\delta_n + \int_0^{\delta_t} \sigma^c_{nt} (\partial\delta_t/\partial\delta_n\, d\delta_n + \partial\delta_t/\partial\sigma^c_{nn}\, d\sigma^c_{nn}) \tag{2"'}$$

Now, near the origin of the displacement field, for δ_n tending to zero, the first integral in the RHSide of eq.(2"') tends to zero, while the second integral tends to zero only on condition that both the derivatives $\partial\delta_t/\partial\delta_n$ and $\partial\delta_t/\partial\sigma^c_{nn}$ tend to zero, which means that only the paths having the following equation are admissible (Fig.5):

$$\delta_t = c\ \delta_n^a \tag{7}$$

where c is a constant, and a must be larger than unity.
Due to the condition $\partial\delta_t/\partial\delta_n = 0$,

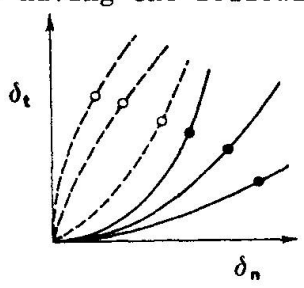

Fig.5
● allowable paths
o not-allowable paths

the first displacement of the crack must be normal (pure opening mode, Fig.6 a) and only later can slip occur.

The constants c and a can be evaluated through a careful analysis of what happens when the crack starts to open. Near the origin, since $\partial\delta_t/\partial\delta_n = 0$, also the value of the ratio $r = \delta_t/\delta_n$ tends to zero; as a consequence, eqs. (3) and (4) can be simplified:

$$\sigma^c_{nn} = -\frac{a_1 a_2 a_3}{\delta_n}\tau_o r \qquad \sigma^c_{nt} = a_3\tau_o r \qquad (3'), (4')$$

With reference to a crack of unit length, the internal forces and the steel forces have the following expressions:

$$\begin{cases} \sigma_{nn} = \frac{1}{2}\sigma_1[(1+m)+(1-m)\cos 2\alpha] \\ \sigma_{tt} = \frac{1}{2}\sigma_1[(1+m)-(1-m)\cos 2\alpha] = \frac{(1+m)-(1-m)\cos 2\alpha}{(1+m)+(1-m)\cos 2\alpha}\sigma_{nn} = k_1\sigma_{nn} \\ \sigma_{nt} = \frac{1}{2}\sigma_1(1-m)\sin 2\alpha = \frac{(1-m)\sin 2\alpha}{[(1+m)+(1-m)\cos 2\alpha]}\sigma_{nn} = k_2\sigma_{nn} \end{cases} \qquad (8)$$

$$\begin{cases} \sigma^s_{nn} = E_s\,\varepsilon_{nn}(p_x\cos^4\theta + p_y\sin^4\theta) \\ \sigma^s_{nt} = E_s\,\varepsilon_{nn}\sin\theta\cos\theta(-p_x\cos^2\theta + p_y\sin^2\theta) \end{cases} \qquad (9)$$

where $\varepsilon_{nn} = \delta_n/s$, if the solid concrete deformations are disregarded, and p_x, p_y, θ are the steel ratios of the reinforcing net, and the net orientation. In eqs. (8) the principal stress σ_1 may be considered always positive (because of the nature of the problem, which would be meaningless in the case of prevailing compression); as a consequence, the sign of the expression $[(1+m)+(1-m)\cos 2\alpha]$ turns out to be very important because the case $[\ldots] > 0$ means that the internal normal force σ_{nn} tends to open the crack; the case $[\ldots] = 0$ means that the internal forces in the plane parallel to the crack are only shear, which neither helps nor opposes crack opening; the case $[\ldots] < 0$ means that the internal normal force σ_{nn} is compressive, i.e. tends to keep the crack closed (but the presence of an internal shear force induces crack dilatancy and then the crack opens anyway).

Three different cases must be examined:

CASE A: $[(1+m) + (1-m)\cos 2\alpha] > 0$, i.e. $\sigma_{nn} > 0$

When the crack starts to open, due to the pure opening mode ($\delta_n \geq 0$, $\delta_t = 0$) there is no confinement stress, and aggregate interlock cooperates with the reinforcement in the transmission of shear:

$$\sigma^c_{nn} = 0 \rightarrow \sigma^s_{nn} = \sigma_{nn}, \quad \sigma^c_{nt} = \sigma_{nt} - \sigma^s_{nt}$$

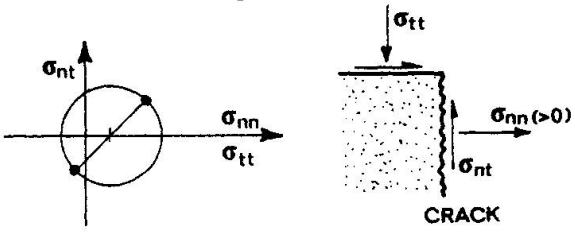

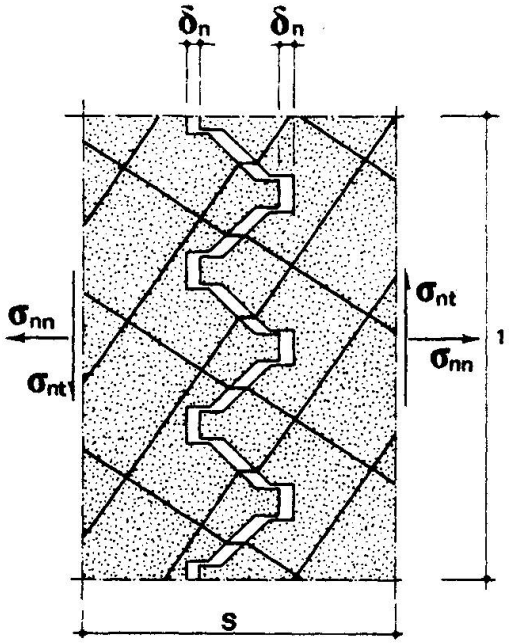

Fig.6a - Pure opening mode when the crack starts to open. (bar reorientation is highly exagerated, being in fact negligible at this stage)

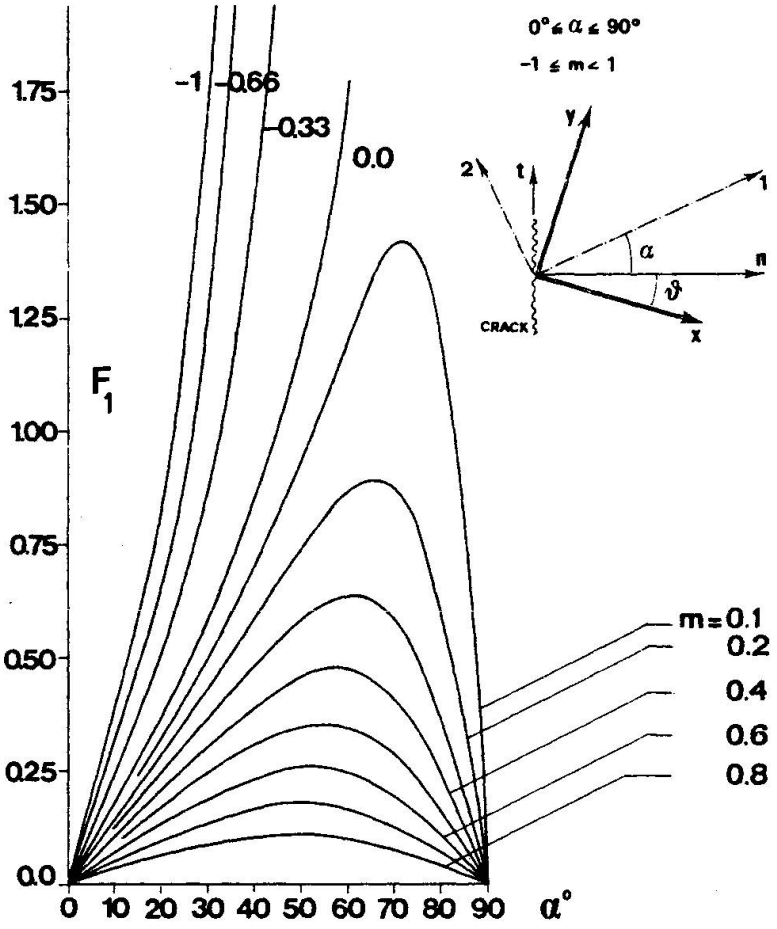

Fig.6b - Plot of the function F_1 for various values of the ratio m between the principal stresses.

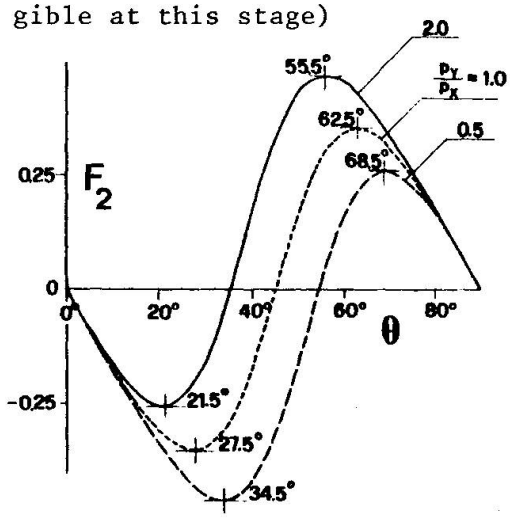

Fig.6c - Plot of the function F_2 for various values of the parameter p_y^2/p_x.

From eqs. (3')(4')(8)(9) the relation between δ_t and δ_n can be worked out:

$$\delta_t = \frac{E_s}{a_3 \tau_o s} (p_x \cos^4\theta + p_y \sin^4\theta) \cdot (F_1 - F_2)\, \delta_n^2 \qquad (10)$$

where $F_1 = \dfrac{(1-m)\sin 2\alpha}{[(1+m)+(1-m)\cos 2\alpha]} = k_2$, $\quad F_2 = \dfrac{-\sin\theta\cos\theta(p_x\cos^2\theta - p_y\sin^2\theta)}{(p_x\cos^4\theta + p_y\sin^4\theta)}$

Depending on the sign of (F_1-F_2), the crack slip has the same sign as the internal force σ_{nt}, or opposite sign, this fact being a somewhat unexpected characteristic of the crack kinematics (Fig.6b,c).

Note that F_1 depends only on the assigned load history (m and α), while F_2

□ y bars yield in tension

○ x bars yield in tension

f'_c = 28 N/mm2 f_{sy} = 280 N/mm^2

s(crack spacing)= 50 mm

$p_x = p_y$ = 0.02 (isotropic reinforcement)

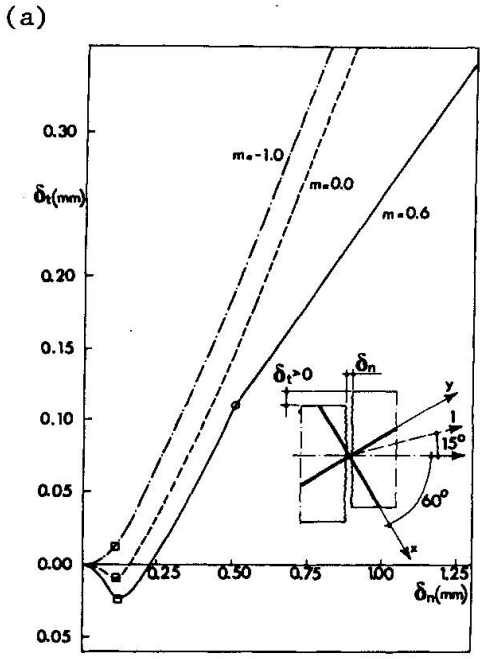

Fig.7 - Paths in the displacement field (a). Interface stresses versus crack opening (b),(c),(d). Internal shear force and steel shear force (e).

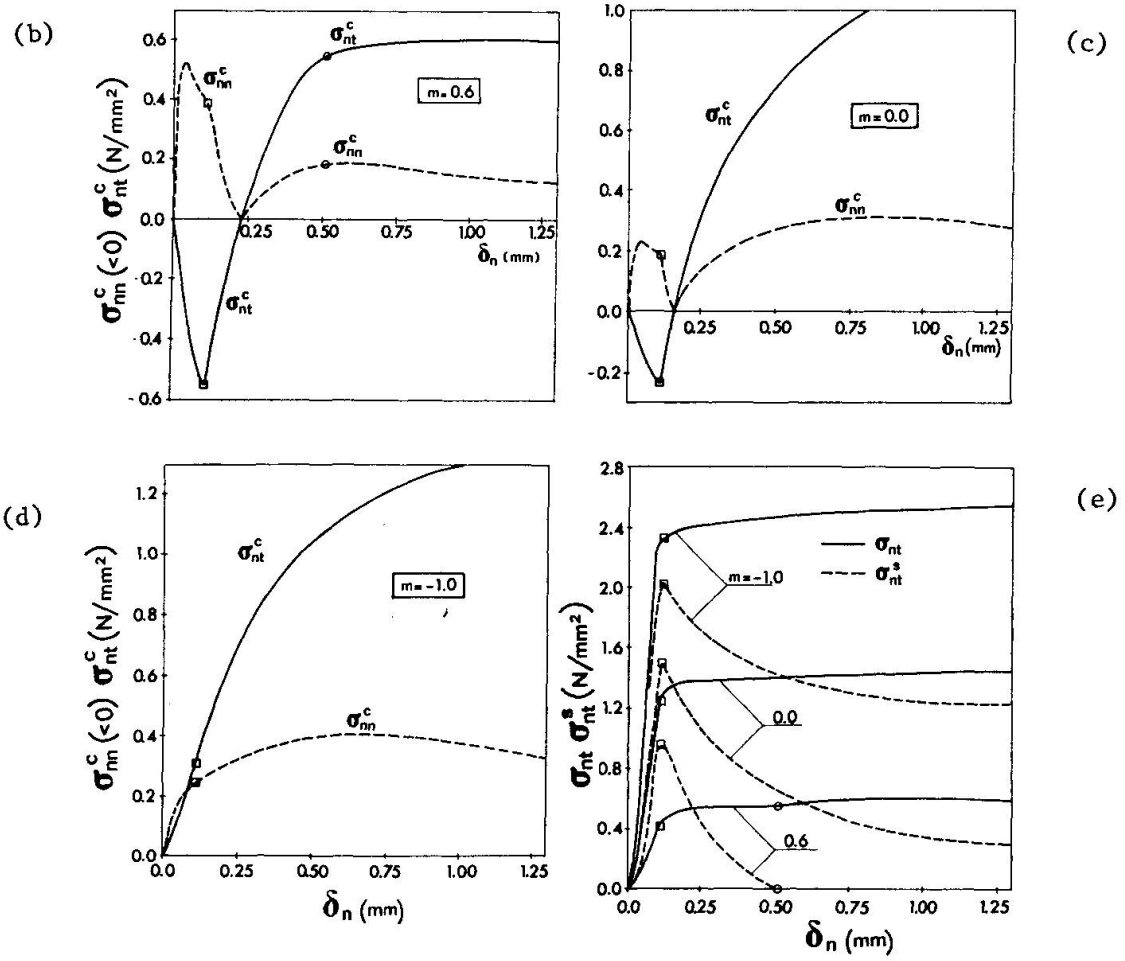

depends only on the steel characteristics (p_x, p_y, θ).

When the sign of the crack slip does not agree with the sign of the applied shear, the reinforcement must carry not only the applied shear σ_{nt}, but also the interface shear σ^c_{nt}, which has the same sign as the crack slip.

The reversal of the slip sign occurs after the reinforcement has started to yield, as can be seen in Fig. 7, for m = -1.0, 0.0. As a general rule, should the reinforcement be strongly non-aligned with crack axes ($\theta > 35° \div 45°$) and should the internal normal force σ_{nn} prevail over the internal shear force σ_{nt}, the signs of δ_t and σ_{nt} will be opposite, until the reinforcement partly yields, compelling the aggregate interlock mechanism to help in the transmission of the applied shear (this help is possible only if the sign of the slip aggrees with the sign of the applied shear).

CASE B: $[(1+m)+(1-m)\cos 2\alpha] = 0$, i.e. $\sigma_{nn} = 0$, $\sigma_{nt} \neq 0$

In this case, which includes also the case of internal forces reduced to pure shear, the confinement stress σ^c_{nn} must balance the normal stress σ^s_{nn} in the reinforcement:

$$\sigma_{nn} = \sigma^s_{nn} + \sigma^c_{nn} = 0 \rightarrow \sigma^c_{nn} = -\sigma^s_{nn}$$

From eqs. (3')(9) the relation between δ_t and δ_n can be worked out:

$$\delta_t = \frac{E_s}{a_1 a_2 a_3 \tau_o s}(p_x \cos^4\theta + p_y \sin^4\theta)\, F_3 \delta_n^3 \qquad (11)$$

where $F_3 = \dfrac{(1-m)\sin 2\alpha}{|(1-m)\sin 2\alpha|}$

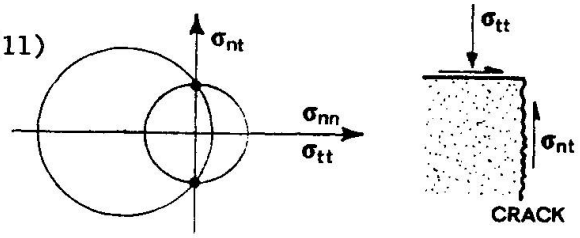

The sign of δ_t must always agree with the sign of σ_{nt}.

In Fig. 8, for various crack spacings and rebars at right angles to the crack, the shear modulus G^{CR} of the (solid+cracked) reinforced concrete is plotted versus crack slip, when the crack opens and slips (note that the value of G^{CR} are 1/3 to 1/6 of the solid concrete shear modulus G^{SC}).

CASE C: $[(1+m)+(1-m)\cos 2\alpha] < 0$, i.e. $\sigma_{nn} < 0$

By introducing the relations (3')(4')(8)(9) into the equilibrium equations

$$\sigma_{nn} = \sigma^s_{nn} + \sigma^c_{nn}, \qquad \sigma_{nt} = \sigma^s_{nt} + \sigma^c_{nt}$$

the following relation ($\delta t, \delta n$) can be worked out:

$$\delta_t = \frac{E_s}{a_3 \tau_o s}\,\frac{F_1 - F_2}{F_1}(p_x \cos^4\theta + p_y \sin^4\theta)\delta_n^3 \qquad (12)$$

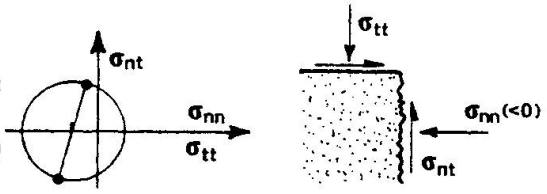

The crack slip must always have the same sign as σ_{nt}: otherwise, when the value of the slip goes back to zero, the internal force σ_{nn} ought to become positive (i.e. tensile), because in this situation ($\delta_t = 0, \delta_n > 0$)

there is no interface confinement stress and the internal normal force σ_{nn} is carried only by the reinforcement, which is in tension due to crack dilatancy (the three relations $\sigma_{nn} = \sigma^s_{nn} \neq 0$, $\sigma^s_{nn} > 0$, $\sigma_{nn} < 0$ cannot be verified at the same time).

It follows that the states with $\delta_t/|\delta_t| \neq \sigma_{nt}/|\sigma_{nt}|$ are impossible and for the corresponding values of m and α the crack does not open.

In Fig. 9 different allowable paths (near the origin $\delta_n = \delta_t \simeq 0$) are shown for different load histories, and for the three cases just examined.

Eqs. (10)(11)(12) give the initial value of δ_t which has to be introduced into the first step of the numerical procedure shown in Fig. 4. As initial value of δ_n, the simplest guess is:

$$(\delta_n)_1 = (\Delta\varepsilon_{nn})_1 \cdot s,$$

where $(\Delta\varepsilon_{nn})_1 \cdot s$ is the actual crack opening if the solid concrete deformations are disregarded.

The above guess for δ_n may cause numerical troubles because the value of σ^c_{nn} may be too high - see eq.(3). Then the assumption of a non-zero initial crack opening $(\varepsilon_{nn})_o \cdot s$ must be adopted; as a consequence, the opening in the first step becomes as follows:

$$(\delta_n)_1 = [(\Delta\varepsilon_{nn})_1 + (\varepsilon_{nn})_o] \cdot s,$$

where the value $(\varepsilon_{nn})_o = 0.0005$ seems satisfactory.

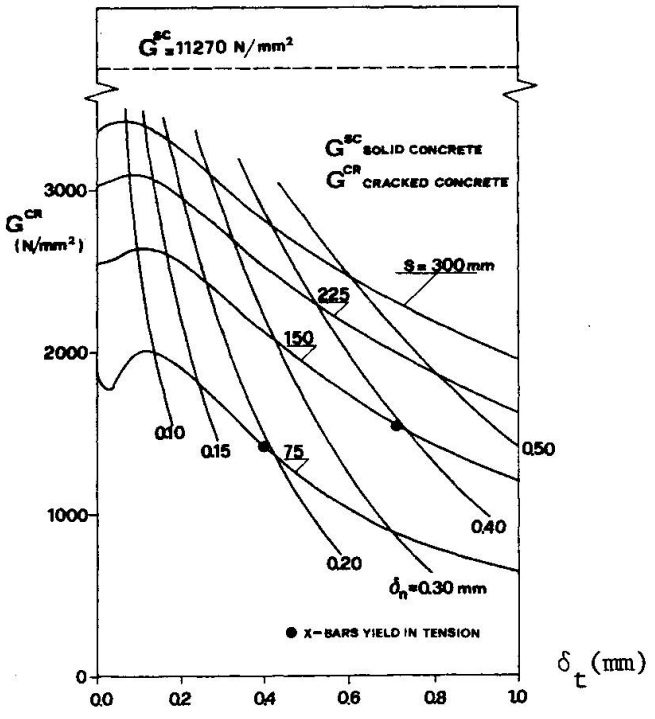

Fig.8 - Curves of the apparent shear modulus G^{CR}(tangent) for cracked reinforced concrete ($f'_c = 31$ N/mm^2, $f_{sy} = 460$ N/mm^2, $p_x = p_y = 0.0112$, $m = -1$, $\alpha = 45°$).

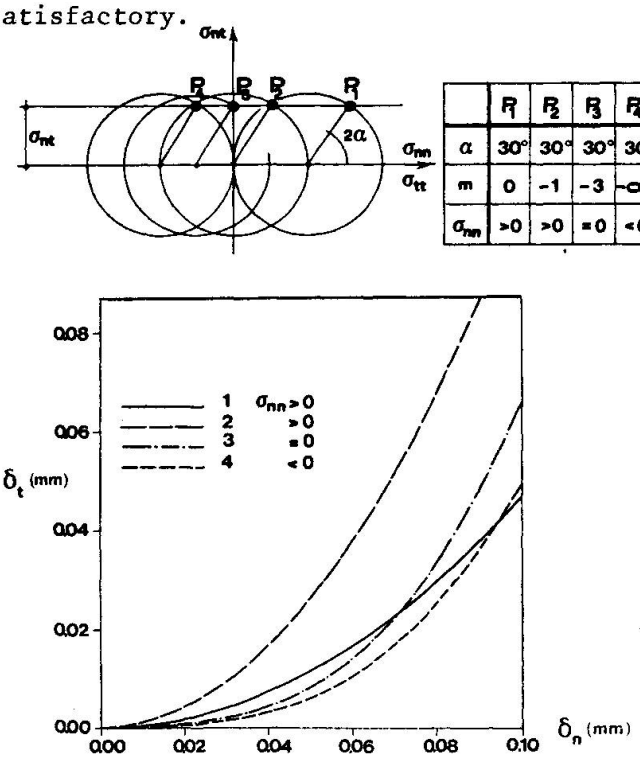

Fig.9 - Allowable paths in the displacement field : the orientation of the principal stresses is constant ($E_s = 200000$ N/mm^2, $\theta = 30°$, $p_x = p_y = 0.01$, crack spacing $s = 100$ mm, $f'_c = 31$ N/mm^2).

5. INTERACTION BETWEEN AGGREGATE INTERLOCK AND TENSION STIFFENING IN THE REINFORCEMENT

The results shown in the two previous sections have been obtained on the assumption that the reinforcement is "external", or in other words that there is no bond between each bar and concrete. As a matter of fact this assumption is never satisfied in practice, with reference to reinforced concrete structures, and consequently the effects of bond must be introduced.

As a general rule, the solid concrete between two contiguous cracks limits the steel deformations through the bar-to-concrete bond, and this phenomenon is enhanced by the presence of compressive stresses (confinement stresses) in the solid concrete. The limitation of steel deformations makes the steel behaviour more stiff (tension stiffening /16,17/). Although related to concrete, tension stiffening may be considered as an exclusive reinforcement property, because it modifies the stress-strain constitutive law of the steel. Tension stiffening makes cracked concrete behaviour less dependent on the steel ratio, because other parameters are involved, such as bar diameter, bond strength, steel and concrete stresses. For these reasons tension stiffening cannot be ignored, especially if the comparison between theoretical and experimental results is at stake.

With reference to a bar (Fig. 10) embedded in a solid concrete element and subjected to a monotonically increasing pull-out force, the bar-to-concrete bond is at first assured by chemical adhesion, then by friction (which is related to the interlock between bar asperities - ribs excluded - and surrounding concrete) and by interlock (between the bar ribs and the concrete, with local concrete crushing and microcracks spreading from the tops of the ribs). The second and third mechanisms are by far the most effective, so that bond stress due to chemical adhesion may be disregarded. After chemical adhesion as been destroyed along part of the bar, friction and interlock assure bar-to-concrete bond with a finite slip at the interface, so that the bar gets "unstuck" from the concrete. At increasing load levels, the bar gets more and more unstuck from the concrete, or in other terms the length of the bar over which bond is assured by friction and interlock increases until this length (λ_x = interlock length, Fig. 11) becomes equal to half the bar length between two contiguous cracks. From this load level on, bar-to-concrete bond is assured only by friction and interlock.

Now assume that: bond stress τ_a due to friction and interlock is constant; bond stress due to chemical adhesion is zero; concrete stresses (Fig. 12) in the direction of the bars are compressive, uniformly distributed and decreasing with the distance from the crack face; concrete behaviour is elastic; steel behaviour is elastic-perfectly plastic; microcracking and crushing are localized in a thin layer of concrete close to the bar. It then becomes possible to evaluate the stresses in the bars and in the concrete at each section, starting from the crack face.

Writing the equilibrium equations in the direction of the bars gives

$$\sigma_x^s(\xi) = \sigma_x^s - \frac{4\tau_a}{\phi}\xi \quad , \quad \sigma_x^c(\xi) = \sigma_x^c + \frac{\tau_a \pi \phi}{b\,\Delta y}\xi$$

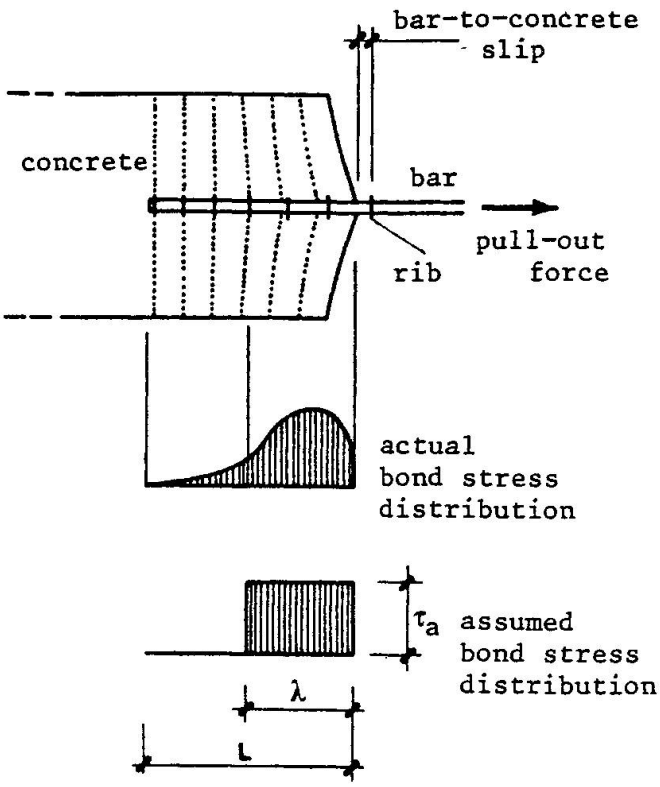

Fig.10-Basic assumptions for the bond stress distribution along an embedded bar, subjected to a pull--out force.

L = bond length

λ = interlock length (bond by friction and interlock)

L-λ = no-slip length (bond by chemical adhesion)

τ_a = bond stress

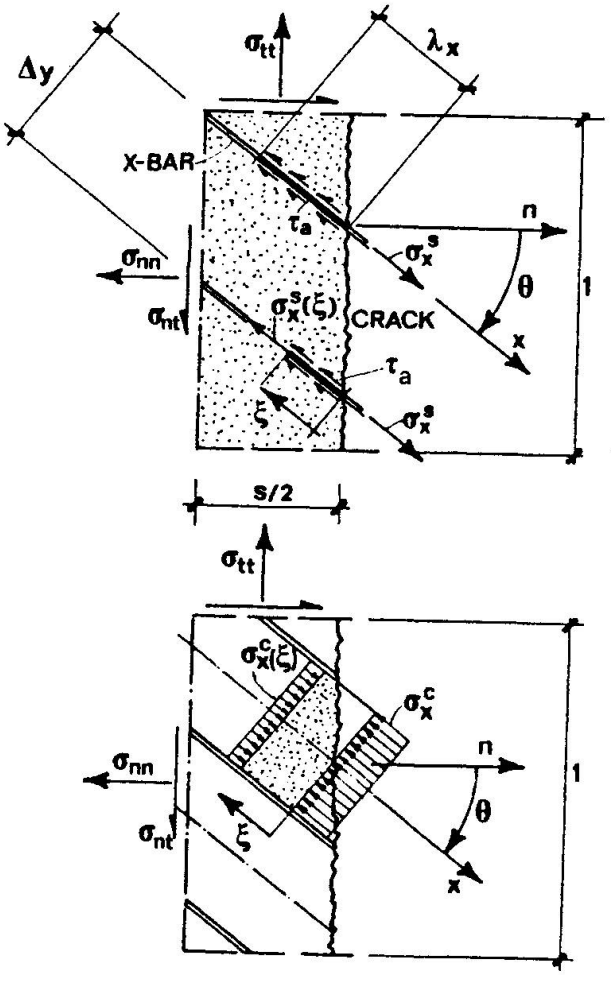

Fig.11-Steel stresses between two contiguous cracks.

$$\sigma_{nn}=\sigma^c_{nn}+\sigma^s_{nn}$$

$$\sigma_{nt}=\sigma^c_{nt}+\sigma^s_{nt}$$

$$\sigma_{tt}=\sigma^c_{tt}+\sigma^s_{tt}$$

Fig.12-Concrete stresses between two contiguous cracks.

$$\sigma^c_x, \sigma^c_x(\xi) < 0$$

$$\sigma^c_x = \sigma^c_{nn}\cos^2\theta + \sigma^c_{tt}\sin^2\theta - 2\sigma^c_{nt}\sin\theta\cos\theta$$

where σ_x^s, σ_x^c are the stresses along the crack face ($\xi = 0$)

τ_a is the bond stress due to friction and interlock

ϕ is the bar diameter

b, Δy are the plate thickness and the x-bar spacing.

The interlock length λ_x can be evaluated through a simple compatibility condition (for $\xi = \lambda_x$, $\varepsilon_x^c(\xi) = \varepsilon_x^s(\xi)$):

$$\lambda_x = \frac{\sigma_x^s \phi}{4\tau_a} \frac{1 - n\,\sigma_x^c/\sigma_x^s}{1 + n\,p_x} \tag{13}$$

where n is the ratio between the Young moduli E_s and E_c.

Eq. (13) shows that the better the bond characteristics (high values of τ_a and p_x, small values of ϕ), the smaller the interlock length and the larger the tension stiffening effects.

Since the crack spacing is a reference distance for the strains (for instance, the strains due to cracking have been obtained by smearing the crack displacements over the crack spacing), it is convenient to introduce the "average" steel strain over the bar length between two contiguous cracks, ε_x^s:

$$\varepsilon_x^s = \frac{2\int_0^{s/2\cos\theta} \varepsilon_x^s(\xi)\,d\xi}{s/\cos\theta} = \frac{2\int_0^{\lambda_x} \varepsilon_x^s(\xi)\,d\xi}{s/\cos\theta} + \frac{2\int_{\lambda_x}^{s/2\cos\theta} \varepsilon_x^s(\xi)\,d\xi}{s/\cos\theta} =$$

$$= \frac{2\int_0^{\lambda_x} \varepsilon_x^s(\xi)\,d\xi}{s/\cos\theta} + \frac{2\int_{\lambda_x}^{s/2\cos\theta} \varepsilon_x^c(\xi)\,d\xi}{s/\cos\theta} \cong \frac{2\int_0^{\lambda_x} \varepsilon_x^s(\xi)\,d\xi}{s/\cos\theta}$$

where concrete and steel strains have been disregarded in the zone with chemical adhesion (see Figs. 10, 11, 12).

Then the following stress/strain relation is obtained:

$$\varepsilon_x^s = \frac{2\lambda_x \cos\theta}{s\,E_s} \left(\sigma_x^s - \frac{2\tau_a}{\phi}\lambda_x\right) \tag{14}$$

With reference to λ_x (which can never exceed $s/2\cos\theta$) two different cases have to be considered:

1) $\lambda_x = \frac{\sigma_x^s \phi}{4\tau_a} \frac{1 - n\,\sigma_x^c/\sigma_x^s}{1 + n\,p_x} < s/2\cos\theta$

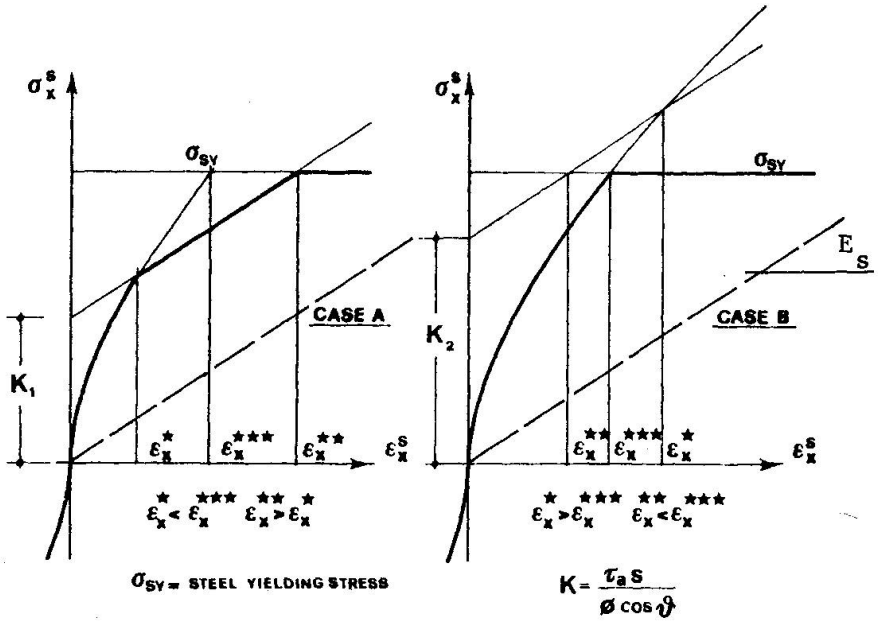

——— without tension stiffening ——— with tension stiffening

Fig.13 - Typical stress-strain curves for steel subjected to tension stiffening : Case A poor bar-to-concrete adhesion ; Case B good adhesion.

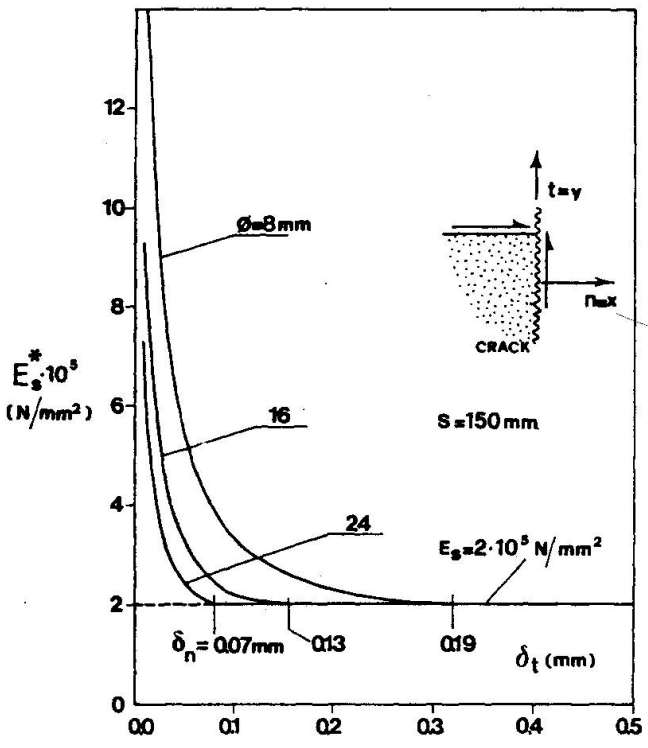

Fig.14 - Curves of the effective Young modulus of the steel, for various bar diameters.

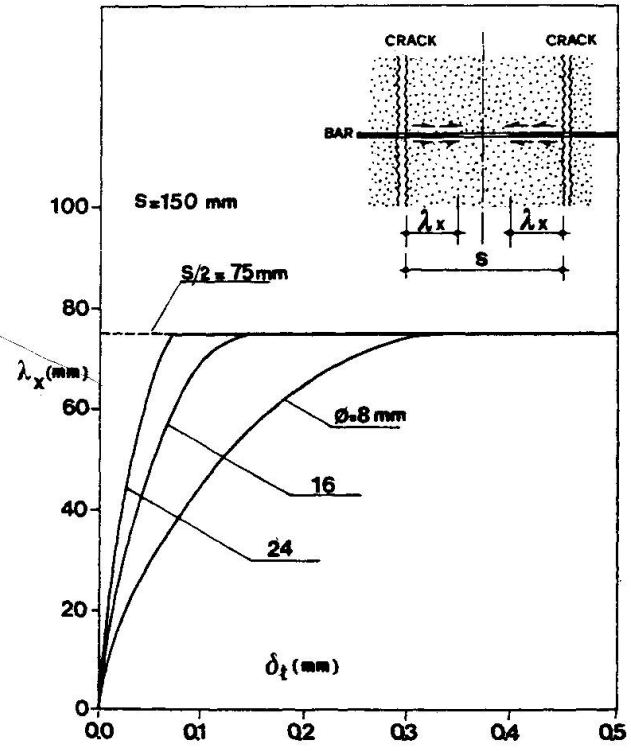

Fig.15 - Curves of the interlock length for various bar diameters.

Fig.14,15 - $f_c' = 31\ N/mm^2$, $f_{sy} = 460\ N/mm^2$, $p_x = p_y = 0.0112$, crack spacing $s = 150mm$

The bars are only partially unstuck from the surrounding concrete. Substituting Eq. (13) into Eq. (14) and disregarding $n\,\sigma_x^c$ with respect to σ_x^s leads to:

$$\sigma_x^s = \pm 2(1 + n\,p_x)\sqrt{\tau_a\,E_s\,\frac{s}{\phi\,\cos\theta}\,\frac{\varepsilon_x^s}{1 + 2\,n\,p_x}} \qquad (15)$$

$$E_x^* = \frac{d\sigma_x^s}{d\varepsilon_x^s} = \frac{|\tau_a|\,E_s\,(s/\phi\,\cos\theta)}{\sqrt{\tau_a\,E_s\,\frac{s}{\phi\,\cos\theta}\,\frac{\varepsilon_x^s}{1 + 2\,n\,p_x}}}\,\frac{(1 + n\,p_x)}{(1 + 2\,n\,p_x)} \qquad (16)$$

where τ_a has to be kept positive if ε_x^s is positive, and viceversa; also the sign + holds when ε_x^s is positive;
E_s^* is the effective steel modulus.

2) $\lambda_x = s/2\cos\theta$

The bars are completely unstuck from the surrounding concrete. Substituting the value of λ_x into Eq. (14), gives:

$$\sigma_x^s = \frac{\tau_a\,s}{\phi\,\cos\theta} + E_s\,\varepsilon_x^s \qquad E_x^* = E_s \qquad (17)\ (18)$$

The relations (15) and (17) may be considered as the constitutive laws of the steel when tension stiffening is introduced. These laws are plotted in Figs. 13a and b : in the former case (Fig.13a) the interlock length reaches the maximum value ($s/2\cos\theta$) before the reinforcement yields, while in the latter case (Fig.13b) the yielding of the reinforcement comes before the complete destruction of the chemical adhesion. The behaviour shown in Fig.13a refers to moderate bond characteristics, while the behaviour shown in Fig.13b is typical of very good bond characteristics.

With reference to the numerical procedure described in Sec. 3 (see also Fig. 4), the stiffness matrix of the reinforcement is updated at each step, in the x and y directions, according to the constitutive laws (15) and (17). At each step the interlock lengths λ_x and λ_y are evaluated - see Eq. (13) where x must be replaced by y in order to evaluate λ_y. If $\lambda_x < s/2\cos\theta$, $\lambda_y < s/2\sin\theta$, the effective moduli E_x^*, E_y^* are given by Eq. (16) - replace x and $\cos\theta$ to get E_y^* -; if $\lambda_x > s/2\cos\theta$, $\lambda_y > s/2\sin\theta$, λ_x and λ_y must be given the values $s/2\cos\theta$ and $s/2\sin\theta$ respectively, and, according to Eq.(18), the effective moduli coincide with the elastic modulus E_s. The evolution of the effective modulus E_x^* and of the interlock length λ_x with the crack displacements is shown in Figs. 14 and 15 , for various bar diameters. The steel effective modulus may be many times larger than E_s. Note that the better the bond characteristics (which are improved by small diameters), the smoother the decrease of E_x^* and the increase of λ_x.

The importance of tension stiffening is shown by the curves of Fig.16 , at constant crack spacing (Fig.16a) and at variable crack spacing (Fig.16b),for various bar diameters and for a given value of the steel ratios ($p_x = p_y = 0.112$). Tension stiffening is more effective when the bond characteristics are good (which may be obtained by adopting smaller bar diameters - Fig.16a) or when the crack spacing is large (which occurs for the largest bar diameters - Fig.16b).

The aforesaid approach to the analysis of tension stiffening, although simple, seems effective and sound, as shown by the agreement between the numerical results and the experimental results (Fig.17) , obtained with the same input data. Of course, crack tension softening is not allowed for in the Rough Crack Model (in the actual form) - as mentioned in Sec. 3 - and some improvements are also necessary in the case of very small steel ratios.

For the lowest steel ratio ($p_x = 0.0056$) two curves are shown: the full line represents the results obtained by means of eqs. (3) and (4), while the dotted line represents the results obtained with an improved formulation of eq. (3), which tentatively introduces both crack stiffening effects due to the local deterioration of concrete produced by the bars crossing the crack interface, and crack strain softening. Crack strain softening is mostly related to the ratio between the crack displacements δ_t and δ_n, and is here introduced through the formulation suggested in Section 3 (see also /19/).

Finally, when comparing theoretical and experimental results (Fig.17), it should be remembered that the bond length is generally larger in a precracked test specimen and so tension stiffening effects are enhanced, while in a real concrete plate the bond length is smaller because it coincides with the crack spacing, provided that the rebars are at right angles to the cracks. It follows that the tests tend to overestimate the crack shear stiffness when the crack is nearly closed and the displacements are small, while for large interface displacements the same tests tend to underestimate the crack shear stiffness, because in this case the earlier yielding of the reinforcement forces the cracks to open earlier, with a decrease in the ultimate shear strength.

6. CONCLUDING REMARKS

As mentioned in the introduction, aggregate interlock mechanism is so important in certain structural cases, that a complete analytical description is necessary. Not only does aggregate interlock (together with dowel action and axial forces in the reinforcement) provide a good level of strength and stiffness to cracked confined concrete, but also cracked concrete ductility is assured by aggregate interlock mechanism, which through crack dilatancy and slip allows the structure to absorb large amounts of energy. The Rough Crack Model seems sufficiently simple and adequate, at least for planar cracks, but further basic phenomena such as crack softening and steel-induced crack deterioration have to be introduced. This introduction could be facilited by further experimental work, but also the general approach of the tests must be somewhat improved. As a matter of fact, it seems that all the pre-

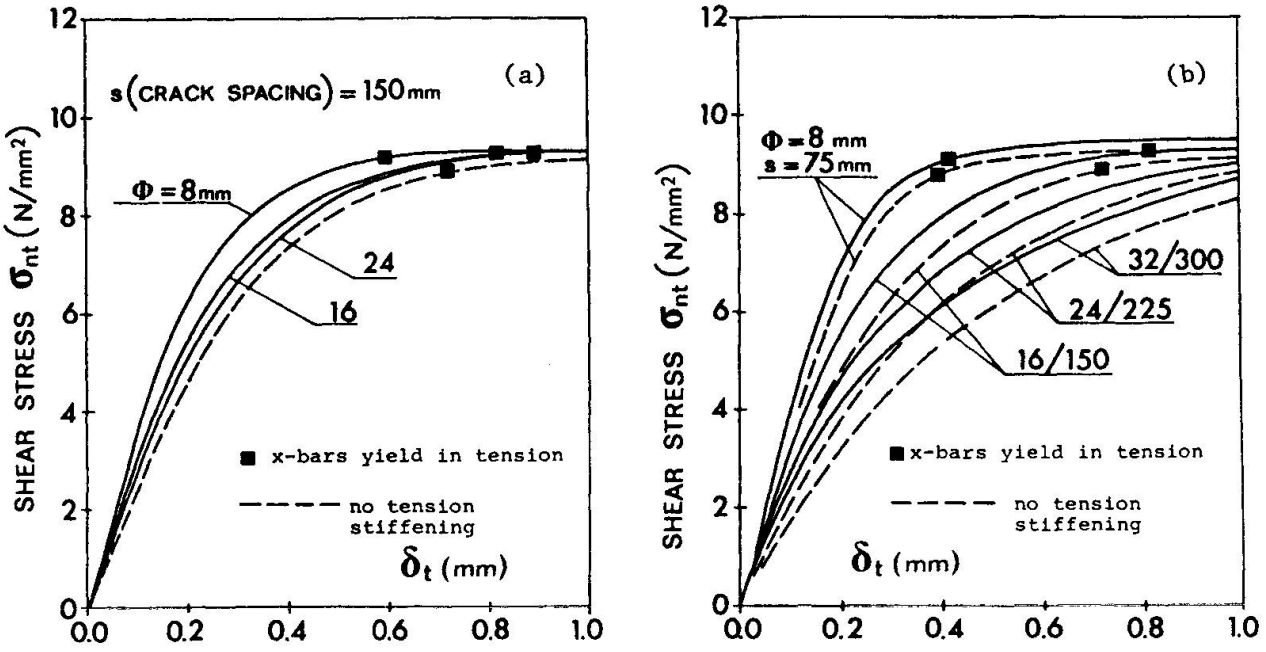

f'_c = 31 N/mm^2 f_{sy} = 460 N/mm^2 $p_x = p_y = 0.0112$

Φ = bar diameter τ_a = bond stress (=10 N/mm^2)

$s = (f_c/2\tau_a)\cdot(\Phi/p_x)$ = crack spacing = bond length of the bars

Fig.16 - Role of tension stiffening for (a) constant crack spacing and various bar diameters, and (b) crack spacing proportional to the diameter.

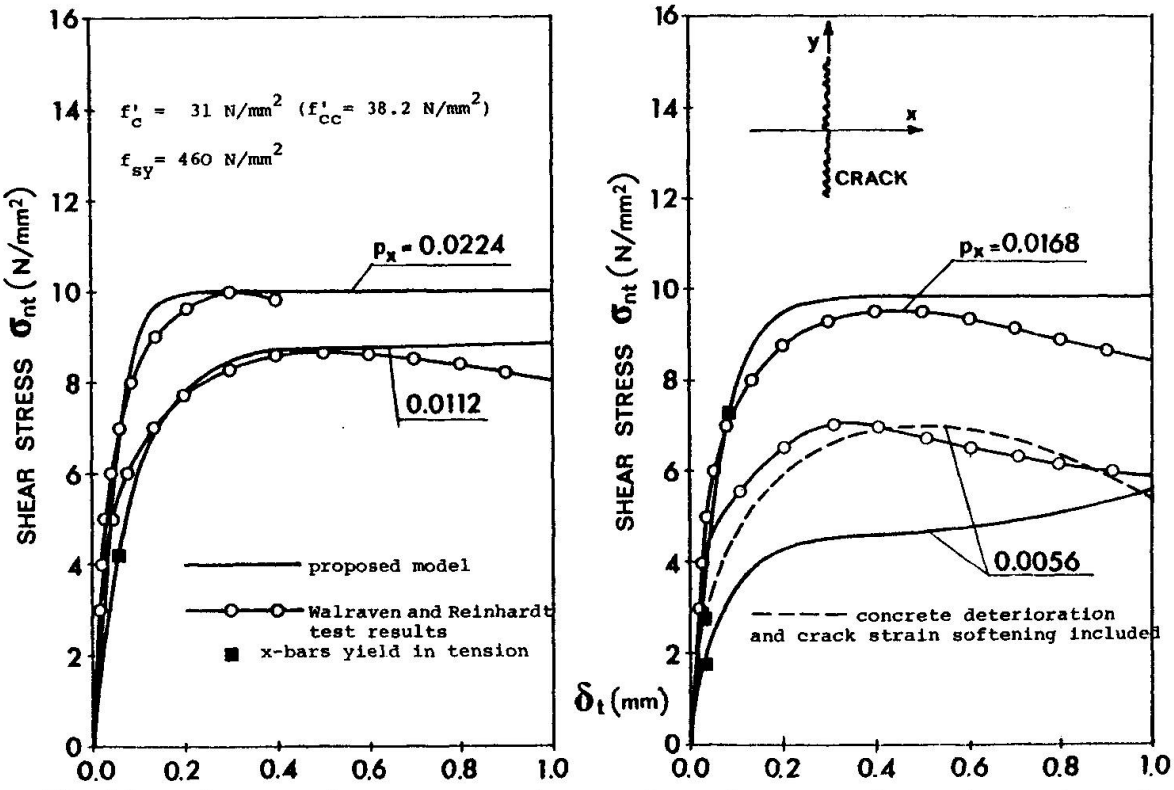

Fig.17 - Fit of Walraven and Reinhardt' results , steel tension stiffening included, for a medium strength concrete (crack spacing s = 50 mm, bond length of the bars in the experimental tests L = 400 mm).

cracked concrete specimens with a single crack tested so far have a weak point, namely an excessive bond length compared to the actual bond length of a densely cracked plate, in which bond length and crack spacing coincide. As a consequence, most of the tests are too much affected by tension stiffening and overestimate aggregate interlock stiffness for the smallest values of crack opening.

With reference to concrete deterioration at the crack interface due to the bars crossing the crack, some studies /12/ suggest that the deteriorated concrete forms compressive struts at an angle to the crack interface; as a consequence, crack shear stiffness is somewhat improved, this improvement being particularly remarkable for small steel ratios, while crack normal stiffness should not be affected by concrete deterioration (°).

Also dowel action plays a non negligible role, but just how important it is remains a problem still open to discussion: for limited crack displacements this role is certainly minor.

REFERENCES

/1/ Fenwick, R.C., "The Shear Strength of Reinforced Concrete Beams", Ph.D. Thesis, University of Canterbury, Christchurch, New Zealand, 1966.

/2/ Paulay, T., and Loeber, P.S., "Shear Transfer by Aggregate Interlock", Shear in Reinforced Concrete, Vol. 1, Special Publication SP-42, American Concrete Institute, Detroit, 1974.

/3/ Taylor, H.P.J., "The Fundamental Behavior of Reinforced Concrete Beams in Bending and Shear", Shear in Reinforced Concrete, Vol. 1, Special Publication SP-42, American Concrete Institute, Detroit, 1974.

/4/ Houde, J., and Mirza, M.S., "Investigation of Shear Transfer Across Cracks by Aggregate Interlock", Research Report No. 72-06, Département de Génie Civil, Division des Structures, Ecole Polytechnique de Montréal, 1972.

/5/ Laible, J.P., White, R.N., and Gergely, P., "An Experimental Investigation of Seismic Shear Transfer Across Cracks in Concrete Nuclear Containment Vessels", Reinforced Concrete Structures in Seismic Zones, Special Publication SP-53, American Concrete Institute, Detroit, 1977.

/6/ Jimenez-Perez, R., Gergely, P., and White, R.N., "Shear Transfer Across Cracks in Reinforced Concrete", Report 78-4, Department of Structural Engineering, Cornell University, Ithaca, New York, 1978.

/7/ Mattock, A.H., "Shear Transfer in Concrete Having Reinforcement at an Angle to the Shear Plane", Shear in Reinforced Concrete, Vol. 1, Special Publication SP-42, American Concrete Institute, Detroit, 1974.

(°) The dotted curve in Fig. 17 was obtained with $\tau_o/f'_c = 0.37$ (instead of 0.31 for the other curves) in eq.(3), and with $\tau_o/f'_c = 0.245$ in eq.(4).

/8/ Mattock, A.H., "The Shear Transfer Behavior of Cracked Monolithic Concrete Subject to Cyclically Reversing Shear", Report SM 74-4, Department of Civil Engineering, University of Washington, 1974.

/9/ Walraven, J.C., and Reinhardt, H.W., "Experiments on Shear Transfer in Cracks in Concrete, Part 1: Description of Results", Report 5 - 79 - 3, Stevin Laboratory, Department of Civil Engineering, Delft University of Technology, 1979.

/10/ Hamadi,Y.D., and Regan,P.E.,"Behaviour of normal and lightweight aggregate beams with shear cracks",The Structural Engineer, Vol.58B,No.4, December 1980,pp.71-79.

/11/ Fardis, M.N, and Buyukozturk, O., "Shear Transfer Model for Reinforced Concrete", Journal of the Engineering Mechanics Division, ASCE, Vol. 105, No. EM2, Proc. Paper 14507, April 1979, pp. 255-275.

/12/ Walraven, J.C., "Experiments on Shear Transfer in Cracks in Concrete, Part 2: Analysis of Results", Report 5 - 79 - 10, Stevin Laboratory, Department of Civil Engineering, Delft University of Technology, 1979.

/13/ Bazant, Z.P., and Gambarova,P.G.,"Rough Cracks in Reinforced Concrete", Journal of the Structural Division, ASCE, Vol. 106, No. ST4, Proc. Paper 15330, April 1980, pp. 819-842.

/14/ Bazant, Z.P., and Gambarova,P.G.,"Ductility and Failure of Net-Reinforced Concrete Shell Walls", Paper J 4/9, Transactions of the 5th Int. Conf. on Structural Mechanics in Reactor Technology, Vol. J, Berlin, August 13-17, 1979.

/15/ Gambarova,P.G.,"Shear Transfer by Aggregate Interlock in Cracked Reinforced Concrete Subject to Repeated Loads", Studi e Ricerche, Corso di Perfezionamento per le Costruzioni in Cemento Armato (Reports and Researchworks, Postgraduate Course for Reinforced Concrete Structures), Vol. 1, Department of Structural Engineering (I.S.T.C.), Polytechnic University of Milan, Milan, Italy, 1979, pp. 43-70.

/16/ Clark,L.A., "Tension Stiffening in Reinforced Concrete Beams and Slabs under Short-Term Load", Cement and Concrete Association, Technical Rep. 42.521, London, July 1978 .

/17/ Gilbert,R.I., and Warner R.F., "Tension Stiffening in Reinforced Concrete Slabs, Journal of the Structural Division, ASCE, Vol.104, No.ST12, Proc. Paper 14211, December 1978, pp.1885-1900.

/18/ Gambarova,P.G.,"Ingranamento delle particelle di aggregato e trasmissione delle tensioni in elementi di c.a. fessurati, soggetti a stato piano di tensioni", Studi e Ricerche Vol.2-Reports of the Postgraduate Course for the design of r.c.structures, Politecnico di Milano, 1980, pp.103-164.

/19/ Gambarova,P.G., and Bazant,Z.P.,"Tension Stiffening Effect in Rough Crack Model for Reinforced Concrete", Paper L 1/3, SMiRT 6 Conference, Paris, August 1981.

ACKNOWLEDGEMENTS

Both the Italian National Council for Research (C.N.R.-Engineering,Reinforced and Prestressed Concrete Structures) and the Ministry of Education (M.P.I.) are to be thanked for the financial support given in the period 1978-1980 to the research program which this paper refers to.

Experimental Investigation on the Bond-Slip Law of Deformed Bars in Concrete

Recherche expérimentale sur la relation adhérence-glissement des barres nervurées dans le béton

Versuche zum Verbundgesetz von Rippenstählen in Beton

EZIO GIURIANI
Ass. Professor
Institute of Structural Engineering (ISTC), Politecnico di Milano
Milan, Italy

SUMMARY
The paper shows the results of a series of tests aimed at the analysis of the reinforcement-concrete bond, for very small relative displacements (under 0.1 mm). Several pull-out tests were carried out on cubic specimens, having a single bar with only two ribs embedded in the concrete.
The bond stiffness was analysed for different positions of the ribs, for cyclic loads with or without sign reversal. The effects of the concrete hardness at the interface with the reinforcement are discussed and the bond mechanism is examined in terms of microcracking and concrete crushing.

RÉSUMÉ
Dans cette étude on montre les résultats d'une série d'essais expérimentaux pour la détermination de la loi d'adhérence acier-béton, pour des déplacements relativement petits (inférieurs à 0,1 mm).
Plusieures épreuves de pull-out ont été faites sur des cubes d'essai avec une barre ayant seulement deux nervures faisant prise dans le béton.
On a étudié l'influence sur l'adhérence des diverses positions des nervures dans les cubes pour des charges répétées avec ou sans inversion de signe.
On analyse l'influence de la résistance du béton en contact avec l'acier et on discute le mécanisme de microfissuration et d'écrasement près des nervures.

ZUSAMMENFASSUNG
Der Beitrag zeigt die Ergebnisse einer Versuchsreihe zum Verbundverhalten von Rippenstählen im Beton mit sehr kleinen Relativverschiebungen (< 0,1 mm). Mehrere Ausziehversuche wurden an Würfeln ausgeführt, in die Einzelstäbe mit zwei Rippen einbetoniert waren.
Die Verbundsteifigkeit wurde untersucht für verschiedene Rippenlagen und für Wechselbelastung und Schwingbelastung. Der Einfluss der Betonhärte in Stabnähe auf des Verbundverhalten wurde mithilfe von Mikrorissbildung und Betondruckversagen erläutert.

1. INTRODUCTION

The bond between reinforcing bars and concrete is a very important factor not only in anchorage but also in cracking.

In /1/ it was shown that the deformations in r.c.beams,at the beginningof the second stage (when the main cracks begin and extend progressively), are largely conditioned by the bond which affects also the so-called tension stiffening in the advanced second stage. According to the model proposed in /1/, and with reference to beams in bending, in the first stage the micro-cracks (*) begin to propagate starting from the extreme tensile fiber until reaching the reinforcement. Their progressive opening up is compatible with the elastic strains in the concrete between the microcracks, and there is no slip at the interface between reinforcement and concrete (chemical adhesion phase).

After this phase, the chemical adhesion is progressively destroyed, starting from the flexural cracks, and in this same zone the bar-to-concrete slip begins (^).

This gradual loss of chemical adhesion progresses until it involves the entire surface of the reinforcement between two main consecutive cracks (+), thus setting up different static conditions for the steel in which bond decreases in importance.

All of this justifies a thorough study of the bond-slip law, particularly for small displacements. In fact, very little work has so far been done in this field (').

2. PURPOSE OF THE RESEARCH

The researchwork, which this paper refers to, is focused on the local bond behaviour, with reference to the bond law of a single rib within the range of very small slip values.

The tests are limited to one type of deformed bar with a nominal diameter of 14 mm (Fig.2) (") and consist of load cycles, with maximum slip less than one tenth of a millimeter; after the last cycle (generally the third cycle), the loads were monotonically increased up to failure with much larger displace-

---

(*) With a maximum amplitude of only some thousandths of a millimeter, and so visible only through a microscope.

(^) The bar length, over which the slip occurs, plays an important role also with reference to other problems, such as for example fracture mechanics of reinforced concrete and shear transmission through aggregate interlock.

(+) The main cracks (which generally develop from micro-cracks) form and advance progressively, all at the same time, up to the end of stage II (as shown by many tests, including those of Leonhardt in Stuttgart).

(') Even the most recent literature, though abounding in experimental and theoretical work on bond, is generally directed towards large strains and displacements.

(") The kind of reinforcing bar chosen for the tests,with slanting ribs (see Fig.2) is becoming more and more widely used in practice.

ments.(*)

During the tests useful information was also gathered on various phenomena that occur in the vicinity of the ribs. Though these phenomena have already been discussed by other authors, their effect on small relative displacements is still uncertain.

As already shown by Goto /2/ (Fig.1), radial micro-cracks form around each rib immediately after the formation of the principal cracks. It has also been shown in /3/, that as slip increases, the high bearing stresses acting on the rib faces provoke local crushing in the concrete, with resulting deformations of a permanent nature. As to bond, the experimental work by Rehm /3/ is particularly valuable, since it was the first and so far still the most significant on the local bond-slip law. For his pull out tests he used a special bar with a single rib placed in the center of a concrete cube (20 cm per side)(^). Rehm was mostly interested in comparing different types of deformed bars, and his main purpose was to determine the strengths of various rib shapes in the range of large relative displacements. He obtained a remarkable number of useful results, one of which showed the importance of the position of the reinforcement with respect to the direction of concrete casting. He noted considerable differences in the cases of a bar parallel to the casting direction or at right angles to this direction, as a result of the different porosity of the concrete surrounding the reinforcement.

In Rehm's opinion this was due to the water, which tends to rise to the surface during compaction(+). He also noted the importance of local crushing of the concrete in contact with the reinforcement, leading to the permanent displacements already mentioned. However, since he used monotonically increasing loads, his tests can supply no certain data on the beginning of crushing('). Furthermore, he located the bar in a central position, while often the reinforcement is located close to one of the faces of the beam, so the analysis for different positions of the rib is certainly useful(").

(*) Beyond this value the reinforcing steel of a beam in bending generally reaches the yield point (stage III) as shown in /1/, for the usual values of crack spacing.

(^) Special lubricated sleeves around the bar, just before and after the rib, were placed to prevent the adhesion between the bar and the concrete.

(+) In the tests herein examined, the bar was always horizontal, so perpendicular to the casting direction. Furthermore, with reference to the particular rib shape, also the rib orientation is important: the lugs (sickle-shaped) were always sub-horizontal (Fig.3).

(') This problem will receive greater attention in sect. 5.

(") The deformed bars tested in the present researchwork, with sickle-shaped lugs, were not available at the time of Rehm's tests.

3. TEST PROCEDURE AND EXPERIMENTAL SET-UP

The usual pull out tests on long bars do not give suitable results for evaluating the local bond stress slip law. They only give the average bond stress and the slip at the bar extremities. Specific tests are necessary to find the local bond stress slip law, using reinforcing elements of very limited length.(*)

In Fig. 2 the reinforcing element used in the test is shown. It has two ribs on each side, and was obtained from a normal deformed bar of 14 mm in diameter (core diameter 13.2 mm); its length is twice the rib spacing (16 mm). Starting from a normal ribbed bar, the two parts adjacent to the test rib are machined at the turning lathe, the diameter being reduced to 8 mm. The two machined spindles are inserted in smooth aluminium sleeves, which are removed after the concrete has hardened(^). The spindles protrude from the cube faces (Fig.3), so that the measurement of the slip is possible at one end of the bar, while at the other end the pull out force is applied.

In Fig. 3-a the four test positions adopted for the reinforcing element are shown. In this way it becomes possible to analyse, within the range of small displacements, the role played by the concrete covering, and also the local bond stress slip law for various positions of the ribs along the bar. In Fig. 3-b the orientation of the lugs and the direction of casting are shown(+).

The concrete test cube was glued along one face (Fig.3) to the loading set-up in order to get as near as possible to the real conditions of the concrete block between two flexural cracks in a beam subjected to bending (fig.3-c)(').

(*) In this way the slip will be the same at all points on the bar.

(^) The external diameter of the sleeves (14.5 mm) is the same as the external diameter of the lugs. The internal diameter of the sleeves is 12 mm. To facilitate the removal, the sleeves are covered with a film of paraffin. The cavity formed after the removal of the fore sleeve (see the sketch) enables the ribs to work in the same conditions as in an actual bar with many ribs embedded in the concrete mass.

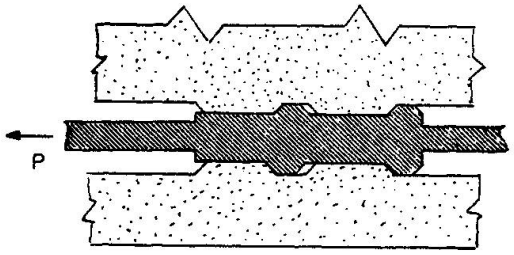

(+) Expanded polystyrene molds were used for the castings to avoid the thermal gradients in the concrete during hardening.

(') In Fig. 3-a the transversal restraints of the bar: the purpose is to avoid misalignments of the load especially when the load is reversed.

In Fig. 3-d the layout of the instruments for the measurement of the displacement is shown(*).

In Figs.4,5 a picture of the test set-up is shown. Because of the length of time (12 to 36 hours) required by each test, a loading device based on levers and water tanks was preferred to a system of hydraulic jacks, also because of the relatively limited value of the loads.

During the test the load was monotonically increased up to a fixed value of the slip (7.5 hundredths of a millimeter). Next, it was reduced to zero, then it was reversed in order to make the bar retract(^). It was not possible to obtain partial retractions, of pre-fixed values, because of the sudden re-entry of the bar.

During the tests, the slip was heavily influenced by the time-rate of load application. However, in each test, at each load step (200N), the load was kept constant until the slip value was stable(+).

Fig.6 shows a typical time-dependent curve of the displacements: for each load step the slip δ tends towards a stable value.

The stabilization of the slip required a considerable length of time in the nearly horizontal branch of the τ/δ curve, with respect to the steep branch at the lowest slip values (see Fig.7).

4. RESULTS

The geometrical characteristics of the reinforcement and the mechanical characteristics of the concrete are given in Fig.2 and tab.I. The curves referring to the bond stress and to the displacement between concrete and bar (slip δ) are shown in Figs. 8-18.

The bond stress is defined as(') :

$$\tau_{ad} = P/(\pi d2c)$$

(*) The deflectometer applied to the bar measures the displacement of the two ribs embedded in concrete, while a second deflectometer measures any possible displacement of the cube in a point at some distance from the zone disturbed by the ribs.

(^) The reversal of the load to thrust the reinforcement simulates the behaviour of a beam in bending which, during the unloading phase, shows partial closure of the cracks, with the bars moving back.

(+) The concrete deformations were considered as stable when the time-rate of the slip was less than 10^{-4} mm per hour. For monotonically increasing loads, this criterion leads to a nearly constant slip velocity.

(') The term "bond" here is used for both chemical adhesion (with zero relative displacements) as well as for the mechanical bond with bar-to-concrete slip. It follows that the bond stress is actually a nominal stress relating the force applied to the bar to the nominal surface of the reinforcement (embedded in concrete). Then the bond stress takes into account all the effects involved, such as the bearing action of the lugs, and the friction produced by the radial pressure of the concrete at the tops of the lugs.

(with P the load, d the nominal diameter of the bar and c the spacing of the ribs).
The $\tau(\delta)$ curves of each test N_i (i = 3,4,7,8) are adimensionalized, the actual values of the bond stress being divided by the value $\bar{\tau}_{Ni}$ which refers to the value 0.075 mm of the slip (the value $\bar{\tau}_{Ni}$ appears at the head of each diagram).

Fig. 8 shows the curves for test N8 with the bar in a central position. During the first cycle the load was increased up to a slip value of 0.075 mm (branch O_1 A_1 B_1 C_1). It was next decreased to zero (C_1 D_1), and then, by reversing the sign(D_1 E_1), the bar was forced to re-enter (E_1 F_1) and this occurred with virtually instantaneous slip starting at E_1 (*).

The slip (at constant reverse load) stopped at a point corresponding to a residual displacement (^) (see point F_1).

The cycle was completed (branch F_1 G_1) by re-setting the load to zero. The following cycles (2 and 3) differ considerably from the first in the loading path. After a first steep short branch (G_1 H_2) the curve flattens off (H_2 K_2) with small sudden displacements in the way that is typical of friction (+).

In the branch K_2 C_2 (and also in K_3 C_3) the load was increased up to the maximum value reached in the first cycle, but the maximum relative displacement was of a higher value. The unloading paths C_2 D_2 and C_3 D_3 are practically identical with the corresponding C_1 D_1 of the first cycle.

Also the branches D_2 E_2 and D_3 E_3 are also practically identical (') with D_1E_1. In all three cases at E_1, E_2 and E_3 there is unrestrainable sudden slip up to F_1, F_2 and F_3, the latter points being very close indeed. In Figs. 9, 10, 11 the curves for the other positions of the bar (tests N 7, N4, N3) are shown. In Fig. 11 a star indicates the point at which splitting parallel to the bar first appeared (the microcrack was detected by means of a microscope). For the sake of comparison, in Fig.12 the curves for these four cases are superimposed. The comparison is limited to the first cycle and the first branch of the second cycle. The loading paths OABS show relatively modest differences (").

(*) Because of the instantaneous re-entry of the bar, the branch E_1F_1 is dashed. Sudden slip may be explained if one thinks that crushing has led to the formation of a cylindrical cavity in which the bar can move freely, apart from some unavoidable friction.

(^) This residual displacement is due to the presence of particles of aggregate in the cavity left by the lugs in the loading phase.

(+) For further details, see sect. 5.

(') The values of the reverse load needed to pass from E_2 to F_2 and from E_3 to F_3 are a little more than half the load needed to pass from E_1 to F_1.

(") The slope of the loading path, at the origin (branch DA) is less steep for peripheral reinforcement, which seems reasonable.

There are also limited differences in the unloading path of the first cycles (branch C D). The curve of test N3 is less steep as a result of a split parallel to the reinforcement.

Fig.13 shows the curves obtained in test N8, with reference to cycles 4-20. The load was limited so as to get a fixed value for the relative displacement (0.17 mm).

The maximum value of the ratio τ_{ad}/τ_{N8} continues to decrease for each cycle, but with a tendency to stabilize around a value which is about two-thirds of the initial value(*) - see the 4th cycle and the 20th cycle.

Fig.14 shows the behaviour of test specimen N8. Here the load was decreased to zero and then increased again without any sign reversal.

In Fig. 15 the curves of the actual bond stress in the four cases examined, are superimposed.

Although the strengths f_c of the concrete were fairly similar, as shown in the figure, the values of τ_{Ni} (^) were very different. τ_{N8} is equal to 0.59 τ_{N4}.

The fact that the bond stresses τ_{Ni} are almost independent of the specific strength fc of the concrete is also underlined in fig.16, where the ratio of the bearing stresses of the lugs to concrete strength are plotted versus bar slip(+).

The value of local bond strength depends rather on the local hardness of the concrete adjacent to the lug, but it is difficult to evaluate(') . An examination of the test cubes cut along the mean plane containing the bar axis, after the tests showed that those with lower values for local bond strength had a more marked porosity, characterized by voids of some tenths of millimeters in diameter (see Fig. 17).

(*) The work dissipated in each cycle decreases as the number of cycles increases. The loading and unloading paths tend to get closer for each successive cycle, but up to a certain limit (see the modest difference between cycles 14 and 20). Crushing of the concrete in contact with the lugs does not seem to progress with the increase in the number of cycles. The gradual decrease in work dissipated is perhaps due to friction between the tops of the lugs and the concrete, which diminishes because of the repeated scraping.

(^) As already pointed out, τ_{Ni} represents the value of local bonding corresponding in the various cases tested to the relative displacement δ = .075 mm.

(+) The concrete compressive strength was measured on prismatic specimens (100x100x200 mm) cut out from the original cubes. The bearing stress σ_n is defined as: $\sigma_n = P/(4a_m \cdot l_R \cdot \cos(90^o-\beta))$ where a_m is the average height, l_R the length and β the orientation of the lug (see Fig.2).

(') To the author's knowledge no data on this problem is yet available in the literature.

Schlerometric tests were carried out on the concrete adjacent to the reinforcement to get some first ideas on the subject(*).

The average values from the schlerometric tests are given in table II . These values of course, are only partly related to the local strength of the concrete, because of the limited section of the prod(^). These results do make it possible to define an index of "relative hardness" for each case, as a ratio between the hardness of the case involved and the hardness of the test piece with central reinforcement (N8). With K_{si} to indicate this relative hardness, Fig.18 shows the curves of the "reduced bond stress" τ_{ad}/K_{si} as a function of the relative displacements. The deviation from the mean value does not exceed $\pm$ 5%. These curves point out the importance of the local hardness of the concrete over other parameters.

Fig.19 shows the curves τ_{ad}/τ_{Ni} for large displacements (1.5 mm). In case N3 the appearance of the first crack (split, see point I) while still in the range of small displacements has no appreciable effect on bond. It is the transversal crack (II) which leads to a reduction in stiffness. However, there is a long softening branch up to failure, which occurs at a relative displacement of 1.7 mm(+).

5. SOME CONSIDERATIONS ON THE BOND MECHANISM

Fig.20 gives the local bond stress slip curve for test specimen N9 with the bar close to one of the faces. As in all cases the curve shows a characteristic trilateral shape (OABC) with decreasing slope.

During this test, four load cycles were performed keeping the displacements very small (less than 3/100 of a millimeter).

In the first branch of the trilateral curve (OC_1) the behaviour is practically elastic (the first cycle has negligible hysteresis) with elastic shear in the concrete and without any relative displacement at the bar-concrete interface (bond is due to chemical adhesion).

After the first cycle, the load was increased up to C_2, not much beyond point A which marks the beginning of the second branch. Then the unloading (to D_2) and reloading up to C were carried out. The virtually elastic behaviour along paths C_2D_2 , D_2C_2 and the residual displacement OD_2, could perhaps be explained as follows.

(*) A small test prod (tab.II) was attached to the schlerometer tip, in order to reach the surface of the groove left after the test cube was split and the bar removed. The readings were repeated about twenty times in different positions along the groove surface.

(^) In tab.II the concrete hardness (obtained with the reduced prod) measured along the groove surface and on the external surface are shown.

(+) This behaviour related to crack II is certainly less remarkable in a real case, with continuous reinforcement.

Once the load goes beyond a value corresponding to point A, radial micro-cracks form around the bar starting from the lug tops (Fig.21-a). When the load is reduced to zero, these micro-cracks do not completely close up. This is partly due to the friction among the aggregate particles protruding from the crack faces, but also to the wedging action of the loose particles.

After the second load cycle the load was progressively increased up to a value corresponding to point B (Fig.20), which marks the beginning of the third branch.

Once again the unloading and re-loading process was performed (C_3 D_3 and D_3 C_3), with again practically elastic behaviour and very limited hysteretic behaviour. The average slope of curves C_3 D_3 and D_3 C_3 is rather less than curves (1) and (2), because the micro-cracks propagate and spread, thus making the concrete adjacent to the lugs less rigid. Starting from C_3 the load was again increased, and crushing of the concrete in contact with the lugs began, as a result of very high bearing stresses on the lugs.

Because of concrete crushing, permanent displacements are possible (Fig.21-b): as a consequence, a cavity forms behind each lug.

Complete unloading (to D_4) was performed starting from point C_4.

During the unloading process the microcracks tend to close up almost completely, but on the surfaces of the lugs the radial compressive stresses P_r continue to be applied, though because of the shape(*) of the cavity produced during the loading process BC_4 these stresses are applied along a part of the top of the lugs.

Because of these radial stresses, the reinforcement subjected to load reversals is partially prevented from slipping back (Fig.20-d). This load, however, does help to close the micro-cracks.

When the load reached a value corresponding to point E_4 (Fig.20) a sudden slip began: this is because the equilibrium of the lug is no longer possible when the lug is pushed out of the cavity, which was produced by concrete crushing during the load process (Fig.21-d).

After the sudden slip (which occurs at constant load), the position of the lug is practically the same as the initial (no-load) position, though a slight residual slip remains, because of the loose particles detached during the loading and unloading process.

In the fourth cycle, for load levels below point K_4 (Fig.20) the bond stiffness is very limited, because the only force acting on the lugs is friction at the top (^).

(*) The nominal failure surface (Fig.21-a) makes the angle α with the deformed surface of the concrete adjacent to the bar; because of the elastic strains, this concrete gets detached from the lateral surface of the bar, between two contiguous lugs.

(^) It is interesting to note that points E_4 (the lug leaves the crush-induced cavity) and K_4 (the lug is engaged in the crush-induced cavity) are characterized by practically the same displacements. Furthermore, the slip δ_{C1} (between E_4 and F_4, Fig.20) coincides with the length of the crush-

./..

Beyond point K_4, the lugs are engaged in the concrete, due to the conical surface of the cavity produced by earlier crushing; as a consequence, the bond stiffness increases (K_4H_4), because of the friction resulting from the radial pressure.

At the same time the micro-cracks again open up around the lug, so that the slope of the branch K_4 H_4 (Fig.20) is on average less steep than the slope of C_4 D_4.

At point H_4 the front face of the lug is again in contact with the crushed concrete: it follows that the value of the bond stress in H_4 is hardly different from the value in B, which marks the beginning of concrete crushing. (Beyond H_4, further crushing occurs).

6. CONCLUSIONS

The local bond stress slip curves in the range of displacements below one tenth of a millimeter do not seem to be markedly affected by the position of the reinforcement with respect to the faces of the test cube and the amount of concrete cover.

As a consequence, the test results suggest that in a beam subjected to bending the rib-to-concrete bond is not markedly affected by the position of the rib with respect to the beam faces and to the flexural cracks.

The test results show that the considerable scattering of the values of the bond stress, for any given slip, is mostly due to the different porosity of the concrete layer immediately surrounding the bar, while the concrete compressive strength seems to be a minor factor.

Should bond stress be related to the hardness of the concrete layer in contact with the ribs (through a suitable "hardness index"), the scattering of the bond stress/slip curves will be reduced to only about 5%: the dependence of the bond strength on the hardness of the concrete along the bars seem to be so important that further tests on a larger scale ought to be carried out to confirm the above statement.

Finally, the experimental curves, obtained with cyclic loads characterized by a limited reversal, clarify the role of microcrack opening and concrete crushing with reference to bond stiffness. This role has different aspects when the load is increased (microcrack opening, possible splitting, concrete crushing) or when the load is decreased and reversed (friction at the top of the ribs, free slip to recover the cavity produced by earlier crushing).

ACKNOWLEDGEMENTS

My thanks are due to Prof.Dei Poli, Director of the post-graduate course on r.c. structures at the Politecnico di Milano, for his constant interest and suggestions all through this research, which was financed by a grant from the Italian National Research Council (CNR) in 1980.

./..

induced cavity. The slip δ_{C2} (between B and C_4) does not coincide exactly with δ_{C1}, because the crushing of the concrete occurs at the same time as the opening of the microcracks.

SYMBOLS

δ : relative displacement (slip) between the reinforcing bar and the surrounding concrete

$\tau_{ad} = P/(\pi d\ 2c)$: nominal bond stress

P : pull-out load

d : nominal diameter of the bar

c : pitch of the ribs

τ_{Ni} : nominal bond stress for each test specimen at $\delta = .075$ mm

$\sigma_n = P/(4a_m l_R \cos(90-\beta^o))$: bearing stress on the ribs

a_m : average height of the ribs

l_R : length of the ribs

β^o : angle of the ribs with respect to the longitudinal axis

f_c : prismatic concrete strength of each test specimen, measured on prisms cut out from each specimen, after the pull-out test

K_{si} : relative hardness index defined as the ratio between the concrete hardness of the generic i^{th} test specimen and the hardness of the specimen with central reinforcement (N8). The hardness is measured (with a suitable sclerometric test) in the groove left by the bar in the concrete, after having cut the test specimen.

REFERENCES

/1/ Giuriani E., "Le curvature di travi in cemento armato tenso e presso-inflesse nel primo e secondo stadio" Costruzioni in Cemento Armato. Studi e Ricerche, vol. 1, 1979, Politecnico, Milano.

/2/ Goto, Y, "Cracks formed in concrete around deformed tension bars" ACI Journal, April 1971.

/3/ Rehm G., "Über die Grundlagen des Verbundes zwischen Stahl und Beton". Dafst, Heft 138, Berlin, W.Ernst u.Sohn, 1961.

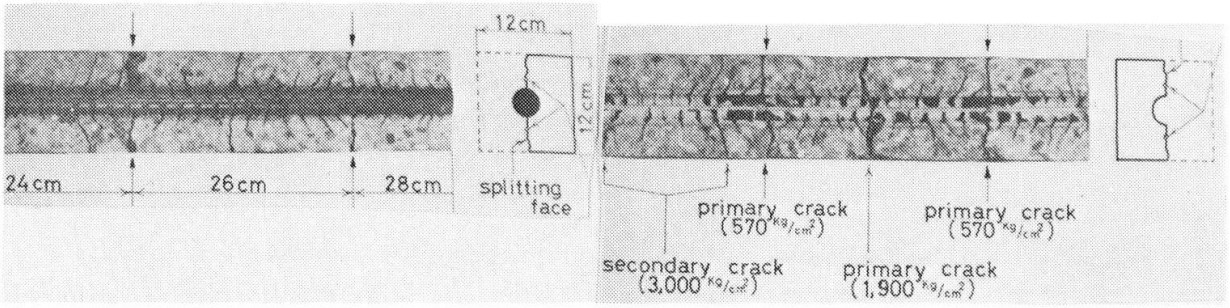

Fig. 1 - Cracking and microcracking of concrete near the ribs of a deformed bar, shown by Goto /2/

d = 14 mm nominal diameter

ϕ = 13.95 mm diameter of the equivalent round bar

D_K = 13.2 mm diameter of the core of the bar

c = 8 mm pitch of the ribs

a_m = .8 mm average height of the ribs

β = 56° angle of the ribs

l_R = 20 mm length of the ribs

$$I_R = \frac{2\, a_m\, l_R \cos(90-\beta)}{\pi\, D_K\, c} = .818 \text{ bond index}$$

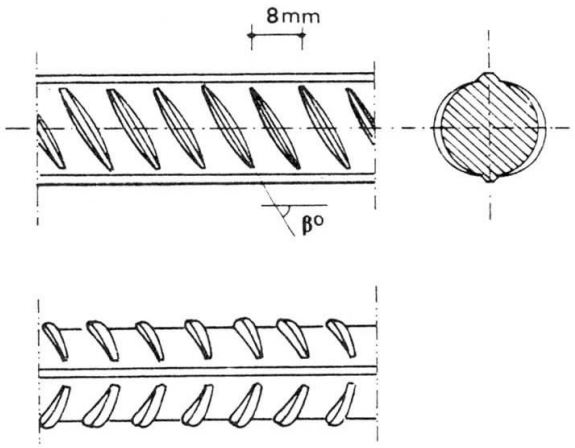

Fig. 2-a Geometrical characteristics of the deformed bar used in the tests

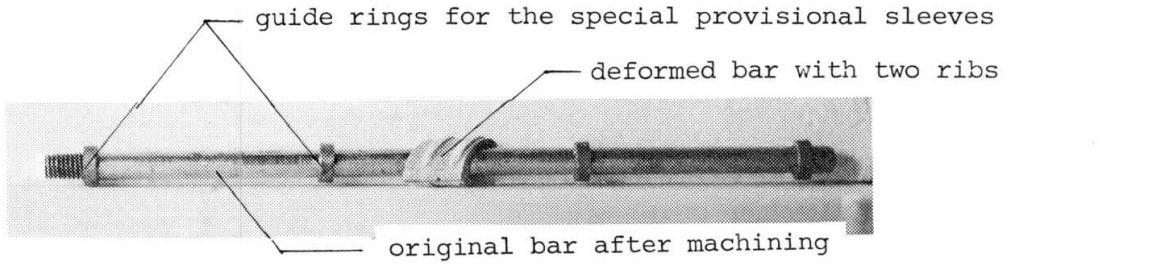

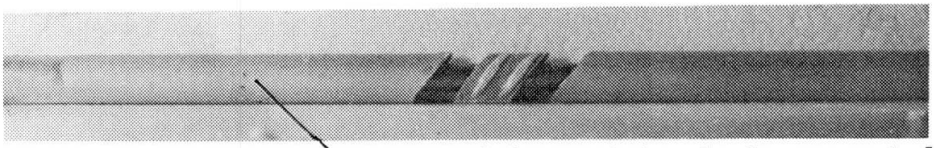

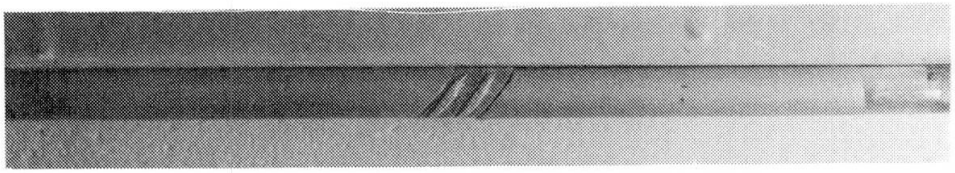

external aspect of the test bar before concrete casting, with the provisional sleeves closed up to the ribbed element

Fig.2-b - The two-ribbed element of deformed bar and the special provisional sleeves

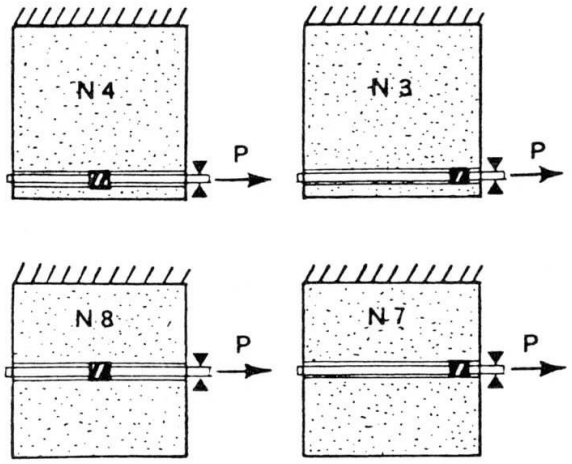

Fig. 3-a - Longitudinal cross-sections of the test specimens to show the position of the bar

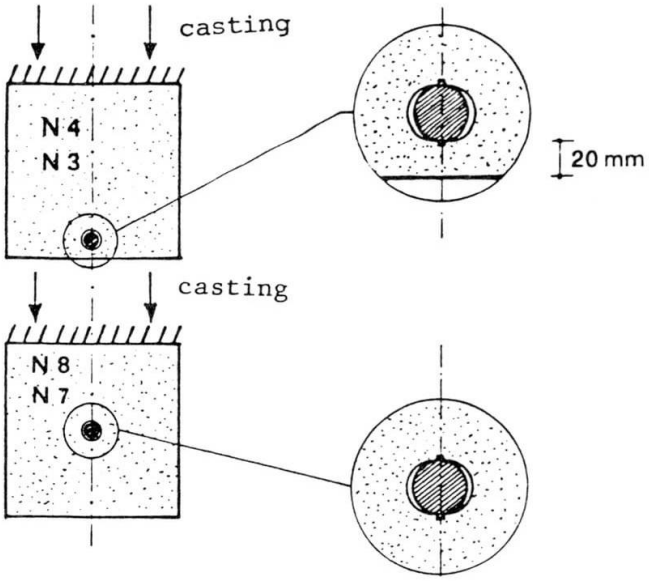

Fig. 3-b - Transversal cross-sections of the test specimens and orientation of the lugs

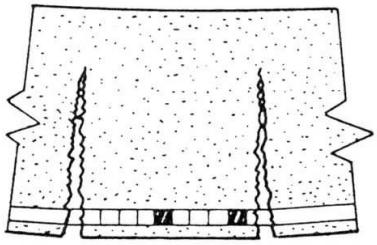

Fig. 3-c - Actual situation of a beam in bending: the test specimens N3 and N4 simulate this situation

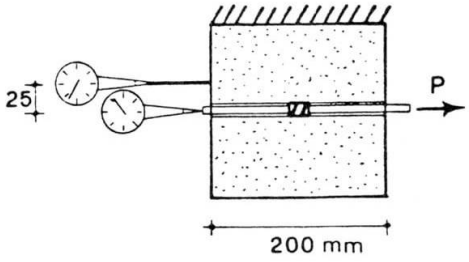

Fig. 3-d - Instruments to measure slip

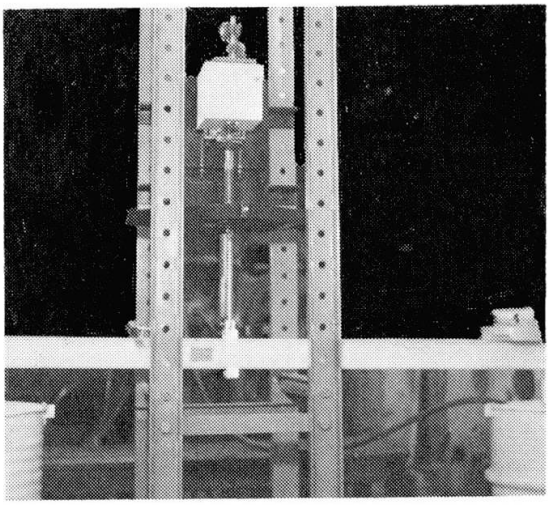

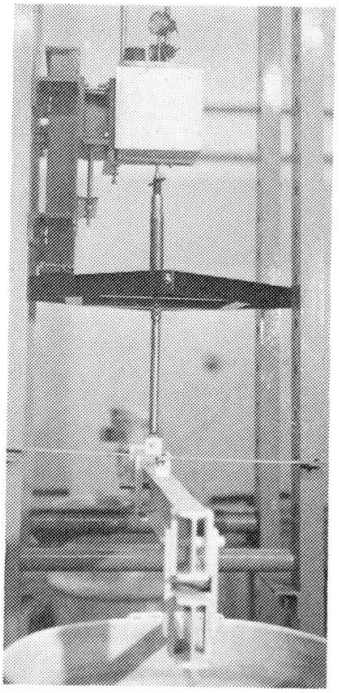

Fig. 4 , 5 - View of the loading set-up: the loads are applied via watertanks and levers, which makes the load reversal possible

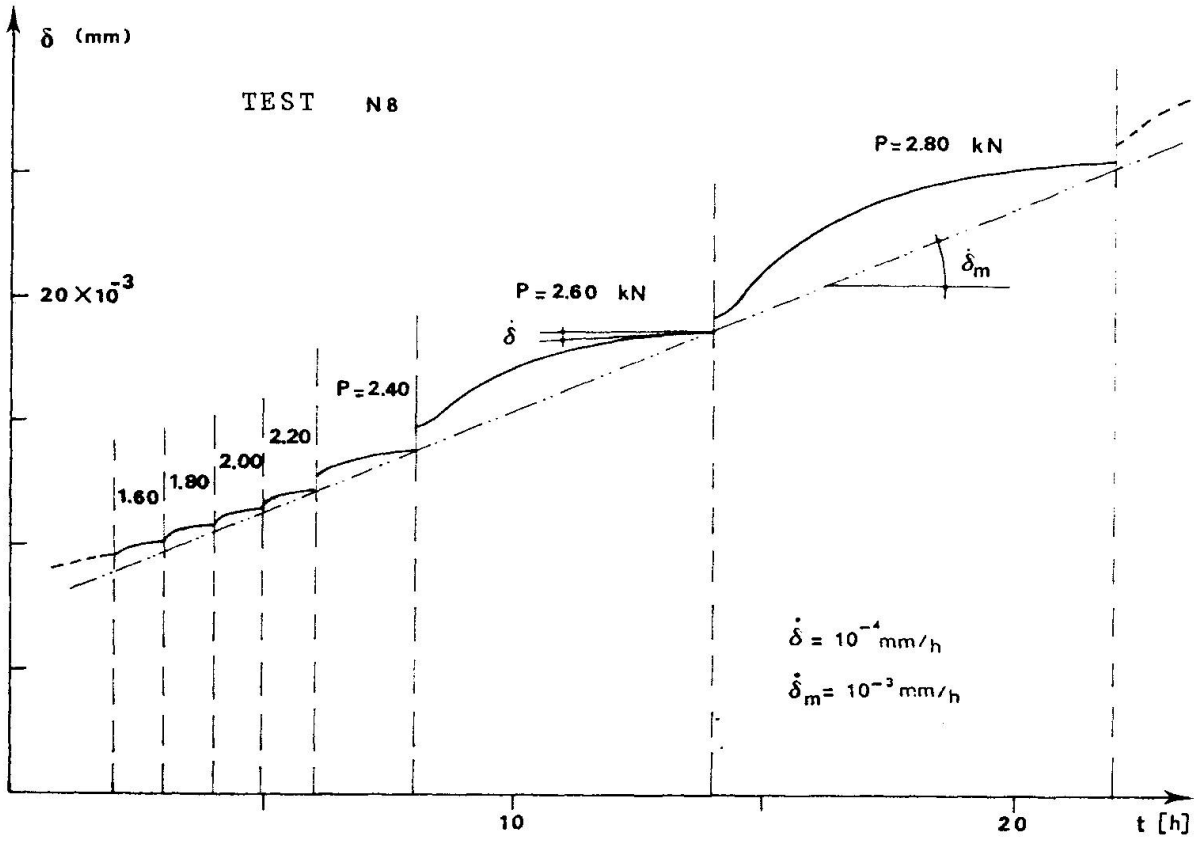

Fig. 6 - Slip curve for different load steps, versus time

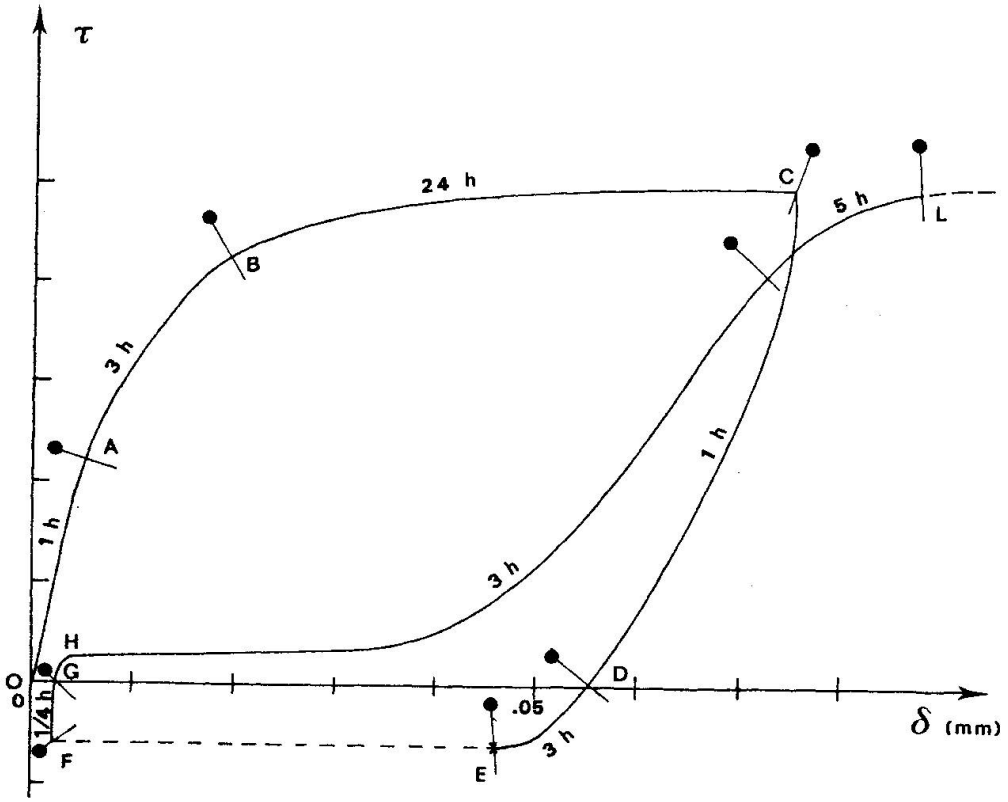

Fig. 7 - Bond-slip curve with the length of time taken by the various phases

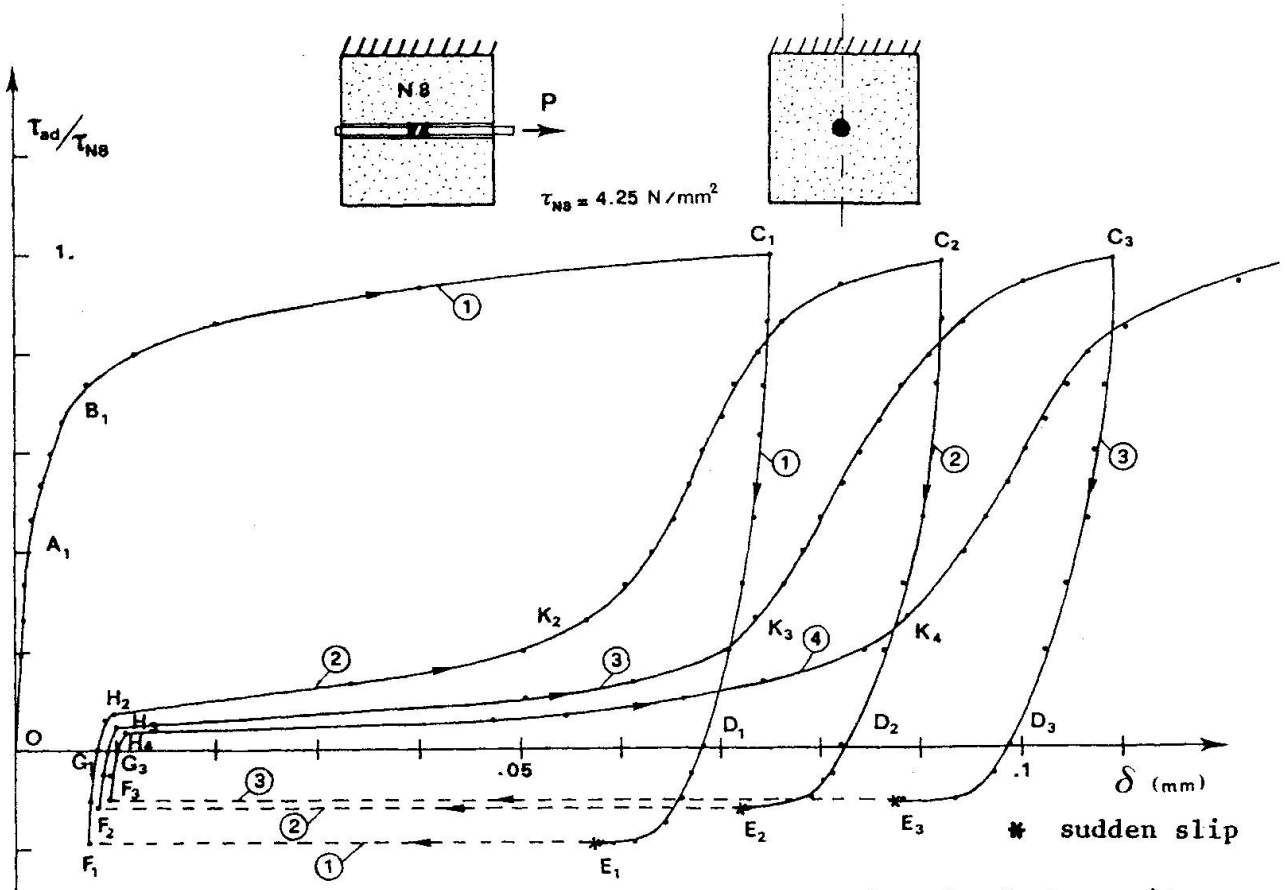

Fig. 8 - Bond-slip curves with cyclic loading (the maximum bond stress is kept constant in each cycle)

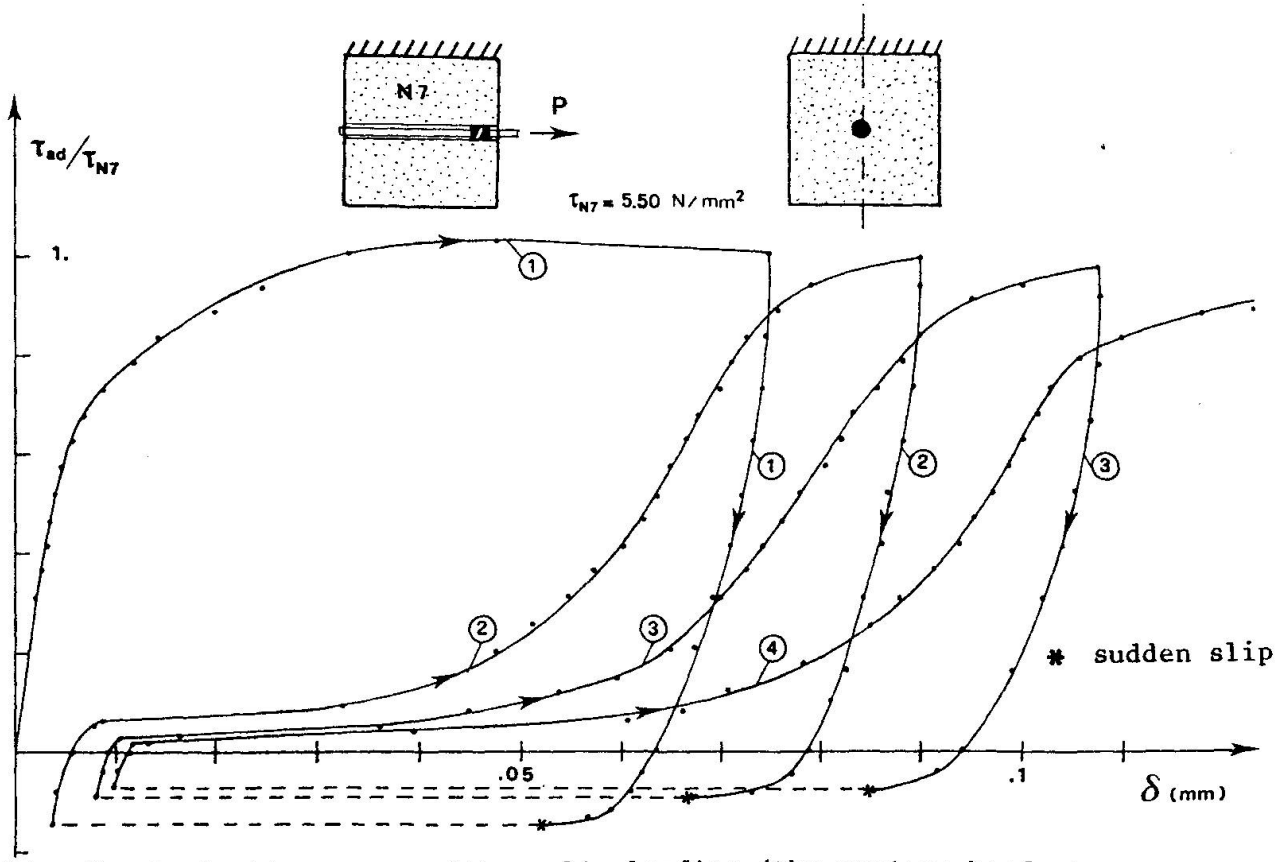

Fig. 9 - Bond-slip curves with cyclic loading (the maximum bond stress is kept constant in each cycle)

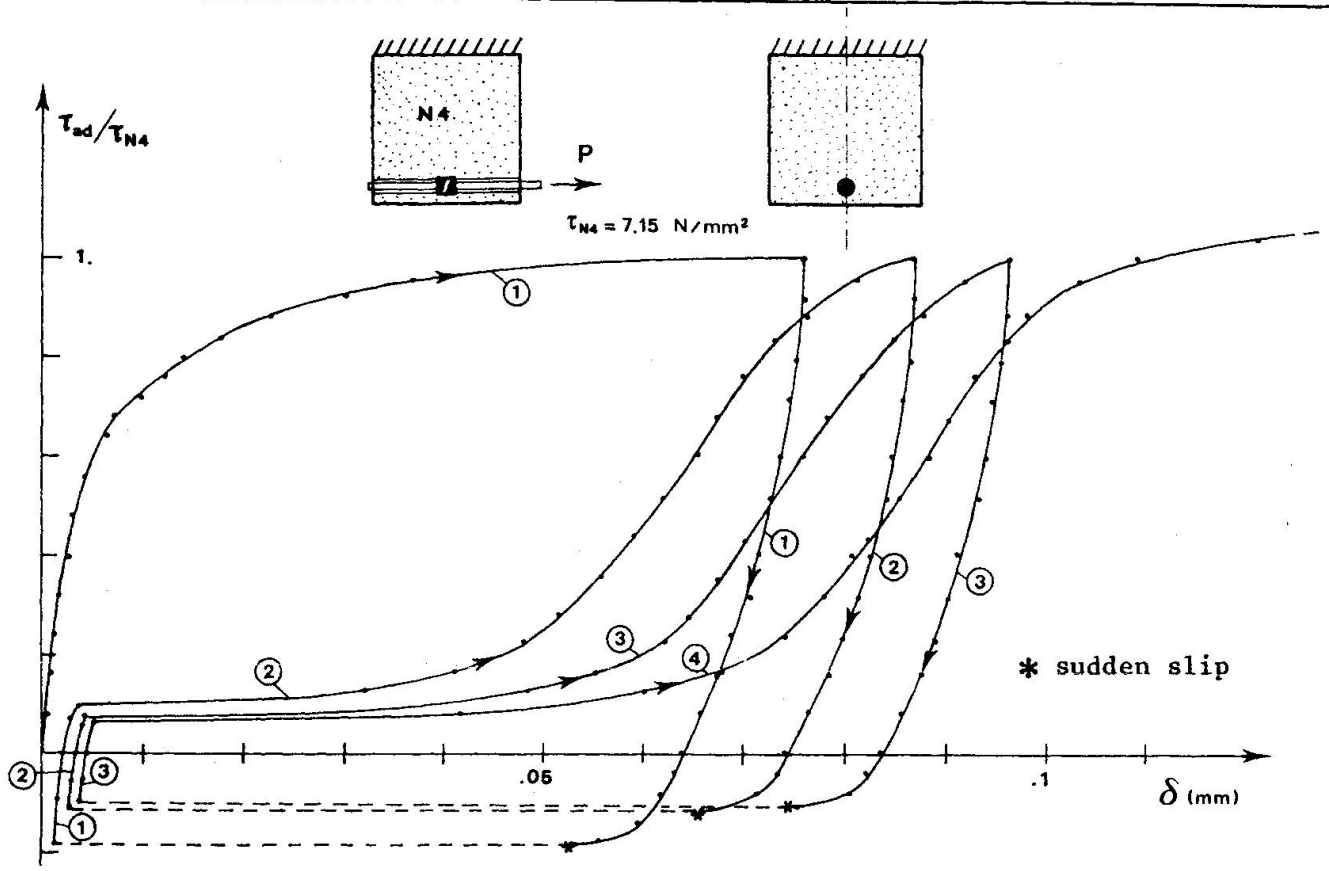

Fig.10 - Bond-slip curves with cyclic loading (the maximum bond stress is kept constant in each cycle).

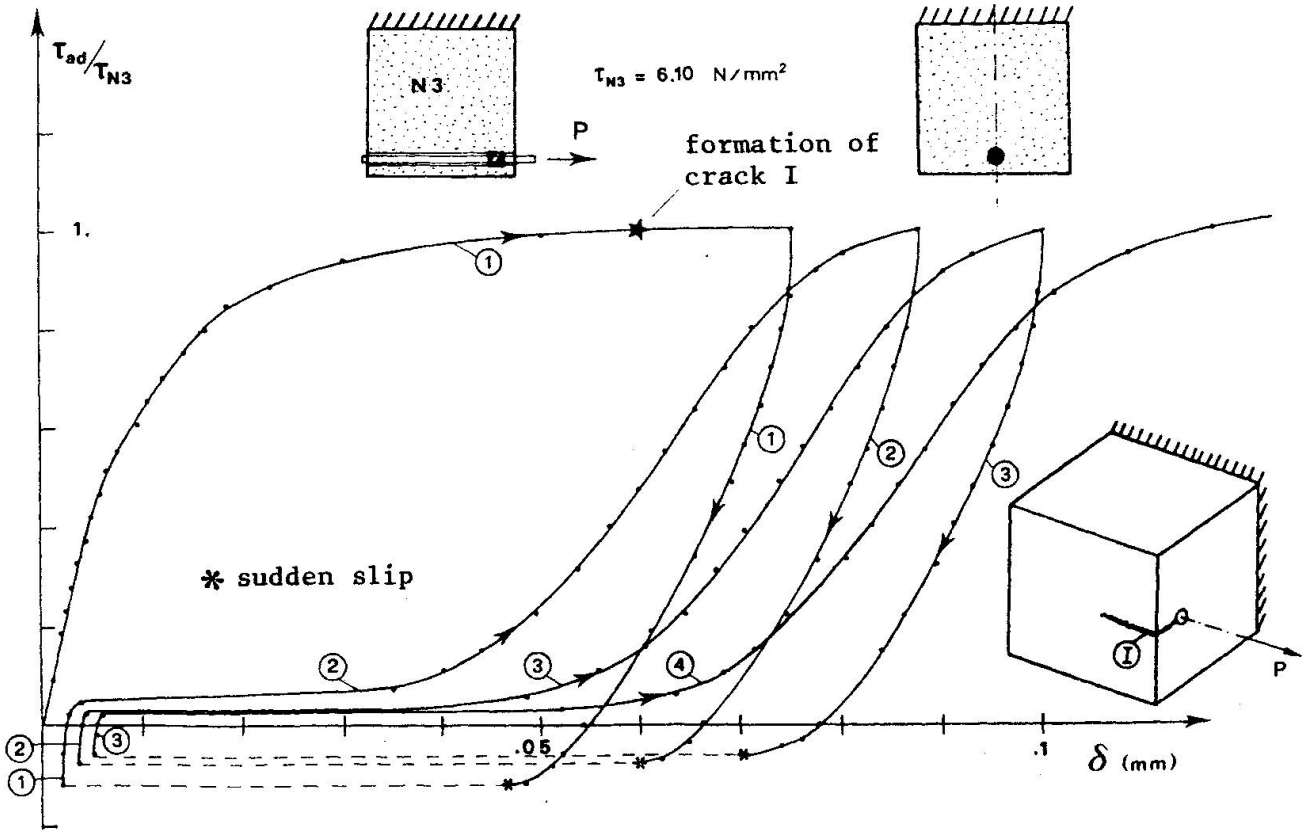

Fig. 11 - Bond-slip curves with cyclic loading (the maximum bond stress is kept constant in each cycle)

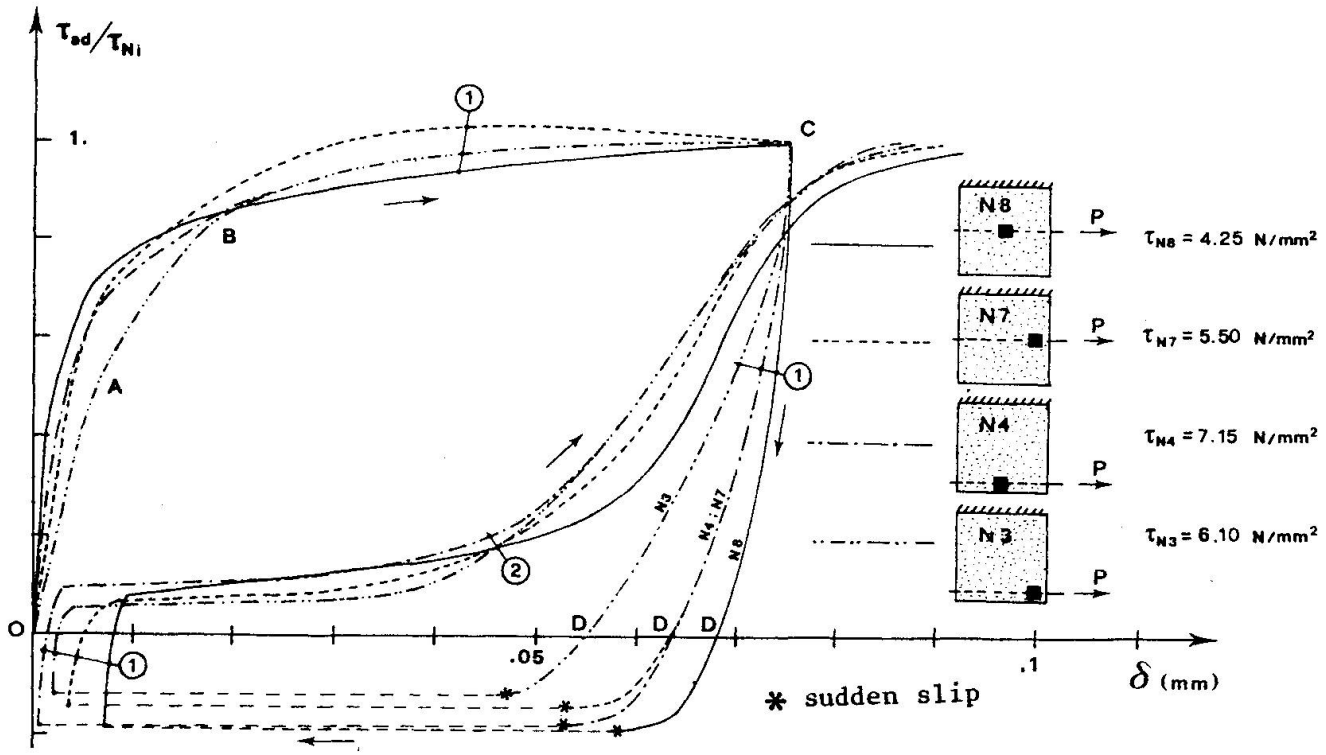

Fig. 12 - Bond-slip test curves, with the bond stress related to the nominal stress τ_{Ni} of each test specimen

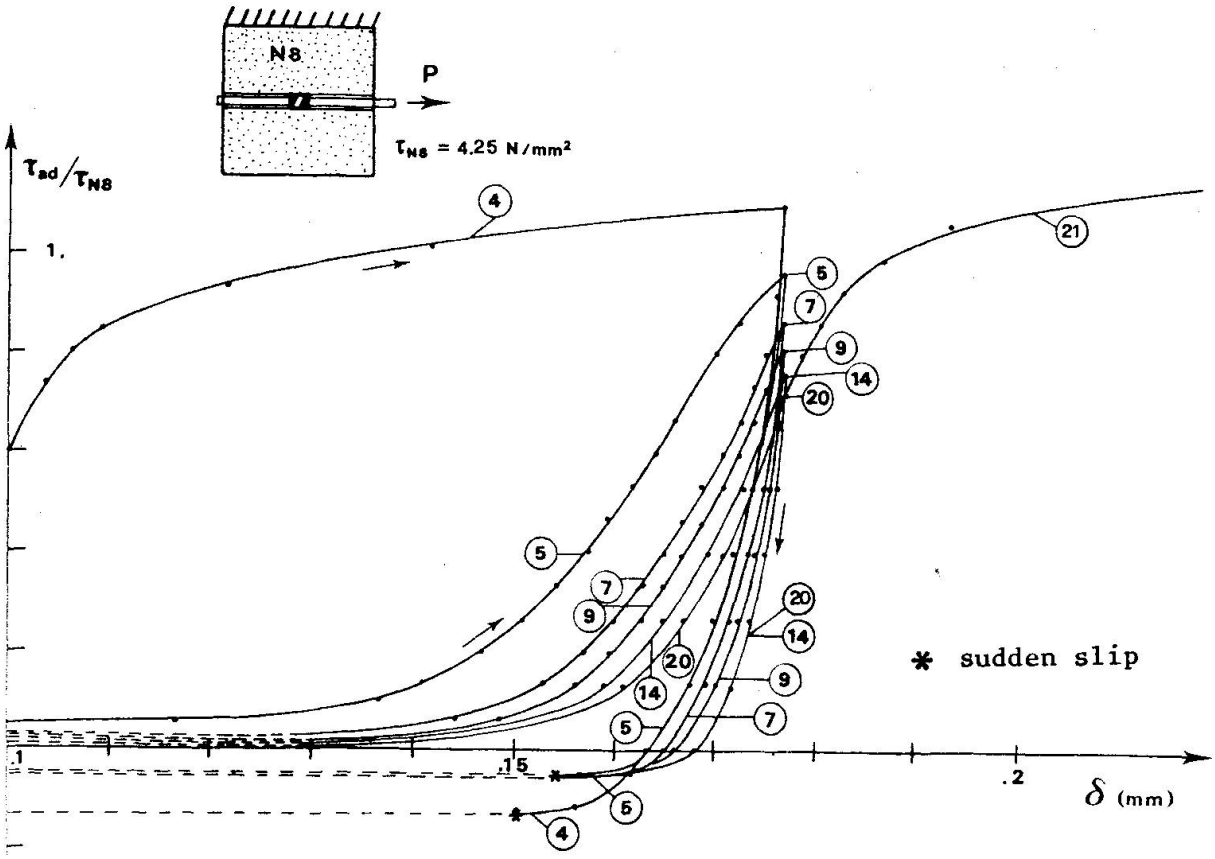

Fig. 13 - Bond-slip curves with cyclic loading (the maximum slip is kept constant in each cycle)

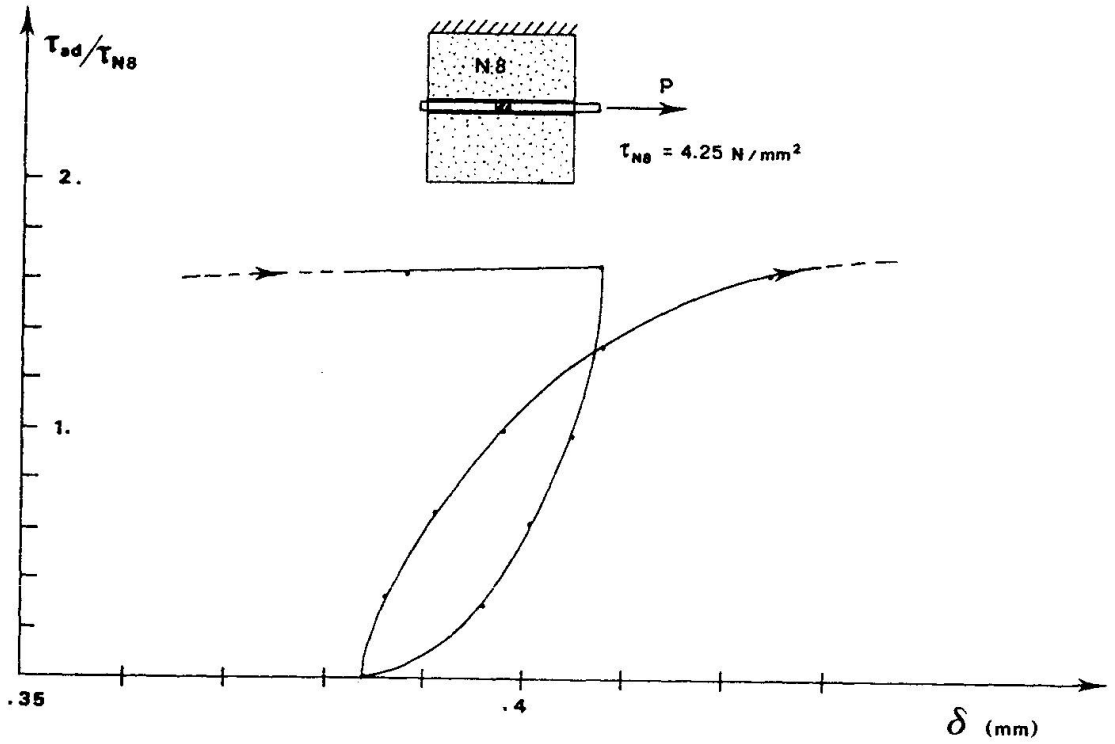

Fig. 14 - Bond-slip curve obtained by reducing the load to zero and re-loading without sign reversal

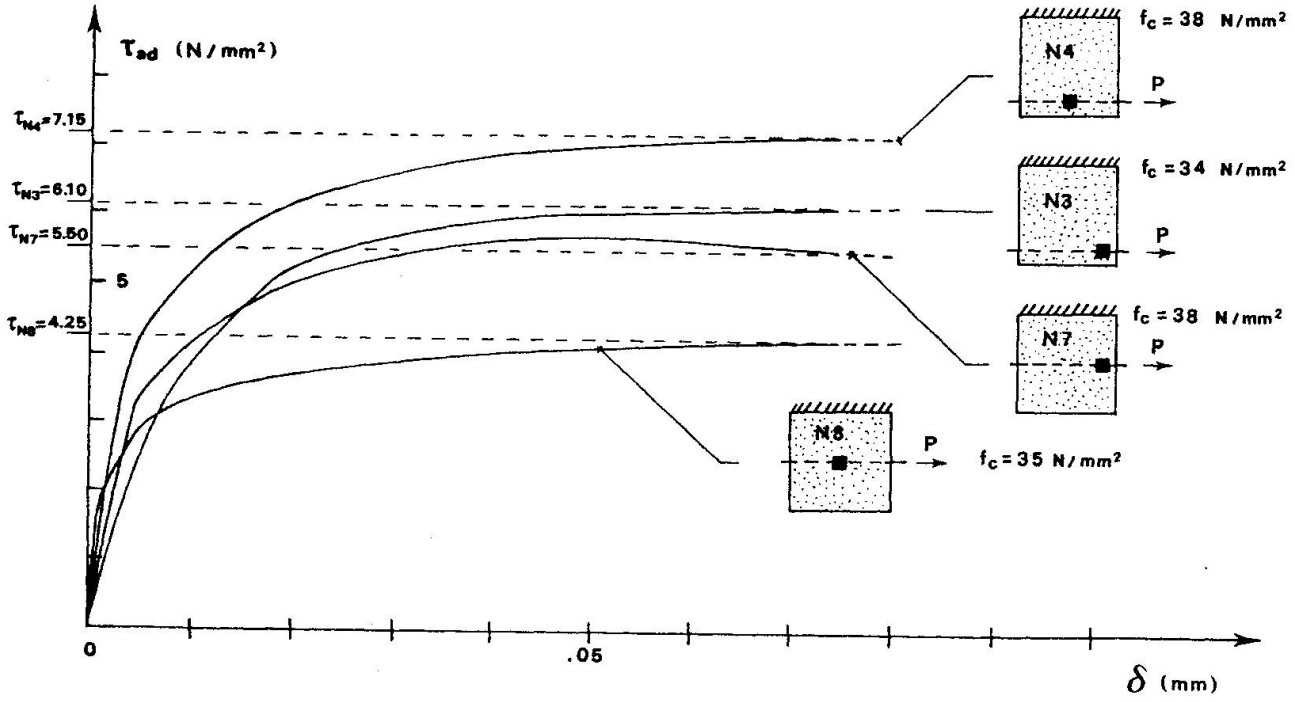

Fig. 15 - Comparison between bond-slip curves for monotonically increasing load

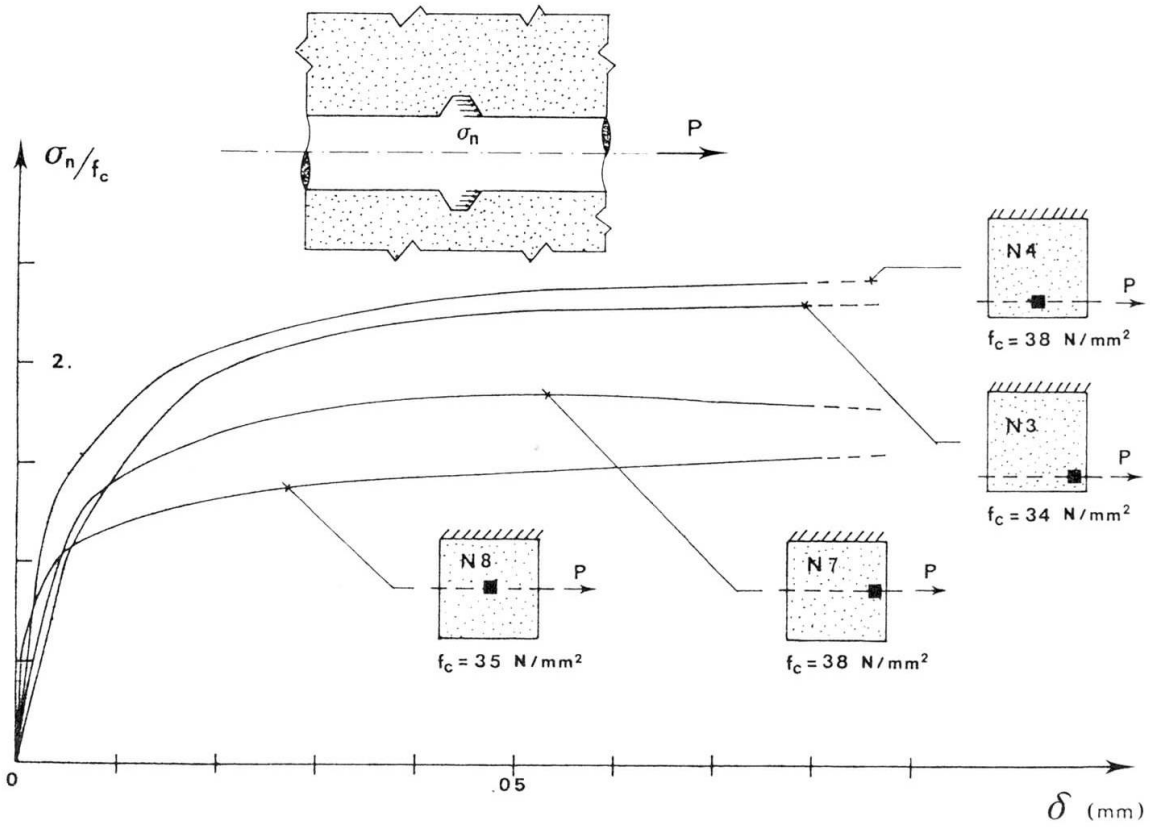

Fig. 16 - Bearing stress on the concrete related to the prismatic strength of each test specimen

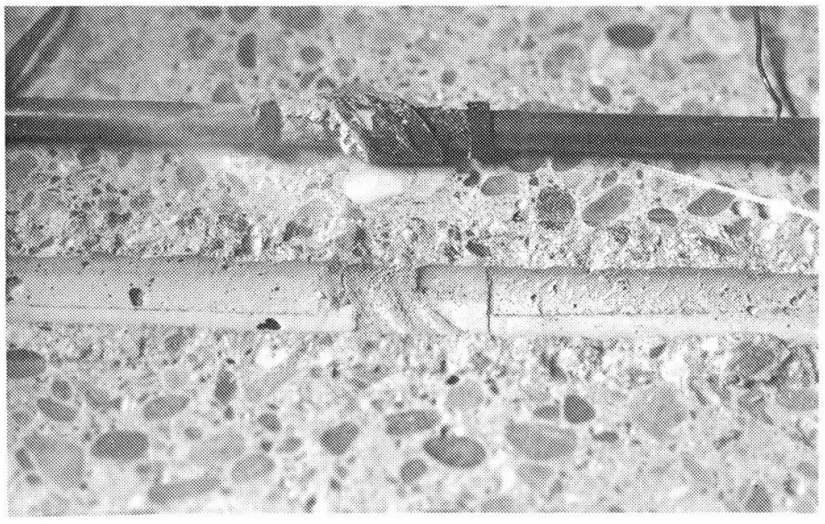

Fig. 17 - Detail of the groove left by the bar

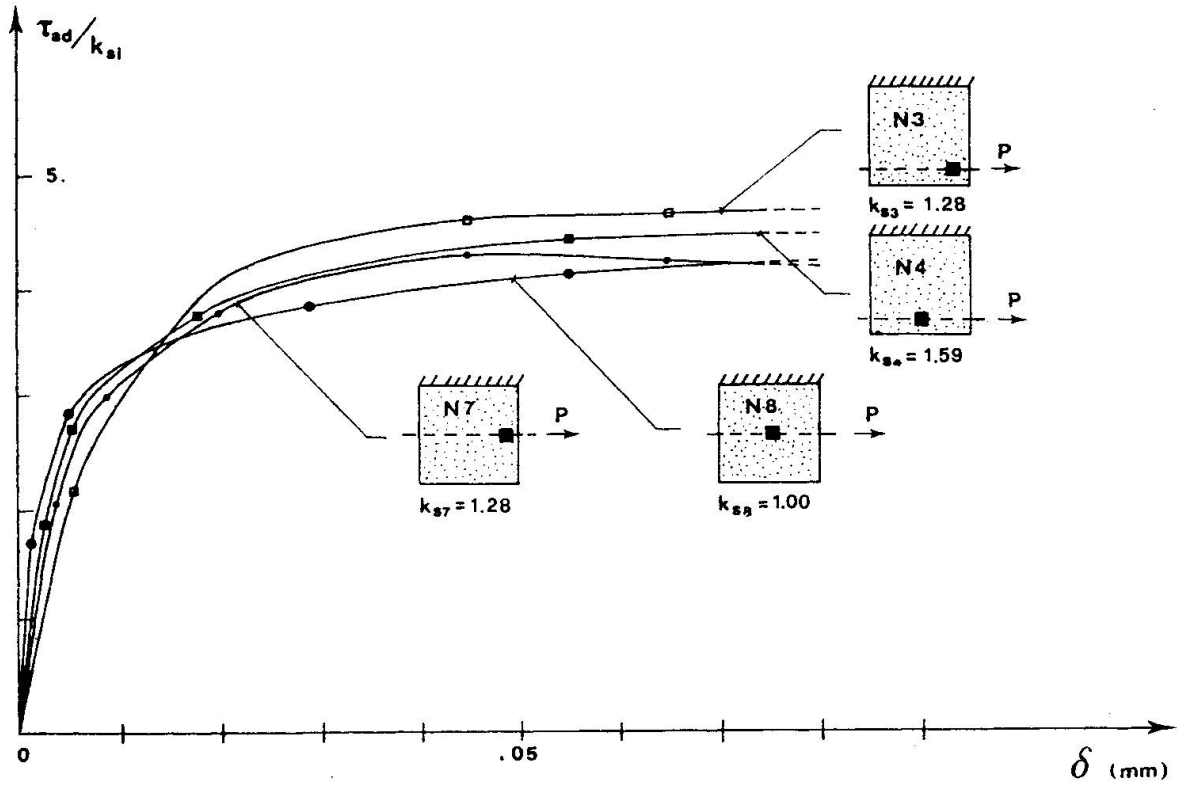

Fig. 18 - Bond-slip curves, with the bond stress divided by the hardness index, for the different specimens

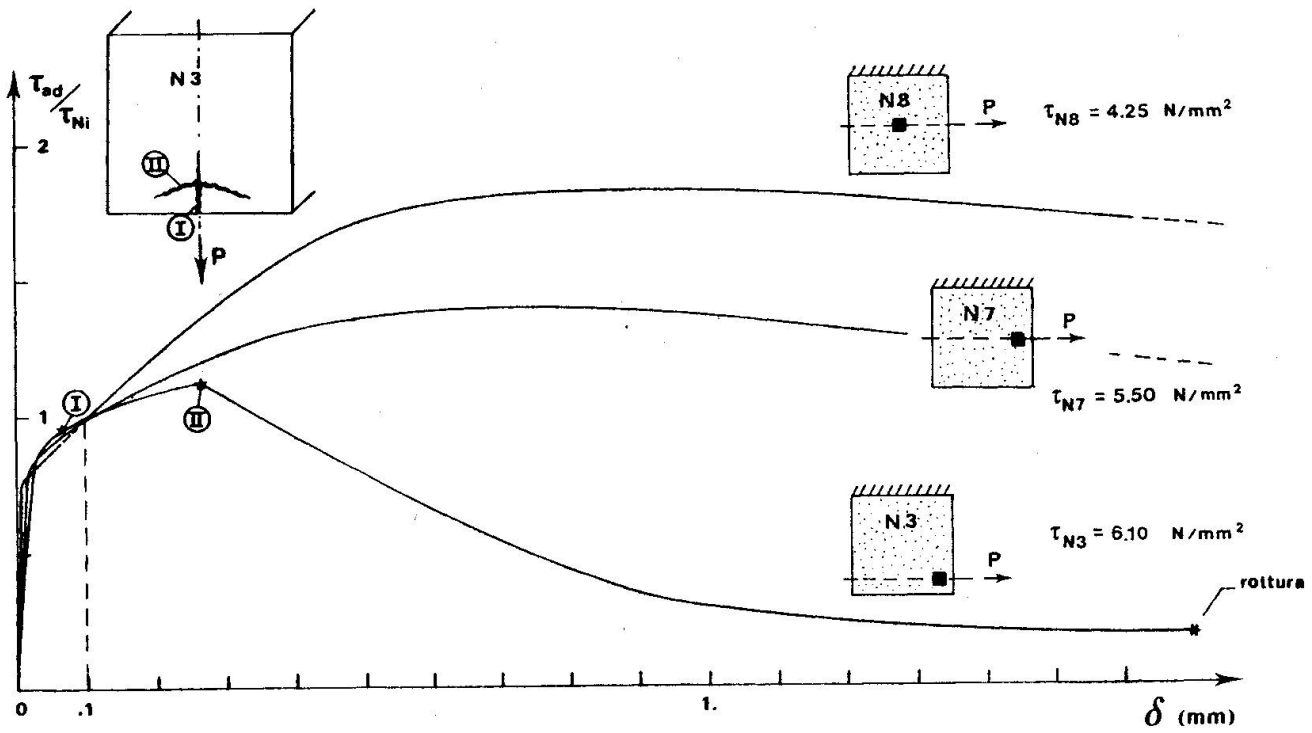

Fig. 19-a - Bond-slip curves for large displacements

Fig. 19-b-Cracking of test specimen N3 at the end of the test.A large transversal crack can be seen on the front face as well as a split

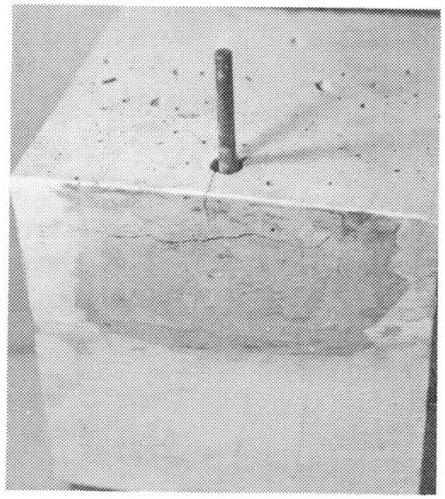

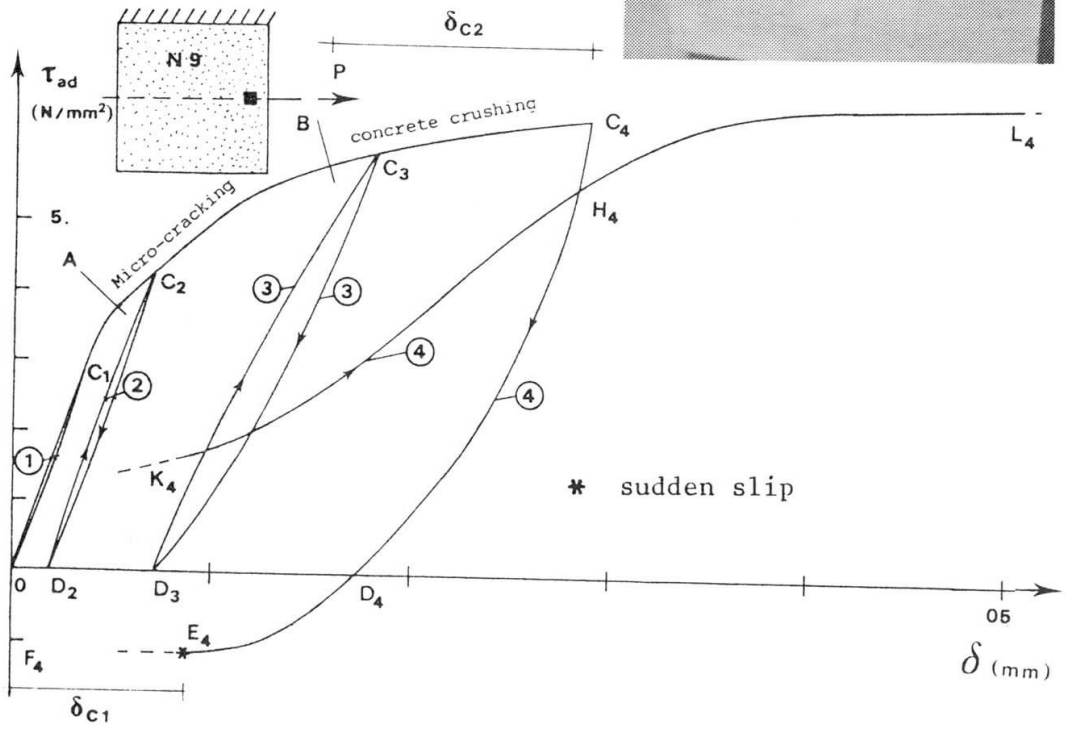

Fig. 20 - Load cycles in the elastic phase and at the beginning of the permanent displacement phase

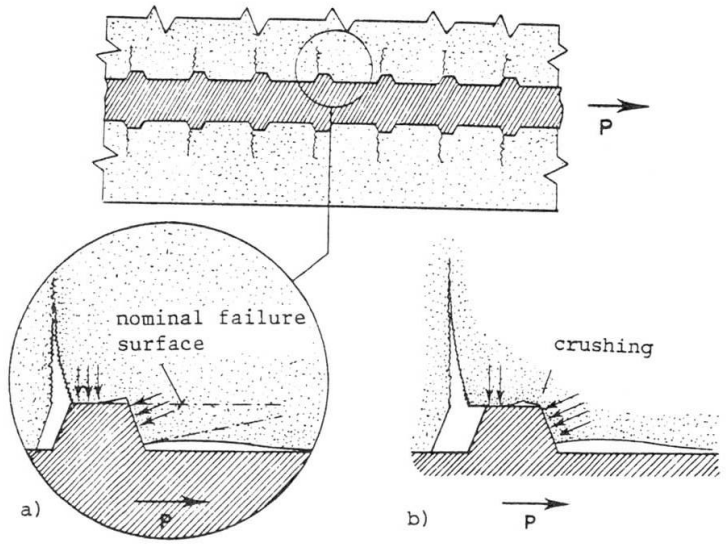

Monotonically increasing loads (branch AB C_4 Fig. 20)

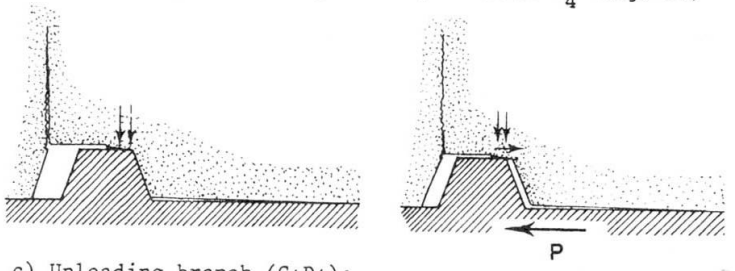

c) Unloading branch (C_4D_4): situation with no load applied (point D_4)

d) Situation for loading of opposite sign (D_4E_4)

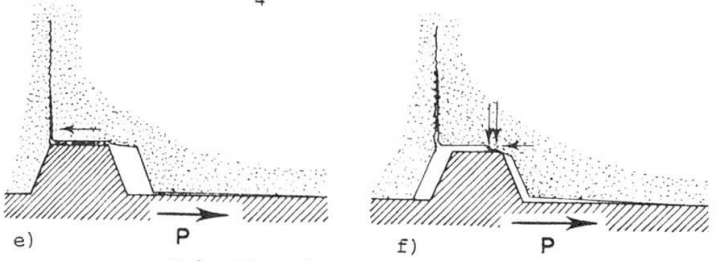

Reloading (branch O K_4 H_4 L_4)

Fig. 21 - Micro-cracking mechanism

Concrete MIX

- Portland Cement (compressive strength = 41.4 N/mm^2)
  nominal cement quantity 3 KN/m^3
  actual cement quantity 3,32 KN/m^3
- water-cement ratio: A/C = .65
- aggregate graduation and size

maximum size (mm)	15-7	7-3	3-1	1-0,5	0,5-0,2	0,2-.075	.075 -0
percentage %	34.1	25.1	20.7	8.3	7.6	3.7	.5

The aggregate are open quarry, natural aggregates.

Casting

- Expanded polystyrene molds for the test specimens (cubes)
- compaction by table vibrator (50 Hz) for 5+5 seconds
- slump: specimens N3 and N4 (1^{st} casting), slump = 5.5 cm
  specimens N7 and N8 (2^{nd} casting), slump = 6.0 cm

Mechanical Characteristics of concrete

- Average cylindrical strength: f = 36.5 N/mm^2 measured on three cylinders with load rate 1.5 (N/mm^2)/sec.
- elastic modulus: E_o = 26500 N/mm^2 measured with load rate 0.015 (N/mm^2)/sec.
- tensile strength 3.08 N/mm^2 (measured) on a cylinder (D = 10 cm; l = 30 mm) with load rate 1.5 (N/mm^2)/sec.

Table I

	N8 P	N7 P	N4 P	N3 P
Prismatic strength at the load rate 1.5 N/mm^2/sec. (+)	f_c = 35	f_c = 38	f_c = 38	f_c = 34
Curing period at start of test (in days)	90	80	70	60
Nominal hardness (+) of the concrete layer around the bar (**)	10.5	13.5	16.7	13.5
Index of hardness K_{si}	1	1.28	1.59	1.28
Nominal hardness of the outer layer of the specimen (+)	16.5	20.7	22.5	22.8

Table II - Mechanical characteristics of the concrete

(+) Measured after 150 days of curing

(**) The hardness was measured by sclerometric tests, averaging 20 readings. A special reduced prod was fitted to a Schmidt sclerometer to reach the concrete groove formed by the bar after having cut the test specimen and removed the bar.

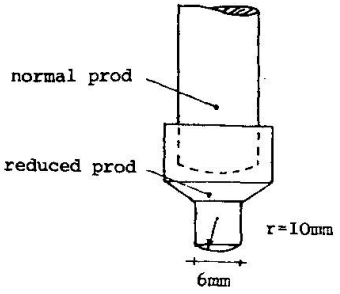

The normal prod for plane surfaces gave values 1,3 times higher than with the smaller prod.

Plain Concrete Under Load - A New Interpretation

Béton non-armé sous charge - Une nouvelle interprétation

Unbewerhter Beton unter Belastung - Eine neue Interpretation

MICHAEL D. KOTSOVOS
Lecturer
Imperial College
London, U.K.

JOHN B. NEWMAN
Senior Lecturer
Imperial College
London, U.K.

SUMMARY
It is propesed that plain concrete in compression suffers a complete loss of load carrying capacity when ultimate strength is exceeded. This hypothesis, which contrasts with the widely held view of post-ultimate behaviour, is supported by experimental evidence and the results of analyses of structural forms. The results of these analyses indicate that the response of the structures investigated is independent of the post-ultimate behaviour of concrete under compressive stress states. It is shown that the large deformations attributed to the post-ultimate characteristics of concrete as a material may be associated with triaxial stress states existing in any structure, but which are usually ignored for purposes of simplicity.

RÉSUMÉ
On avance l'hypothèse qu'en compression, le béton non armé perd toute sa capacité de charge dès que le niveau de résistance ultime est atteint. Bien qu'elle s'inscrive en marge du concept généralement accepté de comportement en régime post-ultime, cette hypothèse réflète néanmoins bien certains résultats d'essais et d'analyse de quelques structures. Les résultats d'analyse suggèrent que le mode d'action des différentes structures soumises à l'étude soit indépendant du régime post-ultime du comportement typique du béton non armé chargé en compression. Les déformations importantes, qui étaient jusqu' à maintenant considérées comme caractéristiques du régime post-ultime du béton, seraient plutôt attribuables à des champs de contraintes triaxiales qui existent dans toute structure, mais qui sont généralement négligés, par souci de simplicité.

ZUSAMMENFASSUNG
Es wird vorgeschlagen, dass unbewehrter Beton die ganze Festigkeit verliert, sobald die Grenzbeanspruchung überschritten wird. Diese Hypothese, die im Wilderspruch zur weitverbreiteten Ansicht des überkritischen Tragverhaltens steht, wurde durch Versuche und analytische Berechnungen erhärtet. Die Resultate dieser Berechnungen weisen darauf hin, dass das Verhalten der untersuchten Tragwerke unabhängig vom überkritischen Bereich der druckbeanspruchten Betonzonen ist. Es wurde gezeigt, dass die g,ossen, den überkritischen Eigenschaften des Betons zugeschriebenen Deformationen mit den dreiachsigen Spannungszuständen in Verbindung gebracht werden können, die in jedem Tragwerk vorhanden sind, aber aus Gründen der Vereinfachung oft vernachlässigt werden.

1. INTRODUCTION

Most constitutive models of concrete behaviour under compressive stress states published to date predict that the deformational response of the material in the direction of the maximum principal compressive stress exhibits a trend similar to that given in Fig. 1 which shows a stress-strain relationship consisting of an ascending and a gradually descending portion. Such predictions result from deriving the models on the basis of the widely held view that, beyond ultimate strength, the load carrying capacity of concrete under a compressive load is progressively reduced with increasing deformation. This view has been reinforced by experimental evidence which has indicated that the deformational response of concrete under uniaxial compression applied by a stiff testing machine is described by a stress-strain curve which exhibits the characteristics of the relationship shown in Fig. 1. Such stress-strain curves have been used to describe the behaviour of concrete in the compression zone of reinforced concrete structural members such as beams, slabs, etc. [1].

However, the validity of the stress-strain data for concrete, as for other materials, depends on the testing techniques adopted and this fact has been recognised by many research workers [2]. As a result techniques have been developed in order to minimise restraint effects due to the interaction between specimen and testing device. However, it is shown in the following that, even when minimal, these secondary effects have a significant effect on material behaviour for stress levels in the region of ultimate strength and beyond. In view of this it is postulated that, if restraint effects could be eliminated completely, concrete would exhibit a complete loss of load carrying capacity when ultimate strength is exceeded. Experimental data which have been produced by tests in which secondary testing effects have been effectively eliminated support this hypothesis.

It is shown that the large deformations attributed to post-ultimate strength stress-strain characteristics could be due to the triaxial state of stress which exists in any structure under load but which is usually ignored for the purposes of simplicity. This consideration is supported by the results obtained by a finite element analysis of plain concrete structural forms under concentrations of load which suggest that the overall behaviour of the structural forms investigated is independent of the post-ultimate strength behaviour of concrete under a compressive state of stress.

2. TESTING METHODS AND STRESS-STRAIN BEHAVIOUR

It is generally accepted that the fundamental deformational response of concrete under increasing stress is realistically described by the stress-strain behaviour measured for laboratory specimens provided definable states of stress are induced. The application of such states of stress is achieved by using testing techniques which have been developed so as to minimise restraint effects due to the interaction between specimen and testing device. The most significant of these effects is the frictional restraint which develops at the specimen-platen interfaces under increasing load.

The use of cylindrical or prismatic specimens with a length to width ratio of between approximately 2 and 2.5 is one method which has been adopted in order to minimise the effect of the above frictional restraint on the specimen behaviour [3]. It has been found by experiment that, while the end zones of such specimens under uniaxial compression are subjected to an indefinable triaxial compressive state of stress caused by this frictional restraint, the central zone of the specimens is effectively free from such effects [3]. Other methods used to minimise frictional effects involve the use of various types of anti-friction

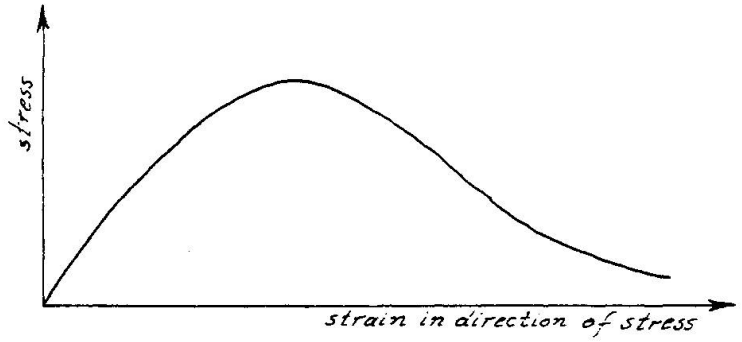

Fig. 1 Generally assumed form of stress-strain relationship for concrete under compressive stress

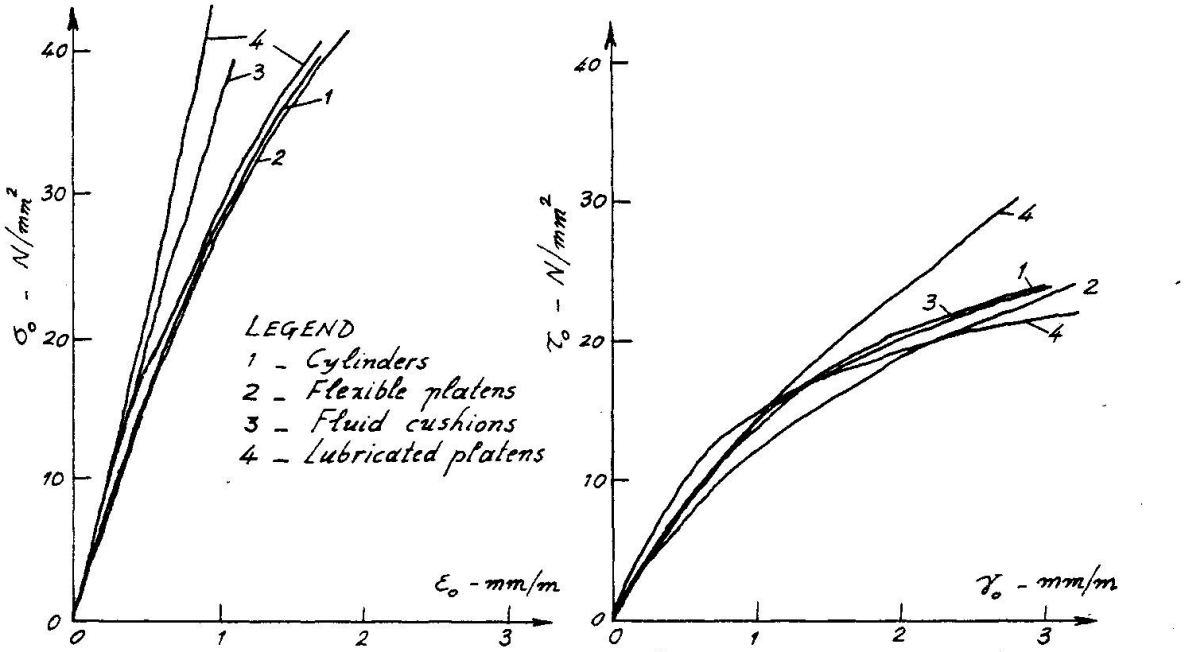

Fig. 2 Volumetric ($\sigma_o - \varepsilon_o$) and deviatoric ($\tau_o - \gamma_o$) stress-strain relationships for concrete under triaxial compression obtained from tests using various friction reducing techniques

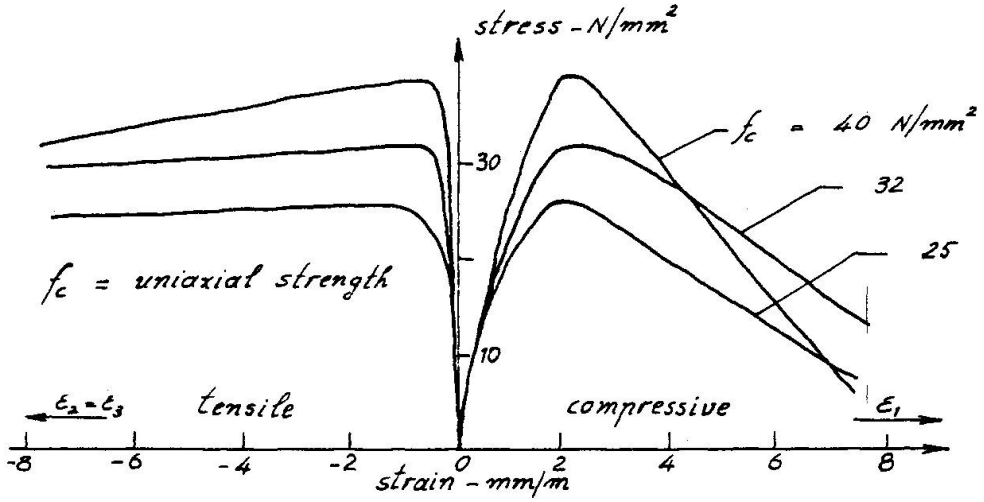

Fig. 3 Stress-strain relationships for concretes under uniaxial compression obtained from tests on cylinders

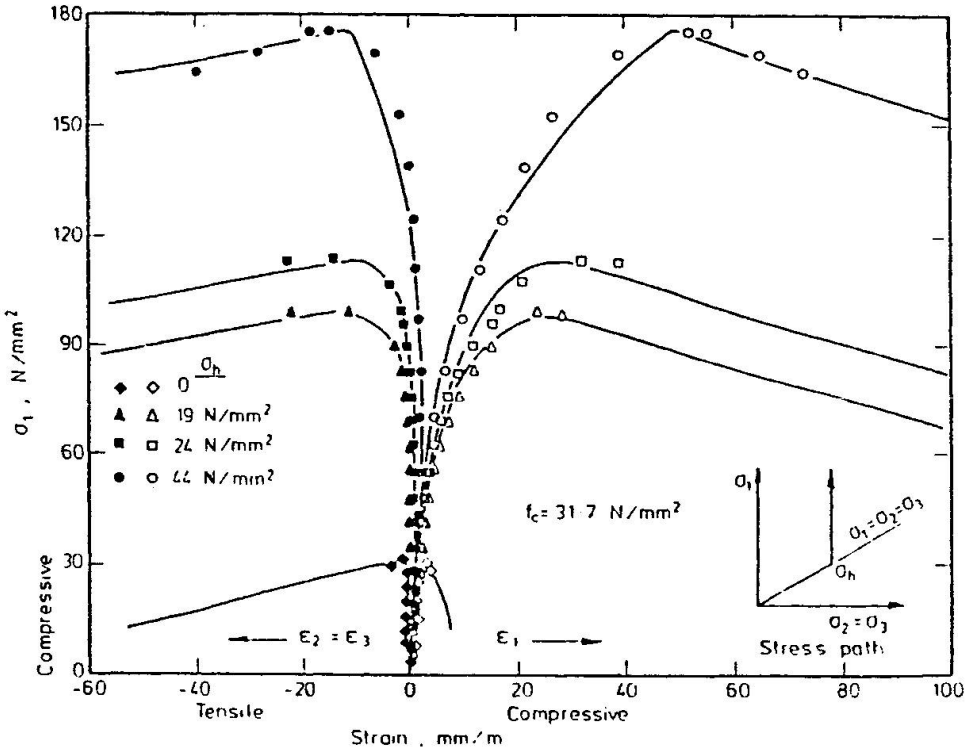

Fig. 4 Stress-strain relationships for concrete under various compressive states of stress obtained from triaxial tests on cylinders

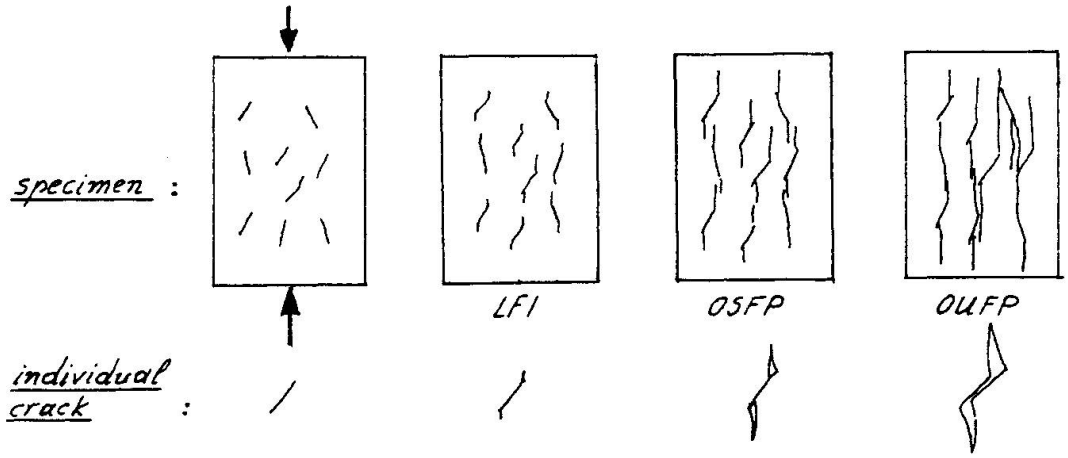

Fig. 5 Stages in the process of crack extension and propagation for concrete under compressive stress

pads [4], brush platens [5], flexible platens [6], fluid cushions [2], etc.

The development of the above testing methods has been based on the assumption that the mechanical properties of concrete during its whole loading history are qualitatively comparable to the mechanical properties of a continuous material. For example, loading devices such as brush and flexible platens are considered to induce a negligible frictional restraint at the specimen-platen interfaces when designed to allow displacements in the direction orthogonal to loading to be compatible with tensile strains in concrete calculated on the basis of Poisson's ratio values up to 0.5 which is the maximum value for a continuous material. As long as this condition is satisfied, most of the above methods have been found to produce stress-strain data which correlate very closely [7] (see Figure 2). It should be noted, however, that most of the above data describe material behaviour under stress levels approaching, but not exceeding, ultimate strength.

Complete stress-strain relationships for concrete (i.e. relationships with both ascending and descending portions) have been obtained mainly from tests on cylinders under uniaxial compression [8] (see Figure 3). There is also some experimental evidence which suggests that similar trends of behaviour are exhibited under triaxial compression [9] (see Figure 4). The description of the specimen behaviour beyond ultimate strength has been achieved by loading the specimens at a constant rate of displacement through a 'stiff' testing machine either by using a loading system capable of releasing rapidly any load in excess of that which can be sustained by the specimen at any time [10] or by loading a steel specimen in parallel with the concrete specimen in a manner such that, as the load carrying capacity of concrete is reduced, the concrete-steel system transfers the excess load from the concrete to the steel specimen to maintain the internal equilibrium of the overall system [11].

It is interesting to note in both Figures 3 and 4 that, for stress levels beyond a level close to ultimate strength, the tensile strain increases at a rate very much higher than that of the compressive strain. Such behaviour can only be attributed to the effect on deformation of void formation caused by the fracture processes of the specimens [12]. Thus it is difficult, if not impossible, to explain the specimen behaviour on the basis of continuum mechanics concepts. Since the development of the testing techniques used to minimise secondary testing procedure effects has been based on assumptions which imply mechanical properties for concrete quantitatively comparable to those of a continuous material, the effectiveness of the testing methods used to induce definable states of stress in specimens for the whole length of a loading path is questionable. The effect, therefore, of the frictional restraint on specimen behaviour must be reconsidered when using all current data.

3. EFFECT OF FRICTIONAL RESTRAINT ON CONCRETE BEHAVIOUR

The nonlinear deformational behaviour of concrete under increasing stress is dictated by internal fracture processes. Therefore, any effect on the deformation due to frictional restraints at the loaded boundaries will cause a modification of the fracture processes.

3.1 Fracture Processes of Concrete

Previous research work [13] has indicated that the fracture processes of concrete under increasing stress take the form of crack extension, due to initiation of crack branches, followed by stable propagation of these branches which eventually becomes unstable and leads to complete disruption. Crack extension and propagation occur in the direction of the maximum principal compressive stress in order

to relieve high predominantly tensile stress concentrations which exist near the crack tips. During the above fracture processes voids are created within the body of the material.

Four stages in the process of crack extension and propagation have been identified under increasing stress [14]. The boundaries to those stages have been termed Local Fraction Initiation (LFI), Onset of Stable Fracture Propagation (OSFP) and Onset of Unstable Fracture Propagation (OUFP) and their variation in stress and strain space have been established by experiment. A schematic representation of the stages of crack extension and propagation is shown in Figure 5. The variation of LFI, OSFP, OUFP and ultimate strength in stress and strain space forms the failure envelopes shown in Figure 6.

3.2 Effect of Frictional Restraint on Fracture Processes

A concrete cylinder subjected to uniaxial compression can be considered as exhibiting 2 principal zones of behaviour as shown in Figure 7. Material in the central zone is generally accepted to be subjected to a near-uniaxial compressive stress state whereas the end zones are subjected to a complex and indefinable compressive stress state caused by the frictional restraint which prevents the specimen from expanding in the direction of the specimen-platen interfaces.

As indicated by the failure envelopes of Figure 6, cracking of the concrete cylinder will initiate in the central zone which is subjected to near-uniaxial compression. For stress levels increasing up to OUFP, cracking occurs in the microscopic level in localised regions within the material in this zone [14]. As a result, the overall deformation response of the specimen is comparable to the deformation response of a continuous material and the effect of the boundary frictional restraint is confined within the end zones of the cylinder.

When OUFP is exceeded cracking becomes continuous and propagates towards the end zones. As discussed previously (see section 3.1) cracking propagates in the direction of the maximum principal stress trajectories which, in the central zone of the specimen, coincide with the direction of the applied compressive stress. Outside this zone, both stress trajectories and propagating cracks deviate from the direction of the initial crack branches due to the indefinable multiaxial state of stress which exists.

The above change in the orientation of the crack propagation path increases the energy required for crack extension and a higher load is required for the fracture process to continue. This will result in an overestimate of both the strength and the strain in the direction of the applied load. Furthermore, the above delay in the fracture process will also reduce the rate of void formation which affects predominantly deformation in the direction orthogonal to the crack propagation path. This may result in a serious underestimate of the lateral tensile strain of the cylinder.

As the applied load increases to a level very close to the maximum load that can be sustained by the specimen (ultimate strength), cracking spreads within the end zones and propagates towards the specimen-platen interfaces. It becomes apparent at this stage that the only reason for the central zone responding as a unit under the applied load is the delay in the fracture process within the end zones caused by the change in orientation of the crack propagation path. This suggests, therefore, that if the state of stress was the same throughout the specimen, no such change in the orientation of the crack propagation path would occur and the specimen would completely collapse due to rapid and unstable fracture propagation. A schematic representation of the fracture processes of concrete specimens (with and without frictional restraint) under increasing load is given in Figure 8.

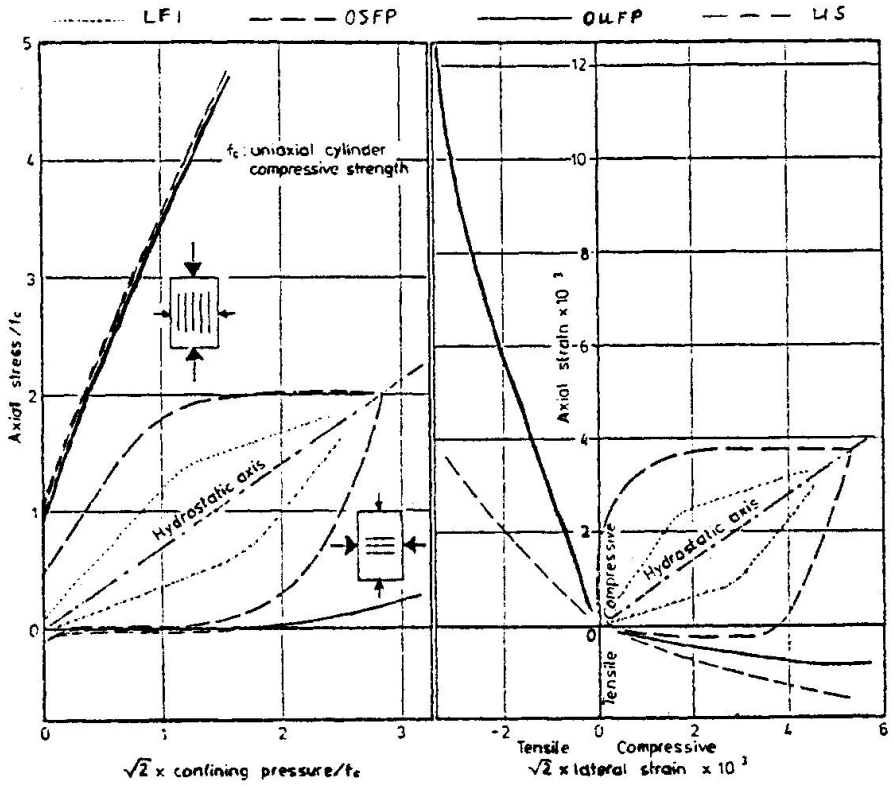

Fig. 6 Failure envelopes for concrete as derived from triaxial tests data for cylinder

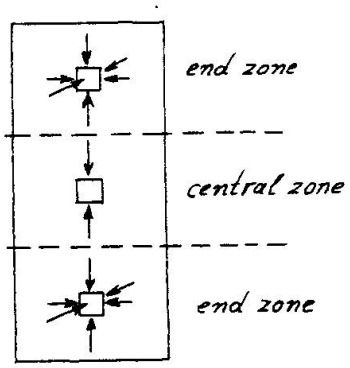

Fig. 7 Schematic representation of the effect of boundary frictional restraint on the state of stress within cylinders

Fig. 8 Schematic representation of the fracture processes for restrained and unrestrained concrete specimens under increasing compressive stress

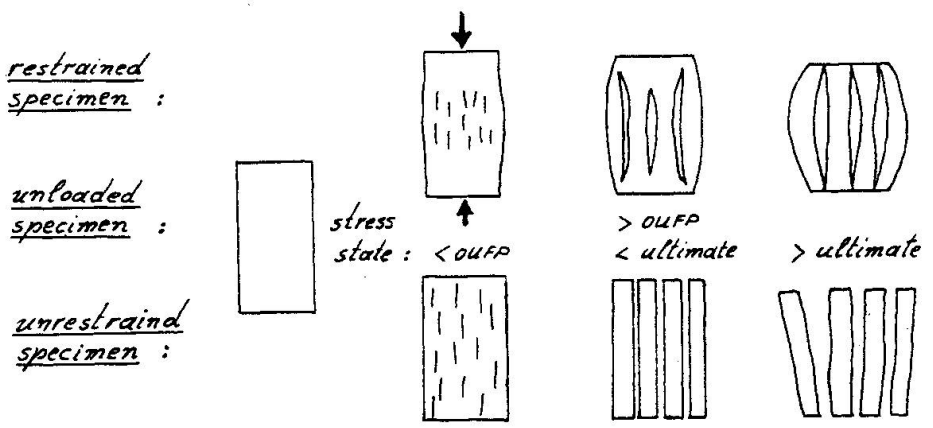

3.3 Effect of Frictional Restraint on Deformation

On the basis of the above considerations the true deformational behaviour of concrete under compression with no secondary effects may realistically be described by the stress-strain relationships proposed in Figure 9. These are characterised by a complete loss of load carrying capacity as soon as the ultimate strength level is exceeded. For comparison the figure also includes a typical form of experimental relationship obtained under monotonically applied compression for concrete cylinders with a height to diameter ratio of 2.5 loaded through rigid platens.

For stress levels up to OUFP, proposed and experimental relationships coincide since, for such levels, the specimen behaviour has been shown previously (see section 3.2) to be essentially unaffected by the frictional restraint which exists at the specimen-platen interfaces. For stress levels between OUFP and ultimate strength, there will be a significant deviation of the two relationships due to the frictional restraint on deformation. The proposal that complete loss of load carrying capacity will occur when ultimate strength is attained, is considered to provide a realistic description of the post-ultimate strength behaviour of an 'unrestrained' material.

A measure of the effect of the frictional restraint on the deformational behaviour of the specimen is given by the deviation of the proposed from the experimental relationships shown in Figure 9.

4. EVIDENCE FOR SUGGESTED NEAR- AND POST-ULTIMATE BEHAVIOUR

An unequivocal experimental proof of the validity of the trends of concrete behaviour proposed in section 3.3 can only be obtained by using testing techniques which eliminate completely any frictional restraint on the specimen-platen interfaces. However, on the basis of the considerations discussed in section 3, such a proof is unlikely to be obtained by using any of the existing testing techniques in isolation, although the fluid cushion technique [2] appears in theory to eliminate frictional restraints. An investigation of the post-ultimate behaviour of concrete under uniaxial compression could be based on a comparative study of the trends of post-ultimate response of concrete specimens tested by using testing methods employing different techniques to reduce friction. Such an investigation forms part of an ongoing programme of research being carried out by the Concrete Materials Research Group (CMRG), which is concerned with the derivation of a constitutive model of concrete and its use with computer-based techniques of structural analysis.

There is, however, published experimental evidence which suggests that under certain types of triaxial compressive stress states concrete suffers a complete loss of load carrying capacity when the ultimate strength is exceeded [9]. Furthermore, an analytical study of the fracture processes of plain concrete structural forms subjected to a wide range of boundary conditions has produced some interesting results regarding the transfer of load from elements which suffer a partial loss of load carrying capacity due to cracking to elements subjected to stress states below ultimate strength [15,16]. These results indicate that the overall behaviour of the structural forms investigated is independent of the post-ultimate strength behaviour of the material under compressive states of stress. A brief description of the above experimental and analytical information is given in the following.

4.1 Information from Experiments

The experimental data which are discussed in this section have been obtained

during a comprehensive programme of research into the behaviour of concrete under multiaxial stress carried out by the CMRG. The testing techniques used in this programme have been fully described elsewhere [17] and the obtained experimental data have formed the basis of a number of publications concerned with the fracture processes [18,19], strength [20], and deformational response [9,12,21, 22] of concrete under generalised stress.

4.1.1. Test Procedure

Concrete cylinders with a height to diameter ratio of 2.5 have been subjected to an axial compression (σ_α) and a lateral confining pressure (σ_c) combined in such a way that the state of stress within the specimen has been always either triaxial 'compression' ($\sigma_\alpha > \sigma_c$) or triaxial 'extension ($\sigma_c > \sigma_\alpha$)(see Figure 10). The axial compression has been applied by using a loading method similar to that described in section 2, whereas the confining pressure has been hydrostatic resulting in the curved surface of the specimen being essentially friction-free. For both triaxial 'compression' and triaxial 'extension' tests the specimens were initially subjected to a given hydrostatic pressure and then the axial compression was either increased (triaxial 'compression') or decreased (triaxial 'extension') to failure (see Figure 10).

4.1.2. Test Results

Typical stress-strain relationships obtained from the above tests are shown in Figure 11 which indicates that while under triaxial 'compression' concrete exhibits a gradual reduction of load carrying capacity for stress levels beyond ultimate strength, under triaxial 'extension' concrete suffers an immediate and complete loss of load carrying capacity. This difference in material behaviour is considered to reflect the effect of frictional restraint on the fracture processes of the specimens. According to the fracture mechanism of concrete discussed in section 3.1, under triaxial 'compression' crack propagation occurs in the axial direction and thus, when cracking spreads in the end zones of the specimen, the frictional restraint will affect the specimen behaviour as discussed in section 3.2. On the other hand, under triaxial 'extension' crack propagation occurs in the lateral direction and thus the fracture processes which take place in the central zone of the specimen are not affected by the frictional restraint existing at the specimen-platen interfaces.

However, in contrast to the complete loss of load carrying capacity exhibited by concrete when ultimate strength is exceeded in an 'extension' test, experimental stress-strain curves obtained for concrete under equal biaxial compression applied through brush platens, which is a particular case of triaxial 'extension' with $\sigma_\alpha = 0$, exhibit a gradually descending portion [5] similar to that obtained from triaxial 'compression' tests (see Figure 12). The difference between the two types of tests are considered to reflect frictional restraint effects. It should be noted, however, that in contrast to the sequential loading path used for the triaxial tests, the above biaxial tests have been performed by using a proportional loading path. Since it has been shown that concrete behaviour is essentially independent of stress path effects for stress levels up to OUFP only [21], the dependence of the material behaviour on stress path for higher stress levels may also reflect the effect of the frictional restraint.

In view of the above, the complete loss of load carrying capacity when ultimate strength is exceeded in a triaxial 'extension' test is considered to be characteristic of material behaviour under any state of stress.

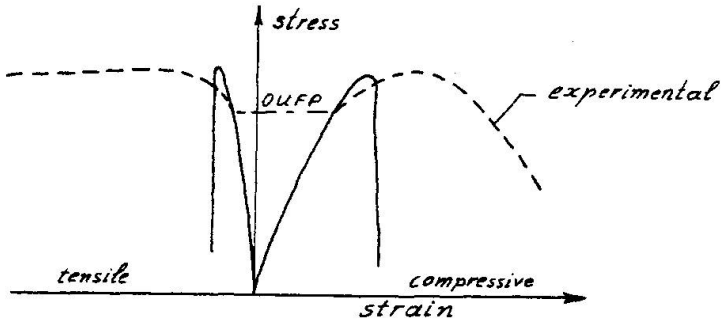

Fig. 9 Proposed form of stress-strain relationships for concrete under compressive stress

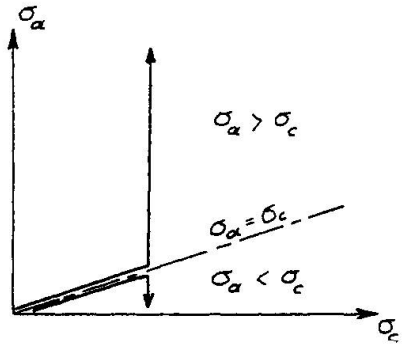

Fig. 10 Stress path used in triaxial tests

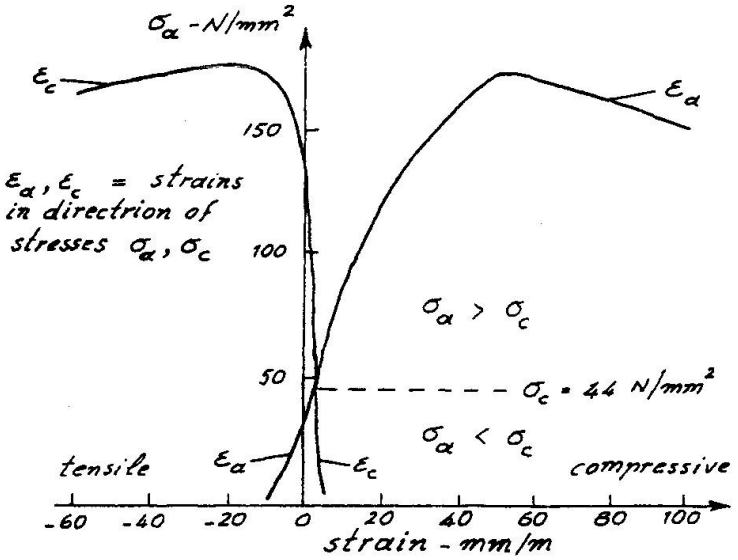

Fig. 11 Typical stress-strain relationships obtained from triaxial 'compression' and 'extension' tests on cylinders

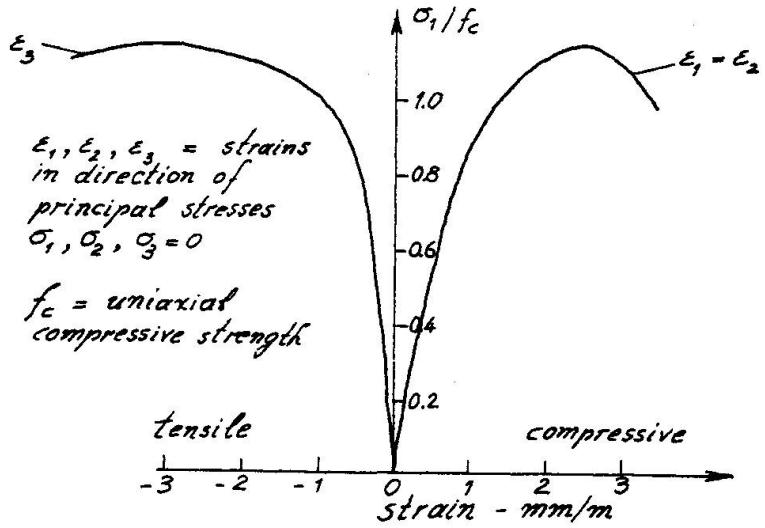

Fig. 12 Typical stress-strain relationships for concrete under equal biaxial compression ($\sigma_1=\sigma_2$) obtained from tests using 'brush' platens

4.2 Information from Analysis

The analytical data which are discussed in this section have been obtained as part of an investigation by the CMRG into the use of constitutive models of concrete when coupled with computer-based methods of analysis. Nonlinear finite element techniques incorporating the constitutive model of concrete behaviour described in references [12] and [20] have been used to analyse plain concrete structural forms under concentrations of load induced by a wide range of boundary conditions (see Figure 13). The analysis has been found to yield realistic predictions of structural response which correlate very closely with published experimental data. The following is concerned only with a brief description of the fracture mechanism of the structural forms investigated predicted by the analysis. A full description of the results obtained has been given elsewhere [15,16].

4.2.1. Constitutive Model

The constitutive model used has been devised so as to describe the effect of the fracture processes of concrete on the material deformation [12]. Its formulation has been based on an analysis of triaxial experimental data [22-24] and as a result it suffers, like any other model, from the inherent disadvantage that it may describe specimen rather than material behaviour. However, unlike other models, it has been expressed in a modular form which allows improvements to be made in the light of any new information regarding the material behaviour without changing the theoretical basis of the model.

The above model describes completely the deformational behaviour of concrete under generalised stress increasing up to and, for 'compressive' states of stress, beyond ultimate strength. When the ultimate strength of concrete under a state of stress with at least one principal stress component tensile is exceeded, the maximum principal tensile stress is set to zero and the material behaviour is defined by the model on the basis of the principal stresses in the orthogonal directions.

4.2.2. Results of Analysis

It has been very interesting to find that for all cases investigated collapse of the structure occurs without the compressive strength of concrete being exceeded anywhere within the structure. The analysis predicts cracking will occur in regions subjected to a state of stress with at least one of the principal stress components tensile. For the cases investigated, the most critical state of stress is that which causes cracking to occur in the region marked B in Figure 14a. With increasing load, this cracking only propagates into other regions subjected to similar states of stress, i.e. with at least one of the principal stress components tensile, up to the formation of a crack pattern corresponding to the collapse stage (see Figure 14b).

Figure 14 also shows that region A, which is subjected to a wholly compressive state of stress, reduces in size as the applied load increases above the level which causes crack initiation. This is due to stress redistribution which transforms the state of stress at the periphery of region A from a wholly compressive state of stress to a state of stress in which at least one of the principal stress components is tensile. When the strength of concrete under this latter state of stress is exceeded cracking occurs and the size of region A is further reduced (see Figure 14b). In all cases investigated collapse of the structure occurs before the strength of concrete in region A is exceeded.

If the fracture process described above is typical of that of any concrete structure, then the post-ultimate strength behaviour of concrete (i.e. the

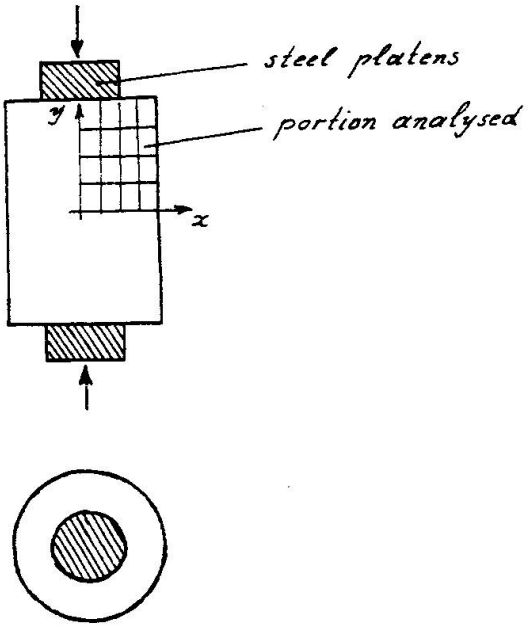

Fig. 13 Typical structural unit investigated

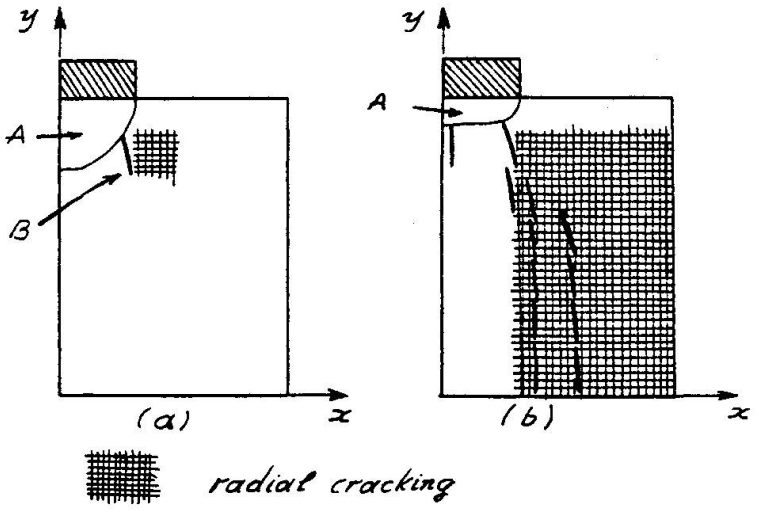

Fig. 14 Typical crack patterns at (a) crack initiation and (b) collapse as predicted by analysis

descending portion of the stress-strain relationship) under a compressive state of stress has no apparent effect on the overall behaviour of the structure. The large deformations attributed to post-ultimate strength stress-strain characteristics may be associated with the triaxial state of stress which exists in any structure but which is usually ignored for the purposes of simplicity. For example, the compression zone of reinforced concrete beams is actually subjected to a triaxial compressive state of stress due to the restraints imposed on the transverse expansion of the beams by the reinforcement, surrounding concrete, etc., but this is not accounted for in the design calculations.

A simplified description of the effect of hoop reinforcement on the strength and deformation of linear concrete structural members subjected to axial compression may be obtained by a finite element analysis in which the hoop reinforcement is simulated as a spring support with a stiffness equivalent to the stiffness of the reinforcement. The results obtained from such an analysis are shown in Figures 15a to 15c.

Figure 15a shows that the load carrying capacity of concrete increases with decreasing the spacing of the hoop reinforcement. The cause of such behaviour is demonstrated in Figure 15b which shows the effect of hoop reinforcement spacing on the stress path to which concrete under increasing load is subjected. Figure 15b also includes the ultimate strength envelope for plain concrete and indicates that the confining pressure (σ_c) induced by the restraint which the hoop reinforcement imposes on the transverse expansion of concrete with increasing applied axial load increases with decreasing the spacing of the reinforcement and thus a higher axial stress (σ_α) is required for the ultimate strength level to be exceeded.

Figure 15c shows the variations of axial and lateral strains with increasing axial stress for various values of reinforcement spacing. The stress-strain relationships obtained from tests on plain concrete under uniaxial compression are also shown in the figure for purposes of comparison. It should be noted that, for values of the reinforcement spacing up to about 0.5 x the diameter of the concrete member, the axial compressive strains corresponding at ultimate strength are comparable, or higher than, the maximum axial strain exhibited by plain concrete under uniaxial compression.

5. CONCLUSIONS

Based on a discussion of secondary testing procedure effects on the fracture processes of concrete specimens under compressive stress states, it is shown that experimental stress-strain relationships may realistically describe material response only for stress levels up to a region close to the ultimate strength level. Beyond this level, the hypothesis that concrete suffers a complete loss of load carrying capacity is considered to provide the most realistic prediction of concrete behaviour.

The above hypothesis is supported by experimental evidence obtained from triaxial tests on concrete subjected to wholly compressive states of stress which indicates that when the fracture processes are not affected by secondary testing effects then the specimens suffer a complete loss of load carrying capacity when ultimate strength is exceeded. Furthermore, results obtained by finite element analysis indicate that the behaviour of plain concrete structural forms subjected to load is independent of the behaviour of concrete under compressive stress states beyond ultimate strength. If such behaviour is typical of any concrete structure then the large deformations attributed to post-ultimate stress-strain characteristics may, in fact, be associated with the triaxial state of stress which exists in any structure but is usually ignored for purposes of simplicity.

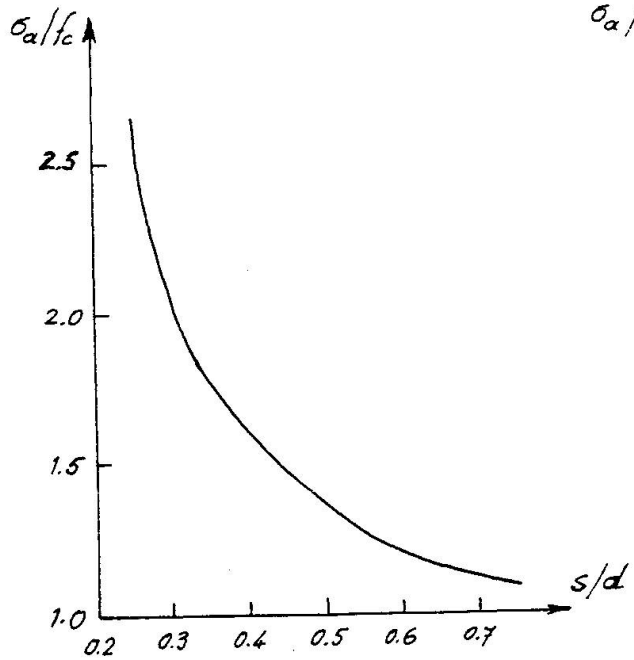

(a) relationship between strength and reinforcement spacing

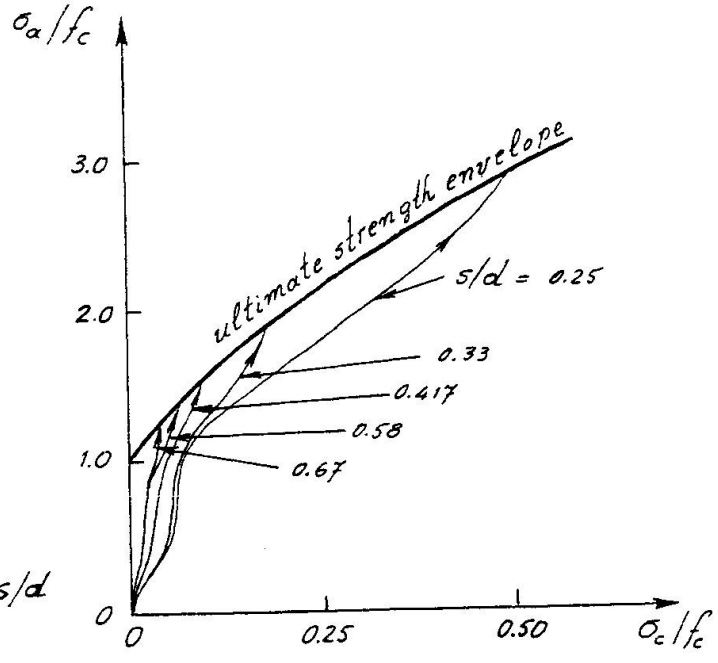

(b) Effect of reinforcement spacing on strength and stress path

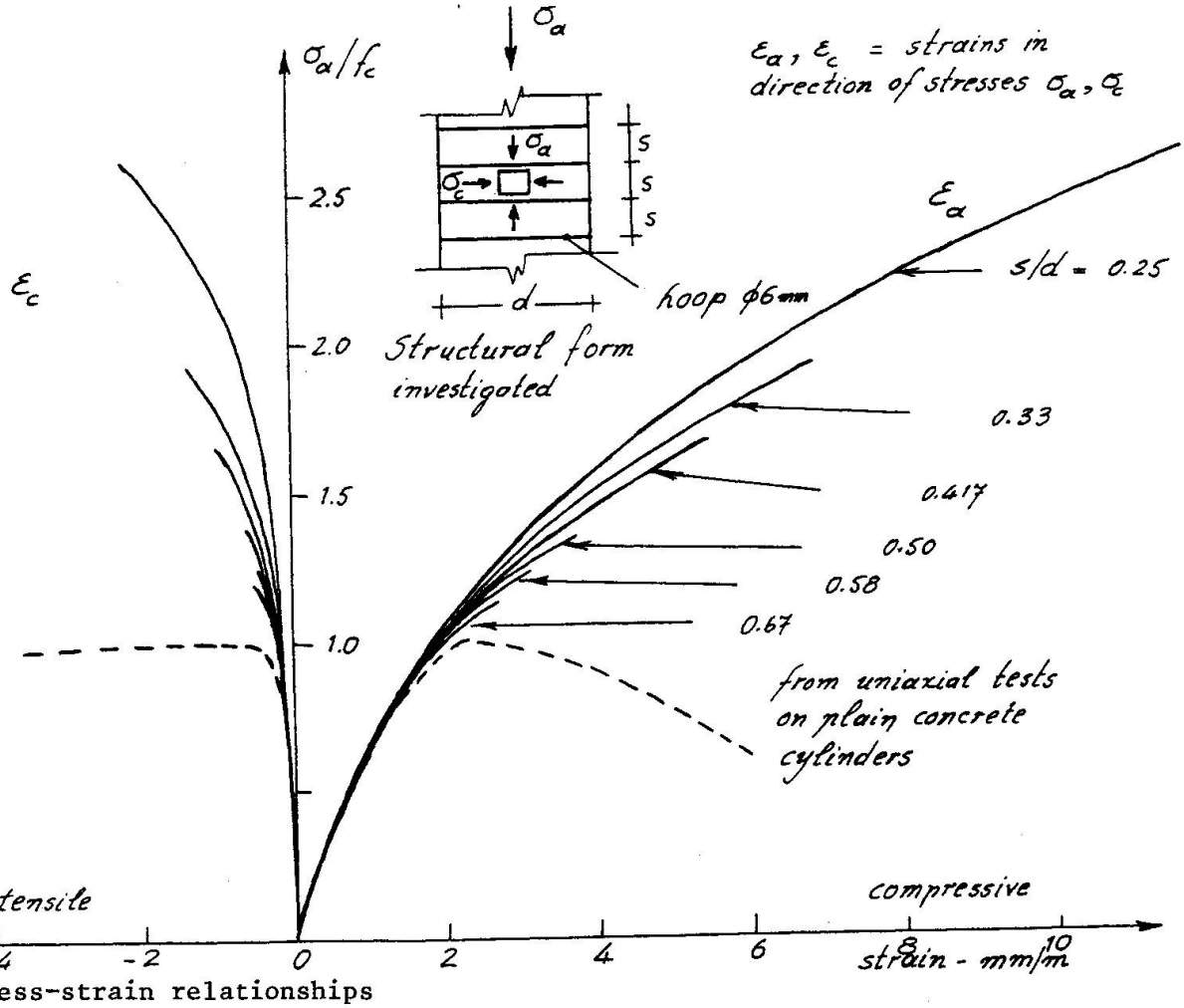

(c) Stress-strain relationships

Fig. 15 Relationships as predicted by analysis for the structural form investigated

REFERENCES

1. Code of Practice for the Structural Use of Concrete, CP110, British Standards Institution, London, 1972, Part 1, "Design, Materials and Workmanship", 154 pp.

2. GERSTLE, K.H., LINSE, D.H., BERTACCHI, P., KOTSOVOS, M.D., KO, H.Y., NEWMAN, J.B., ROSSI, P., SCHICKERT, G., TAYLOR, M.A., TRAINA, L.A., ZIMMERMAN, R.M., BELLOTTI, R., "Strength of Concrete under Multiaxial Stress States", Proceedings Douglas McHenry International Symposium on Concrete and Concrete Structures, ACI Publication SP-55, 1978, pp. 103-131.

3. NEWMAN, K. and LACHANCE, L., "The Testing of Brittle Materials under Uniform Uniaxial Compressive Stress", American Society for Testing and Materials, Proceedings, Vol. 64, pp. 1044-1067.

4. HUGHES, B.P. and BAHRAMIAN, B., "Cube Tests and the Uniaxial Compressive Strength of Concrete", Magazine of Concrete Research, Vol. 17, No. 53, December 1965, pp. 177-182.

5. KUPFER, H., HILSDORF, H.D., RUSCH, H., "Behaviour of Concrete under Biaxial Stresses", ACI Journal, Proceedings, Vol. 66, No. 8, August 1969, pp. 656-666.

6. SCHICKERT, G., "On the Influence of Different Load Application Techniques on the Lateral Strain and Fracture of Concrete Specimens", Cement and Concrete Research, Vol. 3, No. 4, July 1973, pp. 487-494.

7. GERSTLE, K.H., ASCHL, H., BELLOTTI, R., BERTACCHI, P., KOTSOVOS, M.D., KO, H.Y., LINSE, D., NEWMAN, J.B., ROSSI, P., SCHICKERT, G., TAYLOR, M.A., TRAINA, L.A., WINKLER, H., ZIMMERMAN, R.M., "Behaviour of Concrete under Multiaxial Stress States", Journal of the Engineering Mechanics Division, ASCE, Vol. 106, No. EM6, December 1980, pp. 1383-1403.

8. BARNARD, P.R., "Researches into the Complete Stress-Strain Curve for Concrete", Magazine of Concrete Research, Vol. 16, No. 49, December 1964, pp. 203-210.

9. KOTSOVOS, M.D. and NEWMAN, J.B., "Mathematical Description of Deformational Behaviour of Concrete under Generalised Stress Beyond Ultimate Strength", ACI Journal, Proceedings, Vol. 77, No. 5, September-October 1980, pp. 340-346.

10. TURNER, P.W. and BARNARD, P.R., "Stiff Constant Strain Rate Testing Machine", The Engineer, Vol. 214, No. 5557, July 1962, pp. 146-148.

11. WANG, P.T., SHAH, S.P. and NAAMAN, A.E., "Stress-Strain Curves of Normal and Lightweight Concrete in Compression", ACI Journal, Proceedings, Vol. 75, No. 11, November 1978, pp. 603-611.

12. KOTSOVOS, M.D., "A Mathematical Model of the Deformational Behaviour of Concrete under Generalised Stress Based on Fundamental Material Properties", Materials and Structures, RILEM, Vol. 13, No. 76, July-August 1980, pp. 289-298.

13. KOTSOVOS, M.D., "Fracture Processes of Concrete under Generalised Stress States", Materials and Structures, RILEM, Vol. 12, No. 72, November-December 1979, pp. 431-437.

14. KOTSOVOS, M.D. and NEWMAN, J.B., "Fracture Mechanics and Concrete Behaviour", to appear in Magazine of Concrete Research in June 1981.

15. KOTSOVOS, M.D., "An Analytical Investigation of the Behaviour of Concrete under Concentrations of Load", submitted for publication in Materials and Structures.

16. KOTSOVOS, M.D. and NEWMAN, J.B., "Effect of Boundary Conditions on the Behaviour of Concrete under Concentrations of Load", submitted for publication in the Magazine of Concrete Research.

17. NEWMAN, J.B., "Apparatus for Testing Concrete under Multiaxial States of Stress", Magazine of Concrete Research, Vol. 26, No. 89, December 1974, pp. 229-238.

18. KOTSOVOS, M.D. and NEWMAN, J.B., "Behaviour of Concrete under Multiaxial Stress", ACI Journal, Proceedings, Vol. 74, No. 9, September 1977, pp. 443-446.

19. KOTSOVOS, M.D., "Effect of Stress Path on the Behaviour of Concrete under Triaxial Stress States", ACI Journal, Proceedings, Vol. 76, No. 2, February 1979, pp. 213-223.

20. KOTSOVOS, M.D., "Mathematical Description of the Strength Properties of Concrete under Generalised Stress", Magazine of Concrete Research, Vol. 31, No. 108, September 1979, pp. 151-158.

21. KOTSOVOS, M.D. and NEWMAN, J.B., "A Mathematical Description of the Deformational Behaviour of Concrete under Complex Loading", Magazine of Concrete Research, Vol. 31, No. 107, June 1979, pp. 77-90.

22. KOTSOVOS, M.D. and NEWMAN, J.B., "Generalised Stress-Strain Relations for Concrete", Journal of the Engineering Mechanics Division, ASCE, Vol. 104, No. EM4, August 1978, pp. 845-856.

23. NEWMAN, J.B., "Criteria for Concrete Strength", Ph.D. Thesis, University of London, 1973, 583 pp.

24. KOTSOVOS, M.D., "Failure Criteria for Concrete under Generalised Stress States", Ph.D. Thesis, University of London, 1974, 284 pp.

A Constitutive Model for Concrete in High Rate of Loading Conditions

Un modèle constitutif pour le béton sous sollicitations rapides

Ein Stoffmodell für Beton für grösse Beanspruchungsgeschwindigkeiten

LARSGUNNAR NILSSON
Associate Professor
Div. of Structural Engineering, University of Luleå
Luleå, Sweden

RONNY GLEMBERG
Research Associate
Dept of Structural Mechanics, Chalmers University of Technology,
Göteborg, Sweden

SUMMARY
An elastic-viscoplastic-plastic-brittle constitutive theory is chosen for concrete. It is capable of describing rate, strain history, and stress history effects, as well as the ductile and brittle failure of concrete. The model accounts for nonlinearities both in deviatoric and volumetric states of stress and strain. Comparisons with experimental results are presented.

RÉSUMÉ
Un modèle constitutif élastique-viscoplastique-plastique-fragile est choisi pour le béton. Il est capable de décrire les effets de la vitesse, de l'histoire de l'allongement, de l'histoire de la contrainte et aussi la rupture ductile et fragile de béton. Le modèle permet de tenir compte des propriétés non-linéaires dans les états de contrainte et d'allongement déviatriques et volumétriques. Des comparaisons avec des résultats expérimentaux sont présentées.

ZUSAMMENFASSUNG
Ein Stoffmodell für Beton für elastisches, viskoplastisches, plastisches und sprödes Verhalten is gewählt. Es ist möglich, Wirkungen von Geschwindigkeit, Dehnungs-Geschichte und Spannungs-Geschichte zu beschreiben. Auch spröde und duktile Brüche sind beschrieben. Das Modell kann nicht-lineare deviatorische und volumetrische Spannungs- und Dehnungs-Zustände berücksichtigen. Theoretische Ergebnisse sind mit experimentellen Resultaten verglichen.

1. INTRODUCTION

In all inelastic deformation of concrete, as well as most other materials, the response is highly dependent on the rate of stressing or straining. Furthermore, the inelastic deformation is to a large extent non-recoverable and path dependent. A realistic material model must account for these effects.

The present material model uses a combined elastic-viscoplastic-plastic-brittle theory previously presented in Nilsson [1]. This model can be motivated from the physical observations of two main stages of crack propagation: the stable crack propagation and the unstable crack propagation. Thus, the stable crack propagation will be described by the theory of viscoplasticity, and the unstable crack propagation by a combined viscoplastic-plastic, or alternatively, a combined viscoplastic-brittle theory. By the use of rate-hardening functions, the stress at failure will also depend on the strain rate.

The actual material behaviour is governed by the relative location of the stress point to the plastic yielding, brittle failure, and the viscoplastic loading surfaces in the stress space, see Figure 1.

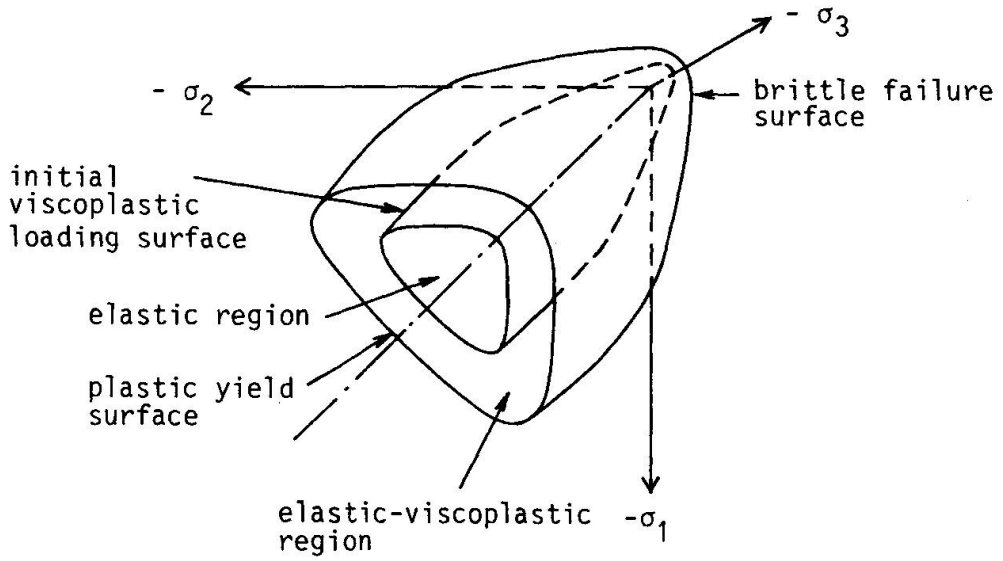

Fig 1 Regions of elasticity, viscoplasticity, plasticity, and brittle failure

2. CONSTITUTIVE EQUATIONS

2.1 Loading, potential, and failure surfaces

From proportional true triaxial tests, it is possible (within the assumption of isotropy) to construct the surface of elastic limit, the crack initiation surface, and the failure surface. Most work on the mathematical modelling of these surfaces has been concerned with the failure surface. In contrast to the failure surface, both the elastic limit surface and the crack initiation surface are closed. In the present theory, their mathematical representations are the static viscoplastic loading surface $F^V = 0$ and the plastic yield surface $F^p = 0$, respectively. For tension or combined tension-compression states of stress, the plastic yield surface is also utilized as a brittle

failure surface.

In concrete and other granular materials, strain softening and dilatancy are obtained for small hydrostatic pressures, while strain hardening and contractancy are obtained for high hydrostatic pressures. A closed loading surface and an associated flow rule are capable of modelling these effects.

A simple geometric surface, which can be made to fit the experimentally found surfaces (i.e. both $F^V = 0$ and $F^p = 0$) fairly well, is the generalized ellipsoidal surface

$$F = \left[\left(\frac{2\,\frac{\sigma_o}{H_r} - \xi_u - \xi_l}{\xi_u - \xi_l}\right)^2 + \left(\frac{\frac{\tau_o}{H_r}}{b(\theta)}\right)^2\right]^{1/2} - 1 \qquad (1)$$

where σ_o, τ_o, and θ are the octahedral normal stress, the octahedral shear stress, and the angle of similarity, respectively, given by

$$\sigma_o = \frac{1}{3}\,\mathrm{tr}\,\underset{\sim}{\sigma}, \quad \tau_o = \left(\frac{1}{3}\,\underset{\sim}{s}:\underset{\sim}{s}\right)^{1/2}, \quad \theta = \frac{1}{3}\arccos\left(\sqrt{2}\,\det(\underset{\sim}{s})/\tau_o^{\,3}\right) \qquad (2)$$

Here $\underset{\sim}{s}$ is the deviator of the stress tensor $\underset{\sim}{\sigma}$. The parameters ξ_u, ξ_l, and $b(\theta)$ can be identified from Figure 2.

The rate-hardening parameter H_r, which will later be discussed, approaches in static loading condition the value of f_{cu}.

The deviatoric semiaxis $b(\theta)$ is approximated as a function of θ (an ellipse). Due to the symmetry conditions, it suffices to interpolate b in its values b_1 and b_2 for 'triaxial extension' ($\theta = 0^o$) and 'triaxial compression' ($\theta = 60^o$)

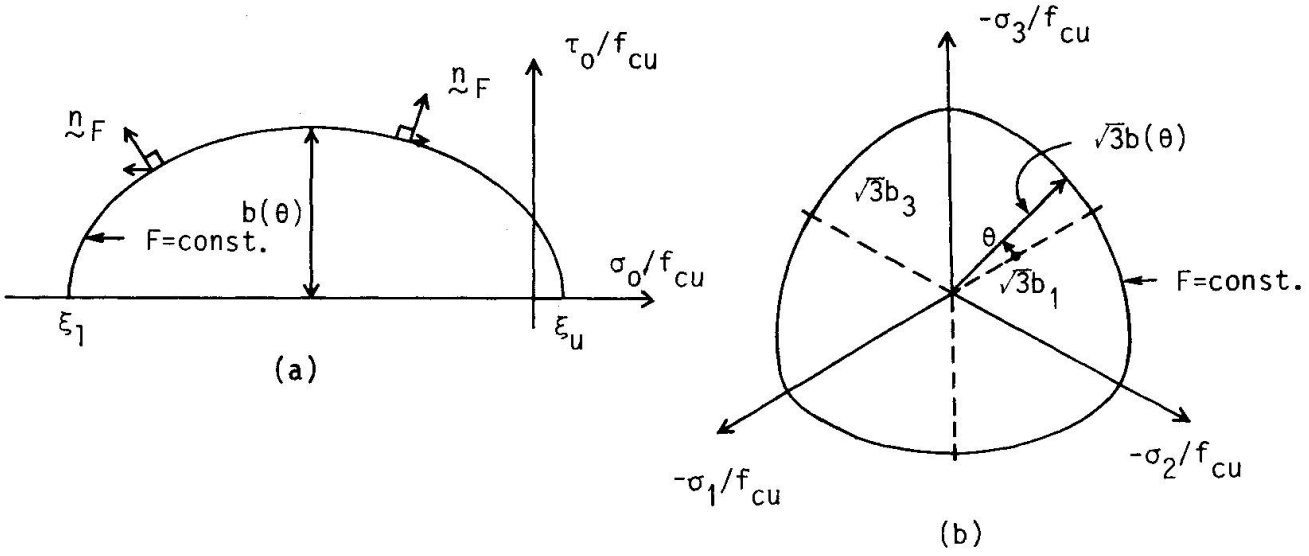

Fig 2 Rendulic (a) and deviatoric section at vertex (b) of the generalized ellipsoidal loading surface. (f_{cu} = uniaxial compressive strength)

tests, respectively. Thus,

$$b(\theta) = [t(\theta) + u(\theta)]/v(\theta) \tag{3}$$

where

$$t(\theta) = 2b_2(b_2^2 - b_1^2)\cos\theta \tag{4a}$$

$$u(\theta) = b_2(2b_1 - b_2)\,[4(b_2^2 - b_1^2)\cos^2\theta + 5b_1^2 - 4b_1b_2]^{1/2} \tag{4b}$$

$$v(\theta) = 4(b_2^2 - b_1^2)\cos^2\theta + (b_2 - 2b_1)^2 \tag{4c}$$

where $b_1 = b(0^o)$ and $b_2 = b(60^o)$, respectively, c f Figure 2(b). With the exception of the hardening and softening parameters, the generalized ellipsoidal surface contains four parameters ξ_1, ξ_1, b_1, and b_2, which must be fitted to experimental data. It is convenient to express some of these parameters in more easily identified ones, which can be obtained from standard tests: the uniaxial compressive strength f_{cu}, the uniaxial tensile strength f_{tu}, the biaxial compressive strength f_{cb}, and the elastic limit in hydrostatic compression f_{ct}. Table 1 summarizes the four different test stress states.

TABLE 1 Identification of test stress states
($\alpha_{tu} = f_{tu}/f_{cu}$, $\alpha_{cb} = f_{cb}/f_{cu}$, $\xi_1 = f_{ct}/f_{cu}$)

Test	Principal stresses	σ_o/f_{cu}	τ_o/f_{cu}	θ	$b(\theta)$
Uniaxial tension	$\sigma_1=f_{tu}$ $\sigma_2=\sigma_3=0$	$\frac{1}{3}\alpha_{tu}$	$\frac{\sqrt{2}}{3}\alpha_{tu}$	0^o	b_1
Uniaxial compression	$\sigma_1=\sigma_2=0$ $\sigma_3=-f_{cu}$	$-\frac{1}{3}$	$\frac{\sqrt{2}}{3}$	60^o	b_2
Biaxial compression	$\sigma_1=0$ $\sigma_2=\sigma_3=-f_{cb}$	$-\frac{2}{3}\alpha_{cb}$	$\frac{\sqrt{2}}{3}\alpha_{cb}$	0^o	b_1
Hydrostatic compression	$\sigma_1=\sigma_2=\sigma_3=-f_{ct}$	ξ_1	0	-	-

The following substitutions for ξ_u, b_1, and b_2 are

$$\xi_u = \frac{\alpha_{cb}^2(\frac{2}{3}\alpha_{tu} - \xi_1)^2 - \alpha_{tu}^2(\frac{4}{3}\alpha_{cb} + \xi_1)^2 - (\alpha_{cb}^2 - \alpha_{tu}^2)\xi_1^2}{2[\alpha_{cb}^2(\frac{2}{3}\alpha_{tu} - \xi_1) + \alpha_{tu}^2(\frac{4}{3}\alpha_{cu} + \xi_1) - (\alpha_{cb}^2 - \alpha_{tu}^2)\xi_1]} \tag{5}$$

$$b_1^2 = \frac{2}{9}\alpha_{cb}^2\left[1 - \left(\frac{\frac{4}{3}\alpha_{cb} + \xi_u + \xi_1}{\xi_u - \xi_1}\right)^2\right]^{-1} \tag{6}$$

$$b_2^2 = \frac{2}{9}\left[1 - \left(\frac{\frac{2}{3} + \xi_u + \xi_1}{\xi_u - \xi_1}\right)^2\right]^{-1} \tag{7}$$

For many occasions a complete set of test data is lacking, and empirical relations must be relied on. With such empirical relations, however, the number of model parameters can be reduced.

Figure 3 shows a fit of the generalized ellipsoidal surfaces to experimental data. A remarkably accurate fit for this concrete is noted for the elastic limit surface. The poorer accuracy for the fit of the initial plastic loading

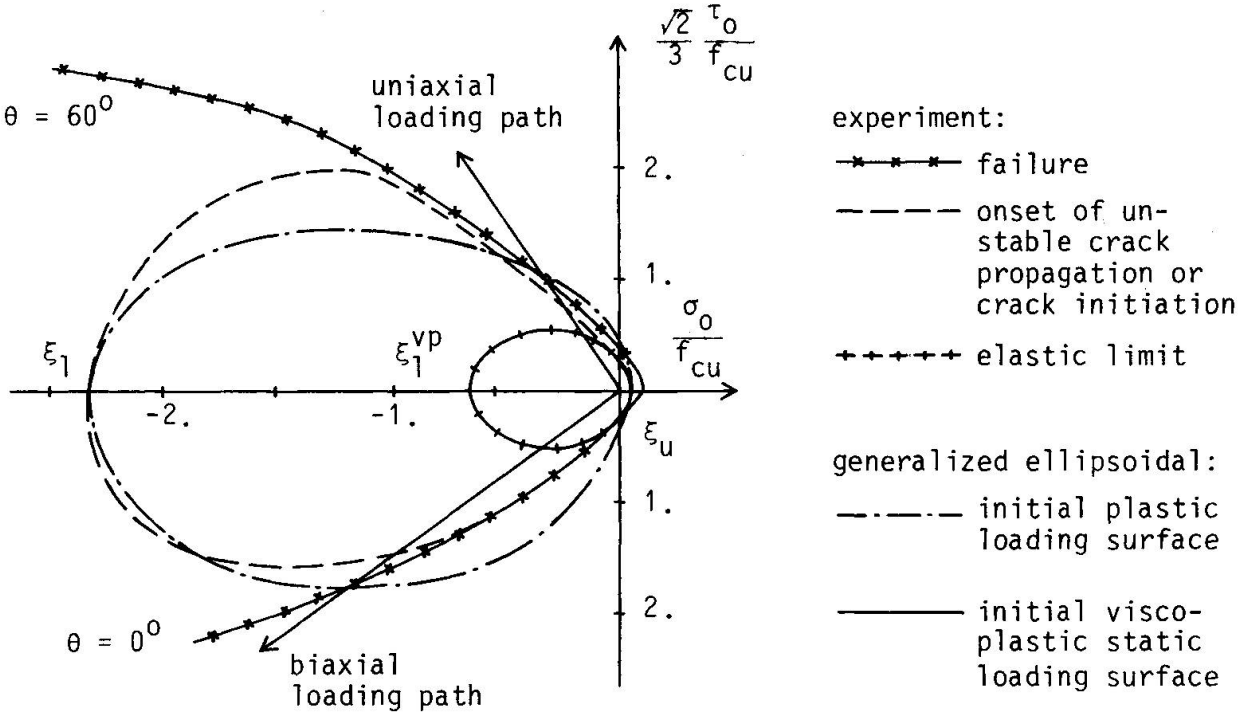

Fig 3 Fit of generalized ellipsoidal surfaces to experimental data of Launay and Gachon [2]. Parameters of the initial plastic loading surface: $\alpha_{tu} = 0.15$, $\alpha_{cb} = 1.8$, $\xi_1 = -2.3$ ($\xi_u = 0.05$, $b_1 = 0.85$, $b_2 = 0.64$). Parameters of the initial viscoplastic static loading surface: $\xi_u = 0.05$, $\xi_1 = -0.67$, $b_1 = 0.24$, $b_2 = 0.25$

surface is explained by the definite form of the ellipse. To obtain closer fits more sophisticated types of loading surfaces are needed. Another possibility for closer fits is to use two different types of loading surfaces; one of the classical type, which conforms to the failure surface, and another which intersects the hydrostatic compression axis.

2.2 Elastic response

For stress points inside the static viscoplastic loading surface, $F^v = 0$ (elastic limit surface), a hypoelastic stress-strain relation is assumed. Thus,

$$d\underset{\sim}{\sigma} = \underset{\sim}{S} : d\underset{\sim}{\varepsilon} \tag{8}$$

where $\underset{\sim}{S}$ is the fourth-order elastic tangential stiffness tensor and $d\underset{\sim}{\varepsilon}$ is the elastic strain increment tensor. Initially, a linear elastic stiffness is assumed, in which case $\underset{\sim}{S}$ contains elastic constants. For representation of stiffness degradation due to micro- and macrocracking, a dependence of the inelastic dilatance on the elastic stiffness $\underset{\sim}{S}$ is introduced in the form

$$K = {}^0K\, e^{-\left(\frac{\varepsilon_o^p}{d_1}\right)^2}, \quad G = {}^0G\, e^{-\left(\frac{\varepsilon_o^p}{d_2}\right)^2}, \quad \varepsilon_o^p > 0 \tag{9}$$

where ${}^0K$ and ${}^0G$ are the initial bulk and shear moduli, respectively, and ε_o^p is the plastic volumetric strain. The parameters d_1 and d_2 control the rate of degradation. In general we have assumed that $d_1 \equiv d_2 \equiv d$.

2.3 Elastic-viscoplastic response

For stress points in the region between the static viscoplastic loading surface, $F^v = 0$, and the plastic yield surface, $F^p = 0$, elastic-viscoplastic response is assumed. The total strain increment is additively resolved into elastic ($d\underset{\sim}{\varepsilon}^e$) and viscoplastic ($d\underset{\sim}{\varepsilon}^{vp}$) parts

$$d\underset{\sim}{\varepsilon} = d\underset{\sim}{\varepsilon}^e + d\underset{\sim}{\varepsilon}^{vp} \tag{10}$$

The elastic-viscoplastic stress-strain relation is thus

$$d\underset{\sim}{\sigma} = \underset{\sim}{S} : (d\underset{\sim}{\varepsilon} - \dot{\underset{\sim}{\varepsilon}}^{vp} dt) \tag{11}$$

The viscoplastic strain rate $\dot{\underset{\sim}{\varepsilon}}^{vp}$ is governed by a generalization of Perzyna's [3] theory

$$\dot{\underset{\sim}{\varepsilon}}^{vp} = \gamma(\dot{\underset{\sim}{\varepsilon}}, \underset{\sim}{\sigma}) < \phi(F^v) > \underset{\sim}{n}_F \tag{12}$$

where the normalized gradient $\underset{\sim}{n}_F$ of the dynamic loading potential surface, $F^v(\underset{\sim}{\sigma}, H^v) = \text{const.}$, gives the direction of the viscoplastic strain rate. The

hardening/softening function H^v will be discussed in Section 2.6. The bracket $\langle \cdot \rangle$ indicates that only values of ϕ with argument $F^v > 0$ are taken as different from zero. The static viscoplastic loading surface is given by $F^v(\underset{\sim}{\sigma}, H^v) = 0$. In short-term static and dynamic loading conditions, the primary nonlinearities of concrete are caused by microcrack growth and pore collapses. Both these physical phenomena manifest themselves as nonrecoverable delay effects. From a physical point of view, a relationship must exist between the velocity of the growth of microcracks and the viscoplastic strain rate. One can therefore interpret the accumulated viscoplastic strain as a measure of microcrack damage. Several proposals of the function $\phi(F^v)$ have been given by Perzyna [3]. They are all derived from fits to experimental data. The function

$$\phi(F^v) = \left(\frac{F^v}{F^{v1}}\right)^{\alpha} \tag{13}$$

is used in this analysis. The value F^v of the dynamic loading function is normalized against F^{v1} in order to give nondimensional values of $\phi(F^v)$. The normalization value F^{v1} has been chosen such that $F^v = F^{v1}$ at plastic yielding for a specified test state of stress. The parameter α determines the curvature of the stress-strain curve at constant rate of straining.

The parameter γ in Eq. (12) is assumed to be a function of the strain rate. This renders it possible to fit stress and strain at failure according to specified values. The following function was proposed in Nilsson [1]

$$\gamma(\dot{\varepsilon}) = \dot{\varepsilon}^{ef}\, e^{-r \ln\left|\frac{\dot{\varepsilon}^{ef}}{\dot{\varepsilon}^{ef}_r}\right|} \tag{14}$$

where $\dot{\varepsilon}^{ef}$ is an invariant function of the strain rate, $\dot{\varepsilon}^{ef}_r$ is a reference value of the effective strain rate, and r is a material constant. In the following numerical analyses

$$\dot{\varepsilon}^{ef} = (\dot{\varepsilon}_o^2 + \frac{1}{4}\dot{\gamma}_o^2)^{1/2} \tag{15}$$

has been utilized.

2.4 Elastic-viscoplastic-plastic response

For a stress point on the surface $F^p = 0$ plastic yielding takes place. The plastic strain increment $d\underset{\sim}{\varepsilon}^p$ gives a contribution to the total strain increment. Thus,

$$d\underset{\sim}{\varepsilon} = d\underset{\sim}{\varepsilon}^e + d\underset{\sim}{\varepsilon}^{vp} + d\underset{\sim}{\varepsilon}^p \tag{16}$$

It is observed that a non-zero viscoplastic strain increment always accompanies the plastic strain increment, unless the static viscoplastic loading surface at the actual stress-point coincides with the plastic yield surface.

Within the assumption of an associated flow rule the plastic strain increment is obtained from

$$d\underset{\sim}{\varepsilon}^{p} = d\lambda \frac{\partial F^{p}}{\partial \underset{\sim}{\sigma}} \tag{17}$$

where the scalar $d\lambda$ will depend on the states of stress, strain, and strain rate. During plastic flow the consistency conditions

$$F^{p}(\underset{\sim}{\sigma}, H^{p}) = 0 \qquad \text{and} \qquad dF^{p}(\underset{\sim}{\sigma}, H^{p}) = 0 \tag{18}$$

must be satisfied. If the hardening and softening of the plastic surface is governed by a function H^{p}, which is a function only of the plastic strain, we find

$$d\underset{\sim}{\sigma} = \underset{\sim}{S}^{ep} : (d\underset{\sim}{\varepsilon} - d\underset{\sim}{\varepsilon}^{vp}) \tag{19}$$

where the elastic-plastic tangential stiffness tensor $\underset{\sim}{S}^{ep}$ is given by

$$\underset{\sim}{S}^{ep} = \underset{\sim}{S} - \frac{1}{D}\left(\underset{\sim}{S} : \frac{\partial F^{p}}{\partial \underset{\sim}{\sigma}}\right)\left(\frac{\partial F^{p}}{\partial \underset{\sim}{\sigma}} : \underset{\sim}{S}\right) \tag{20a}$$

$$D = \frac{\partial F^{p}}{\partial \underset{\sim}{\sigma}} : \underset{\sim}{S} : \frac{\partial F^{p}}{\partial \underset{\sim}{\sigma}} - \frac{\partial F^{p}}{\partial H^{p}} \frac{\partial H^{p}}{\partial \underset{\sim}{\varepsilon}^{p}} : \frac{\partial F^{p}}{\partial \underset{\sim}{\sigma}} \tag{20b}$$

2.5 Elastic-viscoplastic-brittle response

Brittle failure is assumed to occur whenever the failure criterion

$$F^{c}(\underset{\sim}{\sigma}, H^{c}) = 0 \tag{21}$$

is met and at least one principal stress is positive. Before failure, isotropy is assumed, and the failure criterion (21) can be interpreted as a failure surface in the principal stress space. The shape of the failure surface changes according to the hardening and softening parameter H^{c}. The same function has been chosen both for the plastic yielding (ductile failure) and for the brittle failure. Thus, it is assumed that

$$F^{c}(\underset{\sim}{\sigma}, H^{c}) = F^{p}(\underset{\sim}{\sigma}, H^{p}) \tag{22}$$

Prior to failure the material can carry a certain amount of principal tensile stresses in any direction. Whenever the failure criterion (21) is satisfied in a spatial point, a crack plane is formed there. The crack plane induces anisotropy, which will exist for all future time. The normal of the crack plane is assumed to coincide with the direction of the maximal principal (tensile) stress at failure.

After the brittle failure, the tensile strength across the crack plane is assumed to be zero. The compressive strength across a crack plane is, however, assumed to be independent of an existing crack plane. Depending on the roughness of the crack surfaces and on the crack width (distance between the crack surfaces), the shear strength in the crack plane can vary from full strength to zero strength.

Secondary cracks may develop at a cracked point as long as a tensile strength remains in any direction. For every new crack plane that is formed, the order of the stress state will be reduced by one. Thus, prior to cracking the stress state is three-dimensional. After one crack plane has formed, it is two--dimensional, etc.

In the present analysis, the 'tension cut-off' surface is utilized as a post failure surface. Thus,

$$F^f(\underset{\sim}{\sigma}) \equiv \max\,(\sigma_i) \qquad i = 1, 2, 3 \tag{23}$$

where σ_1, σ_2, and σ_3 are the principal stresses.

At failure the following relations are satisfied:

$$F^p(\underset{\sim}{\sigma}, H_k^p) = 0 \qquad \text{and} \qquad F^f(\underset{\sim}{\sigma}) = \mu \tag{24}$$

where $\mu > 0$ is the largest principal stress. Immediately after failure, the following relation must hold

$$F^f(\underset{\sim}{\sigma} + d\underset{\sim}{\sigma}) = 0 \tag{25}$$

where $d\underset{\sim}{\sigma}$ is a stress transfer or stress relaxation. It is assumed that the incremental strain due to brittle failure $d\underset{\sim}{\varepsilon}^c$, can be added to the total incremental strain. Thus,

$$d\underset{\sim}{\varepsilon} = d\underset{\sim}{\varepsilon}^e + d\underset{\sim}{\varepsilon}^{vp} + d\underset{\sim}{\varepsilon}^c \tag{26}$$

In analogy with an associated flow theory of plasticity, it is assumed that the incremental strain due to brittle failure follows from the normality rule

$$d\underset{\sim}{\varepsilon}^c = d\lambda_c \frac{\partial F^f}{\partial \underset{\sim}{\sigma}} \tag{27}$$

where $d\lambda_c$ is dependent on the stress and strain state. Some algebra yields

$$d\underset{\sim}{\sigma} = \underset{\sim}{S}^c : (d\underset{\sim}{\varepsilon} - d\underset{\sim}{\varepsilon}^{vp}) - d\underset{\sim}{\sigma}^c \tag{28}$$

where the tangential stiffness tensor $\underset{\sim}{S}^c$ for the material with one crack plane is given by

$$\underset{\sim}{S}^c = \underset{\sim}{S} - \frac{1}{D^c}\left(\underset{\sim}{S} : \frac{\partial F^f}{\partial \underset{\sim}{\sigma}}\right)\left(\frac{\partial F^f}{\partial \underset{\sim}{\sigma}} : \underset{\sim}{S}\right) \tag{29a}$$

$$D^c = \frac{\partial F^f}{\partial \underset{\sim}{\sigma}} : \underset{\sim}{S} : \frac{\partial F^f}{\partial \underset{\sim}{\sigma}} \tag{29b}$$

and the incremental stress $d\underset{\sim}{\sigma}^c$ due to brittle failure is given by

$$d\underset{\sim}{\sigma}^c = \frac{\mu}{D^c}\ \underset{\sim}{S} : \frac{\partial F^f}{\partial \underset{\sim}{\sigma}} \tag{30}$$

The derivation of the tangential stiffness tensor $\underset{\sim}{S}^{cc}$ and the incremental fracture stress $d\underset{\sim}{\sigma}^{cc}$ due to a secondary crack plane is analogous.

Finally, when the third crack plane is formed, the tangential stiffness tensor for tensile states of stress is reduced to the zero tensor.

2.6 Strain hardening and softening

All four parameters of the generalized ellipsoidal loading surface can be functions of damage measures. This renders it possible to model complex hardening and softening behaviour. Unfortunately, much experimental results on triaxial hardening and softening of concrete are lacking, and the choice of hardening and softening functions must mainly be based on hypotheses.

Experiments show that plastic contractance hardens the material, while plastic dilatance softens the material. Thus, it is natural to use the inelastic volumetric strain as an internal variable (measure of material damage).

The parameter ξ_1 (Eq. (1)) of the generalized ellipsoidal surface is assumed to be a master hardening and softening parameter. The hardening function is obtained by identifying the inelastic strain components of experimental data obtained from hydrostatic compression tests. The exponential hardening function

$$\xi_1 = {}^0\xi_1\, e^{-a\varepsilon_o^p} \qquad (\varepsilon_o^p \leq 0) \tag{31}$$

has been found to fit test data of Green and Swanson [4] fairly well. In Eq. (31) ${}^0\xi_1$ denotes the initial hydrostatic stress at plastic yielding and a is a material parameter.

The softening function can be chosen in a similar manner from tests which exhibit softening behaviour. The following function has been chosen

$$\xi_1 = ({}^0\xi_1 + \xi_u)\, e^{-\left(\frac{\varepsilon_o^p}{b}\right)} - \xi_u \qquad (\varepsilon_o^p > 0) \tag{32}$$

where ξ_1 and ξ_u can be identified from Figure 2 and b is a material parameter. The parameter b controls the rate of softening. It has been found that $b = 5 \cdot 10^{-4}$ yields a good fit to uniaxial compression tests by Linse [5], [6]. Experimental data for the hardening and softening of the elastic limit surface seem to be lacking at present. For this reason very simple hardening and softening rules have been chosen. In the case of viscoplastic dilatancy, the relation between the parameters of the plastic yielding and the static viscoplastic loading surfaces is constant. However, plastic contractancy is assumed to affect this relation in such a way that ξ_1^{vp} tends to ξ_1. Thus

$$\xi_1^{vp} = \begin{cases} {}^0\xi_1^{vp} + \dfrac{H^v}{f_{cu}}\, \varepsilon_o^{vp} & \xi_1^{vp} > \xi_1 \\ \xi_1 & \text{otherwise} \end{cases} \tag{33a}$$

where it has been assumed that

$${}^0\xi_1^{vp} = \kappa\xi_1,\ {}^0b_1^{vp} = \kappa b_1, {}^0b_2^{vp} = \kappa b_2,\ \xi_u^{vp} = \xi_u \tag{33b}$$

and κ is a proportionality constant. The viscoplastic hardening can be explained by the observation of relatively elastic unloading paths from stress states with high hydrostatic pressure components. Furthermore, the existence of creep or relaxation even after excessive cracking can be observed in experiments.

2.7 Strain rate hardening and softening

Experiments have clearly indicated the dependence of the rate of loading or the rate of straining upon the failure. The general observation is that the ultimate stress increases significantly with the rate of loading or straining.

In the present analysis the rate effects upon the ductile yield and brittle failure surfaces are introduced in the form of a single rate hardening parameter H_r, which is a function of an effective strain rate, Eq. (15). It was proposed in Nilsson [7] that the rate hardening can be approximated as the function

$$H_r = f_{cu}\{c_1 + c_2 \ln(\dot{\varepsilon}^{ef}) + c_3[\ln(\dot{\varepsilon}^{ef})]^2\} \tag{34}$$

where the parameters c_1, c_2, and c_3 are obtained by fitting H_r to experimental data, c f Figure 4.

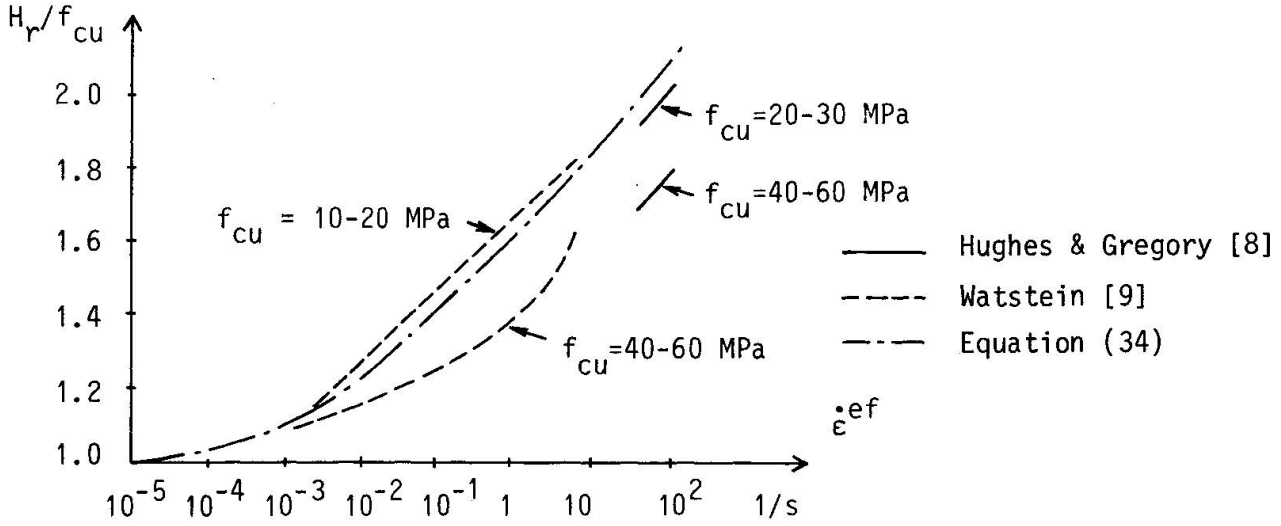

Fig 4 The effect of average strain rate upon compressive strength of concrete. Parameters of Eq. (34): $c_1 = 1.6$, $c_2 = 0.104$, and $c_3 = 0.0045$

The introduction of the hardening parameters H_r into the plastic yield and brittle failure function Eq. (1) yields an isotropic rate hardening or softening. Due to the rate effect, the failure surface can be interpreted as 'breathing'.

3. VERIFICATION OF THE CONSTITUTIVE THEORY

In this section some experimental test results found in the literature are compared to numerical results obtained with the present constitutive model. The simulations are carried out directly on the constitutive equations. Consequently, homogeneous states of stress and strain are assumed in the experimental test specimens.

In general, it is extremely difficult to perform an experimental test with all components of the strain vector prescribed according to a specified history. Most strain controlled tests have been performed with just one pre-determined strain component.

The verifications have been conducted under conditions of controlled strain rate in the smallest principal stress direction, and with a given ratio between the principal stresses. Two types of triaxial tests have been simulated: the triaxial compression test (two principal stresses equal) and the true triaxial test with constant ratio between the principal stresses.

The triaxial compression tests performed by Green and Swanson [4] were conducted on high strength concrete. According to the experimental test $f_{cu} = 48.4$ MPa and $f_{tu} = 5.6$ MPa. The biaxial strength was not tested. The following parameters have been used: $f_{cb} = 1.15$, $f_{cu} = 55.7$ MPa, $\xi_1 = -1.5$, $E_0 = 38.8$ GPa, $\nu_0 = 0.18$, $\kappa = 0.4$ (Eq. (33b)), $a = 80$ (Eq. (31)), $b = 1.0 \cdot 10^{-3}$ (Eq. (32)), $H^v = 24.0\, f_{cu}$ (Eq. (33a)), $\alpha = 0.8$ (Eq. (13)), $\dot{\varepsilon}_r^{ef} = 2.0 \cdot 10^{-6}$ s^{-1}

and $r = 0.0625$ (Eq. (14), and $d = 0.5 \cdot 10^{-3}$ (Eq. (9)). The rate of straining is assumed to be $2 \cdot 10^{-6}$ s^{-1}.

Figure 5 shows the fit of the hydrostatic compression test. With the proposed parameters the deviation between the experimental and the mathematical curves is small.

Figure 6 shows the fit of different triaxial compression tests. The hydrostatic pressure was applied in accordance with the prescribed rate of straining. When the prescribed level of lateral pressure $\sigma_1 = \sigma_2$ was reached, the lateral pressure was fixed and only the axial stress was increased according to the specified rate of straining. It is noted that relatively good fits are obtained for $\sigma_1 = \sigma_2 = 0$ and $\sigma_1 = \sigma_2 = -6.9$ MPa. Due to the lack of independent deviatoric hardening of the plastic surface, the plastic dilatance according to the model appears to be too abrupt at material instability. The disadvantage of the ellipsoidal shape of the plastic loading surface at higher hydrostatic pressures appears for $\sigma_1 = \sigma_2 = -13.8$ MPa. Furthermore, the shear compaction of the proposed model is too small.

The true triaxial tests performed by Linse [5], [6] were conducted with a constant ratio between the principal stresses. The rate of straining in the smallest principal stress direction was $2.0 \cdot 10^{-6}$ s^{-1}. The following common parameters have been used: $f_{cb} = 1.15\, f_{cu}$, $f_{tu} = 0.1\, f_{cu}$, $\xi_1 = -2.0$, $E_0 = 30.0$ GPa, $\nu_0 = 0.18$, $\kappa = 0.4$ (Eq. (33b)), $a = 100$ (Eq. (31)), $b = 0.5 \cdot 10^{-3}$ (Eq. (32)), $H^v = 50\, f_{cu}$ (Eq. (33a)), $\alpha = 0.8$ (Eq. (13)), $\dot{\varepsilon}_r^{ef} = 2.0\ 10^{-6}$ s^{-1}, $r = 0.625$ (Eq. (14)), and $d = 0.5 \cdot 10^{-3}$ (Eq. (9)).

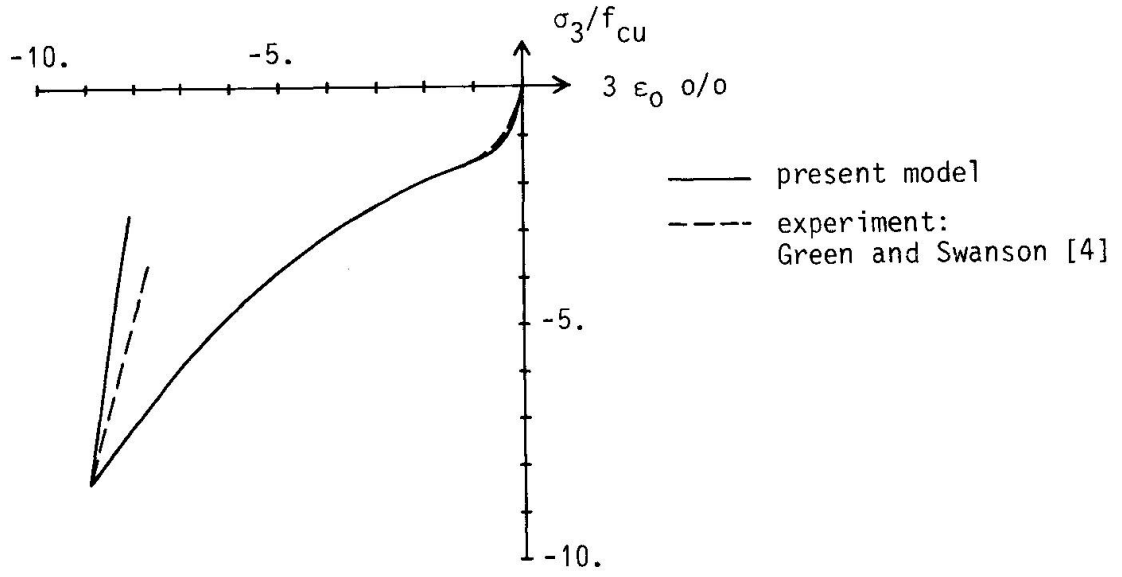

Fig 5 Fit of hydrostatic compression curve

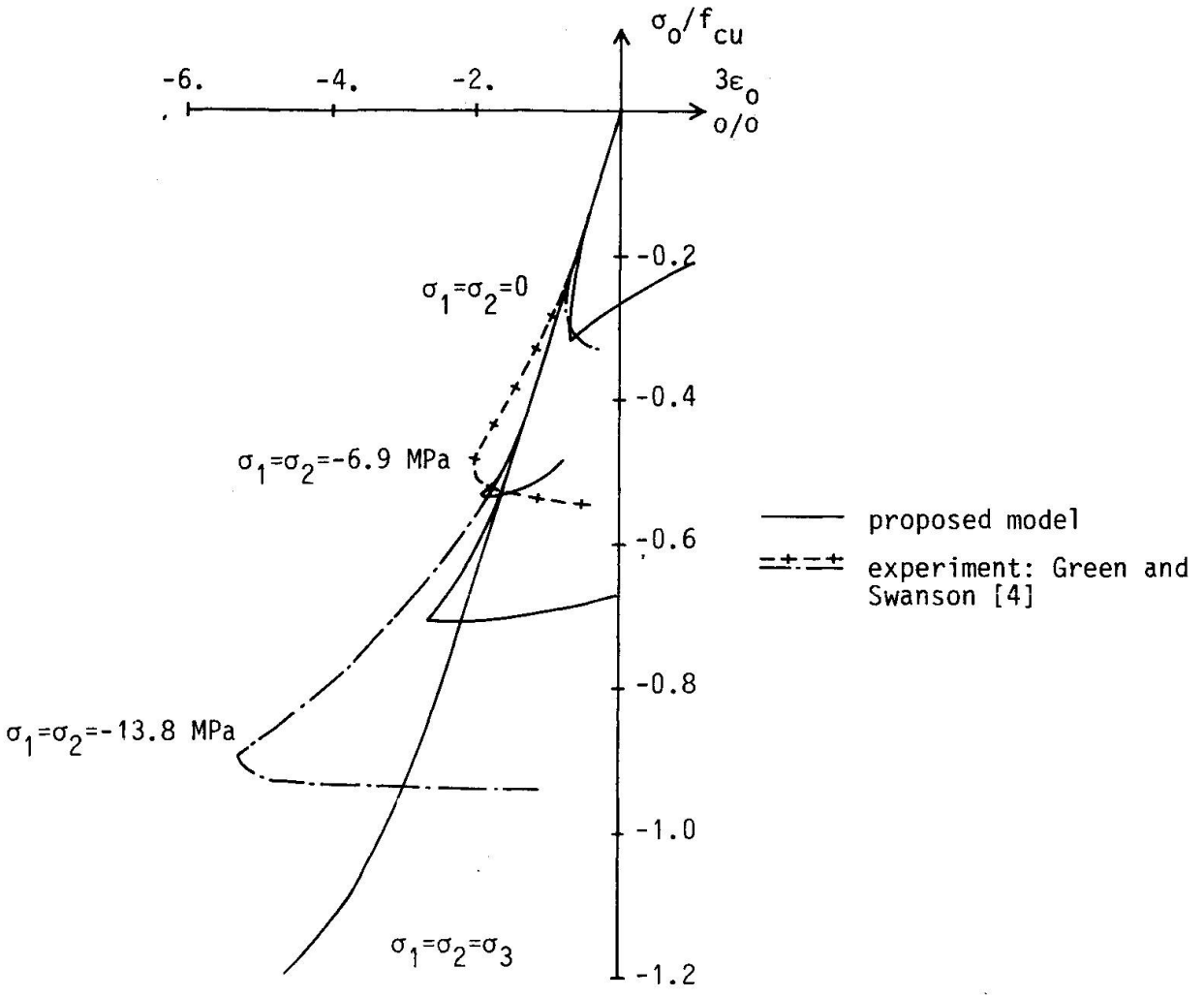

Fig 6 Fit of triaxial compression curves

Figure 7a shows the fit of a uniaxial compression curve. Some deviations between the mathematical and experimental lateral strains are observed. Figure 7b shows the corresponding fit to the biaxial loading curve. The deviations are shown to be small throughout the tested range of strains. Linse did not present any uniaxial tension test. The results from the present model, with the same material parameters as for Linse's compression tests, are shown in Figure 7c.

Figure 8a shows the performance of the present model under different loading--unloading-loading conditions conducted under constant magnitude of strain rate in the direction of maximal load (σ_3). The change of straining direction is assumed to be instantaneous. In its current version, the present model fails to describe the hysteresis loop commonly observed in cyclic tests on concrete.

Figure 8b shows uniaxial compression curves at different constant strain rates as obtained by the present model.

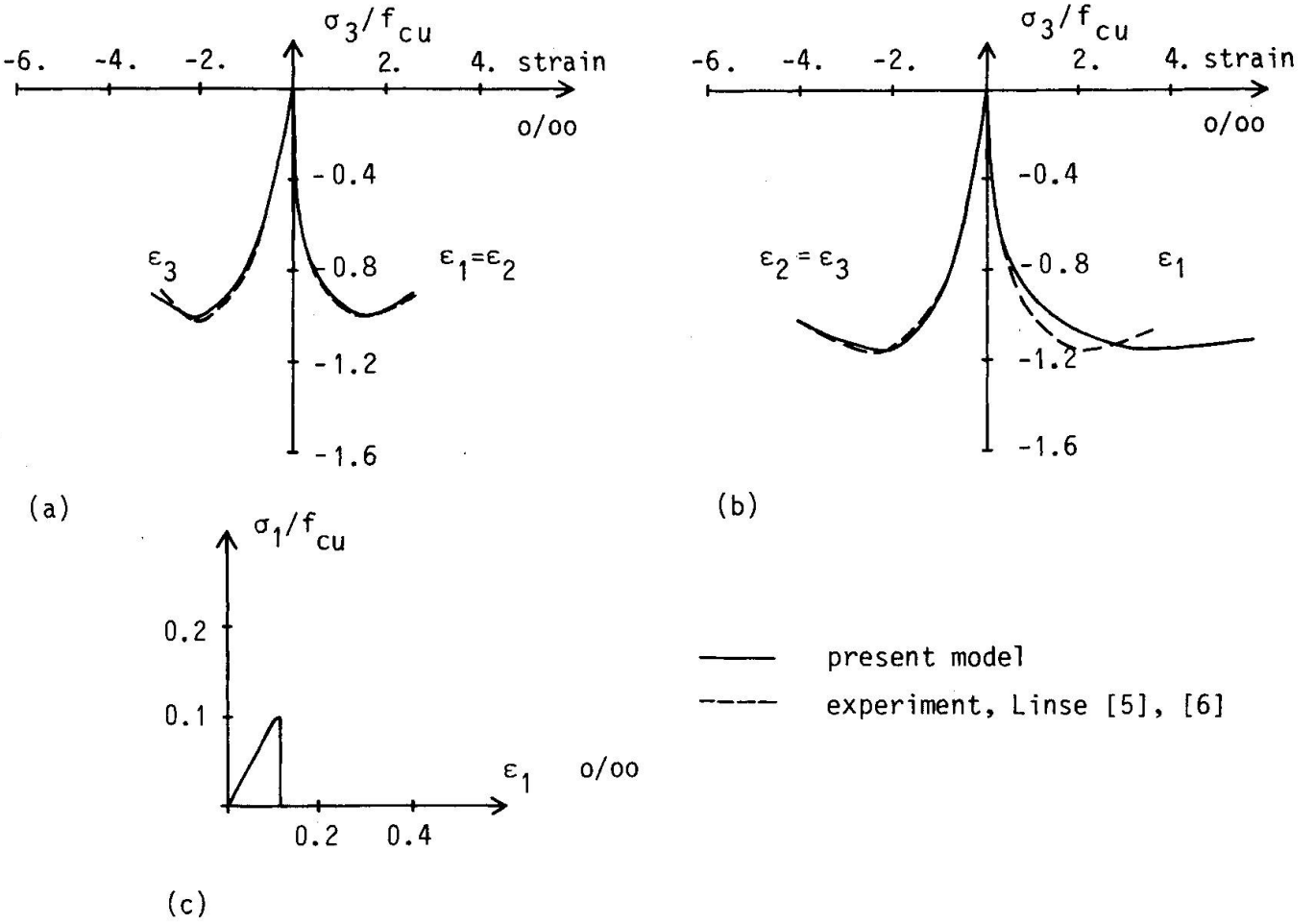

Fig 7 Uniaxial (a) and biaxial (b) compression and uniaxial tension curves (c). (f_{cu} = 30.4 MPa)

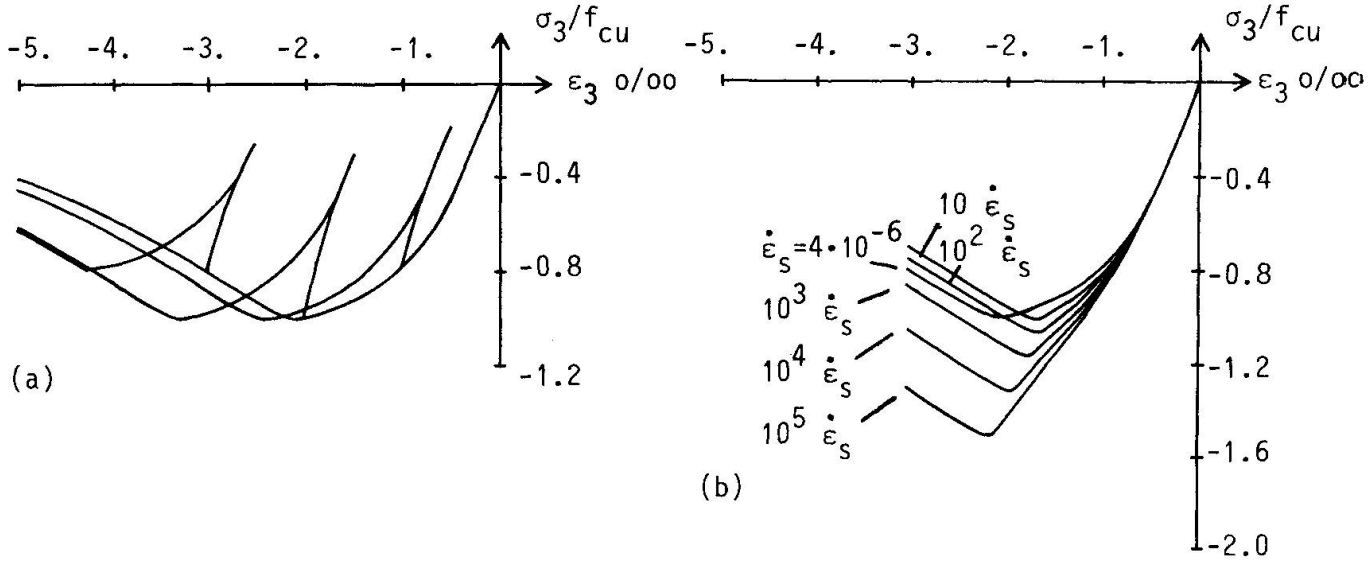

Fig 8 (a) Strain controlled cycling conducted in uniaxial compression test

(b) Uniaxial compression tests conducted at different strain rates. Constant strain rate in the direction of maximal load (f_{cu} = 30.4 MPa)

4. CONCLUDING REMARKS

The stable crack propagation and the unstable crack propagation generally observed in experiments have been modelled by the viscoplastic and plastic-brittle theories, respectively. Rate effects are included in the model both in the sense of viscoplasticity and in the form of strain rate dependent plastic loading and brittle failure relations.

From a number of verification tests, it is concluded that the present constitutive model yields results which qualitatively agree with experimental tests.

Experimental results indicate a degenerated ellipsoidal shape of the loading surface in the principal stress space. Experimental data for hardening and softening of concrete in multi-axial states of stress and strain are still not available. Thus, not much can be said about the appropriate choice of hardening and softening functions. The failure of concrete in tensile states of stress appears as a continuous softening rather than a perfect brittleness. In the present model, the directions of anisotropy of the stiffness tensor are memorized only in the case of a brittle failure. However, every kind of micro- and macro-failure of concrete introduces anisotropy into the stiffness tensor, and the directions of this anisotropy should be memorized by the material for future time.

5. REFERENCES

1. NILSSON, L.: Impact loading on concrete structures, Publication 79:1, Department of Structural Mechanics, Chalmers University of Technology, Göteborg 1979

2. LAUNAY, P. and GACHON, H.: Strain and ultimate strength of concrete under triaxial stress, Paper H1/3, Proceedings of the First International Conference on Structural Mechanics in Reactor Technology, Berlin 1971

3. PERZYNA, P.: Fundamental problems in viscoplasticity, Advances in Applied Mechanics (Eds. Chernyi et al), Vol. 9 (1966), pp 243-377

4. GREEN, S.J. and SWANSON, S.R.: Static constitutive relations for concrete, Air Force Weapons Laboratory, Technical Report No. AFWL-TR-72-2, Kirtland Air Force Base 1973

5. LINSE, D.: Versuchanlage zur Ermittlung der Dreiachsigen Festigkeit von Beton mit ersten Versuchsergebnissen, Cement and Concrete Research, Vol. 3 (1973), No. 4, pp 445-457

6. LINSE, D.: Lösung versuchstechnischer Fragen bei der Ermittlung des Festigkeits- und Verformungsverhaltens von Beton unter dreiachsiger Belastung, Deutscher Ausschuss für Stahlbeton, Heft 292, 1978

7. NILSSON, L.: Finite element analysis of impact on concrete structures, Finite Elements in Nonlinear Mechanics (Eds. Bergan, P. et al), Tapir, Trondheim 1978

8. HUGHES, B.P. and GREGORY, R.: Concrete subjected to high rates of loading in compression, Magazine of Concrete Research, Vol. 24 (1972), No. 78, pp 25-36

9. WATSTEIN, D.: Properties of concrete at high rates of loading, Symposium on Impact Testing, ASTM, STP 176, 1976, pp 156-169

Similitude of Brittle Fracture of Structural Concrete

Similitude de rupture fragile en béton armé

Ähnlichkeit bei sprödem Betonversagen

HANS W. REINHARDT
Prof. Dr.-Ing.
Stevin Laboratory, Delft University of Technology
Delft, The Netherlands

SUMMARY
On three examples of brittle fracture of structural concrete - i.e. bending shear, punching shear, shear in joints between prefabricated floor slabs - it is demonstrated that the absolute size of the member influences the ultimate shear stress. This influence is explained by linear elastic fracture mechanics.

RÉSUMÉ
Par trois exemples de rupture fragile en béton armé - effort tranchant en flexion, poinçonnement de dalles, effort tranchant dans les joints entre éléments de plancher prefabriqués - il est démontré que les dimensions absolues des éléments influencent les tensions de rupture en cisaillement. Cette influence est expliquée par la mécanique de rupture linéaire-élastique.

ZUSAMMENFASSUNG
An drei Beispielen für spröden Bruch von Stahlbetonbauteilen - Biegeschubbruch, Durchstanzen, Schubversagen von Fugen zwischen Fertigteildeckenplatten - wurde gezeigt, dass die absolute Grösse des Bauteils die Bruchschubspannung beeinflusst. Dieser Einfluss wurde mithilfe der linear-elastischen Bruchmechanik erklärt.

1. INTRODUCTION

With the aid of modern computational methods and facilities it is possible to analyse all kinds of structures under almost all loading conditions. Expecially those structures do not give problems which exhibit elastic behaviour in the service state and plastic, or more general ductile, behaviour in the limit state. Most of the concrete structures are designed in such a way that they behave as mentioned. There are only a few cases where brittle fracture or almost brittle fracture occurs. But just these cases are the ones which should receive attention, because they can be dangerous if the governing parameters are not well recognized. This is true of structural design and also of analysis if the engineer is not aware of possible influences which may reduce the safety of the structure.

In the following only one aspect will be discussed in relation to three examples of structures, namely, the size effect in connection with shear failure of beams and slabs, punching shear of slabs, and shear transfer across joints between precast hollow core floor slabs. Common practice is that an average shear stress is calculated and compared with a limiting value which is a certain fraction of the tensile strength of concrete. This is done at finite element level, but also for the structure as a whole. Sometimes the size effect is taken into account by an empirical reduction factor. In the following it is tried to show that fracture mechanics concepts could be applied to explain the influence of the absolute size of the structure on the limit load.

2. EXAMPLE OF BRITTLE FRACTURE

Brittle fracture of concrete structures is the exceptional case and is normally avoided by appropriate reinforcement or prestressing. But sometimes, because of economical advantages, reinforcement is ignored and the concrete alone has to be responsible for the loading capacity. The first example of this is a beam or slab without shear reinforcement. Fig. 1 shows the loading system and the crack pattern after failure. The common behaviour of such a beam is that

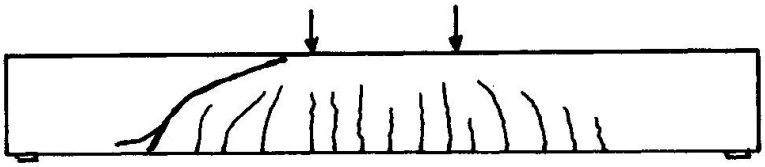

Fig. 1. Loading system and crack pattern of a beam after shear failure

the first cracks occur due to bending. Subsequently the cracks become longer until the extension of one inclined crack leads to failure because of low compressive strength or low tensile strength. Failure is "explosive", without advance announcement by excessive deformation.

A similar example is punching shear of slabs which is shown in Fig. 2. Fracture occurs when a concentrated load which acts on a reinforced concrete slab reaches the loading capacity. After the formation of radial and circular

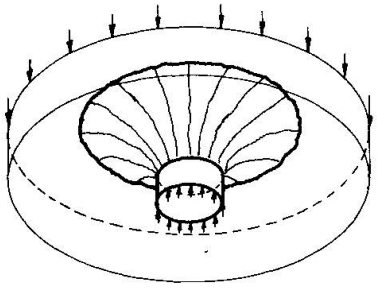

Fig. 2. Punching shear of concrete slab

cracks, sudden fracture occurs without announcement. The difference between bending shear and punching shear lies in the manner of stressing and the accompanying shape of the fractured element, which is a plane in the first case and a cone in the second.

The third example is taken from a precast concrete building in which the floors consist of prestressed hollow core slabs. The slabs are laid side by side and are connected by mortal-filled joints. In most cases a thin topping concrete layer is applied in order to ensure horizontal stiffness and vertical load distribution. Actually, this topping delays the work on the building site and is also an inconvenient feature when the building has to be demolished. Therefore, hollow core slab floors without topping are being investigated in regard to the shear behaviour of the joints under in-plane forces. A typical example of a joint is shown in Fig. 3. Shear stresses in a test specimen are indicated in Fig. 4 exhibiting stress peaks at the ends of the joint. If the joint mortar

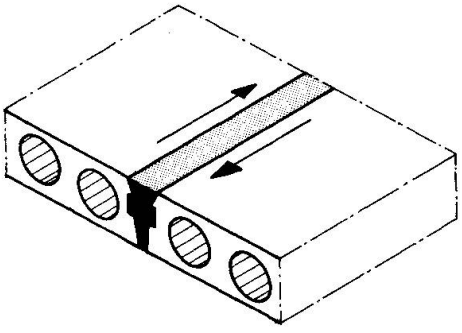

Fig. 3. Hollow core slab with mortar joint

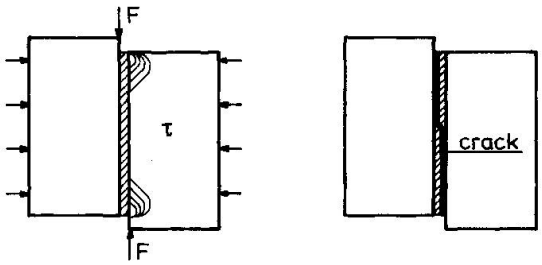

Fig. 4. Shear stresses and crack in the joint

is a brittle material, a crack will start from the end of the joint as soon as the peak stress reaches a certain maximum value and adhesion between mortar and concrete fails. Because this is true for a short joint length and for a large joint length the question arises as to the limiting shearing force F as a function of the joint length. In the case of a plastic material and in the case of a friction mechanism between the slabs, F is linear function of the length, but in the case of a brittle material this is not expected.

3. KNOWLEDGE FROM EXPERIMENTAL INVESTIGATIONS

Much experimental work has been done on bending shear in beams and slabs. The results show a distinct dependence of the ultimate average shear stress on the absolute depth of the beam. Fig. 5 shows the results of various researchers (for details see [1]).
Results of punching shear tests on slabs of various thickness are very scarce, but the few available ones also show a decrease of the punching shear stress with increasing slab thickness, Fig. 6.
In the Stevin Laboratory at Delft research is being carried out on joints between hollow core slabs and also indicates a nonlinear dependence of shear force on the joint length. The results have not yet been fully worked out, however.

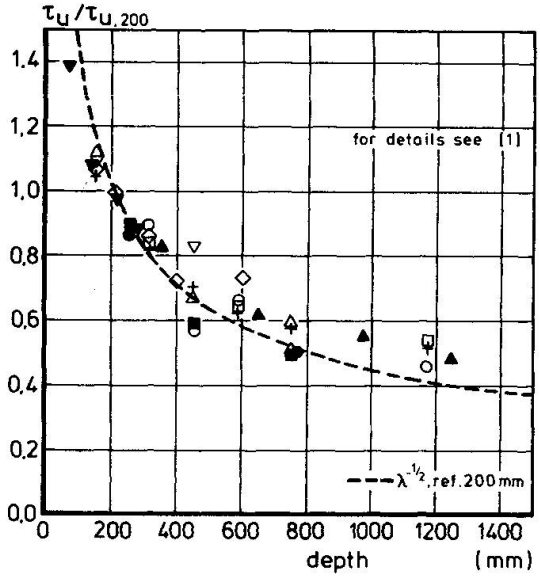

Fig. 5. Relative ultimate shear stress vs. depth of the beam

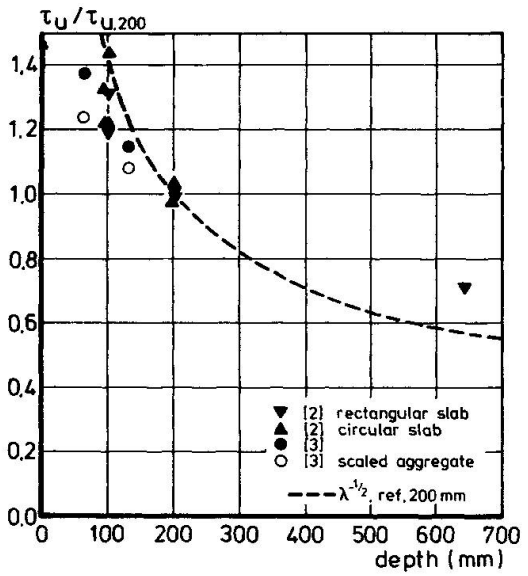

Fig. 6. Relative punching shear stress vs. slab thickness

A common feature of all the experimental results is a significant influence of the absolute size of the specimens on the ultimate average shear stress. This influence is not explicable with the strength of material concept, for which the absolute dimensions do not matter. Therefore fracture mechanics will be applied, which could show a way out of the difficulty.

4. FRACTURE MECHANICS AND CONCRETE

Linear static fracture mechanics as originated by Griffith [4] considers the surface energy at a crack (energy demand) and the elastic energy release around a crack. The condition for a stable crack is that the energy demand is greater than the energy release.
From this condition the maximum nominal stress in an infinite slab with a central crack of length 2a before failure, is

$$\sigma = \sqrt{\frac{2E\gamma}{\pi a}} = \frac{1}{\sqrt{a}} \sqrt{\frac{2E\gamma}{\pi}} \qquad (1)$$

For two specimens of the same material the factor $2E\gamma/\pi$ is constant and therefore the maximum nominal stress σ depends on the absolute value of the crack length. The larger the crack, the lower is σ.
Another approach in fracture mechanics is the determination of the stress field around a crack [5].

$$\sigma = \frac{K}{\sqrt{2\pi a}} \cdot f(\ldots) \qquad (2)$$

where K is the stress intensity factor and f a non-dimensional function which takes the geometry of the specimen or structural member and the loading condition into account. Failure will occur if K is equal to a critical value K_c which is a material constant. Thus, eq. (2) can be rewritten as

$$\sigma = \frac{1}{\sqrt{a}} \cdot \frac{K_c}{\sqrt{2\pi}} \cdot f(\ldots) \qquad (3)$$

which gives essentially the same result as eq. (1).

Until now, fracture mechanics has been widely used in mechanical, ship and airplane engineering for failure analysis of metal structures. The application of fracture mechanics to concrete is rather limited.
At micro-level it is used for the treatment of the influence of sustained [6] and short-time loading [7] on the strength of concrete, at macro-level for the strength of a beam [8] and the failure criterion of a large dam [9]. All these examples relate to plain concrete.

In general, linear elastic fracture mechanics presumes elastic behaviour until failure, i.e., there is no plastic deformation near the crack tip. Concrete does not exactly satisfy this condition; there are always microcracks around the aggregate particles and also around the tip of the discrete crack. But if this microcracking zone is small compared with the size of the crack, linear elastic fracture mechanics may be applied [10].
Whereas plain concrete always develops brittle failure in a tensile stress field, this is not true of reinforced concrete, where the tensile forces are taken over by the reinforcement and ductile behaviour occurs. Only in cases where the concrete is responsible for the loading capacity does brittle failure occur. This is one condition for the application of fracture mechanics to reinforced concrete. Another is that there is a decisive macrocrack which determines the behaviour of the structure. A third is the same as for plain concrete, namely that the microcracked zone is small compared with the visible crack. These requirements are fulfilled in the three examples given in Chapter 2.

5. SIMILITUDE OF BRITTLE FRACTURE OF REINFORCED CONCRETE

Stress intensity factors of members with discrete reinforcing bars are not available in the literature and no attempt will here be made to establish them. The configuration most closely related to the shearing and punching problems is a beam with an inclined crack treated by Bowie [11]. In regard to the joint between slab units there is a solution by Erdogan [12] and subsequent papers by several authors [13, 14, 15]. All these solutions have the general form as given in eq. (3). This means that the square root of the absolute crack length is inversely proportional to the failure stress. If the crack pattern in two members of different size (scale factor λ) is similar, the failure shear stress is also inversely proportional to the square root of the scale factor λ

$$\tau_u \sim \lambda^{-1/2} \tag{4}$$

The occurrence of similar crack patterns in scaled beams has been recognized [16] and has been observed in current research on joints. So it is not surprising that eq. (4) can yield good results, as illustrated by the dotted line in Fig. 5 and 6. Punching shear (Fig. 6) does not appear to conform so closely, but experimental results are admittedly very scarce. So far as joints are concerned, the experiments have not yet been completed and worked out.

6. FINITE ELEMENT ANALYSIS

Bazant states in the introductory report [17] that the analysis of crack propagation leads to different results for different choices of the finite element mesh if the strength of material approach is used. He gives a possible solution by means of an energy criterion which is applied in each single element. Argyris, Faust and Willam [18] also mention fracture mechanics, but prefer a stress-strain concept (J-integral) than the linear elastic fracture mechanics which actually can predict only the limit state and not the state of stable crack growth.

Gergely and White [19] also emphasize the fracture mechanics approach and show the result of a finite element analysis of a beam on the basis of fracture mechanics. Crack formation and deflection of the beam show close agreement with experimental verification.
It is not completely clear whether in these calculations fracture mechanics have been applied to the single element only or also to the whole structure. As can be concluded from the foregoing chapters, it should be required that also - in the case of brittle failure - the whole structure should be checked by means of fracture mechanics and, as a first step, by linear elastic fracture mechanics. A comparative calculation for similar beams (as in Fig. 1) could show the feasibility of such a finite element analysis.

7. CONCLUSIONS

Advanced mechanics of reinforced concrete implies also fracture mechanics concepts which can be applied at micro-level (finite elements, inhomogeneous structure of concrete) but also at macro-level. To demonstrate the applicability at macro-level, three examples of brittle failure have been considered: bending shear in beams, punching shear in slabs, and in-plane shear in joints between hollow core slabs. Using linear elastic fracture mechanics it was found that

$$\tau_u \sim \lambda^{-1/2}$$

where τ_u is the ultimate average stress and λ the scaling factor between similar structures. This relation was confirmed by experimental results. In the future, stress-intensity factors should be derived for reinforced structures which allow a quantitative analysis, not merely a comparative one.
It should be emphasized that fracture mechanics can only be applied to reinforced concrete in the case of brittle fracture. Normally those cases are avoided by appropriate reinforcing, but if they can occur, fracture mechanics should be used.
If brittle failure of concrete is analysed by means of finite element programs, fracture mechanics should be applied not only within single elements but also to the whole structure or a major part of it.

8. NOTATION

a half crack length

d effective depth

E Young's modulus

F force

K stress-intensity factor

V shear force

γ surface energy

λ scale factor

σ normal stress

τ shear stress
(nominal, computed acc. to CEB-FIP)

subscripts:

c critical

U ultimate

9. REFERENCES

[1] REINHARDT, H.W. Massstabseinfluss bei Schubversuchen im Licht der Bruchmechanik. Beton & Stahlbetonbau 76(1981) no. 1, pp. 19-21.

[2] KINNUNEN, S., NYLANDER, H., TOLF, P. Punching tests at the Institution for Building Statics, KTH Stockholm. Nordisk Betong (1978), no. 3, pp. 25-27.

[3] REGAN, P.E., WALKER, P.R., ZAKARIA, K.A.A. Tests of reinforced concrete flat slabs. Polytechnic of Central London, May 1978.

[4] GRIFFITH, A.A. The phenomena of rupture and flow in solids. Phil. Trans. Roy. Soc. (London), Series A, 221(1920), p. 163-198.

[5] IRWIN, G.R. Fracture dynamics. In Fracturing of Metals - Am. Soc. Metals, Cleveland (1948), pp. 147-166.

[6] WITTMANN, F.H., ZAITSEV, J. Verformung und Bruchvorgang poröser Baustoffe bei kurzzeitiger Belastung und Dauerlast. DAfStb, Heft 232, Berlin 1974.

[7] MIHASHI, H., IZUMI, M. A stochastic theory for concrete fracture. Cement and concrete research 7(1977), pp. 411-422.

[8] ZIEGELDORF, S., MÜLLER, H.S., HILSDORF, H.K. A model law for the notch sensitivity of brittle materials. Cement and concrete research 10(1980) pp. 589-599.

[9] KRAPHOV, L.P. et al. The application of fracture mechanics to the investigation of cracking in massive concrete construction elements of dams. In Fracture 1977, Vol. 3, ICF4, Waterloo, Canada, June 19-24, 1977.

[10] HILSDORF, H.K. Sinn und Grenzen der Anwendbarkeit der Bruchmechanik in der Betontechnologie. In Forschungsbeiträge für die Baupraxis, Verlag von Wilh. Ernst & Sohn, Berlin, München, Düsseldorf, 1979.

[11] BOWIE, O.L. Solutions of plane crack problems by mapping technique. In Mechanics of fracture, Vol. I, ed. by G.C. Sih, Noordhoff Intern. Publ., Leiden 1973.

[12] ERDOGAN, F. Stress distribution in a nonhomogeneous elastic plane with cracks. J. Appl. Mech. 30(1963), No. 2, pp. 232-236.

[13] MULVILLE, D.R., HUNSTON, D.L., MAST, P.W. Developing failure criteria for adhesive joints under complex loading. J. Eng. Materials and Technology 100(1978), pp. 25-31.

[14] MALYSHEV, G.M., SALGANIK, R.L. The strength of adhesive joints using the theory of cracks. Intern. J. Fracture Mechanics 1(1965), No. 2, pp. 114-128.

[15] ERDOGAN, F., GUPKA, G. The stress analysis of multilayered composites with a flaw. Intern. J. Solids and Structures 7(1971), No. 6, pp. 56-61.

[16] WALRAVEN, J.C. The influence of depth on the shear strength of lightweight concrete beams without shear reinforcement. Stevin report 5-78-4, Delft University of Technology, Delft 1978.

[17] BAZANT, Z.P. Advances in deformation and failure models for concrete. Introductory report, IABSE Colloquium Delft 1981, pp. 9-84.

[18] ARGYRIS, J.H., FAUST, G., WILLAM, K.J. Finite element modelling of reinforced concrete structures. Introductory report, IABSE Colloquium Delft, 1981, pp. 85-106.

[19] GERGELY, P., WHITE, R.N. Applications and experimental verification. Introductory report, IABSE Colloquium Delft 1981, pp. 109-133.

Stress Analysis of Structural Members Taking Complex Materials Behaviour into Consideration

Analyse des contraintes d'éléments structurels en tenant compte du comportement complexe des matériaux

Spannungsanalyse von Bauteilen unter Berücksichtigung des komplexen Materialverhaltens

P.E. ROELFSTRA
Research engineer

F.H. WITTMANN
Prof. Dr.

Laboratory for Building Materials, Swiss Federal Institute of Technology, Lausanne, Switzerland

SUMMARY

In structural analysis it is essential to introduce realistic materials laws. In this contribution creep and shrinkage of concrete are calculated on the basis of a rather general materials model. In addition heat and moisture diffusion are taken into consideration. Concrete need not be considered as a homogeneous material. The actual heterogeneous macrostructure can be simulated. The materials laws derived in this report are used to analyse a conventional cross-section of a prestressed concrete bridge.

RÉSUMÉ

Dans l'analyse des structures, il est essentiel d'introduire des lois réalistes pour décrire le comportement des matériaux. Dans cette contribution, le retrait et le fluage du béton sont calculés sur la base d'une modélisation assez générale des matériaux. De plus, la diffusion de chaleur et d'humidité est également prise en considération. Le béton ne peut pas être considéré comme un matériau homogène. La macrostructure hétérogène est simulée sur ordinateur. On utilise les lois obtenues pour analyser la section transversale conventionnelle d'un pont en béton précontraint.

ZUSAMMENFASSUNG

Bei der Berechnung von Betonkonstruktionen ist es besonders wichtig realitätsnahe Materialgesetze zu verwenden. In diesem Beitrag werden Kriechen und Schwinden auf der Basis eines allgemeinen Gefügemodells formuliert. Zusätzlich werden Wärme- und Feuchtigkeitsdiffusion berücksichtigt. Beton muss nich notwendigerweise als ein homogenes Material betrachtet werden; das heterogene Gefüge kann vielmehr im Grossrechner generiert werden. Die hier abgeleiteten Materialgesetze werden beispielhaft zur Berechnung eines Querschnittes einer üblichen vorgespannten Betonbrücke verwendet.

1. INTRODUCTION

Recently in many countries serious defects have been observed on prestressed and normally reinforced bridges. These difficulties can be traced back to a number of reasons such as agressive climatic conditions caused by a dense industrialisation and corrosion problems caused by the application of de-icing salts. There remains, however, another purely mechanical reason. By this we mean the use of non-appropriate or over-simplified materials laws in structural analysis and partly also the sheer lack of knowledge on materials properties.

This obvious deficiency is contrasted by sophisticated modern computer facilities. In a number of reports the potential of computerized structural analysis has been demonstrated in a convincing way (see f.e. /1,2/). Until now the application of these elegant methods is, however, seriously limited because there exists no comparable advanced approach on the materials science side.

The essential aim of this report is to help to fill this gap. Therefore we tried to simulate materials behaviour under varying conditions on the basis of the physical and chemical processes involved /3,4/. It is shown how these model laws can be introduced in structural analysis. As an example we choose arbitrarely a conventional cross section of a prestressed concrete bridge. Our approach is outlined in particular by means of the analysis of one characteristic corner of the structure.

This contribution clearly points out the urgent need for a close link between materials science and structural engineering. The common effort of these two different disciplines is nowadays often called concrete mechanics.

2. SIMULATION OF TIME-DEPENDENT DEFORMATION

2.1 Model for Creep and Shrinkage

In recent years much progress has been made in materials science in describing the time-dependent behaviour of hardened cement paste with models based on real mechanisms. One of these models by which good results have been obtained is the Munich-model /5/. By means of this model it is possible to describe the main influence on time-dependent deformation of hardened cement paste such as temperature and humidity.

This model describes quantitatively the unrestrained shrinkage. The unrestrained shrinkage or unrestrained swelling is the immediate hygral relative volume change of an infinite small volume element of hardened cement paste if the water content is changed. Klug /6/ and Feldman /7/ have determined experimentally the relationship between unrestrained shrinkage and the relative humidity. It turned out that unrestrained shrinkage ε_u can be described satisfactorily as function of relative humidity H by a linear relationship if the extreme regions are excluded :

$$\varepsilon_u = aH + b \qquad (1)$$

It is important to notice that unrestrained shrinkage is not time-dependent.

In the Munich-model creep is described as a rate process. The rate theory provides a solid theoretical basis for a rather general approach to study creep processes of materials.

The rate of creep of loaded hardened cement paste is then given by the following equation :

$$\frac{\partial \varepsilon}{\partial t} = Ce^{-\frac{Q}{RT}} \sinh \frac{V}{RT} \sigma \qquad (2)$$

In this equation the symbols have the following meaning :

Q = activation energie;
V = activation volume;
R = gas constant;
T = temperature;
σ = stress;
C = a quantity proportional to the density of creepcenters in a unit volume.

Q and V do not depend on the duration of the applied stress. The time-dependence of the rate of creep is given by quantity C. For constant stress, humidity and temperature the change of C as function of time can be written as :

$$C = C_1 t^{-m} \qquad (3)$$

This assumption leads to the well known creep formulea :

$$\varepsilon = at^n \sinh b\sigma \qquad (4)$$

C_1 is dependent on the type of concrete and the age of loading. A reasonable assumption leads to the well-known double power law.

2.2. Diffusion Processes

2.2.1. Moisture movement

Pihlajavaara /8/ and Bazant /9/ showed that the diffusion equation for drying of hardened cement paste can be written as :

$$\dot{H} - \text{div} (D_H \text{ grad } H) = 0 \qquad (5)$$

In this equation the symbols have the following meaning :

H = pore humidity;
D_H = hygral diffusion coefficient.

D_H depends on the pore humidity H because the pore system and the transport mechanisms change when drying proceeds. The drying process is thus nonlinear. So far very little is known on the exact relationship between D_H and H. The calculations described in this report are carried out by assuming a dependence of D_H as indicated by Bazant /9/.

2.2.2 Heat of hydration

The general equation governing the temperature distribution in a real solid can be written as :

$$\alpha\rho\dot{\Theta} - \text{div} (K\text{grad } \Theta) - \dot{S} = 0 \qquad (6)$$

α = specific heat
ρ = density
K = conductivity
Θ = temperature C
$\dot{S}$ = rate of liberation of heat of hydration

This problem can be solved numerically if the boudary conditions are given and all the materials parameters are known.

In the formulae (1) to (6) the coefficients are materials parameters and thus depend on water/cement-ratio, degree of hydration and type of cement apart from other influences. Some of these parameters are not known well enough. There is a urgent need for further experimental work.

2.3 Influence of Heterogeneous Structure of Concrete

So far we have considered concrete to be a homogeneous material. In order to be able to study the influence of parameters such as grain size and grain geometry or cement content it is necessary to take the real macrostructure of concrete into consideration. This can be done by generating random structures in a computer. In Figure 1 two runs of the structure generation program are shown as a typical example.

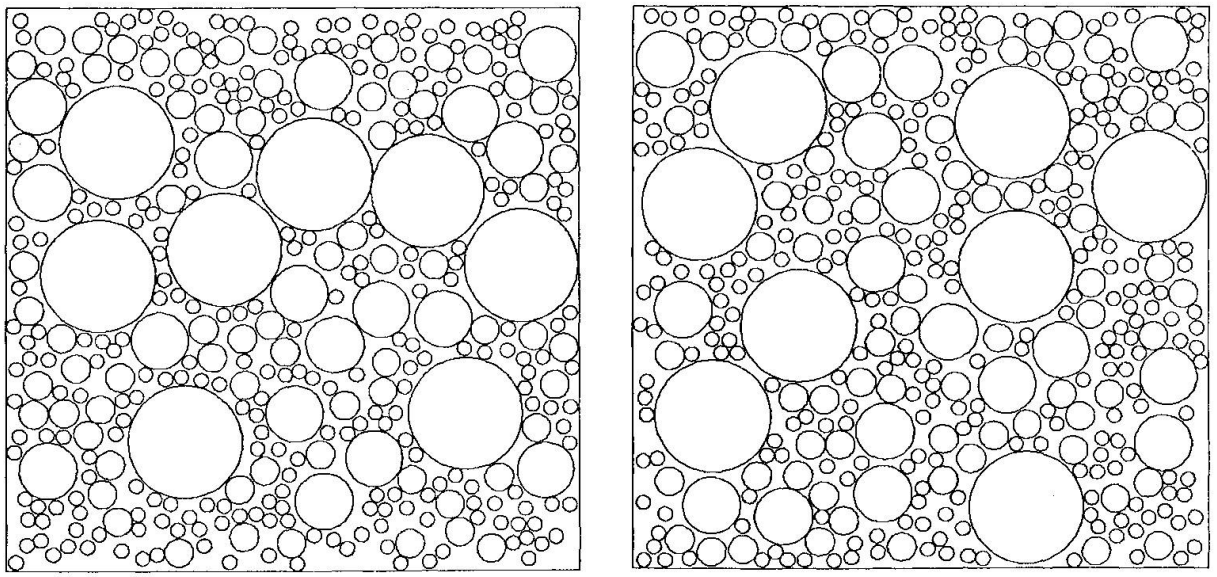

Figure 1 : Two computer generated random structures of concrete.

In this example all aggregates are chosen to be circular. This is, however, not a necessary condition and arbitrary geometries can be generated as well. Any granulometry and arbitrary shape factors can be simulated.

Once the diffusion coefficient of the mortar is known, the behaviour of the composite material can be predicted. The method of finite element analysis has proved to be successful in this connection.

3. ANALYSIS OF REAL STRUCTURES BY APPLYING BASIC MATERIALS LAWS

The materials laws as described in section 2 will now be used to analyse a real

structure. As an example a bridge has been chosen. Figure 2 shows a side-view and two cross-sections of a serial lanced prestressed concrete bridge.

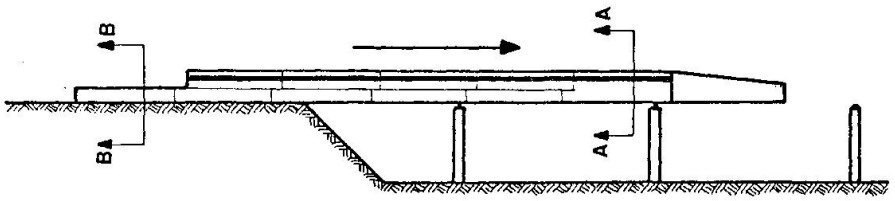

SIDE-VIEW

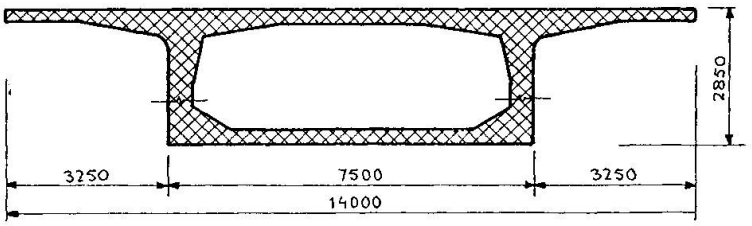

CROSS SECTION A-A

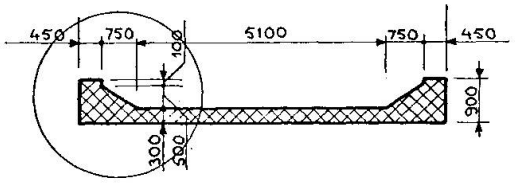

CROSS SECTION B-B

Figure 2 : Side view and cross sections of a typical serial lanced prestressed concrete bridge.

The floor and the two corners of the box-girder (cross-section B-B) are usually concreted one week before the upper-section is concreted. First of the temperature distribution in cross-section B-B due to heat of hydration is calculated. The assumption has been made that the flow of heat is two-dimensional in this cross-section. It is also assumed that the flow of heat through surfaces with shuttering is 5 times smaller than through boundaries without shuttering. The temperature of the fresh concrete was supposed to be 18 C.

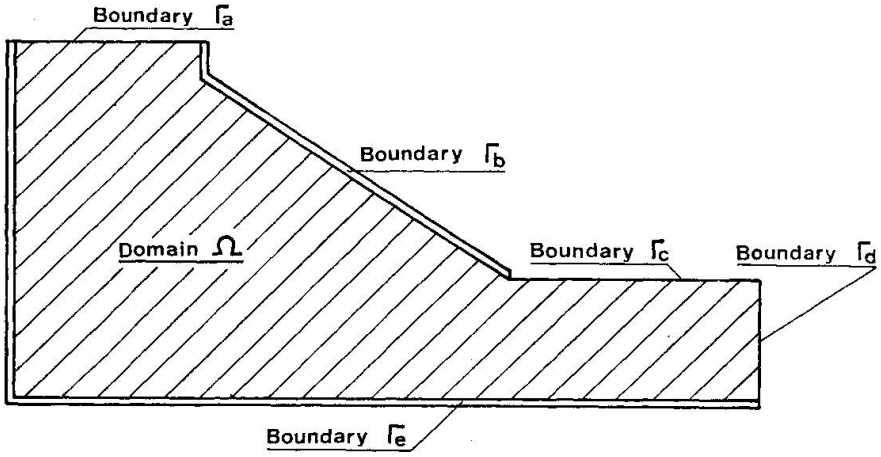

Differential Equation in Domain Ω : $\alpha\rho\dot{\Theta} - \mathrm{div}(K\,\mathrm{grad}\,\Theta) - \dot{S} = 0$

α = specific heat 800 $\frac{J}{kg\,^oC}$

ρ = density 2500 $\frac{kg}{m^3}$

K = conductivity 8000 $\frac{J}{m\,^oC\,h}$

Θ = temperature ^oC

$\dot{S}$ = rate of liberation of heat of hydration =

$$162000 \times 2^{0.1(\Theta|t|-20)} e^{-0.009 \int_0^t 2^{0.1(\Theta|\tau|-20)} d\tau} \quad \frac{J}{m^3 h}$$

Boundary Conditions : on Γ_a and Γ_c : $q_n = 1000000\,(\Theta - 20)\ \frac{J}{m^2 h}$

on Γ_b : $q_n = 200000\,(\Theta - 20)\ \frac{J}{m^2 h}$

on Γ_e : $q_n = 200000\,(\Theta - 15)\ \frac{J}{m^2 h}$

on Γ_d : $q_n = 0\ \frac{J}{m^2 h}$

Initial Condition : $\Theta(x,y,0) = 18\ ^oC$

Figure 3 : Differential equation, boundary, and initial conditions for temperature development.

In figure 3 the mathematical "translation" of this problem is indicated.

Figure 4 shows how domain Ω is subdivided into smaller domains, representing the finite elements.

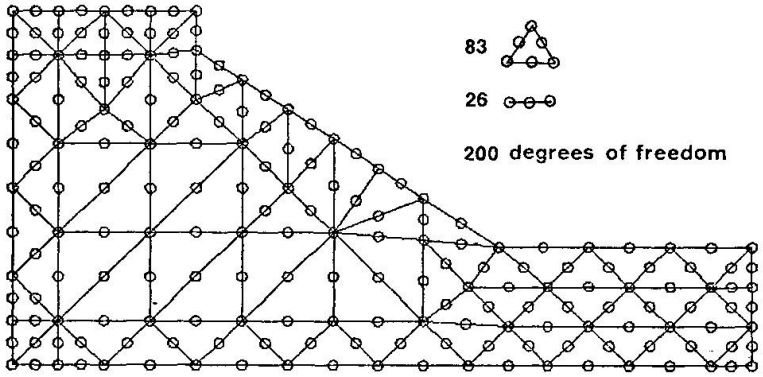

Figure 4 : Finite element idealization.

For the analysis 83 triangle elements with 6 nods and 26 membrane elements with 3 nods have been used. In Figure 5 the calculated temperature distribution at 3 different times after concreting are drawn by means of isotherms.

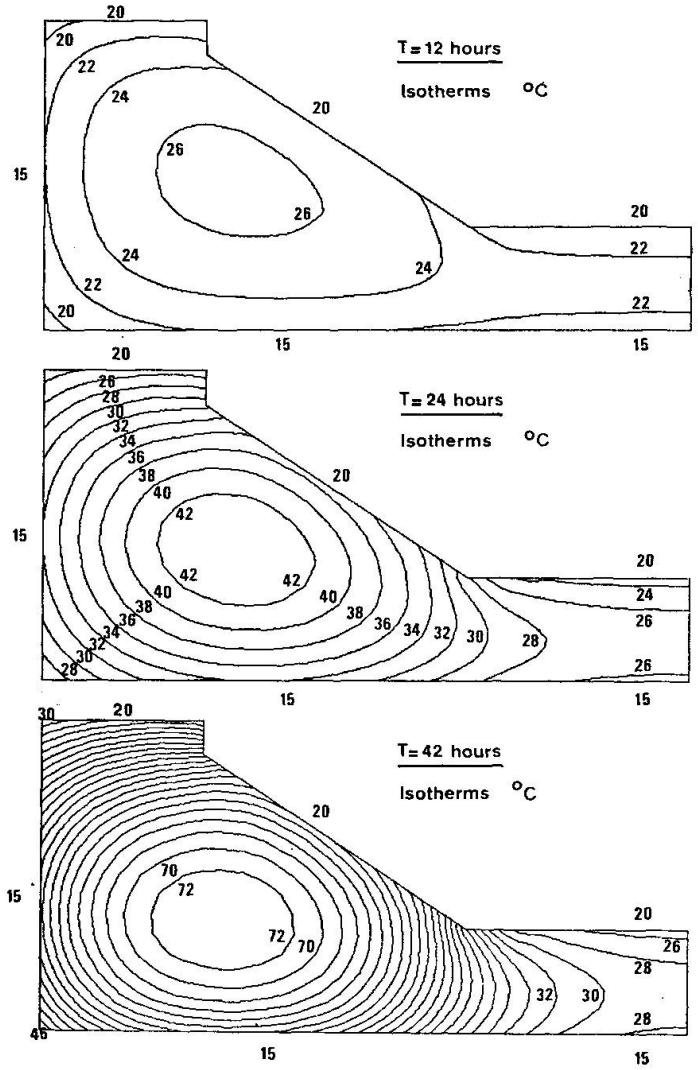

Figure 5 : The calculated temperature distributions at three different times of hydration.

42 hours after concreting the temperature in the core of the corner is about 72 C and the temperature gradients in the directions of the boundaries have reached their maximum. In this situation concrete has become rigid and when the temperature goes down again due to diffusion and the gradients have disapeared this will result in initial stresses which can introduce cracking and which influence total deformation.

Next the drying process of this cross section is simulated. The same finite element idealization has been used. The relative humidity inside the box-girder and of the surrounding air are supposed to be 80 and 70 % respectively. In figure 6 the applied differential equation, the boundary, and the initial conditions are indicated.

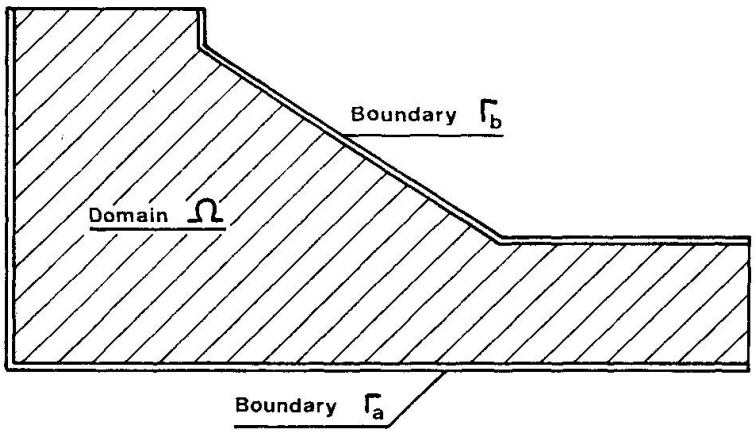

Differential Equation in Domain Ω : $\dot{H} - \mathrm{div}(D_h \, \mathrm{grad} H) = 0$

With : $D_h = 2\left[0.05 + \frac{0.95}{1 + \left(\frac{100 - H}{25}\right)^4}\right] \frac{mm^2}{h}$

On boundary Γ_a : $q_n = 10(H - 70) \frac{mm}{h}$

On boundary Γ_b : $q_n = 10(H - 80) \frac{mm}{h}$

Initial Condition : $H(x,y,0) = 100$ in domain Ω

Figure 6 : Differential equation, boundary and initial conditions for drying.

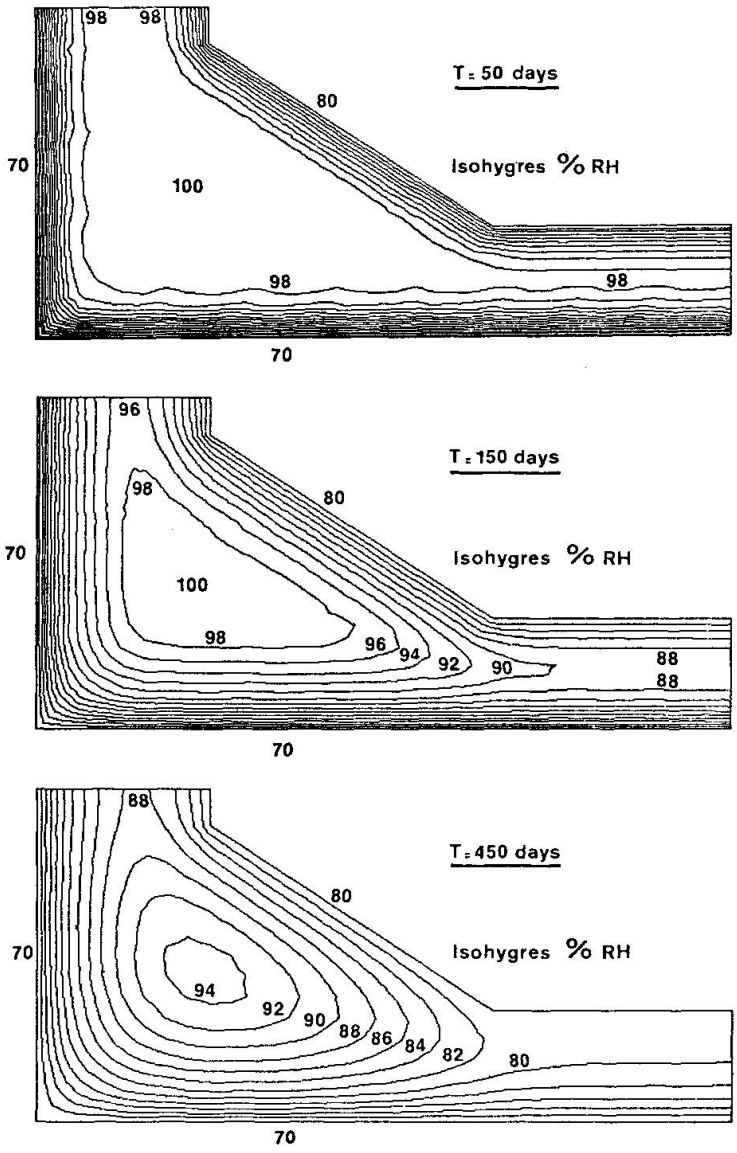

Figure 7 : The calculated moisture distribution at given times after demoulding.

In figure 7 the calculated moisture distribution at three different times after demoulding (duration of drying) are drawn by means of iso-hygres (lines of constant pore humidities).

After 50 days the main part of the corner is still wet. Near the surface there is a big gradient of humidity. This gradient results in tensile stresses which can overcome the tensile strength and thus introduce small cracks (tensile softening).

After 450 days the smaller parts of the cross-section have allmost reached an equilibrium while the core of the corner just has started to dry.

This complex moisture distribution during drying will introduce so-called "drying induced bending moments" which again will influence the total deformation of the structure.

In figure 8 it is indicated how the calculated moisture and temperature distributions can be used in a routine analysis. By means of the derived materials laws these distributions can be translated into initial strains which have to be superimposed to the global state of stress. In this way it is possible to take into consideration the influence of moisture and temperature gradients on the overall response in structural analysis in a realistic way and based on actual materials behaviour.

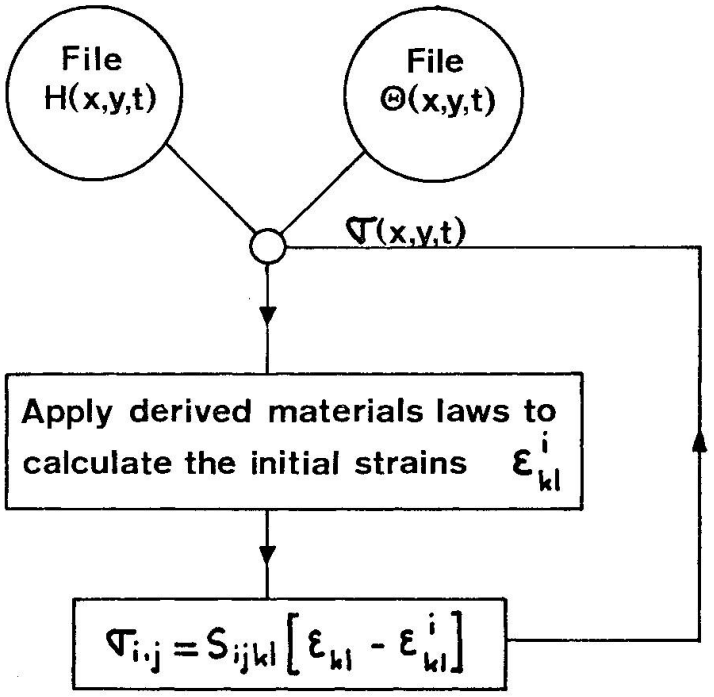

Initial strains: shrinkage
creep
tensile softening
thermal strains

Figure 8 : Flow-chart for a routine analysis.

4. CONCLUSIONS

There exists a huge gap between structural analysis and materials science. It is possible nowadays to formulate materials properties in a complex and realistic way. By means of finite element analysis it is possible to describe the behaviour of composite materials such as concrete on the basis of elementary processes within the different components. Arbitrary structural members can be analyzed by using computer generated materials laws.

In this contribution an approach is outlined in which the materials parameters used in computerized structural analysis are derived by using numerical methods in materials science. This general concept will be further developed.

It is obvious that the method outlined in this contribution is not meant to be applied in every routine analysis. In all these cases where a detailed analysis is justified and needed, however, this approach can serve as a powerful tool. In a more general way this complex analysis enables us to point out and quantify the risk for mechanical damage in critical parts of a construction.

5. REFERENCES

/1/ Argyris, J.H., Warnhe, E.P. and Willam, K.J., "Berechnungen von Temperatur- und Feuchtefeldern in Massivbauten nach der Methode der finiten Elemente", Deutscher Ausschuss für Stahlbeton, Schriftenreihe, Heft 278 (1977).

/2/ Anderson, C.A., "Numerical creep of structures", International Symposium on Fundamental Research on Creep and Shrinkage of Concrete, Lausanne, Switzerland (1980, to be published).

/3/ Wittmann, F.H. and Roelfstra, P.E., "Total deformation of loaded drying concrete", Cement and Concrete Research, Vol. 10, 601-610 (1980).

/4/ Roelfstra, P.E. and Wittmann, F.H., "Een rekenmodel ter bepaling van de totale tijdsafhankelijke vervorming van uitdrogend beton", Cement 6, 348-351 (1980).

/5/ Wittmann, F.H., "Grundlagen eines Modells zur Beschreibung charakteristischer Eigenschaften des Betons", Deutscher Ausschuss für Stahlbeton, Schriftenreihe, Heft 290 (1977).

/6/ Klug, P., "Kriechen, Relaxation und Schwinden von Zementstein", Dissertation, TU München (1973).

/7/ Feldman, R.F., Fifth International Symposium on the Chemistry of Cement, Tokyo, Japan (1968).

/8/ Pihlajavaara, S.E., "On the main features and methods of investigation of drying and related phenomena in concrete", State Inst. for Techn. Research, Helsinki, Finland, Ph.d.Thesis, Publ. No 100 (1965).

/9/ Bazant, Z.P. and Najjar, L.J., "Nonlinear waterdiffusion in nonsaturated concrete", Mat. et Constr. 5, 3-20 (1972).

Leere Seite
Blank page
Page vide

Inelastic Analysis of Reinforced Concrete Shear Wall Structures - Material Modelling of Reinforced Concrete -

Analyse inélastique de la structure asismique des refends en béton armé - Un essai pour obtenir la formule modèle mathématique pour le béton armé -

Inelastische Berechnung von erdbebenfesten Stahlbetonwandkonstruktionen - Modellierung von Stahlbetonmaterialien -

NOBUAKI SHIRAI
Assistant

TOSHIO SATO
Professor

Department of Architecture, College of Science and Technology, Nihon University, Tokyo, Japan

SUMMARY

A finite element formulation capable of clarifying inelastic behavior of reinforced concrete shear wall structures is presented. Inelastic effects such as tensile cracking of concrete, nonlinear stress-strain response of concrete and steel, bond between steel and concrete, aggregate interlock between cracked concrete surfaces and dowel action of reinforcing bars are considered and particular attention is given to a constitutive modelling of these effects which have an important effect upon hysteresis characteristics of reinforced concrete structures. Finally, an incremental self-correcting approach used as a numerical procedure is briefly explained.

RÉSUMÉ

On présente une formule par la méthode des éléments finis capable d'éclairer le comportement inélastique de la structure asismique des refends en béton armé. Compte tenu des effets inélastiques tels que de la fissuration dans le béton due à la traction, de la contrainte non-linéaire et de la réponse de déformation du béton et de l'acier, de l'adhérence entre l'acier et l'armature, de l'effet d'engrènement des faces en béton fissurées et de l'effet goujon, plus particulièrement on a essayé d'obtenir la formule modèle mathématique de constitution desdits effets qui donnent une grande influence sur les caractéristiques d'hystérèsis des structures en béton armé. Finalement, on explique en bref le mode d'accès auto-correction incrémental employé comme un procédé numérique.

ZUSAMMENFASSUNG

Es wird eine Formel nach der Methode der finiten Elemente zur Klärung des inelastischen Verhaltens von erdbebenfesten Stahlbetonwandkonstruktionen präsentiert. Es werden inelastische Effekte wie Zugrissbildung im Beton, nichtlineare Spannungsdehnungslinie von Beton und Stahl, Verbund zwischen Stahl und Beton, Rissverzahnung zwischen Betonrissoberflächen, Dübelwirkung des Armierungsstahls betrachtet. Der Modellierung dieser Effekte, die eine wichtige Auswirkung auf die Hysteresecharakteristiken von Stahlbetonkonstruktionen haben, wird besondere Aufmerksamkeit gewidmet. Abschliessend wird kurz eine inkrementelle, selbstkorrigierende Methode erläutert, die als numerische Analysemethode verwendet wurde.

1. INTRODUCTION

The reinforced concrete shear strucrure is a structural system being composed of columns, beams and wall panels and is the most efficient earthquake resistant element. Therefore, it is necessary for investigating inelastic behaviors of reinforced concrete shear wall structures subjected to cyclic loads such as seismic forces to consider all sorts of inelastic effects including cyclic behaviors. Attempts to model inelastic effects have been carried out by many investigators so far, but it is felt that simple and effective models for a finite element formulation have not been proposed yet.

The inelastic effects included in this paper are 1)brittle fracture of concrete (tensile cracking), 2)nonlinear stress-strain response of concrete and steel, 3)bond between concrete and reinforcing bar, 4)aggregate interlock and 5)dowel action. Particularly, the bond model based upon a new concept of bond behaviors and the modelling of aggregate interlock and dowel action evaluated as equivalent shear moduli by introducing crack spacing and width are described in detail.

An incremental initial stress approach or an incremental self-correcting approach which is able to minimize computational time is used as a numerical procedure and here the latter approach, which has not been applied materially nonlinear problems, is briefly explained.

2. MATERIAL IDEALIZATION

Reinforced Concrete is a composite material being made of concrete and steel, and mechanical properties of each component material are idealized as follows.

2.1 Concrete

Uncracked concrete is assumed as a homogeneous isotropic material, and on the other hand cracked concrete is considered to be anisotropic and capable of resisting normal stress parallel to average crack direction.
The uniaxial stress-strain relationship for uncracked concrete is assumed to be elasto-plastic of tri-linear type including strain-softening with a negative slope in compression, and elastic up until to the tensile strength and thereafter concrete changes to a brittle material as shown in Fig.1. In order to simulate compressive behaviors, the yield criterion for plasticity in compression is assumed of either the Von-Mises's formula[1] or the Drucker-Prager's formula[1] and associated flow rule(see Section 3.1),

$$F = A_1 \cdot \sigma_m + A_2 \cdot \bar{\sigma} = A_3 \qquad \text{--------} \quad (2.1)$$

where $\sigma_m = (\sigma_x + \sigma_y + \sigma_z)/3$; $\bar{\sigma} = [(s_x^2 + s_y^2 + s_z^2)/2 + \tau_{xy}^2 + \tau_{yz}^2 + \tau_{zx}^2]^{1/2}$; σ_x, σ_y, σ_z, τ_{xy}, τ_{yz}, τ_{zx}: the stress components in the orthogonal coordinates X, Y and Z ; s_x, s_y, s_z : the deviatoric stresses of σ_x, σ_y , σ_z and the coefficients A_1, A_2 and A_3 are defined in Table 1.

The fracture criterion of Mohr-Coulomb[1] is applied to tensile failure in order to take a reduction of tensile strength due to lateral compressive stresses into consideration,

$$F = (f_c - f_t)(\sigma_m - \bar{\sigma}\sin\phi/\sqrt{3})/(f_c + f_t) + \bar{\sigma}\cos\phi - f_c f_t/(f_c + f_t) = 0 \quad \text{-----} \quad (2.2)$$

where $\phi = \frac{1}{3}\sin^{-1}[-3\sqrt{3}J_3/2\bar{\sigma}^3]$ with $-\pi/6 \leq \phi \leq \pi/6$; $J_3 = s_x s_y s_z + 2\tau_{xy}\tau_{yz}\tau_{zx} - s_x\tau_{yz}^2 - s_y\tau_{zx}^2 - s_z\tau_{xy}^2$; f_c : the uniaxial compressive strength; and f_t : the uniaxial tensile

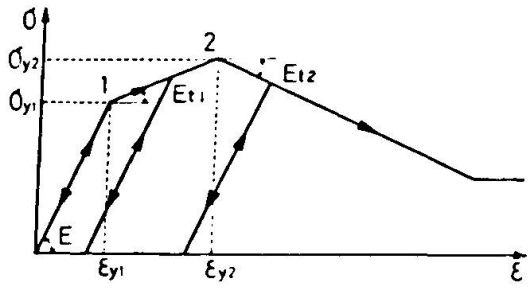

Fig.1 Uniaxial Stress-Strain Relationship for Concrete

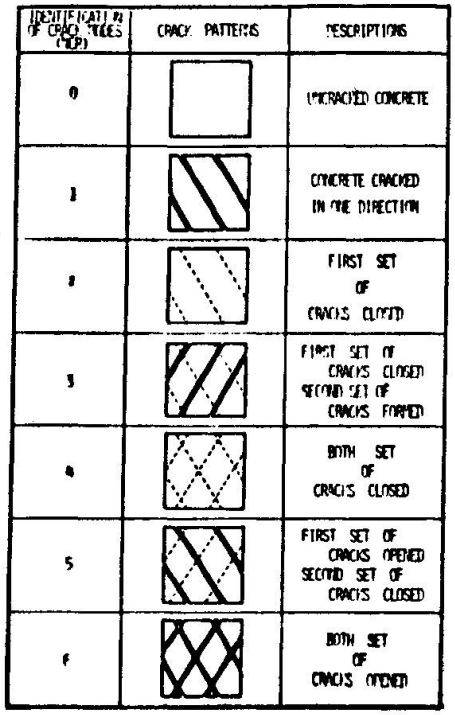

Fig.3 Assumed Cracking Modes

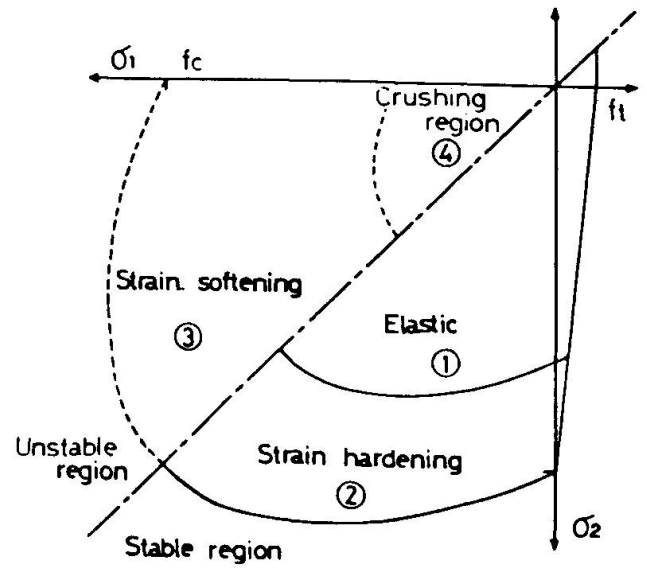

Fig.2 Assumed Fracture and Yield Surfaces of Concrete

Table 1. Coefficients for Yield Criteria

Yield Criterion	A_1	A_2	A_3
Von - Mises	0	$\sqrt{3}$	$\lvert Y(k)\rvert$
Drucker - Prager	3α	1	K

where $\alpha = 2\sin\theta/\sqrt{3}(3-\sin\theta)$; $K = 6C\cos\theta/\sqrt{3}(3-\sin\theta)$; Y(k): the critical points of uniaxial stress on the trilinear curve and k = 1, 2 and 3 ; θ: the angle of friction ; and C: the cohesion.

strength. Fig.2 shows the assumed fracture and yield surfaces in the two-dimensional principal stress plane. The direction of concrete cracks is defined to be perpendicular to principal tensile stress in uncracked concrete just prior to crack formation. In order to be able to pursue behaviors under cyclic loading excursions, six different cracking modes[2] representing the opening and closing of cracks are considered in the present study as shown in Fig.3.

2.2 Steel Reinforcement

The reinforcing bar is regarded as one-dimensional continuous medium in which the area of reinforcing bar distributes uniformly within any concrete element and therefore it is in uniaxial stress state. The stress-strain relationship for reinforcing bar is assumed to be elasto-plastic of bi-linear type with the strain-hardening effect as shown in Fig.4.
The subscripts of σ, E, etc. in the left hand side shall indicate the corresponding materials, and the subscript s is used for steel and c for concrete is omitted in this paper.

Fig.4 Stress-Strain Relationship for Reinforcing Bar

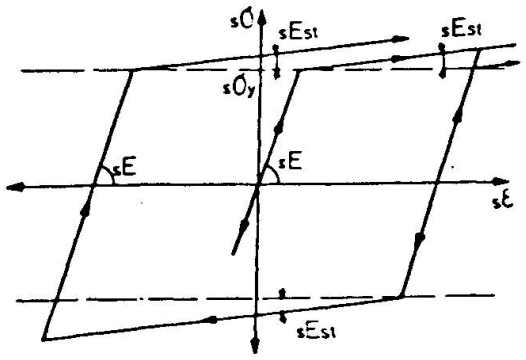

3. MATERIAL STIFFNESS FORMULATION

The material stiffness for reinforced concrete is assumed to be obtained by a linear superposition of component stiffnesses of concrete, reinforcing bar, bond , aggregate interlock and dowel ation to be described below.

3.1 Concrete

The material stiffness for elastic uncracked concrete shall follow Hooke's Law for plane stress in an isotropic material. The relation between the incremental stress $\Delta\{\sigma\}$ and the incremental strain $\Delta\{\varepsilon\}$ for palstic uncracked concrete was derived on the basis of the Theory of Plasticity along with the yield conditions defined in Eq.(2.1) and associated flow rule[3],

$$\Delta\{\sigma\} = ([D]_e - [D]_p)\Delta\{\varepsilon\} = [D]_{ep}\Delta\{\varepsilon\} \qquad \text{------ (3.1)}$$

where $[D]_e$:the elastic matrix for concrete; $[D]_{ep}$: the elasto-plastic matrix and the plastic matrix $[D]_p$ for plane stress is defined as follows,

$$[D]_p = \frac{E^2}{(1-\upsilon^2)^2}\cdot\frac{1}{H'+\bar{\beta}}\begin{bmatrix} d_{11} & d_{12} & d_{13} \\ & d_{22} & d_{23} \\ \text{SYM.} & & d_{33} \end{bmatrix} \qquad \text{------ (3.2)}$$

$$\bar{\beta} = E[2A_1^2/9(1-\upsilon) + \sigma_m A_1 A_2/3(1-\upsilon)\bar{\sigma} + \{\sigma_m^3 + 2(1-\upsilon)J_3\}A_2^2/4\bar{\sigma}^2\sigma_m(1-\upsilon^2)]$$

$$d_{11} = D_1^2\ ,\quad d_{22} = D_2^2\ ,\quad d_{33} = D_3^2\ ,\quad d_{12} = D_1D_2\ ,\quad d_{13} = D_1D_3\ ,\quad d_{23} = D_2D_3,$$

$$D_1 = (1+\upsilon)A_1/3 + (S_x + \upsilon S_y)A_2/2\bar{\sigma}\ ,\quad D_2 = (1+\upsilon)A_1/3 + (\upsilon S_x + S_y)A_2/2\bar{\sigma}\ ,$$

$$D_3 = (1-\upsilon)\tau_{xy}A_2/2\bar{\sigma}$$

where E : the initial Young's modulus ; υ : the Poisson's ratio ; $H' = \Delta Y/\Delta\varepsilon_p$ for the Von-Mises's formula and $(1-\sqrt{3}\alpha)^2\Delta Y/\Delta\varepsilon_p$ for the Drucker-Prager's formula ; ΔY : the increment of uniaxial yield stress ; and $\Delta\varepsilon_p$: the increment of uniaxial plastic strain.

Cracked concrete is subjected to the normal stress σ_u parallel to crack directions and thus the uniaxial stress-strain relation in the U-direction, as indi-

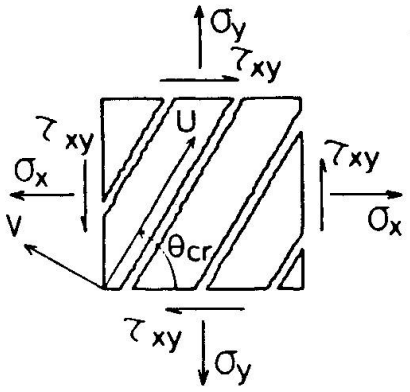

Fig.5 Idealization for Cracked Concrete Element

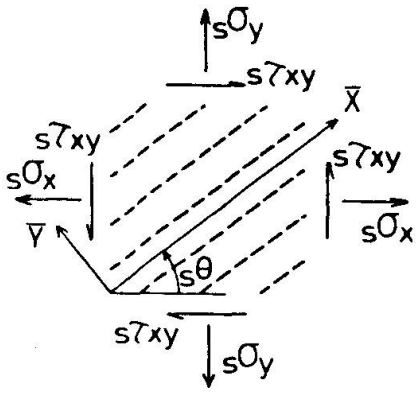

Fig.6 Idealization for Steel Element

cated in Fig.5, is written as follows,

$$\sigma_u = E\varepsilon_u \qquad \text{with} \quad Y(1) \leq \sigma_u \leq f_t \qquad \text{------ (3.3)}$$

If the crack direction makes an angle of θ_{cr} with the X-axis, the stiffness matrix in the local coordinates U,V is converted into that in the global coordinates X,Y by using a appropriate transformation[2],

$$\{\sigma_x\} = [D]_{cr}\{\varepsilon_x\} \qquad \text{------- (3.4)}$$

in which $\{\sigma_x\} = \{\sigma_x, \sigma_y, \tau_{xy}\}^T$ $\{\varepsilon_x\} = \{\varepsilon_x, \varepsilon_y, \gamma_{xy}\}^T$ and

$$[D]_{cr} = E \begin{bmatrix} \cos^4\theta_{cr} & \cos^2\theta_{cr}\sin^2\theta_{cr} & \cos^3\theta_{cr}\sin\theta_{cr} \\ & \sin^4\theta_{cr} & \cos\theta_{cr}\sin^3\theta_{cr} \\ \text{SYM.} & & \cos^2\theta_{cr}\sin^2\theta_{cr} \end{bmatrix} \qquad \text{----- (3.5)}$$

The stiffness formulation for cracked concrete in the plastic range($\sigma_u \leq Y(k)$, where k = 1, 2 and 3) is to be done in the same way as the case for elastic cracked concrete($Y(1) \leq \sigma_u \leq f_t$) by using the tangential moduli E_{t1} and E_{t2} on the uniaxial stress-strain curve corresponding to the strain induced in the crack direction instead of E in Eq.(3.5).

3.2 Steel Reinforcement

Since the reinforcing bar is one-dimensional element, a derivation of the elastic stiffness matrix for reinforcing bar inclined by an angle of $_s\theta$ with the X-axis is similar to the case of cracked concrete. The stress-strain relation for reinforcing bar in the $\bar{X}$-direction, as indicated in Fig.6, is written as follows by assuming the compatibility of deformation,

$$_s\sigma_{\bar{x}} = p_{\bar{x}} \cdot {}_sE\varepsilon_{\bar{x}} \qquad \text{with} \quad -{}_s\sigma_y \leq {}_s\sigma_{\bar{x}} \leq {}_s\sigma_y \qquad \text{------ (3.6)}$$

$$p_{\bar{x}} = {}_sA_{\bar{x}}/A \qquad \text{------ (3.7)}$$

where $_sE$: the Young's modulus of steel ; $_sA_{\bar{x}}$: the area of one bar reinforced in the $\bar{X}$ -direction ; A : the cross sectional area of concrete between reinforcing bars ; and hereafter the subscript s shall indicate steel.
The stiffness matrix of Eq.(3.6) in the global coordinates X,Y takes the following form[2],

$$\{\sigma_x\} = {}_s[D]_e\{\varepsilon_x\} \qquad \text{-------- (3.8)}$$

in which

$$ {}_s[D]_e = p_{\bar{x}} \cdot {}_sE \begin{bmatrix} \cos^4{}_s\theta & \cos^2{}_s\theta\sin^2{}_s\theta & \cos^3{}_s\theta\sin{}_s\theta \\ & \sin^4{}_s\theta & \cos{}_s\theta\sin^3{}_s\theta \\ \text{SYM.} & & \cos^2{}_s\theta\sin^2{}_s\theta \end{bmatrix} \qquad \text{----- (3.9)}$$

The stiffness formulation for reinforcing bar in the plastic range is to be done in the same way as the case for reinforcing bar in the elastic range by using the tangential Young's modulus ${}_sE_{st}$ on the stress-strain curve corresponding to the strain instead of ${}_sE$ in Eq.(3.9).

3.3 Bond between Concrete and Steel Reinforcement

It has been already known that bond between concrete and reinforcing bar after crack formation gives some resistance to concrete(tension stiffening effect) and its resistance gradually deteriorates with an increase in number of cracks, that is, an increase of strain as shown in Fig.7[4 and 5].
Reffering to experimental results on tensile bond tests[4 and 5],bond effect was replaced by the equivalent stress which indicates the nominal concrete stress, without idealizing it into the discrete element such as the linkage element, and the equivalent stress due to bond is modelled as shown in Fig.8.
It is assumed that the equivalent stress under monotonic loading is represented by the 3rd orders of polynomial function,

$$\left.\begin{aligned} &\sigma_{\bar{x},eq} = f_t \cdot (a_0 + a_1X + a_2X^2 + a_3X^3) \\ \text{with}\quad &0 \le \sigma_{\bar{x},eq} \le f_t \ , \quad \varepsilon_{cr} \le \varepsilon_{\bar{x}} \le \varepsilon_{Bu} \quad \text{and} \\ &X = (\varepsilon_{\bar{x}} - \varepsilon_{cr})/(\varepsilon_{Bu} - \varepsilon_{cr}) \end{aligned}\right\} \text{----- (3.10)}$$

where $\sigma_{\bar{x},eq}$: the equivalent stress(kg/cm^2) of concrete in the reinforcing direction $\bar{X}$ and the subscript eq indicates an equivalence to the stress σ, τ, etc.; $\varepsilon_{\bar{x}}$ (or ${}_s\varepsilon_{\bar{x}}$): the average strain of concrete(or reinforcing bar) in the $\bar{X}$-direction ; ε_{cr}: the cracking strain ; ε_{Bu}: the strain at which bond over the element length disappears; and the coefficients a_0, a_1, a_2 and a_3 are 1.0, -2.748, 2.654 and -0.906 respectively.

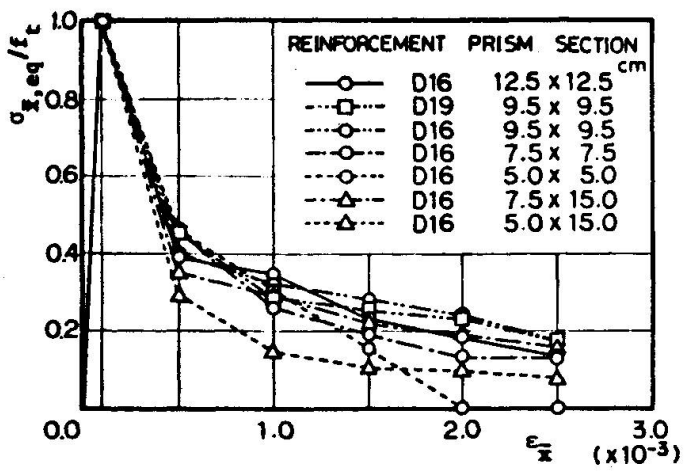

Fig.7 Experimental Equivalent Stress-Average Strain Relation

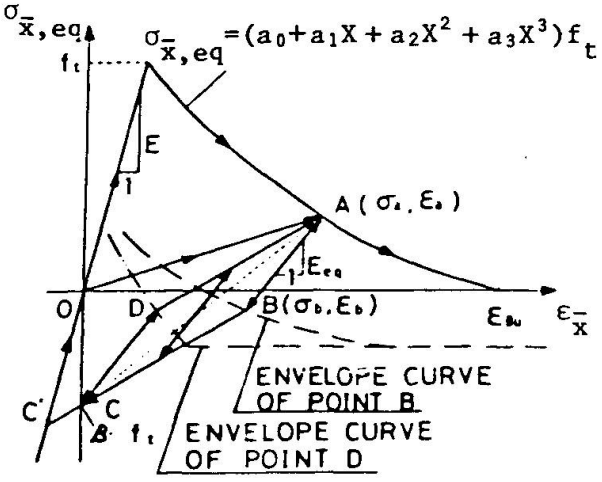

Fig.8 Modelling for Equivalent Stress -Average Strain Relation

Furthermore, the hysteresis for unloading from an arbitrary point A on the curve of Eq.(3.10) was assumed on the basis of a line AC connecting a point A(σ_a ,ε_a) and a point C(βf_t , 0) on the zero-strain axis as follows,

.for region AB ($\sigma_b \leq \sigma_{\bar{x},eq} \leq \sigma_a$)

$$\sigma_{\bar{x},eq} = E_{eq}(\varepsilon_{\bar{x}} - \varepsilon_a) + \sigma_a \quad , \quad E_{qe} = \alpha E \quad , \quad \alpha = (\sigma_a + f_t)/E\varepsilon_a \qquad \text{----- (3.11)}$$

where E_{eq}: the equivalent Young's modulus(kg/cm^2) and the equivalent stress σ_b of the point B is set equal to an average of σ_a and σ_c.

.for region BC ($\beta.f_t \leq \sigma_{\bar{x},eq} \leq \sigma_b$)

$$\sigma_{\bar{x},eq} = E_{eq}.\varepsilon_{\bar{x}} + \beta.f_t \quad , \quad E_{eq} = (\sigma_a - \beta f_t)/2\varepsilon_b$$
$$\varepsilon_b = (\beta f_t - \sigma_a)/2\alpha E + \varepsilon_a \quad , \quad \beta = -0.5 \qquad \text{------ (3.12)}$$

Nextly, the hysteresis for reloading from a point C or C', where C' is an arbitrary point in the compression range, takes either a path(C→D→A) before the closing of cracks or a path(C'→ O→A) after the closing of cracks,

.for region CD ($\beta f_t \leq \sigma_{\bar{x},eq} \leq \sigma_d$)

$$\sigma_{\bar{x},eq} = E_{eq}\varepsilon_{\bar{x}} + \beta f_t \quad , \quad E_{eq} = \alpha.E \qquad \text{------ (3.13)}$$

where the equivalent stress σ_d of a point D is set equal to an average of σ_a and σ_c.

.for region DA ($\sigma_d \leq \sigma_{\bar{x},eq} \leq \sigma_a$)

$$\sigma_{\bar{x},eq} = E_{eq}(\varepsilon_{\bar{x}} - \varepsilon_a) + \sigma_a \quad , \quad E_{eq} = (\sigma_a - \beta f_t)/2\varepsilon_b \qquad \text{------ (3.14)}$$

.for region OA ($0 \leq \sigma_{\bar{x},eq} \leq \sigma_a$)

$$\sigma_{\bar{x},eq} = E_{eq}\varepsilon_{\bar{x}} \quad , \quad E_{eq} = \sigma_a/\varepsilon_a \qquad \text{------- (3.15)}$$

The equivalent stress $\sigma_{\bar{x},eq}$ defined in the above is converted into the stresses $\{\sigma_{\bar{x},eq}, \sigma_{\bar{y},eq}, \tau_{\bar{x}\bar{y},eq}\}$ in the orthogonal coordinates X,Y as follows,

$$\begin{Bmatrix} \sigma_{x,eq} \\ \sigma_{y,eq} \\ \sigma_{xy,eq} \end{Bmatrix} = \begin{bmatrix} \cos^2_s\theta & \sin^2_s\theta & -2\cos_s\theta\sin_s\theta \\ \sin^2_s\theta & \cos^2_s\theta & 2\cos_s\theta\sin_s\theta \\ \cos_s\theta\sin_s\theta & -\cos_s\theta\sin_s\theta & \cos^2_s\theta - \sin^2_s\theta \end{bmatrix} \begin{Bmatrix} \sigma_{\bar{x},eq} \\ 0 \\ 0 \end{Bmatrix} \qquad \text{---- (3.16)}$$

3.4 Equivalent Shear Stiffness due to Aggregate Interlock

In order to evaluate the shear stress induced along cracked surfaces of concrete due to aggregate interlock after crack formation, Paulay et al.[6] conducted the test on aggregate interlock whose variable factors were concrete strength and crack width, and proposed the shear stress-relative displacement relation. However, since their predicting equation gives a rather high evaluation, it is modified to the following,

$$\tau_{uv,eq1} = (0.141/W - 1.0)(1.526\sqrt{f_c} - 7.365)(\delta_s - 0.0436W) \qquad \text{------ (3.17)}$$

where $\tau_{uv,eq1}$: the shear stress acting along cracked surfaces of concrete(kg/cm^2) ; W : the crack width(cm) ; δ_s : the relative displacement across cracked surfaces

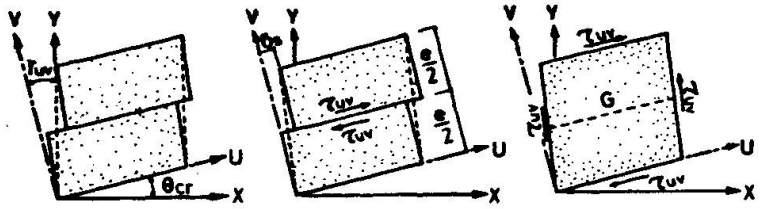

Fig.9 Assumed Shear Strain for Cracked Concrete

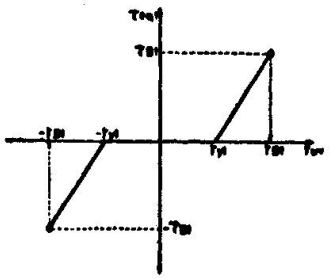

Fig.10 Assumed Equivalent Shear Stress-Strain Relation of Aggregate Interlock for Constant Crack Spacing and Width

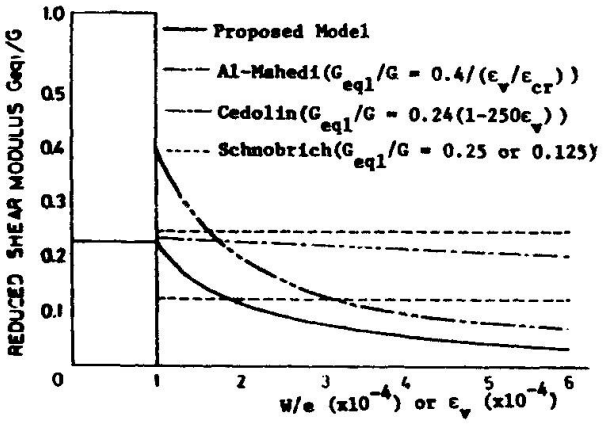

Fig.11 Shear Stiffness Reduction in Cracked Concrete

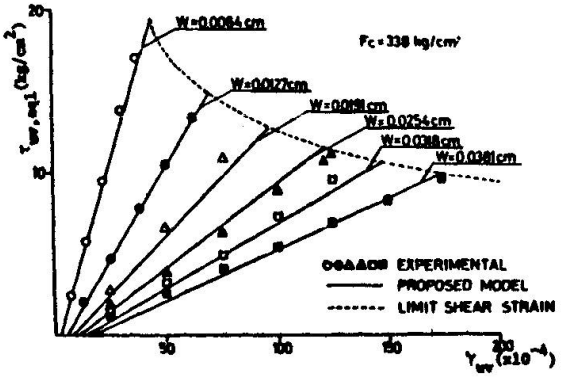

Fig.12 Comparison between Assumed and Observed Equivalent Shear Stress-Shear Strain Relation

(cm) ; and the subscript s in the right hand side indicates slip.
The strain of cracked concrete γ_{uv} is considered to be a sum of the elastic shear strain and the shear strain due to the relative displacement as shown in Fig.9,

$$\gamma_{uv} = \tau_{uv}/G + \delta_s/e \qquad \text{------} \quad (3.18)$$

where G : the elastic shear modulus(kg/cm^2) ; τ_{uv} : the elastic shear stress in the local coordinates U,V(kg/cm^2) ; and e : the crack spacing(cm).
Assuming that the first term in Eq.(3.18) can be negligible as compared with the second term, then Eq.(3.18) can be reduced to,

$$\gamma_{uv} = \delta_s/e \quad \text{with} \quad \gamma_{y1} \leq |\gamma_{uv}| \leq \gamma_{B1} \qquad \text{-------} \quad (3.19)$$

Substituting Eq.(3.19) into Eq.(3.17) and arranging it, then the following equivalent shear stress-strain relation is derived (see Fig.10),

$$\tau_{uv,eq1} = G_{eq1}(\gamma_{uv} - |\gamma_{y1}|) \quad , \quad \gamma_{y1} = 0.0436W/e$$
$$G_{eq1} = (0.141/W - 1.0)(1.526\sqrt{f_c} - 7.365)e \qquad \text{------} \quad (3.20)$$

where $G_{eq1} = 0$ for $-\gamma_{y1} \leq \gamma_{uv} \leq \gamma_{y1}$; $\tau_{uv,eq1}$: the equivalent shear stress(kg/cm^2) ; G_{eq1} : the equivalent shear stiffness(kg/cm^2) ; and γ_{y1}: the shear strain at which aggregate interlock becomes effective.
The limit shear strain at which aggregate interlock disappears is assumed as follows on the basis of the experimental result[6],

$$\gamma_{B1} = (0.01799 + 4.1857W)/e \qquad \text{-------} \quad (3.21)$$

The equivalent shear stiffness of cracked concrete becomes maximum when crack just occurs and is roughly equal to 0.1 E.
Now, the equivalent shear stress in the local coordinates U,V defined in the above is converted into the stresses $\{\sigma_{x,eql}, \sigma_{y,eql}, \tau_{xy,eql}\}^T$ in the global coordinates X,Y as follows,

$$\begin{Bmatrix} \sigma_{x,eql} \\ \sigma_{y,eql} \\ \tau_{xy,eql} \end{Bmatrix} = \begin{bmatrix} \cos^2\theta_{cr} & \sin^2\theta_{cr} & -2\cos\theta_{cr}\sin\theta_{cr} \\ \sin^2\theta_{cr} & \cos^2\theta_{cr} & 2\cos\theta_{cr}\sin\theta_{cr} \\ \cos\theta_{cr}\sin\theta_{cr} & -\cos\theta_{cr}\sin\theta_{cr} & \cos^2\theta_{cr}-\sin^2\theta_{cr} \end{bmatrix} \begin{Bmatrix} 0 \\ 0 \\ \tau_{uv,eql} \end{Bmatrix} \quad (3.23)$$

Fig.11 shows the reduction of shear modulus due to cracking which is evaluated from Eq.(3.20) and those which have been used by different investigators[7], and a discrepancy among them is considerable, ranging from ablout 40 to 3 percents for very wide cracks. Fig.12 shows a comparison between the equivalent shear stress-strain relation calculated from Eq.(3.20) and that observed by the experiment[6] for several crack widths and constant concrete strength.

3.5 Equivalent Shear Stiffness due to Dowel Action

Dulacscka[8] conducted the dowel test whose variable factors were concrete strength and diameter and angle of reinforcing bar, and he proposed the relative displacement-dowel force relation,

$$\delta_s = \Delta\ (358T_y/D\sqrt{f_c})\ \times 10^{-6} \qquad \text{------} \quad (3.24)$$

$$\Delta = (T/T_y)\sqrt{\tan[(T/T_y)(\pi/2)]} \qquad \text{------} \quad (3.25)$$

$$T_y = 0.2D^2{}_s\sigma_y\{\sqrt{\rho^2\sin_s\theta_{cr} + \rho f_c/0.03_s\sigma_y} - \rho\sin_s\theta_{cr}\} \qquad \text{-----} \quad (3.26)$$

where $\rho = 1 - ({}_s\sigma/{}_s\sigma_y)^2$; T_y : the dowel strength of one reinforcing bar(kg) ; T : the dowel force(kg) ; $_s\sigma$: the steel stress(kg/cm^2) ; $_s\sigma y$: the yield stress of steel(kg/cm^2) ; D : the diameter of reinforcing bar(cm); and $_s\theta_{cr}$: the angle between the axis perpendicular to the crack direction and the reinforcing bar.

Δ in Eq.(3.25) is a function of the non-dimensional dowel force T/T_y and gives the curve as shown in Fig.13. This curve is approximated by the elasto-palstic relation,

.for elastic case ; $T/T_y = \alpha.\Delta$ ------ (3.27)

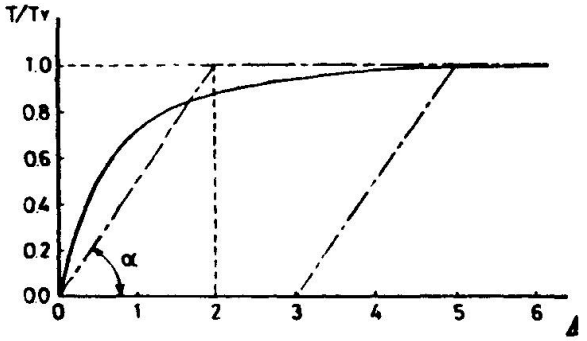

Fig.13 Non-Dimensionized Dowel Force Curve

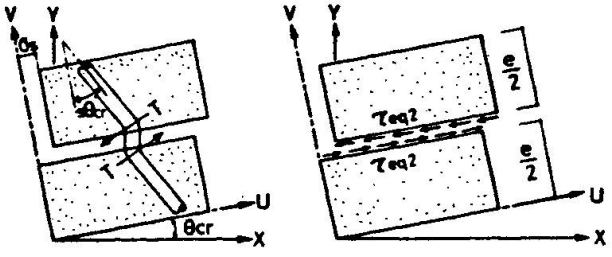

Fig.14 Idealization for Dowel Force

.for plastic case ;

$$T/T_y = 1.0 \quad \text{---- (3.27)}$$

where α indicates the elastic slope and is set equal to 0.2.

In the next place, in order to evaluate the equivalent shear stiffness due to dowel action, the dowel force is replaced by the equivalent shear stress as shown in Fig.14,

$$\tau_{uv,eq2} = p_{\bar{x}} T \cos_s\theta_{cr} / {}_sA \quad \text{----(3.28)}$$

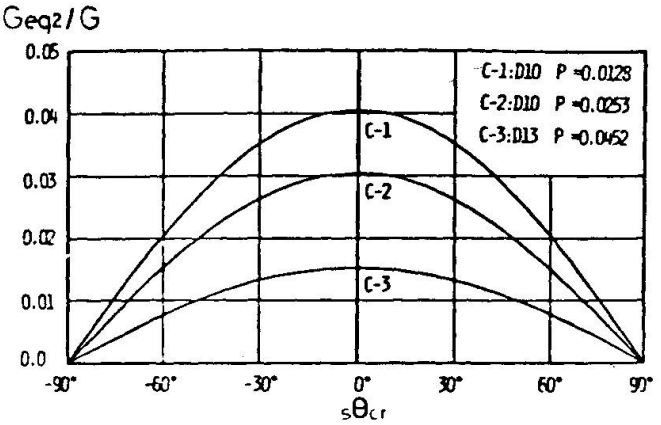

Fig.15 Equivalent Shear Stiffness due to Dowel Action

Substituting Eqs.(3.19), (3.27) and (3.28) into Eq.(3.24) and arranging it, then the following equivalent shear stress-strain relation is obtained,

.for elastic case ($|\gamma_{uv}| \leq \gamma_{y2}$) ;

$$\left.\begin{aligned} \tau_{uv,eq2} &= G_{eq2} \cdot \gamma_{uv} \\ G_{eq2} &= (\alpha . D\sqrt{f_c} . e . p_{\bar{x}} \cos_s\theta_{cr}) \times 10^6 / 358\, {}_sA \end{aligned}\right\} \text{------ (3.29)}$$

.for plastic case ($|\gamma_{uv}| \geq \gamma_{y2}$) ;

$$\left.\begin{aligned} |\tau_{uv,eq2}| &= p_{\bar{x}} . T_y \cos_s\theta_{cr} / {}_sA \\ |\gamma_{y2}| &= 358 T_y \times 10^{-6} / \alpha . D\sqrt{f_c} . e \end{aligned}\right\} \text{------ (3.30)}$$

A transformation of the equivalent shear stress $\tau_{uv,eq2}$ in the U,V-coordinate system to that $\{\sigma_{x,eq2}, \sigma_{y,eq2}, \tau_{xy,eq2}\}^T$ in the X,Y-coordinate system is to be done in the same way as Eq.(3.23). The relation between ratios G_{eq2}/G of equivalent shear stiffnesses G_{eq2} of Eq.(3.29) to the elastic shear stiffness G and angles $s\theta_{cr}$ of reinforcing bars is plotted in Fig.15 for several steel ratios, and it is found that an effect of dowel action is relatively small.

4. CRACK SPACING AND CRACK WIDTH

It is necessary for evaluating aggregate interlock and dowel action described in the previous section and also checking up the opening and closing of cracks in cyclic analysis to determine crack spacing and width.
Morita et al.[9] found from their own experiment that there was a linear relationship between average minmum crack spacing e_{min} and ratios D/p of bar diameters D to steel ratios p. Thus, assuming that when steel yields average crack spacing e_{av} becomes e_{min}, the equation predicting $e_{\bar{x},av}$ is proposed,

$$e_{\bar{x},av} = 0.1476 + 0.19 . D/p_{\bar{x}} + 0.0023/{}_s\varepsilon_{\bar{x}} \quad \text{------ (4.1)}$$

where $e_{\bar{x},av}$ indicates average crack spacing in the reinforcing direction $\bar{X}$, and note that this is a nominal crack spacing for any one of cracked concrete element.

Fig.16 shows a comparison between crack spacings of the experiment[10, 11 and 12] and those calculated from Eq.(4.1) for sevearl ratios D/p, and they have

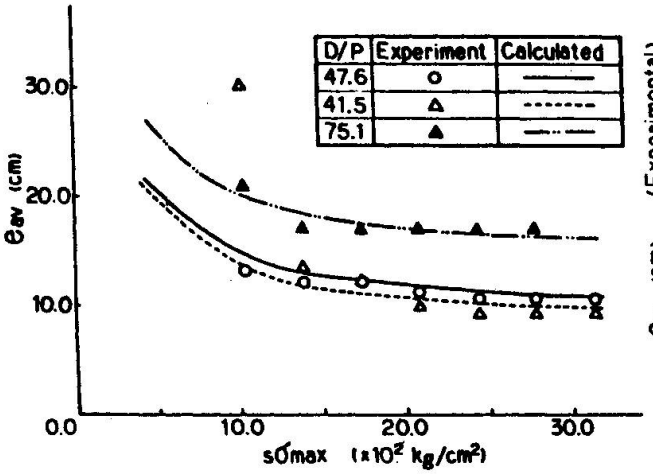

Fig.16 Comparison between Assumed and Observed Average Crack Spacing-Steel stress Relation

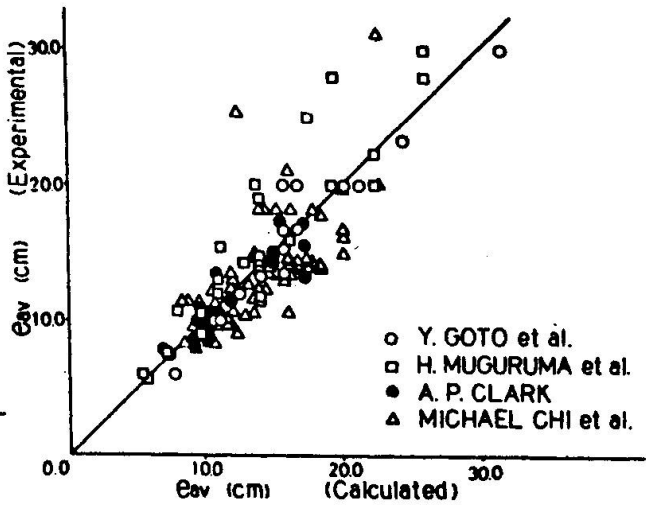

Fig.17 Comparison between Calculated and Experimental Crack Spacings

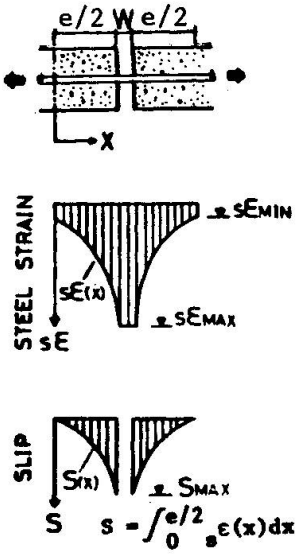

Fig.18 Distributions of Steel Strain and Slip along Reinforcing Bar in Cracked Concrete

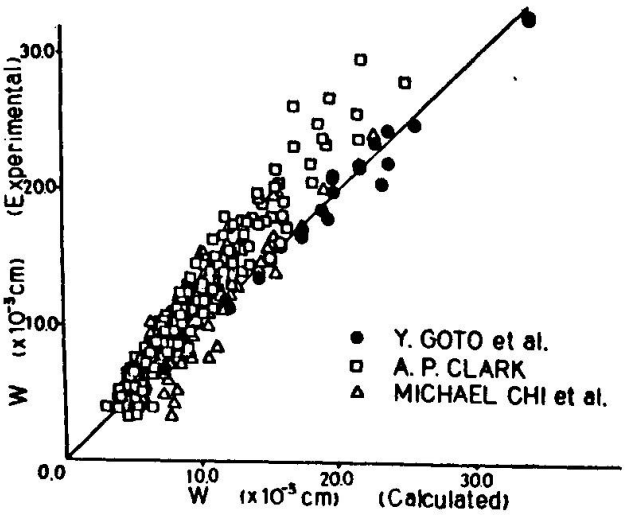

Fig.19 Comparison between Calculated and Experimental Crack Widths

some scatters at low stress levels but they fairely agree to each other with an increase of steel stresses.
Fig.17 shows plots of experimental crack spacings[9, 11, 12 and 13] against calculated values by Eq.(4.1) and it can be seen that although a discrepancy between them exists for big crack spacings, they coincide as crack spacings become smaller.

In the next place, a derivation of crack width based upon the conventional bond theory is presented. The slip increment dS over the interval dX is generally defined as a difference between elongations of concrete and reinforcing bar, and assuming that concrete strain after crack formation is negligible as compared with steel strain, then the slip is approximately expressed as follows,

$$S(x) = \int_0^x {}_s\varepsilon(x)dx \qquad \text{------ (4.2)}$$

The maximum slip is obtained from Eq.(4.2) as follows, provided that distributions of steel strain and slip over crack spacing e are given as shown in Fig.18,

$$S_{max} = \int_0^{e/2} {}_s\varepsilon(x)dx \qquad \text{-------- (4.3)}$$

Therefore, crack width W is defined as a function of maximum slip S_{max} and steel strain ${}_s\varepsilon_{max}$ at the cracking part,

$$W = 2.S_{max}(1 + {}_s\varepsilon_{max}) \qquad \text{-------- (4.4)}$$

However, it is hard to evaluate S_{max} since strain distribution of reinforcing bar along its length is unknown, so the average strain ${}_s\varepsilon_{\bar{x}}$ defined in Section 3.3 is adopted in this paper. But since strain at the cracking part is included in this average strain, it needs to redefine the net average strain excluding that strain,

$${}_s\varepsilon_{\bar{x}}' = {}_s\varepsilon_{\bar{x}} - W_{\bar{x}}({}_s\varepsilon_{max} - {}_s\varepsilon_{\bar{x}})/e \qquad \text{-------- (4.5)}$$

Thus, S_{max} is derived by using Eq.(4.5) instead of ${}_s\varepsilon(x)$ in Eq.(4.3) as follows,

$$S_{max} = e._s\varepsilon_{\bar{x}}/2 - W_{\bar{x}}({}_s\varepsilon_{max} - {}_s\varepsilon_{\bar{x}})/2 \qquad \text{------ (4.6)}$$

An introduction of Eq.(4.6) into Eq.(4.4) results in the following crack width,

$$W_{\bar{x}} = e._s\varepsilon_{\bar{x}}(1 + {}_s\varepsilon_{max})/\{1 + (1 + {}_s\varepsilon_{max})({}_s\varepsilon_{max} - {}_s\varepsilon_{\bar{x}})\} \text{ ------ (4.7)}$$

where $${}_s\varepsilon_{max} = {}_s\varepsilon_{\bar{x}} + \sigma_{\bar{x},eq}/p_{\bar{x}}.{}_sE$$

Fig.19 shows plots of experimental crack widths observed in the tensile test (black circles)[13] and the flexural test of beams[11 and 12] against calculated values by Eq.(4.7).

Although the proposed equations for crack spacing and width give an evaluation on each reinforcing direction, it is useful from an analytical point of view to define crack spacings and widths normal to crack directions.
Consider the general case in which concrete is reinforced in the orthogonal directions $\bar{X},\bar{Y}$.
Letting $e_{\bar{x},av}$, $e_{\bar{y},av}$, $W_{\bar{x}}$ and $W_{\bar{y}}$ be average crack spacings and crack widths evaluated by Eq.(4.1) and (4.7), then the average crack spacing e_{av} perpendicular to the crack direction shall be either smaller one between the following two equations (see Fig.20),

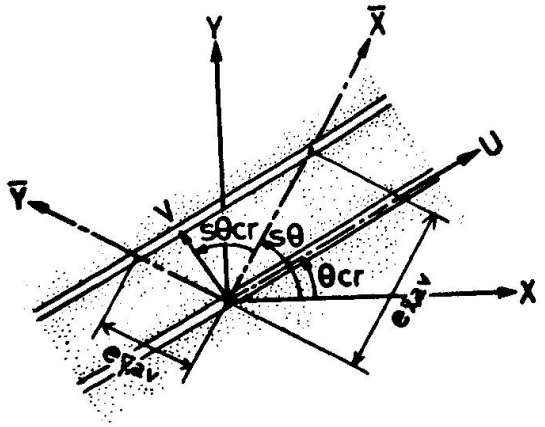

Fig.20 Representation of Crack Spacing

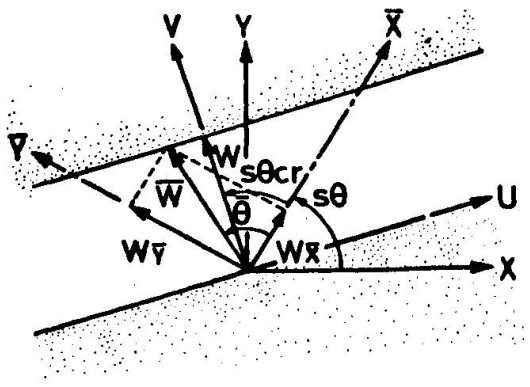

Fig.21 Representation of Crack Width

$$e_{av} = e_{\bar{x},av}\cos_s\theta_{cr} \quad \text{or} \quad e_{av} = e_{\bar{y},av}\sin_s\theta_{cr} \qquad \text{----- (4.8)}$$

and crack width normal to the crack direction is given as follows(see Fig.21),

$$W = \bar{W}.\cos(\bar{\theta} - {}_s\theta_{cr}) \qquad \text{------ (4.9)}$$

$$\bar{W} = \sqrt{W_{\bar{x}}^2 + W_{\bar{y}}^2}\ , \qquad \bar{\theta} = \tan^{-1}(W_{\bar{y}}/W_{\bar{x}})$$

5. NUMERICAL PROCEDURE

5.1 Finite Element

In order to improve accuracy and reduce number of degrees of freedom, the composite element with four nodes and eight degrees of freedom is developed from four constant strain quadrilaterals with nine nodes and eighteen degrees of freedom through the conventional condensation process as shown in Fig.22 and we refer this to as the Super Element[14].

5.2 Solution Procedure

An incremental initial stress approach or an incremental self-correcting approach is used to solve governing nonlinear equations. However, the latter approach is suitable from a viewpoint of a stability and a computational time when cyclic behaviors are to be followed.
Now, the incremental self-correcting approach proposed by Stricklin et al.[15] in which a nonlinear analysis is performed by using the initial stiffness all over the computaional process without iterations is briefly described.
According to this approach, the incremental deflection $\Delta\{\delta\}$ is calculated from the following equations for materially nonlinear problems,

$$\Delta\{\delta\} = [K_0]^{-1}(\Delta P\{\bar{P}\} + \Delta\{Q_p\} + \Delta P.Z\ \{f\}) \qquad \text{------ (5.1)}$$

$$\{f\} = -[K_0]\{\delta\} + P\{\bar{P}\} + \{Q_p\} \qquad \text{------ (5.2)}$$

where $\{f\}$: the force in unbalance induced by the deflection $\{\delta\}$ which does not satisfy equilibrium ; $[K_0]$: the initial stiffness ; $\{Q_p\}$: the fictitious load due to material nonlinearities ; P : the load parameter; $\{\bar{P}\}$: the normalized load vector ; Z : the correcting factor ; and ΔPZ is conventionally set equal to 1.2.

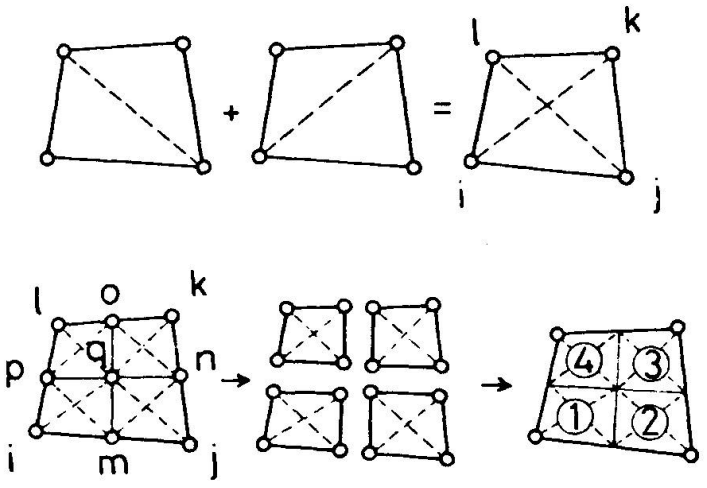

Fig.22 Composition of Super Element

REFERENCES

1. G.C.Nayak and O.C.Zienkiewicz, "Convenient Form of Stress Invariants for Plasticity," Proceedings of A.S.C.E., Vol.98, No.ST4, April 1972.

2. V.Cervenka and K.H.Gerstle," Inelastic Analysis of Reinforced Concrete Panels, Part I ; Theory," IABSE Publications, Vol.31-II, 1971.

3. T.Sato and N.Shirai," Analysis of Nonlinear Behaviors of Concrete by Finite Element Method," The Summary of the Joint Meetings of Applied Mechanics, No.25, 1975 (in Japanese).

4. S.Morita," Study on Bond Effect of Reinforced Concrete Members by Tensile Tests," The Annual Report of Cement Engineering, Vol.XVII, 1963 (in Japanese).

5. S.Morita et al.," Study on Bond Effect of Reinforced Concrete Members by Tensile Tests," The Annual Report of Cement Engineering, Vol.XVIII, 1964 (in Japanese).

6. T.Paulay et al.," Mechanism of Shear Resistance of Concrete Beams," Proceedings of A.S.C.E., Vol.94, No.ST10, 1968.

7. K.H.Gerstle," Material Modelling of Reinforced Concrete," Advanced Mechanics of Reinforced Concrete, Introductory Report, IABSE COLLOQUIUM DELFT 1981.

8. H.Dulacscka," Dowel Action of Reinforcement Crossing Cracks in Concrete," Journal of ACI, 1972, pp.754 - 757.

9. S.Morita et al.," Control of Cracking in Reinforced Concrete Member," The 2nd Symposium on Deformed Bars, Concrete Library, No.14, 1965(in Japanese).

10. Edward G. Nawy," Crack Control in Reinforced Concrete Structures," Journal of ACI, October 1968.

11. A.P.Clark," Cracking in Reinforced Concrete Flexural Members," Journal of ACI, April 1956.

12. Michael Chi et al.," Flexural Cracks in Reinforced Concrete Beams," Journal of ACI, April, 1958.

13. Y.Goto et al.," Investigation on Tension Cracks in Reinforced Concrete Members - An Experiment by Tensile Bond Specimen-," The 2nd Symposium on Deformed Bars, Concrete Library, No.14, 1965 (in Japanese).

14. T.Sato and N.Shirai," Inelastic Analysis of Reinforced Concrete Shear Walls under Combined Stresses," The Annual Report of Architectural Institute of of Japan, 1977 (in Japanese).

15. J.A.Stricklin et al.," Self-Correcting Incremental Approach in Nonlinear Strucrural Mechanics," Journal of AIAA, Vol.9, no.12, 1971.

Stress-Strain Characteristics of Reinforced Concrete in Pure Shear

Les relations tensions-déformations du beton armé soumis au cisaillement pur

Spannungsdehnungsverhalten von Stahlbeton unter reinem Schub

F. VECCHIO
Doctoral Student
University of Toronto
Toronto, Canada

M.P. COLLINS
Professor
University of Toronto
Toronto, Canada

SUMMARY
Experiments in which reinforced concrete panels were loaded in pure shear are described. It is shown that the observed behaviour of the panels can be predicted by using basis equilibrium and compatibility conditions in addition to appropriate stress-strain relationships for the concrete and the steel.

RÉSUMÉ
Des essais sont décrits concernant des panneaux en béton armé soumis au cisaillement pur. On démontre que le comportement des panneaux, tel qu'observé, peut être prédit en utilisant les conditions usuelles d'équilibre et de compatibilité, en plus des relations appropriées entre contraintes et déformations unitaires pour le béton et l'acier.

ZUSAMMENFASSUNG
Versuche, in denen Stahlbetonscheiben nur mit Schubkräften belastet werden, werden beschrieben. Es wird gezeigt, dass man das beobachtete Verhalten der Scheiben durch die Benützung von elementarem Gleichgewicht und Verträglichkeitsbedingungen wie auch von geeigneten Spannungs-Dehnungs Linien für Beton und Stahl beschreiben kann.

1. INTRODUCTION

Developing a rational theory capable of predicting the behaviour of reinforced concrete subjected to shear has been the goal of a large number of research engineers for very many years. Achieving this goal would enable current empirical shear design procedures to be replaced by methods comparable in rationality and generality to the procedures now used in the design of reinforced concrete for flexure and axial load.

In the past many researchers have tackled the shear problem by testing simply supported beams subjected to point loads. A fundamental difficulty inherent in such tests is that no substantial region of the specimen is subjected to uniform stress conditions. The local disturbances caused by the point loads and the reactions plus the changing moments along the span mean that (apart from end-to-end symmetry) no two points on the specimen behave in quite the same manner.

It is the authors' belief that before we can understand the behaviour of reinforced concrete in complex load situations involving shear we must first understand its behaviour in pure shear. Hence, as part of an ongoing research programme at the University of Toronto [1], an experimental project in which reinforced concrete elements were loaded in pure shear was undertaken. This paper will describe the preliminary results of this "pure shear" project.

2. LOADING REINFORCED CONCRETE IN PURE SHEAR

The test specimens were concrete panels, 890 mm square by 70 mm thick, reinforced with two layers of welded wire fabric, Fig. 1. Five steel shear keys, anchored with shear studs, were cast into each edge of the specimen.

The specimens were loaded via links pinned to the steel shear keys. Each key was acted upon by two inclined links, one at +45° to the normal to the specimen edge and the other at -45°, Fig. 2. When one link pulled, while the other pushed with the same force, a resultant force parallel to the edge of the specimen was produced.

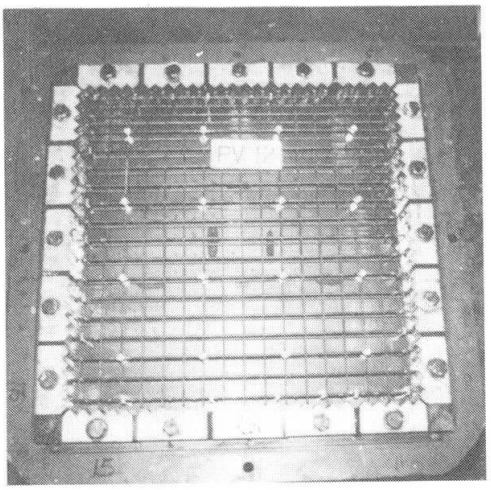

Fig. 1 Specimen Ready for Casting

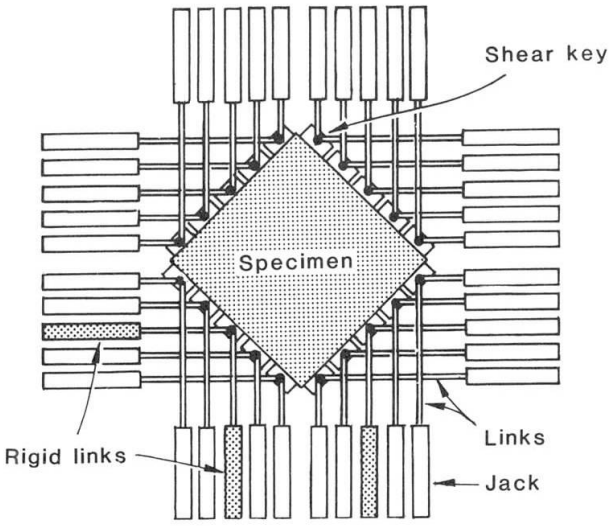

Fig. 2 Hydraulic Jack and Link Assembly

The forces in the 40 links (2 x 5 x 4) were produced by 37 double-acting hydraulic jacks acting on 37 of the links. The remaining three links were fixed in length in order to stabilize the overall position of the specimen within the rig.

To prevent out-of-plane movement of the panel the shear keys were attached to an auxiliary frame by means of tie-rods with spherical rod ends, Fig. 3.

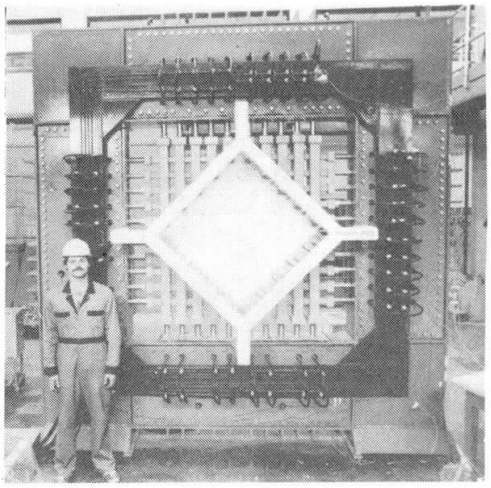

Fig. 3 Rear View of Shear Rig

3. DESCRIPTION OF SPECIMENS

Table 1 summarizes the parameters of the 17 specimens tested to date. The pure shear tests were subdivided into two groups. In the Series I tests, the amount of reinforcing was varied; but, for a given specimen, the amount of reinforcing in the transverse direction was always equal to that in the longitudinal direction (longitudinal and transverse were defined as directions parallel to the edges of the specimen, Fig. 1). For the Series II tests, the amount of reinforcing in the longitudinal direction was held constant while the transverse reinforcement was varied. The two panels of Series III were tested in uniaxial compression to calibrate the performance of the test set-up.

TABLE 1. SPECIMEN PARAMETERS

Specimen	Percentage of Steel Reinforcement		Steel Yield Strength (MPa)		Concrete Strength	Cylinder Strain at Peak
	Long.	Trans.	Long.	Trans.	f'_c (MPa)	ϵ_o ($\times 10^{-3}$)
Series I						
PV2	0.18	0.18	430	430	23.5	2.25
PV3	0.48	0.48	660	660	26.6	2.30
PV16	0.74	0.74	250	250	21.7	2.00
PV5	0.74	0.74	620	620	28.3	2.50
PV4	1.06	1.06	240	240	26.6	2.50
PV14	1.79	1.79	460	460	20.4	2.23
PV6	1.79	1.79	270	270	29.8	2.50
PV7	1.79	1.79	450	450	31.1	2.50
PV8	2.62	2.62	460	460	29.8	2.50
Series II						
PV13	1.79	-	250	-	18.2	2.70
PV12	1.79	0.45	470	270	16.0	2.50
PV10	1.79	1.00	280	280	14.5	2.70
PV11	1.79	1.31	240	240	15.6	2.60
PV1	1.79	1.68	480	420	34.5	2.20
PV9	1.79	1.79	460	460	11.6	2.80
Series III						
PV15	0.74	0.74	250	250	21.7	2.00
PV17	0.74	0.74	250	250	20.4	2.00

Brass strain targets were fixed onto the reinforcing steel and protruded to the surfaces of the specimen. Sixteen targets, on a 200 mm grid, were used on each side of the specimen.

Strains were read (using a demountable mechanical strain gauge) in the longitudinal, transverse, and the two diagonal (+45° and -45°) directions; resulting in a total of 84 separate readings.

4. TESTING OF THE SPECIMENS

In the Series I tests, the initial cracks formed at 45° to the steel grid at a shear stress of approximately $0.33\sqrt{f'_c}$ (MPa). As the load increased the number and width of the cracks also increased, but the direction of the cracks did not change. Failure occurred either by a mass yielding of the steel, Fig. 4, or by a sliding shear failure of the concrete, Fig. 5. The mode of failure depended on the amount and strength of the reinforcing relative to the concrete. The ultimate shear stress, as a fraction of f'_c, increased with the percentage of reinforcing. The maximum shear stress attained was $0.32\ f'_c$.

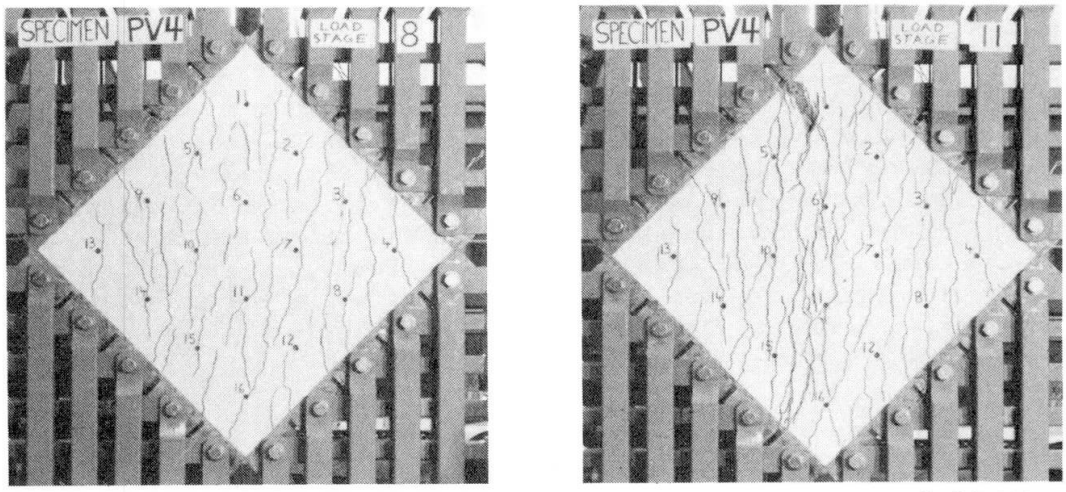

(a) Prior to yielding, v = 2.40 MPa (b) Yielding at v = 2.89 MPa

Fig. 4 Specimen PV4: Steel Yielding Failure

In the Series II tests, the initial cracks also formed at 45°. In this case, however, as the load increased the cracks began to shift direction to become more acute to the longitudinal steel direction, Fig. 6. Failure at ultimate occurred either by: (i) yielding of both the transverse and longitudinal steel; (ii) sliding shear failure of the concrete after the transverse steel had yielded but prior to the yielding of the longitudinal steel, or (iii) sliding shear failure of the concrete prior to yielding of the transverse steel. The mode of failure and ultimate shear strength was influenced mostly by the percentage and strength of the transverse reinforcing.

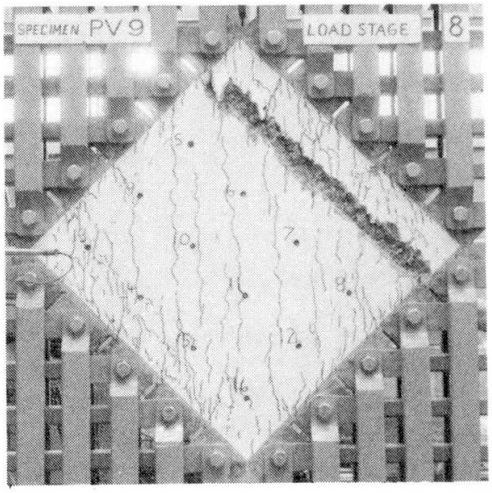

Fig. 5 Specimen PV9: Sliding Shear Failure of Concrete

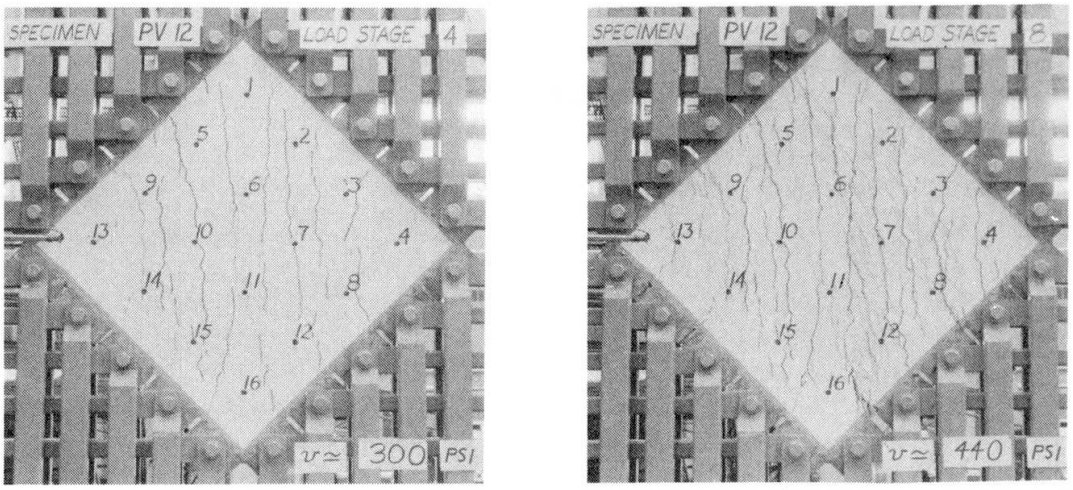

(a) Shortly after cracking, v = 2.1 MPa (b) At ultimate, v = 3.13 MPa

Fig. 6 Specimen PV12: Cracks Shifting Direction

One specimen tested, PV2, was under-reinforced in both directions. It failed immediately after the formation of the diagonal cracks, Fig. 7.

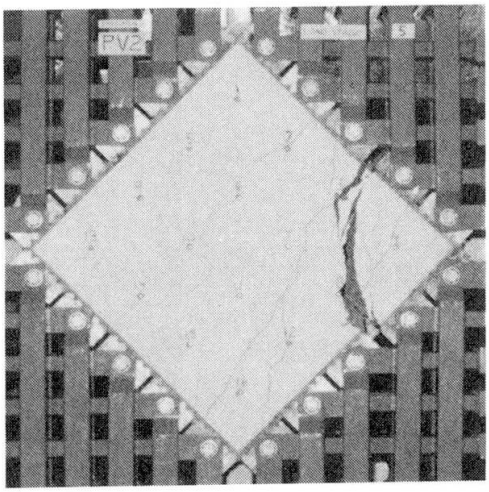

Fig. 7 Specimen PV2: Failure of Under-reinforced Panel Upon First Cracking

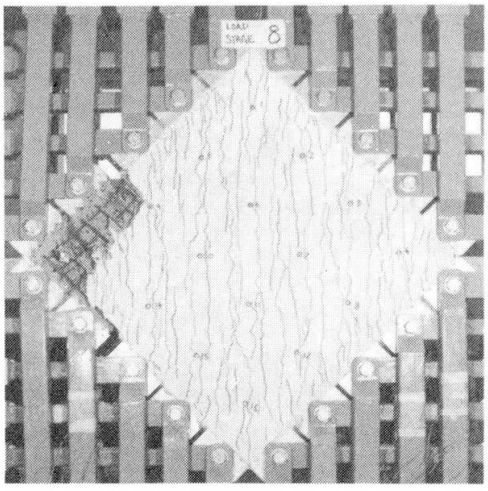

Fig. 8 Specimen PV1: Premature Failure Due to "Pull-Out" of Shear Keys

Unfortunately, some of the test specimens failed prematurely due to a local pull-out failure of the shear keys, Fig. 8. These occurred mostly in the earlier tests where a uniform concrete mix was used throughout the specimen. In later tests, a band of strong concrete was used in the peripheral areas to help alleviate the load transfer problem. A summary of the cracking stresses, ultimate stresses, and mode of failure is given in Table 2.

The two specimens of Series III were tested in uniaxial compression applied in the longitudinal direction. The test on specimen PV15 had to be halted prior to failure because the applied load was approaching the capacity of the rig and a leak had developed in the hydraulic system resulting in severe pressure losses.

TABLE 2: TEST OBSERVATIONS

Specimen	v_{cr} (MPa)	v_u (MPa)	Mode of Failure
PV1	2.21	8.00	Pull-out
PV2	1.10	1.16	Cracking [1]
PV3	1.66	3.07	Steel rupture [2]
PV4	1.79	2.89	Yielding
PV5	1.73	4.24	Pull-out
PV6	2.00	4.55	Local yielding
PV7	1.93	6.81	Pull-out
PV8	1.73	6.67	Pull-out
PV9	1.38	3.74	Concrete shear
PV10	1.86	3.97	Concrete shear
PV11	1.66	3.56	Local yielding
PV12	1.73	3.13	Concrete shear
PV13	1.73	2.01	Concrete shear
PV14	1.93	5.24	Pull-out
PV16	2.07	2.14	Yielding

1 Initially cracked at 90°
2 Non-stress relieved wires ruptured at welds, Fig 9

With Specimen PV17, loading proceeded to failure. At ultimate, there was an explosive failure of the concrete, Fig. 10, with large pieces of concrete thrown as far as 20 m. Prior to failure, only one or two small longitudinal cracks were visible.

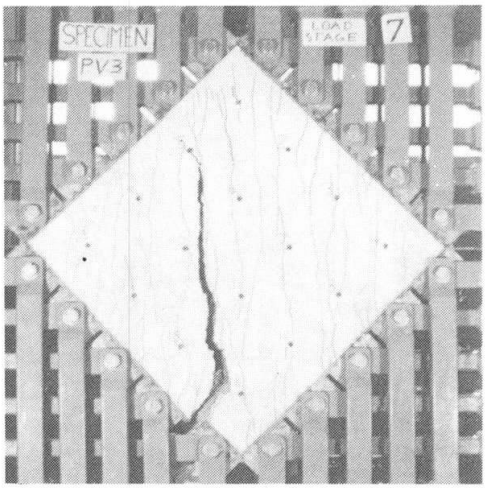

Fig. 9 Specimen PV3: Brittle Failure Due to Fracture of Steel

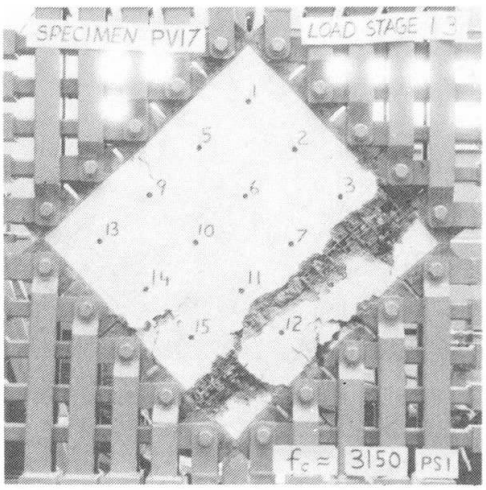

Fig. 10 Specimen PV17: Explosive Failure of Panel in Uniaxial Compression

At ultimate, the concrete compressive stress in PV17 reached 1.04 f'_c.

5. ANALYSIS OF TEST DATA

The data gathered from a particular specimen was analyzed such that Mohr's circles of stress and strain could be drawn at every load stage.

The strain readings were reduced to average strains in the longitudinal, transverse, + 45° diagonal and - 45° diagonal directions; ε_ℓ, ε_t, ε_{+45} and ε_{-45}

respectively. These strains were used to define a Mohr's circle of average strains, Fig. 11. Since four separate items of information were being used to define a circle, there existed one redundant point. The fact that all four points lay very close to it inspired confidence in the accuracy of the strain data.

Defining the strain circle fixed the values of: (i) the principal compressive strain, ε_d; (ii) the principal tensile strain, ε_{dt}; (iii) the normal shear strain, $\gamma_{\ell t}$; (iv) the maximum shear strain, γ_m; and (v) the angle of inclination of the principal compression, θ'.

From the strains in the longitudinal and transverse directions, the average steel tensile stresses ($f_{s\ell}$ and f_{st}) were determined from the stress-strain relationship of the reinforcement. These steel stresses, in turn, permitted the average concrete compressive stresses in the longitudinal and transverse directions, f_ℓ and f_t, respectively, to be calculated ($f_\ell = \rho_\ell f_{s\ell}$ and $f_t = \rho_t f_{st}$). Given the applied shear stress, v, and the calculated concrete stresses f_ℓ and f_t, the Mohr's circle of concrete stress could be drawn, Fig. 12. From the stress circle, the principal compressive stress, f_d, and principal tensile stress, f_{dt}, in the concrete were found.

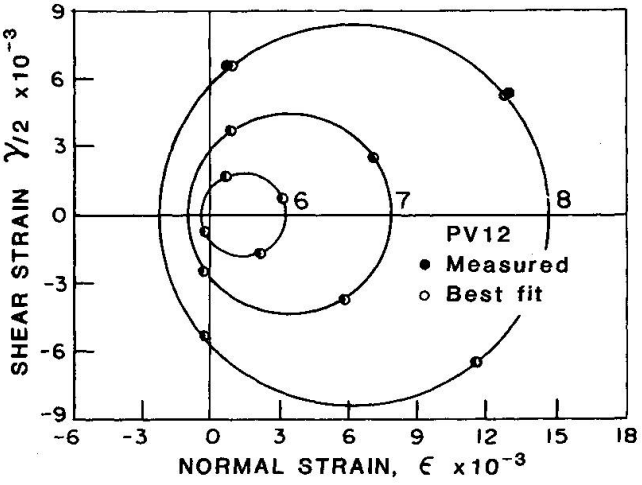

Fig. 11 Mohr's Circles of Strain for Specimen PV12

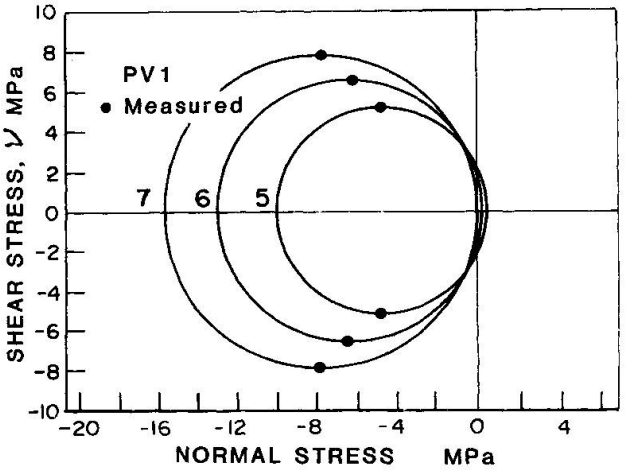

Fig. 12 Mohr's Circles of Stress for Specimen PV1

6. STRESS-STRAIN CHARACTERISTICS OF THE CONCRETE IN COMPRESSION

In Fig. 13, the observed relationships between principal compressive stress and principal compressive strain are shown for four of the panels. It can be seen that the principal compressive stress is not solely a function of the principal compressive strain. As has been previously suggested [2], it would appear that these relationships are influenced by the magnitude of the maximum co-existing shear strains, γ_m.

To further investigate the effects of shear strain, separate plots of the f_d:ε_d data were made for specific

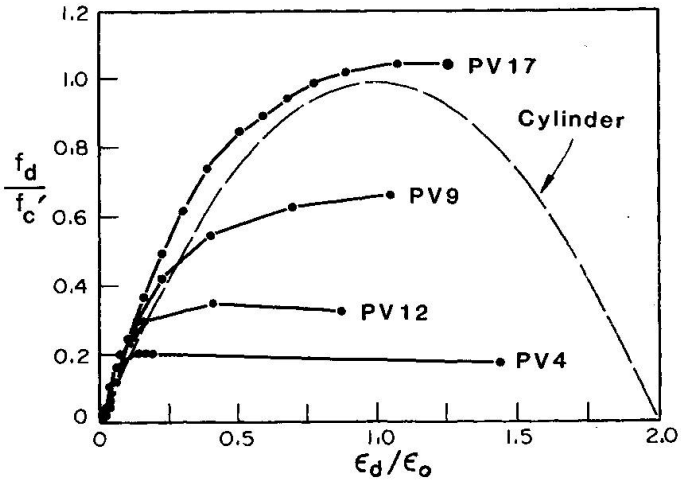

Fig. 13 Principal Compressive Stress vs. Principal Compressive Strain

ranges of the ratio γ_m/ε_d (see Fig. 14). It could be concluded that shearing strains had a degrading effect on the compressive stress-strain response of concrete. Furthermore, the magnitude of this effect appeared related to the ratio of maximum shear strain to principal compressive strain, γ_m/ε_d.

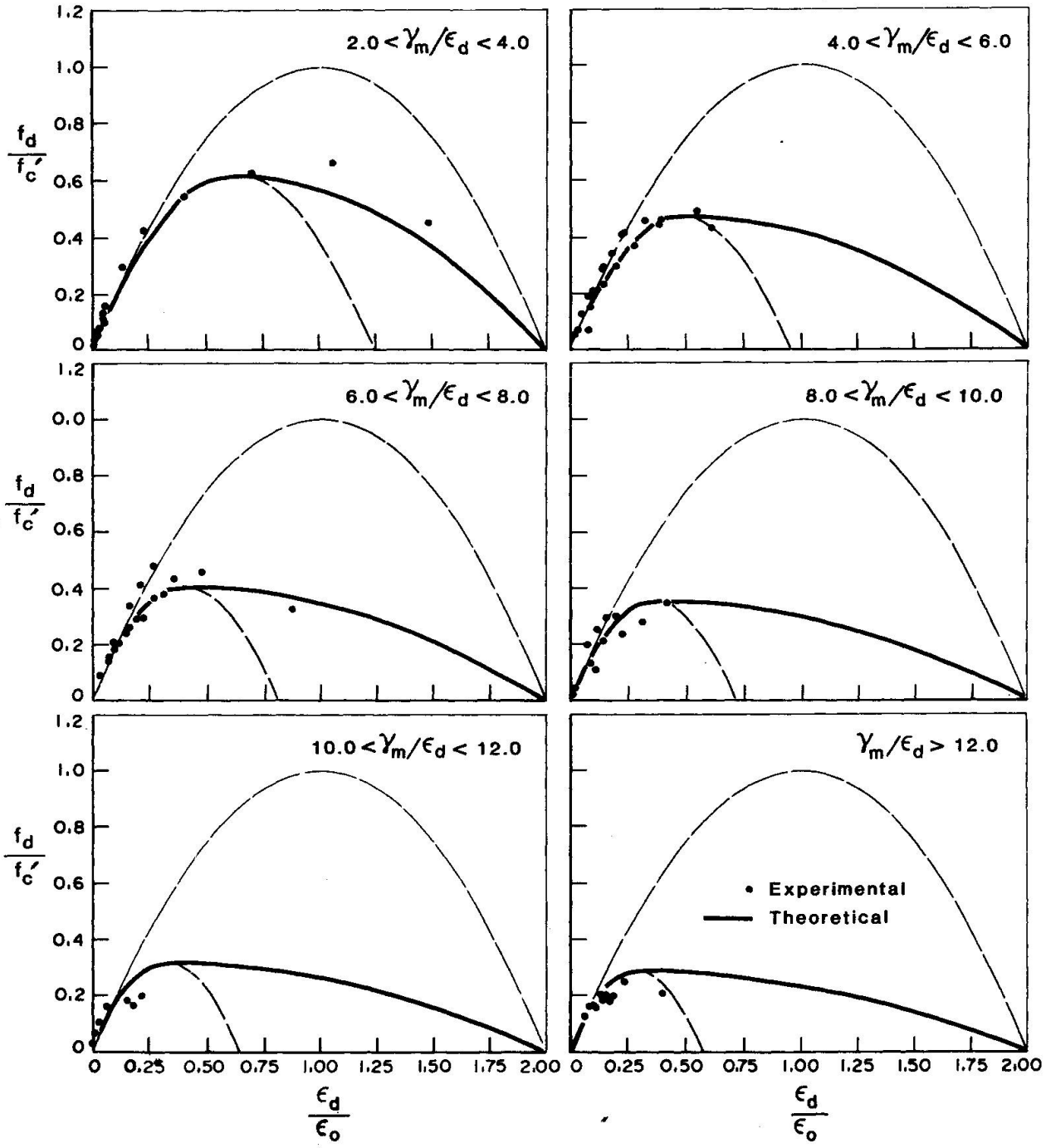

Fig. 14 Influence of Shear Strain on Principal Compressive Stress-Strain

An expression was derived to model the observed behaviour. It involved the addition of a modifying term in the commonly used parabolic stress-strain curve for concrete. The modified expression was:

$$f_d = f'_c \left[2 \left(\frac{\varepsilon_d}{\varepsilon_o}\right) - \lambda \left(\frac{\varepsilon_d}{\varepsilon_o}\right)^2 \right] \quad \ldots (1)$$

where $$\lambda = (\gamma_m/\varepsilon_d - \mu)^{0.5} \quad \ldots (2)$$

Poisson's ratio, μ, is taken equal to 0.30; a value commonly observed near failure in concrete cylinders. The term 'λ' degenerates to 1.0 in the case of uniaxial compression, leaving the customary parabolic curve passing through (ε_o, f'_c).

For a given ratio of γ_m/ε_d, the peak concrete compressive stress attainable, f_p, is:

$$f_p = f'_c/\lambda \qquad \ldots (3)$$

The strain at which this peak stress is achieved, ε_p, is:

$$\varepsilon_p = \varepsilon_o/\lambda \qquad \ldots (4)$$

Thus, all peak stresses for various values of γ_m/ε_d lie on the line passing through the points (0, 0) and (ε_o, f'_c).

The experimental f_d:ε_d data indicated that the concrete had considerably more ductility after peak strain than that predicted by Eq.(1). Thus, a more gradual unloading portion of the stress-strain curve was required. This was achieved by a transition curve between Eq.(1) and the usual parabolic expression, after peak stress.

In summary, given the principal compressive strain (ε_d) and the maximun shear strain (γ_m), the principal compressive stress (f_d) can be determined as follows:

(i) Determine shear strain coefficient, λ:

$$\lambda = (\lambda_m/\varepsilon_d - 0.3)^{0.5} \qquad \ldots (5)$$

(ii) Determine peak stress and peak strain, f_p and ε_p respectively:

$$f_p = f'_c/\lambda \qquad \ldots (6)$$

$$\varepsilon_p = \varepsilon_o/\lambda \qquad \ldots (7)$$

(iii) If $\varepsilon_d \leq \varepsilon_p$:

$$f_d = f'_c\left[2\left(\frac{\varepsilon_d}{\varepsilon_o}\right) - \lambda\left(\frac{\varepsilon_d}{\varepsilon_o}\right)^2\right] \qquad \ldots (8)$$

(iv) If $\varepsilon_d > \varepsilon_p$:

$$f_d = f_p.(1-\eta^2) \qquad \ldots (9)$$

where

$$\eta = \frac{(\varepsilon_d - \varepsilon_p)}{(2\varepsilon_o - \varepsilon_p)} \qquad \ldots (10)$$

The correlation between the test data and the prediction model was quite good (see Fig. 14). A coefficient of variation of 16% was obtained for points where f_d/f'_c was greater than 0.15.

7. STRESS-STRAIN CHARACTERISTICS OF CONCRETE IN TENSION

The stress circles determined for each of the pure shear test specimens showed that the concrete continued to carry some average tensile stresses even after cracking. These stresses, which are the result of the tensile stresses in the concrete between the cracks, must be less than the tensile cracking strength of the concrete, f_{cr}, but are significantly greater than zero, Fig. 15.

While equilibrium relationships are written in terms of average stresses, it will still be necessary for the reinforcement to transmit the loads across the cracks. At these locations tensile stresses in the concrete cannot assist the

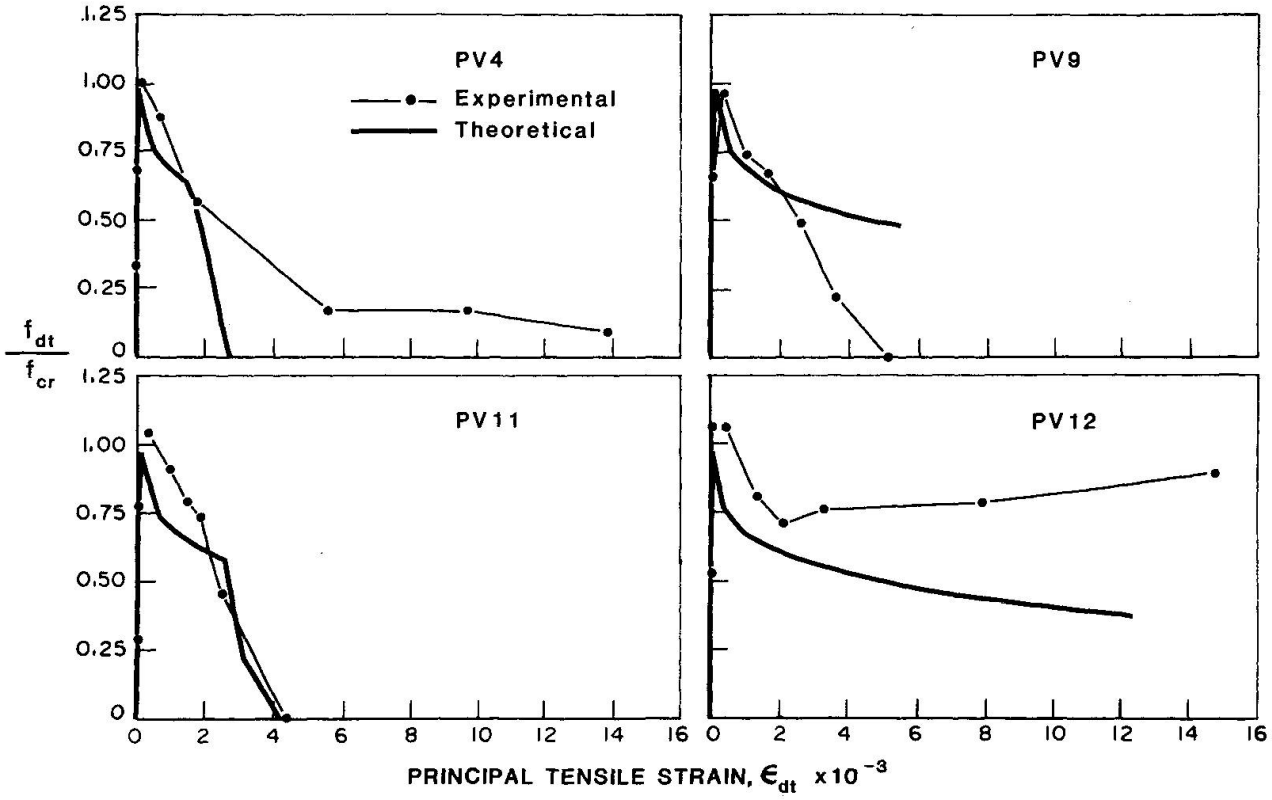

Fig. 15 Principal Tensile Stress-Strain Behaviour of Concrete

reinforcement. Hence, when the average stresses in the reinforcement approach yield, the average tensile stresses in the concrete are assumed to approach zero.

Based on the observed behaviour of the panels, the following procedure is suggested for calculating the average principal tensile stress, f_{dt}, from the average principal tensile strain, ε_{dt}.

(i) Prior to cracking:

$$f_{dt} = (\varepsilon_{dt} - 0.15\,\varepsilon_d) \cdot E_c \leq f_{cr}$$

$$\text{where} \quad E_c = \frac{2f'_c}{\varepsilon_o} \quad \text{and} \quad f_{cr} = 0.33\sqrt{f'_c(\text{MPa})}$$

(ii) After cracking:

$$f_{dt} = f_{cr} \frac{1}{1 + \left(\frac{\varepsilon_{dt}}{.005}\right)^{0.5}}$$

$$\leq \rho_\ell (f_{s\ell y} - f_{s\ell}) \sin^2\theta + \rho_t (f_{sty} - f_{st}) \cos^2\theta$$

It can be seen from Fig. 15 that the predictions of the above model follow the trend of the experimental data. However, as might be expected for a phenomenon dependent on the tensile strength of the concrete and the bond characteristics of the reinforcement, there is considerable scatter in the data. Fortunately, the tensile stresses are only a small component of the total stress circle (Fig. 12). Hence, large errors in the predicted tensile stress will not necessarily result

in large errors in the predicted behaviour. It is, however, necessary to include the contribution of the concrete tensile stresses if accurate predictions of deformation at all stages of loading are to be made.

8. PREDICTING THE RESPONSE OF THE PANELS

The complete shear response of the reinforced concrete elements can be traced by solving for stress and strain conditions as the principal compressive strain, ε_d, is incremented.

For a given value of ε_d, solving for all stress and strain requirements involves an iterative procedure. Two other strain conditions, typically ε_ℓ and θ, must be estimated. Conditions of equilibrium and compatibility are checked, and the estimates adjusted accordingly, until convergence is achieved.

A schematic representation of this solution procedure is given in Fig. 16. A detailed, step by step description follows.

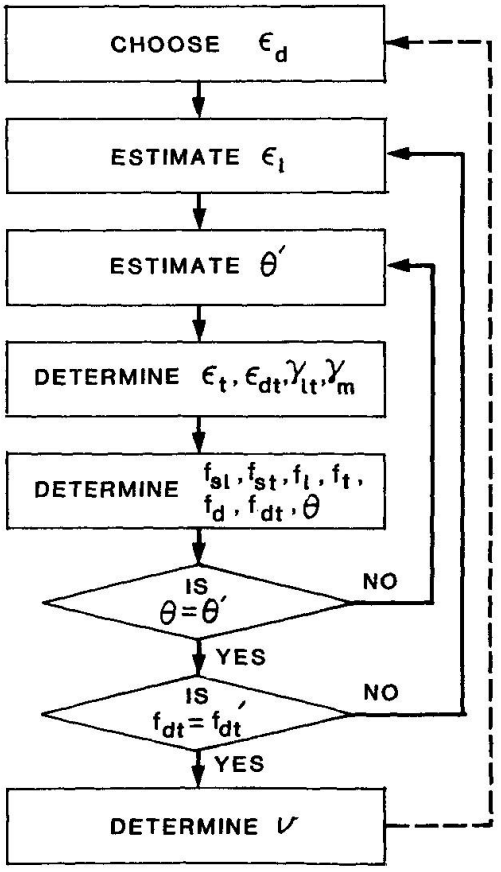

Fig. 16 Solution Procedure for Pure Shear Response of Reinforced Concrete Element

Step 1: Choose value of principal compressive strain, ε_d.

Step 2: Estimate longitudinal strain, ε_ℓ.

Step 3: Estimate angle of inclination of principal compressive strain, θ'.

Step 4: Determine all other strain conditions from the circle of strain, Fig. 17:

(i) Normal shear strain $\gamma_{\ell t}$:

$$\gamma_{\ell t} = \frac{2\,(\varepsilon_\ell + \varepsilon_d)}{\tan\theta'}$$

(ii) Transverse steel strain, ε_t:

$$\varepsilon_t = \frac{\gamma_{\ell t}}{2\,\tan\theta'} - \varepsilon_d$$

(iii) Principal tensile strain, ε_{dt}:

$$\varepsilon_{dt} = \varepsilon_\ell + \varepsilon_t + \varepsilon_d$$

(iv) Maximum shear strain, γ_m:

$$\gamma_m = \varepsilon_t + \varepsilon_\ell + 2\varepsilon_d$$

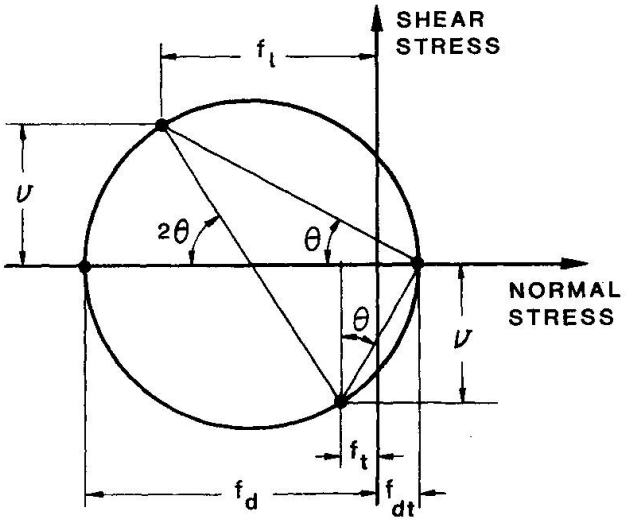

Fig. 17 Equilibrium Conditions for Average Stresses in Concrete

Step 5: Determine stress conditions:

(i) Longitudinal steel tensile stress, $f_{s\ell}$:

$$f_{s\ell} = \varepsilon_\ell \cdot E_s \leq f_{s\ell y}$$

(ii) Transverse steel tensile stress, f_{st}:

$$f_{st} = \varepsilon_t \cdot E_s \leq f_{sty}$$

(iii) Longitudinal concrete compressive stress, f_ℓ:

$$f_\ell = \rho_\ell \cdot f_{st}$$

(iv) Transverse concrete compressive stress, f_t:

$$f_t = \rho_t \cdot f_{st}$$

(v) Concrete principal compressive stress, f_d:

$$\lambda = (\gamma_m/\varepsilon_d - 0.3)^{0.5}$$

$$\varepsilon_p = \varepsilon_o/\lambda$$

$$f_p = f'_c/\lambda$$

$$\eta = (\varepsilon_d - \varepsilon_p)/(2\varepsilon_o - \varepsilon_p)$$

- If $\varepsilon_d \leq \varepsilon_p$, then

$$f_d = \left[2\left(\frac{\varepsilon_d}{\varepsilon_o}\right) - \lambda\left(\frac{\varepsilon_d}{\varepsilon_o}\right)^2\right]$$

- If $\varepsilon_d > \varepsilon_p$, then

$$f_d = f_p.[1.0 - \eta^2]$$

(vi) Concrete principal tensile stress, f_{dt}':

$$f_{cr} = 0.33\sqrt{f'_c\ (\text{MPa})}$$

$$E_c = 2\ f'_c/\varepsilon_o$$

Prior to cracking:

$$f_{dt}' = E_c.(\varepsilon_{dt} - 0.15\ \varepsilon_d) \leq f_{cr}$$

After cracking:

$$f_{dt}' = f_{cr}/\left[1 + \left(\frac{\varepsilon_{dt}}{0.005}\right)^{0.5}\right]$$

but $f_{dt}' < \rho_\ell(f_{s\ell y} - f_{s\ell})\ \sin^2\theta' + \rho_t(f_{sty} - f_{st})\ \cos^2\theta'$

(vii) Angle of inclination of principal compressive stress, θ:

From stress circle, Fig. 18,

$$\theta = \tan^{-1}\left[\sqrt{\frac{f_d - f_\ell}{f_d - f_t}}\right]$$

Step 6: Check compatibility:

Is $\theta = \theta'$?

If yes, go to step 7.
If no, go to step 3.

Step 7: Check equilibrium:

From stress circle, Fig. 18,

$f_{dt} = f_d - f_\ell - f_t$

Is $f_{dt} = f_{dt}'$?

If yes, go to step 8.
If no, go to step 2.

Step 8: Determine shear stress, v, from stress circle, Fig. 18,

$v = (f_d - f_t) \cdot \tan\theta$

Step 9: Increment ε_d and repeat.

$0 < \varepsilon_d \leq 1.5\ \varepsilon_o$

$\Delta\varepsilon_d \approx 0.05\ \varepsilon_o$ to $0.10\ \varepsilon_o$.

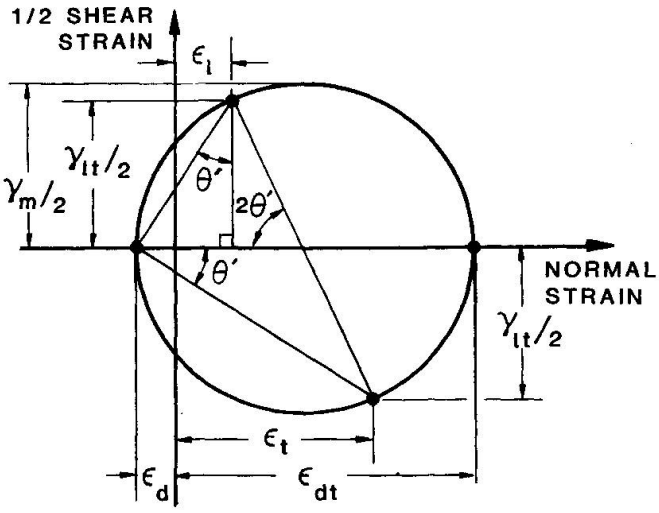

Fig. 18 Compatibility Conditions for Average Strains in Concrete

The above procedure was used to predict the response of the 15 panels loaded in shear. The resulting predicted shear stress - shear strain relationships for these panels are compared with the experimentally determined response in Fig. 19. It can be seen that the theoretical predictions agree well with the experimental observations.

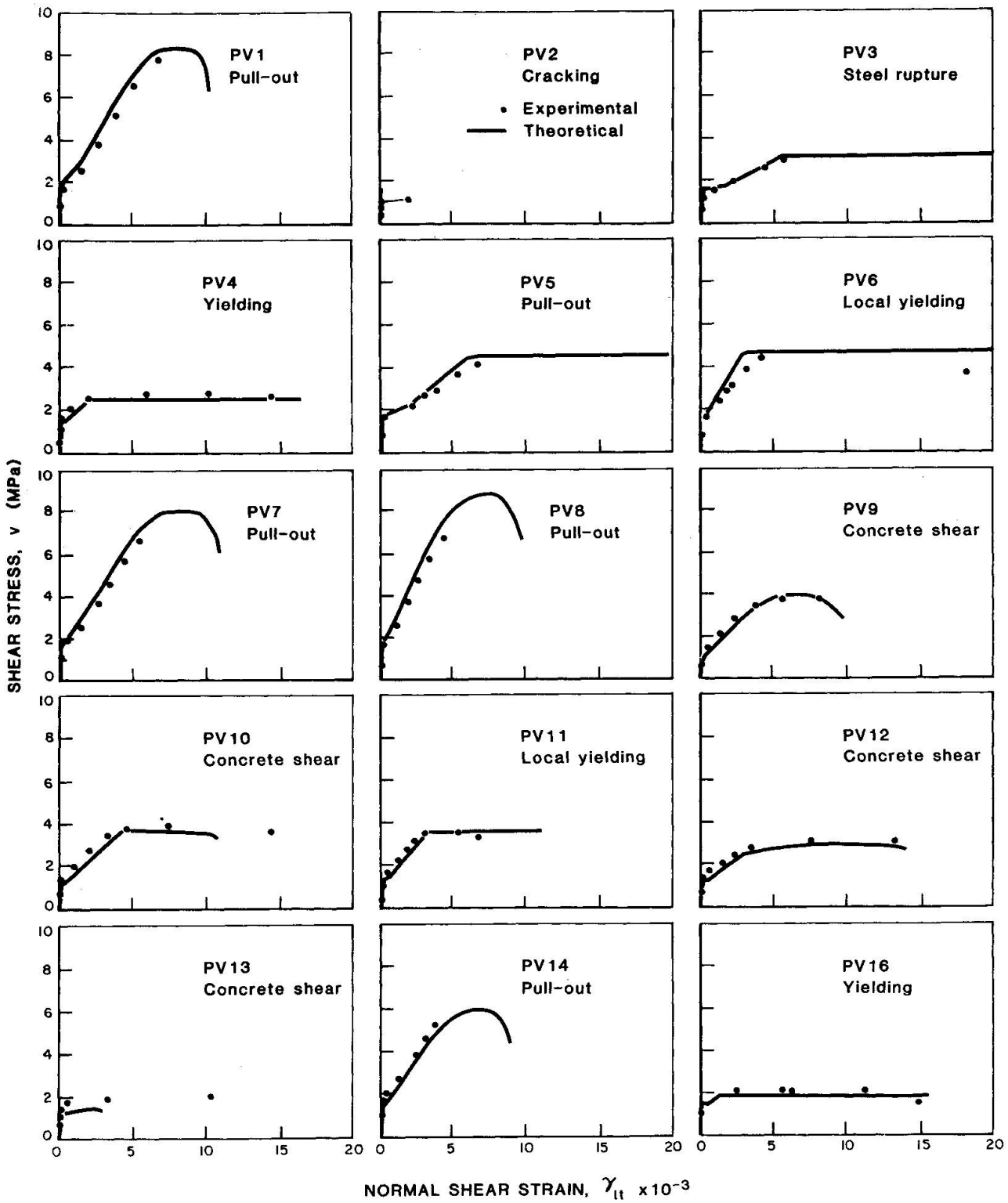

Fig. 19 Shear Stress - Shear Strain Response of 15 Specimens Tested

9. CONCLUDING REMARKS

The results of the 17 panels tested to date have demonstrated that the relationship between the principal compressive stress in the concrete and the principal compressive strain in the concrete is strongly dependent on the co-existing maximum shear strain. Further, it has been found that in order to predict accurately the deformation characteristics of the panel, it is necessary to account for the tensile stresses in the concrete.

Mathematical models were developed to represent the concrete stress-strain characteristics. Using these models, equilibrium conditions based on average stresses, and compatibility conditions based on average strains, it proved possible to predict accurately the behaviour of the panels.

Experimental work currently underway is aimed at investigating the applicability of the models to more complex stress combinations, specifically combined tension and shear, and combined compression and shear. Studies on the influence of reversed cyclic loading are also planned. Hopefully, the material properties determined in this study can be incorporated into general mathematical models which will enable complex reinforced concrete structures to be designed for shear in a rational manner.

10. ACKNOWLEDGEMENT

The research reported in this paper was made possible by a series of grants from the Natural Sciences and Engineering Research Council of Canada. This continuing support is gratefully acknowledged.

11. REFERENCES

1. Collins, M.P.: "Reinforced Concrete Members in Torsion and Shear", IABSE Colloquium on Plasticity in Reinforced Concrete, Copenhagen, May 1979, pp. 119-130.

2. Collins, M.P.: "Investigating the Stress-Strain Characteristics of Diagonally Cracked Concrete", IABSE Colloquium on Plasticity in Reinforced Concrete, Copenhagen, May 1979, pp. 27-34.

Leere Seite
Blank page
Page vide

The Behaviour of Cracks in Plain and Reinforced Concrete Subjected to Shear

Le comportement des fissures en béton armé et non armé

Das Verhalten von Rissen in bewehrtem und unbewehrtem Beton

JOOST C. WALRAVEN
Dr. ir., Research engineer
Stevin Laboratory, Delft University of Technology,
Delft, The Netherlands

SUMMARY
Due to the roughness of their surfaces, cracks in concrete can transmit substantial shear forces. Constitutive equations are derived for cracks in plain and reinforced concrete on the basis of a realistic description of the physical behaviour, in such a way that the influence of the concrete mix properties can be taken into account. Comparisons between theoretical and experimental results are presented. Bearing capacities are derived for cracks in plain concrete under different loading conditions and for cracks in reinforced concrete subjected to pure shear loading. Comparisons are made with existing shear-friction equations.

RÉSUMÉ
Suite à la rugosité de leurs surfaces, les fissures dans le béton ont la possibilité de transmettre des efforts tranchants considérables. Des rélations entre les contraintes et les déplacements sont données pour des fissures en béton armé et non armé, sur base d'une description réaliste du comportement physique, de telle manière qu'il est possible de tenir compte de l'influence des propriétés du béton.
Des comparaisons sont établies entre les résultats théoriques et expérimentaux. Les résistances sont données pour des fissures en béton non-armé, soumises à des sollicitations différentes et pour des fissures en béton armé soumises au cisaillement pur.

ZUSAMMENFASSUNG
Infolge der Rauhigkeit ihrer Rissufer können Risse im Beton beträchtliche Schubkräfte übertragen. Die Beziehungen zwischen Spannungen und Verschiebungen sind auf der Grundlage einer wirklichkeitsnahen Beschreibung des Materialverhaltens für Risse in unbewehrtem und bewehrtem Beton abgeleitet, derart dass auf den Einfluss der Betonzusammensetzung Rücksicht genommen werden kann. Theoretische und experimentelle Ergebnisse sind verglichen.
Die Tragfähigkeit von Rissen in unbewehrtem Beton unter verschiedenen Beanspruchungsarten und von Rissen in bewehrtem Beton unter reiner Schubbeanspruchung ist abgeleitet.

1. INTRODUCTION

In many concrete structures the capacity of cracks to transmit shear forces plays an important role. Cracks, which have been formed due to flexural action, may be subjected to shear forces as a result of other loading configurations. Such a situation occurs for instance in a long bridge, which is supported on hinged columns in the longitudinal axis, so that the torsional moments have to be resisted by the abutments. In such a case open cracks have to be able to transmit shear forces, to warrant the full load bearing capacity. In the design of nuclear power vessels the behaviour of cracks subjected to shear loading is directly taken into account. Design criteria [1] require that the structure be designed to withstand the simultaneous occurence of an internal pressurization, so that horizontal and vertical cracks are formed, and the inertia forces generated by a strong motion earthquake.

The variation of external loading conditions is not a necessary condition for the occurence of shear forces in cracks. The anisotropic properties of cracked reinforced concrete may as well cause shear action in the cracks. The shear capacity of beams without shear reinforcement depends essentially on the resistance of the cracks against shear displacements [2,3,4].
Up to now the understanding of what really happens in a crack subjected to shear forces was not satisfactory. Examples of some frequently encoutered simplifications are shown in Fig. 1a,b. In Fig. 1a the whole mechanism is reduced to the case of simple friction between two interfaces ($\tau = \mu.\sigma$). Fig. 1b considers the possibility of crack dilatancy. If the undulations of the crack faces are considered to be rigid and frictionless, the mechanism can be described by a similar relation $\tau = (\text{tang. } \phi)\,\sigma$. If the undulations are considered as elastic a description is more difficult: during shear displacement at constant crack width both a shear stress τ and a normal stress σ are developed. Further complications occur if it is assumed that the undulations are not perfectly elastic and frictionless. Due to all these incertainties only provisional equations were available for the use in non linear finite element programs, so that even the most advanced programs could not be used with full profit.
It was concluded that there is a need for a better understanding of the phenomenon, improved constitutive equations and better defined strength limits. This paper focusses on these questions. The work was carried out within the scope of the project "Concrete Mechanics" supported by the CUR-VB, the Netherlands Committee of Concrete Research.

2. CONSTITUTIVE EQUATIONS

2.1 Cracks in plain concrete

In order to obtain constitutive equations with a wide range of applicability it is necessary to describe the physical reality as accurate as possible. Hence first the fundamental behaviour is studied.
In general the strength and the stiffness of the aggregate particles are higher than those of the matrix, consisting of hardened cement paste and small particles (f.i. < 0.1 mm). The contact area between the two materials, the bond zone, is the weakest link of the system. Hence, cracking occurs commonly through the matrix, but along the circumference of the aggregate particles. Only in the case of high strength concretes (with high matrix strength) and lightweight concrete (with low particle strength) are cracks observed running both through the ma-

trix and the particles. Generally crack faces are encountered which have a structure as indicated in Fig. 2.

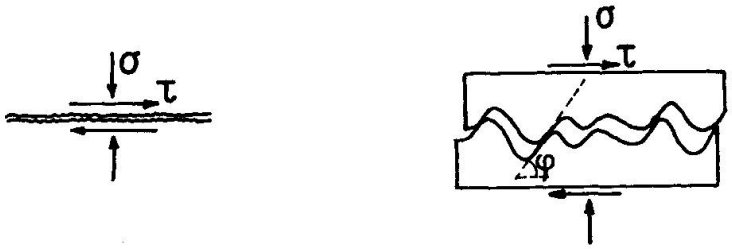

Fig. 1 a, b. Simplified representation of crack behaviour

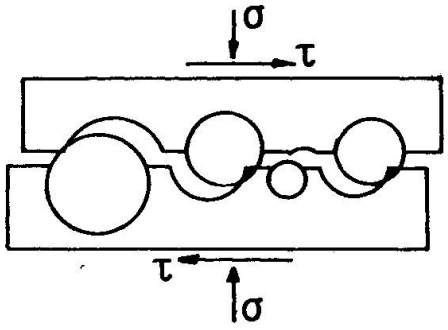

Fig. 2. More realistic representation of crack behaviour

It can be expected that, during shear displacement of the crack faces, contact areas develop on the surface of the particles exceeding from one of the crack faces. The behaviour in detail, for a single particle, is represented in Fig. 3.

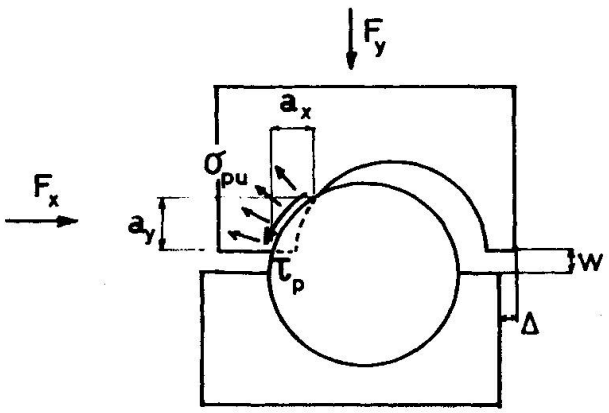

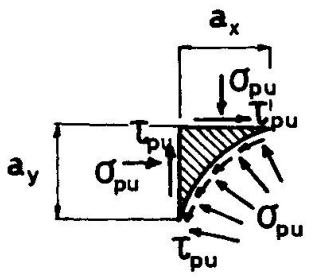

Fig. 3a. Formation of a contact area b. Equilibrium at a contact area

If the shear stress τ on the plane of cracking is increased and crack opening is counteracted by a restraining stress σ, a mechanism will develop, which can be described as follows: the contact areas tend initially to slide: as a result of this sliding, the contact areas are reduced, which results in high contact stresses, so that further deformation occurs. Hardened cement paste is a visco-elastic material: the deformation, provoked by stresses is only partially elastic, for the other part plastic. Under multi-axial stresses, as in the area between the aggregate particles in concrete, large plastic deformations can

occur as a result of pore volume reduction. Since the plastic deformations are expected to dominate the elastic deformations, the stress-strain relation of the matrix is assumed to be rigid-plastic, with a yielding stress σ_{pu}. If we consider the case that both τ and σ are monotonically increasing, the contact areas are always about to slide, so that (Fig. 3a)

$$\tau_p = \mu \sigma_{pu} \tag{1}$$

The equilibrium conditions for one particle (Fig. 3b) can be formulated as:

$$F_x = \sigma_{pu}(a_y + \mu a_x) \tag{2a}$$

$$F_y = \sigma_{pu}(a_x - \mu a_y) \tag{2b}$$

a_x and a_y being the projected contact areas, parallel and normal to the crack plane. Taking into account all particle contributions over a unit crack area, the equilibrium is described by

$$\tau = \sigma_{pu}(\Sigma a_y + \mu \Sigma a_x) \tag{3a}$$

$$\sigma = \sigma_{pu}(\Sigma a_x - \mu \Sigma a_y) \tag{3b}$$

Since Σa_x and Σa_y are functions of the crack displacements w and Δ, the equations 3a,b are the generalized constitutive equations. In order to obtain expressions for concretes with a particular strength and composition, the values of the parameters σ_{pu}, μ should be known, and Σa_x and Σa_y should be expressed as functions of the crack width w, the shear displacement Δ and the aggregate characteristics.
The matrix yielding strength σ_{pu} must have a direct relation with the uniaxial concrete compressive strength f'_{cc}. Although no adequate data are found in literature concerning this relation, it can be expected that the value σ_{pu} is higher than the uniaxial compressive strength f'_{cc}, because this value f'_{cc} is limited by progressive microcracking between particles and matrix and not by the matrix strength.
Also about the coefficient of friction μ no specific data are found in the literature. An indication is given by tests of Weiss [5], who found for concretes and concrete components (aggregates, mortars) values, ranging from 0.4-0.6.
The projected contact areas Σa_x and Σa_y depend on both the displacements between the crack faces and the concrete mix composition, particularly the volume fraction of the aggregate particles and their grading curve. If it is assumed that the central crack line is straight, the aggregate particles are spherical (Fig. 2) and the distribution of the particles over the volume is random, the most probable values of Σa_x and Σa_y can be found by a statistical analysis. The expressions for Σa_x and Σa_y are derived in [6].

Experiments

Tests have been carried out for two reasons: to find out if the theoretical model makes sense anyhow and, if it does, to establish the expressions for σ_{pu} and μ.
The set-up of the tests is represented in Fig. 4. The specimens were precracked before actual testing. Crack opening during the actual shear test was counteracted by external restraining bars, clamping the two specimenhalves together.

The displacements between the crack faces, both in normal and parallel direction were recorded by two combinations of displacement gauges at both sides of the specimen. Variables were:

- the concrete strength: f'_{cc} = 13, 35, 59 N/mm^2
- the maximum aggregate particle diameter: D_{max} = 16, 32 mm
- the concrete type: normal, lightweight
- the initial crack width: w = 0.01, 0.20, 0.40 mm
- the stiffness of the external restraining system

All the concrete mixes were composed according to ideal Fuller curves.

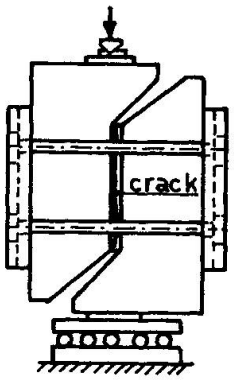

Fig. 4. Specimen with external restraining bars for tests on cracks in plain concrete

Results

For all the concrete mixes the grading curve (Fuller), the maximum particle diameter D_{max}, and the aggregate volume fraction p_k, were known. Writing the constitutive equations 3a, b as

$$\tau = \sigma_{pu} \{ \Sigma a_y(p_k, D_{max}, \Delta, w) + \mu \Sigma a_x(p_k, D_{max}, \Delta, w) \} \quad (4a)$$

$$\sigma = \sigma_{pu} \{ \Sigma a_x(p_k, D_{max}, \Delta, w) - \mu \Sigma a_y(p_k, D_{max}, \Delta, w) \} \quad (4b)$$

the only unknown values are σ_{pu} and μ.
Apart from the theoretical relations a large number of combinations (τ,σ,Δ,w) were obtained from the tests. Comparing the theoretical with the experimental relations, it was found that excellent fitting of the curves was obtained for

$$\sigma_{pu} = 6.39\, f'^{0.56}_{cc} \quad (N/mm^2) \quad (5)$$

$$\mu = 0.40 \quad (6)$$

for all the concrete mixes (except lightweight concrete). These comparisons are shown for four mixes in the Figures 5-8*).

It should be noted that only two parameters (σ_{pu},μ) are available for curve fitting, so that only two lines per diagram (f.i. for w = 1.0 mm) can actually be fitted. The fact that it turns out that automatically all the other lines fit, demonstrates the validity of the theory.

*) The agreement between theory and experiments in these figures is even slightly better than shown earlier in [6], since here a correction is applied for the elastic deformation of the concrete between the measuring points (located 50 mm from the crack to both sides) which was earlier neglected.

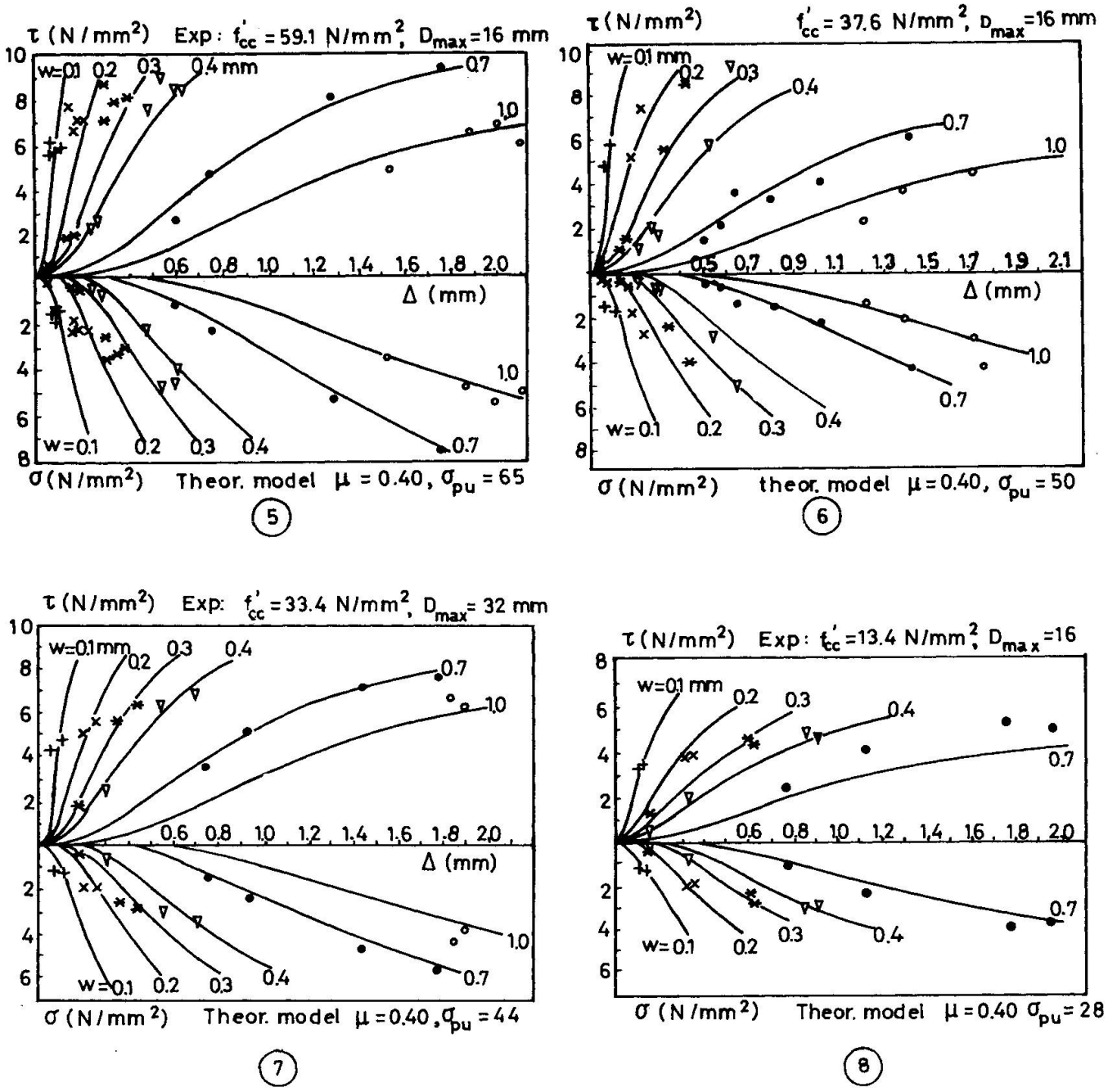

Fig. 5-8. Comparison between experimental values and theoretical lines for several concrete mixes

Fig. 5: f'_{cc} = 59.1 N/mm^2, D_{max} = 16 mm, p_k = 0.75
" 6: f'_{cc} = 37.6 " , D_{max} = 16 mm, "
" 7: f'_{cc} = 33.4 " , D_{max} = 32 mm, "
" 8: f'_{cc} = 13.4 " , D_{max} = 16 mm, "

Because τ and σ are proportional to $f_{cc}'^{0.56}$ (eq. 5) it is possible to represent the relations in a more general way. This is done in Fig. 9 and 10.

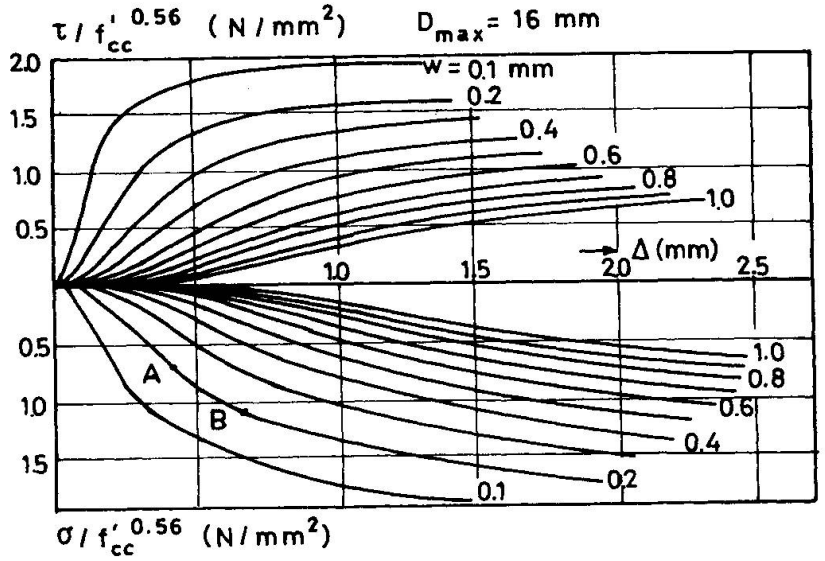

Fig. 9. Generalized constitutive relations for a crack in plain concrete ($13 < f_{cc}' < 60$ N/mm^2, D_{max} = 16 mm, p_k = 0.75)

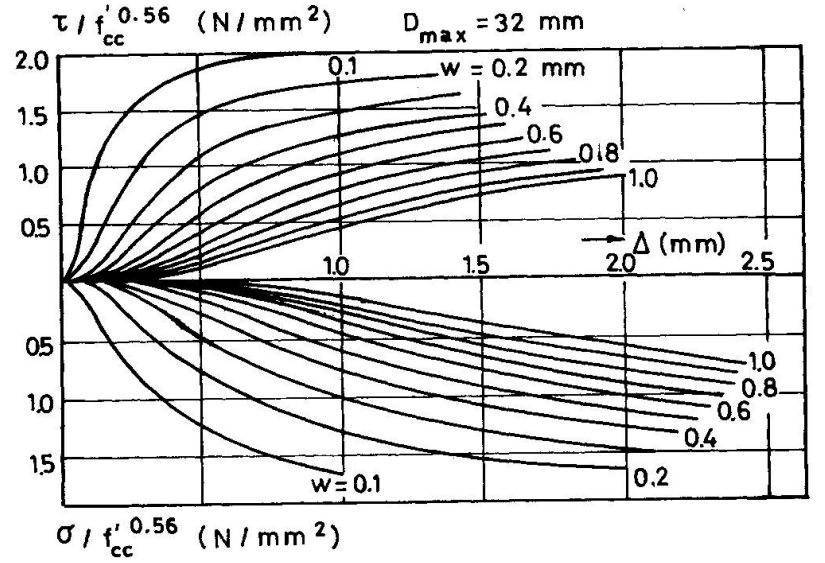

Fig. 10. The same as Fig. 9, but for $13 < f_{cc}' < 60$ N/mm^2, D_{max} = 32 mm, p_k = 0.75

Comparing both figures 9(for D_{max} = 16 mm) and 10 (for D_{max} = 32 mm), it is seen that the differences are very small. Only for large crack widths the differences in the development of τ as a function of Δ are not insignificant. This phenomenon is also exhibited by the test (Fig. 6 and 7). The theoretical model enables a parameter study. Detailed data about this study, focussing on the influence of μ, the contribution of individual aggregate fractions, the influence of the grading curve and the behaviour under cyclic loading, are found in [6].

For the range of values tested simplified linear relations have been derived:

$$\tau = -\frac{f'_{cc}}{30} + \{1.8\, w^{-0.80} + (0.234\, w^{-0.707} - 0.20) f'_{cc}\}\Delta \quad (\tau \geq 0) \qquad (7a)$$

$$\sigma = -\frac{f'_{cc}}{20} + \{1.35 w^{-0.63} + (0.191\, w^{-0.552} - 0.15) f'_{cc}\}\Delta \quad (\sigma \geq 0) \qquad (7b)$$

(N/mm^2).
Fig. 11 shows these graphs for two of the concrete mixes.

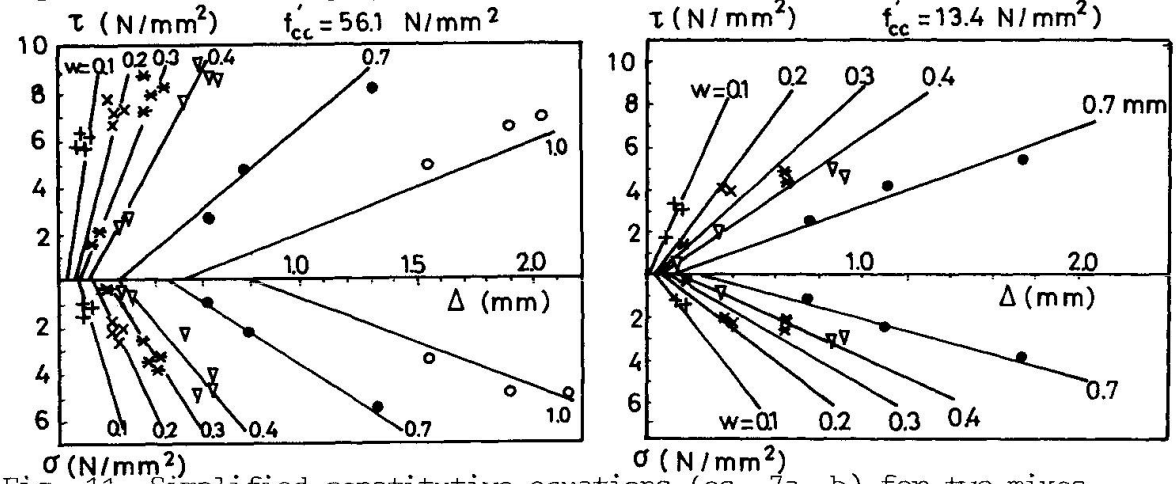

Fig. 11. Simplified constitutive equations (eq. 7a, b) for two mixes (f'_{cc} = 56.1 N/mm^2, left) and f'_{cc} = 13.4 N/mm^2, right)

2.2 Cracks in reinforced concrete

It is obvious to expect that cracks in reinforced concrete behave essentially in the same way as cracks in plain concrete, because the mechanism seems to be only slightly different: the restraining force against crack widening is not provided by an external system but internally by the reinforcing bars. The stiffness of this internal restraining system is governed by bond between bars and concrete and the yielding stress of the steel. Furtheron dowel action of the reinforcing bars is an additional component. It can however be demonstrated that, within practical limits, dowel action can be neglected without committing a significant error [6].

Experiments

Test have been carried out on specimens as represented in Fig. 12. Variables were:
- concrete strength: f'_{cc} = 20, 30-35, 56 N/mm^2
- maximum particle diameter: D_{max} = 16, 32 mm
- grading curve (continuous, discontinuous)
- reinforcement ratio: ρ_o = 0.14 - 3.35%
- bar diameter
- concrete type: normal, lightweight
- inclination of the reinforcing bars (45-135° to the crack plane)

The specimens were precracked (w ≈ 0.01-0.03 mm) and subsequently subjected to a monotonically increasing shear load. The displacements between the crack faces in normal and parallel direction were measured.
A full description is given in [7].

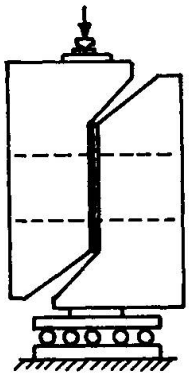

Fig. 12. Experimental set-up for tests on cracks, crossed by embedded reinforcement

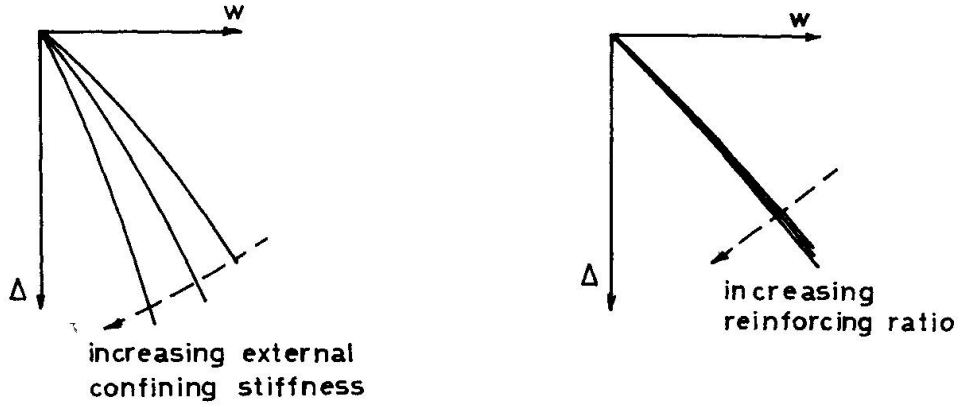

Fig. 13. Crack opening paths for cracks in plain (a) and reinforced (b) concrete with varying restraining stiffness

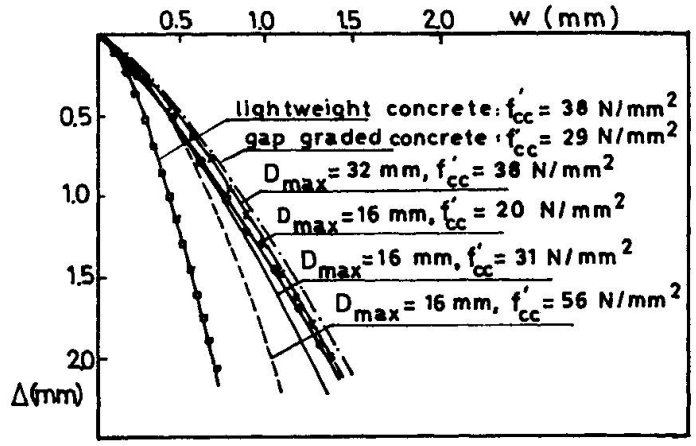

Fig. 14. Average crack opening paths for different mixes

Results

The results of the tests on specimens with embedded reinforcement appeared to be essentially different from the results of the tests on cracks in plain concrete.
In the tests on unreinforced cracks it appeared that the external restraining stiffness has a significant influence on the crack opening path (w,Δ path). This can be shown with the aid of Fig. 9. Point A is attended with an arbitrary restraining stiffness (normal stress σ_A for a crack width w = 0.2 mm). If the restraining stiffness is higher ($\sigma_B > \sigma_A$ for the same crack width) this results in a larger value of Δ . So the dependency of the crack opening path on the external restraining stiffness can, in a general way, be represented as in Fig. 13a. In the tests on specimens with embedded bars the crack opening direction remained unaffected by the restraining stiffness (or reinforcement ratio) (Fig. 13b).
A similar type of behaviour was earlier reported by Mattock [8]. So, apparently the relations between stresses and displacements cannot be described on the basis of the relations derived for cracks in plain concrete (eq. 4, 5, 6) even if the restraining stiffness (load-slip relations) of the reinforcing bars were accurately known. The average crack opening paths for the different series, each of which consisted of 4 specimens of one concrete quality and reinforcement ratios of 0.56, 1.12, 1.68 and 2.23%, are represented in Fig. 14.

Four different concrete mixes with strengths of $20 < f'_{cc} < 40$ N/mm^2 displayed hardly any difference. The high strength mix (f'_{cc} = 56 N/mm^2) exhibited a slightly steeper crack opening path, possibly caused by breaking through of a number of the aggregate particles. The lightweight concrete showed a considerably steeper crack opening path (all lightweight particles break through). Apparently there is a fundamental difference in behaviour between unreinforced and reinforced cracks. This difference may be caused by the bond between the deformed steel and the concrete. It is known that, due to this bond, the crack width in reinforced concrete is not constant, but decreases coming nearer to the bars (Fig. 15a). It is probable that, due to this local crack width reduction higher stresses occur in the concrete around the bars, resulting in secondary cracking. In this way local compressive struts could be formed (Fig. 15b), which force the two halves of the specimen to follow a certain "cri-

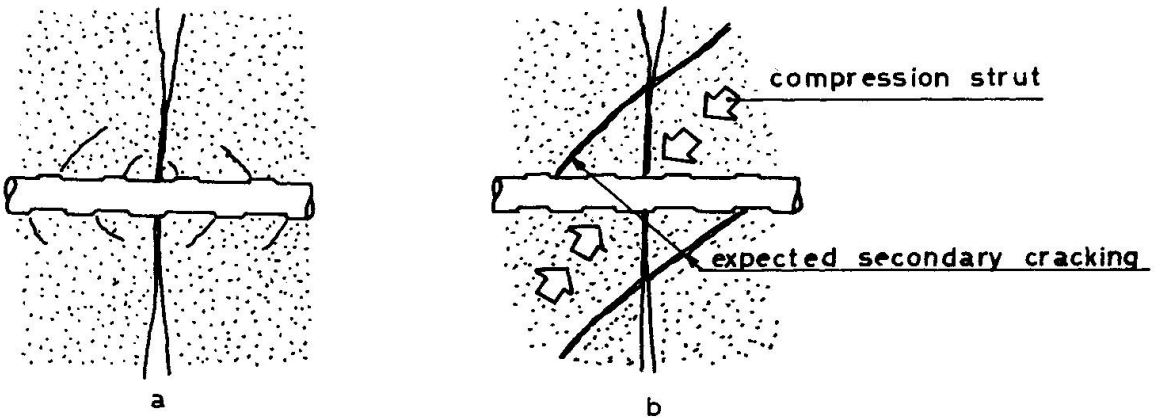

Fig 15 a. Decrease of crack width around reinforcing bar
b. formation of compression struts

tical" crack opening path. The presence of such a mechanism seems the more probable because additional tests on specimens, in which soft sleeves were secured around the reinforcing bars over a short distance to both sides of the crack, so that not such a severe crack width reduction has to be expected, displayed a behaviour similar to that of the specimens with external bars.
It turned out that the relation between τ, σ, w and Δ could be described by a model as shown in Fig. 16. Here is

F_s = the axial force in the embedded steel reinforcement (the pull-out stiffness should be known)

F_d = dowel force provided by the reinforcement. On basis of tests of other authors it was derived that the dowel force for one bar can be approximated by

$$F_d = 10(w + 0.2)^{-1} \Delta^{0.36} \phi^{1.75} f'^{0.38}_{cc} \qquad (N, mm, N/mm^2)$$

F_{iv}, F_{ih} = the forces due to pure aggregate interlock as described by eq. (4) or (7)

S = strut action, provided by hinged compression struts with infinite stiffness. The direction of the struts depends on the position of the crack faces (w,Δ) and is defined such that the critical w, Δ path cannot be exceeded. The struts are only active if compressed. The direction is always normal to the w,Δ path. The critical crack opening path for the concretes with $20 < f'_{cc} < 40$ N/mm^2, defined such that both the author's and Mattocks [8] tests (with large initial crack widths) could be described as

$$\frac{d\Delta}{dw} = w^{0.18} (1.65 + 2.10\, w) - 1.5\Delta \qquad (mm)$$

Undoubtfully these phenomena need further study. It should be investigated if the profilation of the bars has a governing influence on the behaviour (smooth bars may be expected to give no crack width reduction and consequently to display a behaviour similar to that of external bars. Furtheron it should be studied if such type of behaviour also occurs in the case of combined shear and tension, perpendicular to the crack.

3. ULTIMATE BEARING CAPACITIES

3.1 Cracks in plain concrete

On the basis of the theory and the experiments a number of different conditions can be analysed.

3.1.a Cracks in plain concrete, not subjected to a normal compressive stress

Studying the nature of the equations (4a,b) represented in the Figs. 9 and 10, an interesting property is found: if a pair of lines for an arbitrary, constant crack width is considered, it is seen that the σ,Δ line intersects the abscis and that the τ-Δ line goes through the origin (Fig. 17). This shows that a crack can resist a shear stress even in the case that no normal compressive stress is available. For a crack width w, equilibrium is obtained for $\tau=\tau_1$, $\Delta=\Delta_1$, $\sigma = 0$.
If $\tau > \tau_1$, and the same crack width should be maintained, equilibrium can only be obtained for $\sigma > 0$: if $\sigma = 0$ an increase of the crack width (overriding of the crack faces) will occur. However, no equilibrium is possible any more (Fig. 17 $\tau_2 < \tau_1$).

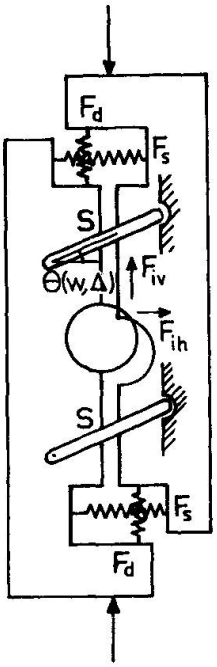

Fig. 16. Schematic representation of forces in a reinforced crack

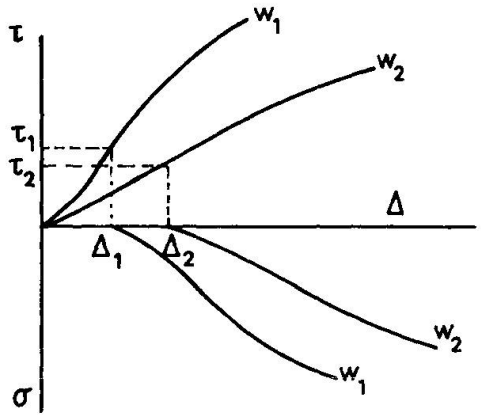

Fig. 17.

This "stick-slip" behaviour can be explained considering the crack on particle level.
Fig. 18a shows the equilibrium condition for a small shear force: the external shear force is internally reacted by the shear and normal stresses at the contact area. If the external shear force increases, the contact area is enlarged, resulting in internal stresses which are larger but the resultant of which is inclined in another direction. The external shear force is limited due to the fact that at a certain degree a deformation, the direction of the internal reaction is turned to such an extent that no equilibrium can be obtained any more and sliding occurs (Fig. 18b).

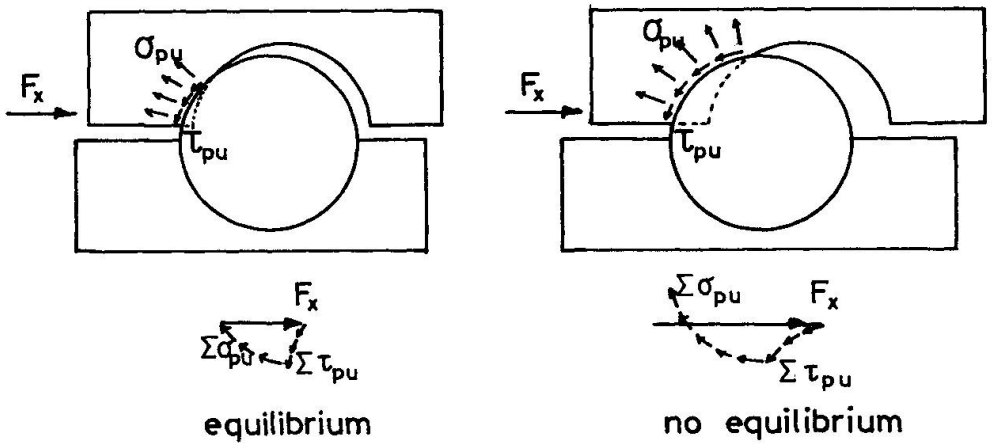

Fig. 18. Stress conditions at pure shear loading

Fig. 19 shows a number of results obtained in the tests with external bars (Fig. 5); the maximum shear stress τ_u was supposed to be reached at the load increment just before the external bars were observed to be stressed (smallest reading $\sigma = 0.003$ N/mm^2).

3.1.b Cracks in plain concrete, the widening of which is prevented

Fig. 9 and 10 show that, theoretically, a maximum shear stress level is reached for every crack width. This maximum is reached if the maximum total contact area is reached (Fig. 3).
Due to the set-up of the tests, permitting an increase of the crack width during loading, no values were available to control the ultimate shear level, reached for constant crack widths. Therefore the theoretical values (Figs. 9,10) have been compared with the results of tests carried out at the TU-Munich [9]. Fig. 20 represents this comparison. It turned out that the theoretical lines (for D_{max} = 16 mm) are slightly conservative compared with the experimental values (D_{max} = 8-16 mm).

3.1.c Cracks in plain concrete, subjected to a normal compressive stress

If a crack, after opening, is subjected to a normal compressive stress, it will not close perfectly. Basing oneself on a residual value of w = 0.1 mm, the ultimate shear stress τ_u can be read as a function of the normal compressive stress in the diagrams of the Figs. 9 and 10. Fig. 21.a shows the theoretical function, compared with a number of experimental results. The values of the coefficient of friction for the crack on macro-scale $\mu_e = \tau/\sigma$ are represented in Fig. 21b. It is shown that μ_e decreases with increasing values of the normal compressive stress.

3.2. Cracks in reinforced concrete

The ultimate resistance of cracks in reinforced concrete, subjected to shear loading, has been discussed many times and several expressions for the bearing capacity have been suggested [10,11,12]. It is striking that in these expressions only a subordinate role has been attributed to the concrete strength, whereas the previous analysis of the mechanism demonstrates that the matrix strength (directly related to the concrete strength) is one of the most important variables.
The expression which is most frequently used, providing a lower bound is

$$\tau_u = 1.4 + 0.8\ \rho f_{sy} \qquad (N/mm^2) \qquad (10)$$

with

$$\tau_u < 0.3\ f'_{ccyl}$$

which is known as the "modified shear-friction equation".
The concrete strength has here only been used as an upper limit, but not as an influencing variable for lower values of ρf_{sy}.

Fig. 21a showed a curve for an unreinforced crack, subjected to an external compressive stress. If reinforcement is applied, the force which is developed in the bars acts roughly in the same way: it prevents the crack from opening. However, there are a number of differences which should be noted:

- whereas in an unreinforced crack the confining stress acts to close the crack, in a reinforced crack the maximum restraining force is only reached at yielding of the steel, at a considerably larger crack width.

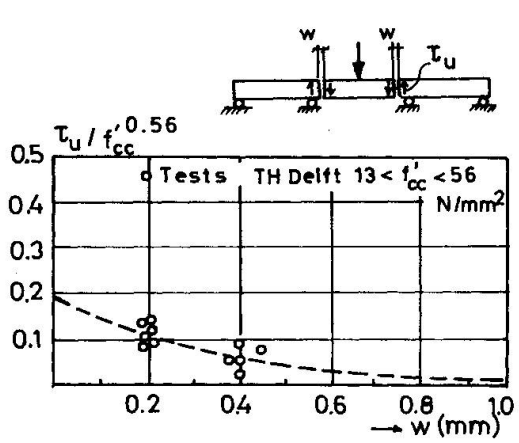

Fig. 19. Shear resistance of an unreinforced crack not subjected to any external normal force

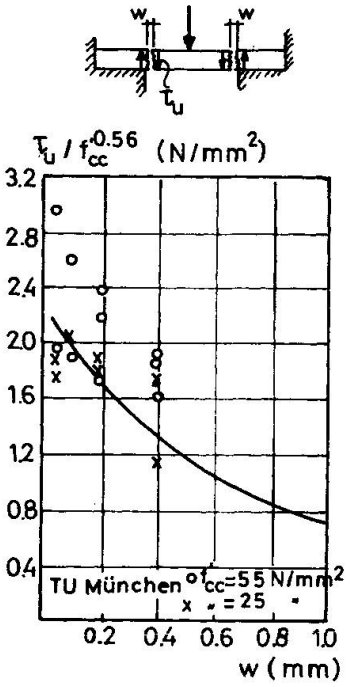

Fig. 20. Shear resistance of an unreinforced crack, the widening of which is prevented

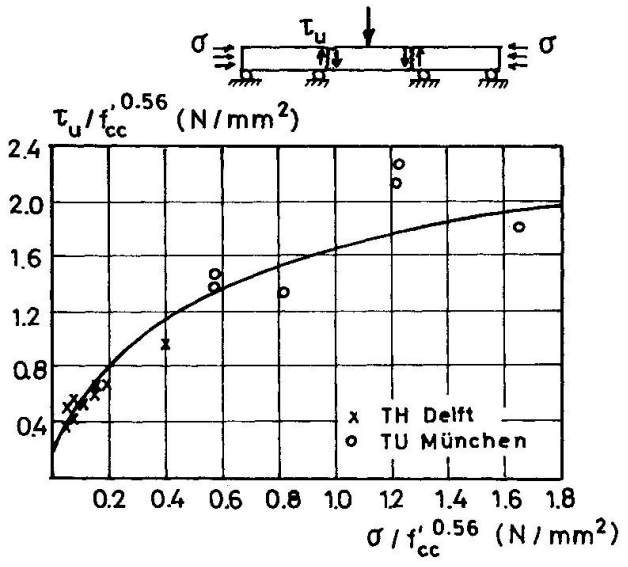

Fig. 21a. Shear resistance of an unreinforced crack, subjected to a normal compressive stress

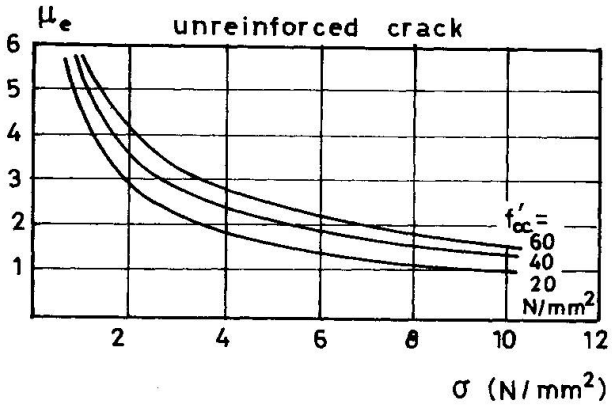

Fig. 21b. Effective coefficient of friction of an unreinforced crack

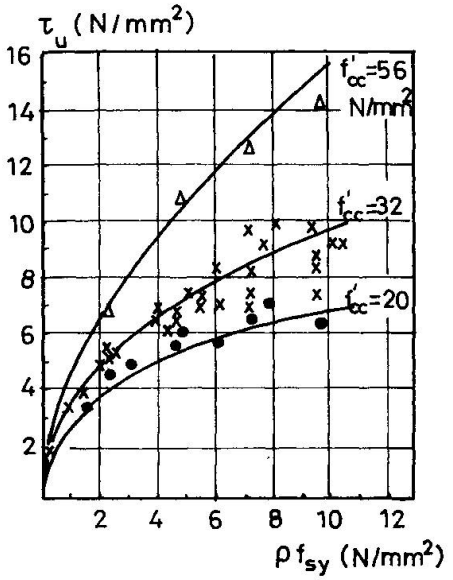

Fig. 22. Shear resistance of a reinforced crack

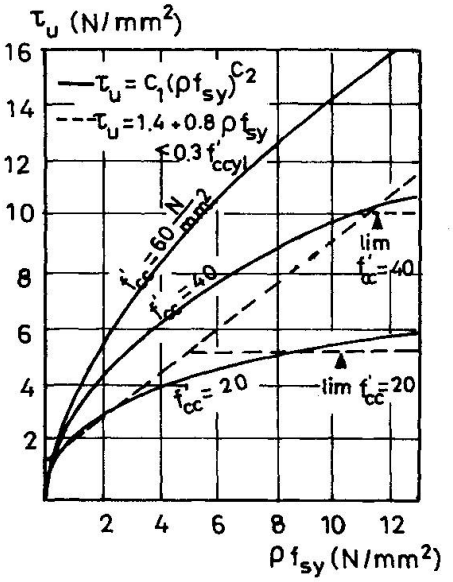

Fig. 23. Comparison between lower bounds according to eq. (10) and (12)

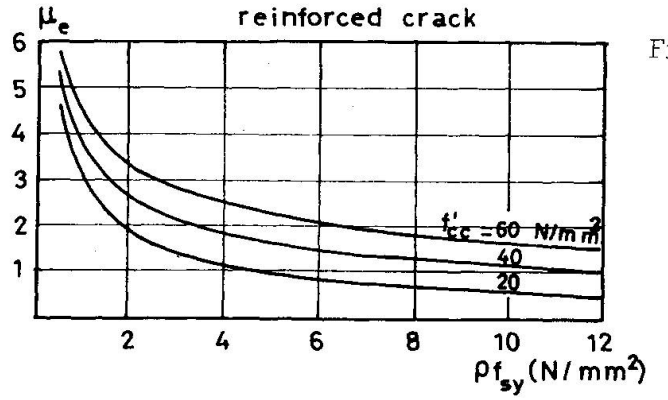

Fig. 24. Effective coefficient of friction for a reinforced crack

- as it was demonstrated before, there is a fundamental difference between the behaviour of unreinforced and reinforced cracks, probably due to crack width reduction (Fig. 15). However, the utmost part of the shear is still transferred across the crack via the contact areas between particles and matrix [6].

An increase of the concrete strength may be expected to have a positive influence on the shear resistance for three reasons:

- the matrix strength is enlarged so that a greater resistance against deformation of the crack faces is obtained.
- better bond between bars and concrete causes yielding at a smaller crack width [13] so that a larger potential contact area is available.
- by virtue of the increase of the shear resistance, resulting from the two previous points, the transverse stresses on the reinforcing bars will be larger, improving again the bond characteristics: a greater pull-out stiffness is obtained, which results in a secondary reduction of the crack width at yielding.

It seems to be realistic to assume that the relation between the ultimate shear stress τ_u and the restraining normal stress ρf_{sy} is of comparable shape as the relation between τ_u and σ for an unreinforced crack (Fig. 21a). In a generalized way this relation can be expressed as:

$$\tau_u = c_1(\rho f_{sy})^{c_2} \qquad (N/mm^2) \qquad (11a)$$

where c_1 and c_2 are constants, defining the exact shape and position. For the previously discussed reasons c_1 and c_2 may be expected to be primarily functions of the concrete strength f'_{cc}. An analysis of the own results (28 tests) and a number of tests carried out by Mattock (21 tests - series 2, 3, 4, 5 [14]) showed that good agreement is obtained for

$$c_1 = f'^{0.36}_{cc} \qquad (N/mm^2) \qquad (11b)$$

$$c_2 = 0.09\, f'^{0.46}_{cc} \qquad (\text{"} \quad) \qquad (11c)$$

The average value of $\tau_{u,exp}/\tau_{u,th}$ for the 49 tests (all normal weight concrete) was 0.98 with a standard deviation of 0.10 (Fig. 22). So a 5%-lower bond is obtained with

$$\tau_u = 0.85\, c_1(\rho f_{sy})^{c_2} \quad (N/mm^2) \qquad (12)$$

Fig. 23 displays a comparison between the lower bounds according to the "modified shear friction equation" (10) and the improved equation (12). It is seen that the "modified shear friction equation" is rather conservative for higher concrete strengths. The use of (12) could result in a saving of up to 50 % of the reinforcement.
Fig. 24 shows the effective coefficient of friction μ_e based on eq. (11). It is seen that the lines are lower than the comparable ones for unreinforced cracks.
As was argued before the stress condition in the specimens is important. This was confirmed by comparing the equation (11) with the results of "pull-off" specimens, where tensile stresses instead of compressive stresses are acting perpendicular to the bars (Mattock [10], series 8, 6 tests). The average value of $\tau_{u,exp}/\tau_{u,th}$ (eq. 9) was indeed only 0.77, which can be explained by worse bond behaviour of the reinforcing bars.

4. CONCLUSIONS

- The transmission of shear and normal stresses across cracks in plain concrete can be explained on the basis of the behaviour on particle level. Constitutive equations can be derived, based on physical considerations, taking into account all concrete mix properties.
- There is a fundamental difference in behaviour between cracks in plain concrete and cracks in reinforced concrete.
- The shear-friction equations as actually used in practive give too conservative results for high strength concretes. An improved formulation for the shear resistance can be derived taking account of the concrete strength f'_{cc} and the mechanical reinforcement ratio ρf_{sy}.

5. NOTATIONS

a_x, a_y	projected contact areas parallel and normal to the crack
f'_{cc}	cube crushing strength (150 mm^3)
f_{sy}	yielding stress of the steel
p_k	volume fraction of the aggregate
w	crack width
D_{max}	maximum particle diameter
ρ	reinforcement ratio
μ	coefficient of friction (particle-matrix)
μ_e	effective coefficient of friction (crack on macro scale)
σ	stress normal to crack
σ_{pu}	matrix yielding stress
τ	shear stress
τ_p	shear stress on particle
Δ	shear displacement
ϕ	bar diameter

6. REFERENCES

[1] ACI-Committee 349: "Criteria for reinforced concrete nuclear power containment structures", ACI-journal, Vol. I, January 1972, pp. 2-28.

[2] TAYLOR, H.P.J.: "The fundamental behaviour of reinforced concrete beams in bending and shear", ACI-Special Publication SP-42, "Shear in reinforced concrete", 1974, Vol. I, pp. 43-78.

[3] FENWICK, R.C., PAULAY, T.: "Mechanisms of shear resistance of concrete beams", Journal of the Structural Division ASCE, vol. 94, No. ST10, Proc. Paper 2325, 1968, pp. 2325-2350.

[4] WALRAVEN, J.C.: "The influence of depth on the shear strength of lightweight concrete beams without shear reinforcement", Report No. 5-78-4, May 1978, Stevin Laboratory, Delft University of Technology, The Netherlands.

[5] WEISS, R.: "Ein Haufwerkstheoretisches Model der Restfestigkeit geschädigter Betone", Dissertation TU Braunschweig 1978, pp. 37-47.

[6] WALRAVEN, J.C.: "Aggregate interlock: a theoretical and experimental analysis", Dissertation, Delft University of Technology, The Netherlands, Oct. 1980.

[7] WALRAVEN, J.C., VOS, E., REINHARDT, H.W.: "Experiments on shear transfer in cracks in concrete. Part I: Description of results", Report No. 5-79-3, January 1979, Stevin Laboratory, Delft University of Technology, The Netherlands.

[8] MATTOCK, A.H.: "Effect of aggregate type on single direction shear transfer strength in monolithic concrete", Report SM 74-2, Department of Civil Engineering, University of Washington, Seattle, Washington, August 1974.

[9] DASCHNER, F.: "Schubkraftübertragung in Rissen von Normal- und Leichtbeton", Preliminary report, TU München, March 1980.

[10] MATTOCK, A.H., HAWKINS, N.M.: "Research on shear transfer in reinforced concrete - recent research", PCI-Journal, V. 17, No. 2, March-April 1972, pp. 55-75.

[11] RATHS, C.H.: Discussion of the paper "Design proposals for reinforced concrete corbels", by A.H. Mattock, PCI-Journal, V. 22, No. 2, March-April 1977, pp. 93-98.

[12] FATTAH-SHAIKH, A.: "Proposed revisions to shear-friction provisions", PCI-Journal, March-April 1978.

[13] MARTIN, H.: "Zusammenhang zwischen Oberflächenbeschaffenheit, Verbund und Sprengwirkung von Bewehrungsstählen unter Kurzzeitbelastung", Deutscher Ausschuss für Stahlbeton, Heft 228, Berlin, 1973.

[14] HOFBECK, J.A., IBRAHIM, I.O., MATTOCK, A.H.: "Shear transfer in reinforced concrete", ACI-Journal, V. 66, No. 2, Febr. 1969, pp. 119-128.

DISCUSSION

Session 1, part 1: Modelling of Material Behaviour

Introductory Report by Bazant, U.S.A.

Braestrup (Denmark): Why should be the mesh size at least 3 times the aggregate size?

Bazant: I meant it should not be less. It can be larger (e.g. 5 times the aggregate size). However, if the mesh size is much larger, you need fracture mechanics in your computational model.

Paper by Vecchio/Collins, Canada

Gambarova (Italy): Looking at the crack patterns in your tests, most of the cracks are extended over the whole plate. Did you measure for these cracks the crack width and slip?

Collins: No, this would have taken too much time. We measured the local strains and occasionally the width of some characteristic cracks.

Bazant (U.S.A.): How closely did you achieve a uniform strain, and did you try to keep the stresses or the strains constant on the boundary?

Collins: We kept the stresses constant on the boundary. We tried to apply pure shear. The strains were surprisingly uniform as appeared from our measurements.

Blaauwendraad (The Netherlands): Is it basically a good point of view that you make a superposition of cracks in three directions, which in fact presupposes that the cracks form an orthogonal system?

Schnobrich (U.S.A.): It is stated in the paper and I do not like it.

General discussion

Blaauwendraad (The Netherlands): Is it possible to make some new arguments which put you to promote the approach of plasticity in reinforced concrete?

Braestrup (Denmark): The main argument is that it works; it is a simple model and it can be used as a basis for sound consistent design rules.

König (F.R.G.): Referring to fig. 4 and fig. 5 of prof. Reinhardt's paper, there must be an asymptotic line with increasing depth of the beams. The test results show this asymptotic line, but not your theory.

Reinhardt (The Netherlands): I looked for a theoretical background in order to explain the size effect. I started with a linear fracture mechanics approach, knowing that this is not optimal. In fig. 5 for beams with greater depths the dotted line represents a lower bound.

Because there are no experimental results available it cannot be proved whether the theory is correct or there exists an asymptote. More FEM-calculations are necessary in order to find out if this linear fracture mechanics approach is to be justified.

Schäfer (F.R.G.): In Stuttgart a very thick foundation slab, measuring 3,00 x 3,00 x 0,80 m, was tested recently and its punching load compared with others. It turned out that the relative ultimate shear stress is governed by the span-depth ratio rather than the absolute thickness. Is it possible that because of not equal span/depth-ratio's the tests mentioned in Reinhardt's paper cannot be compared?

Reinhardt (The Netherlands): I compared similar beams with the same shear span.

Braestrup: I refer to Section 4 of the Introductory Report of Prof. Bazant. I think this would be a very appropriate opportunity to try and clarify the relationship between your slip-free limit design and the classical approach, which you insist on calling frictionless design.
Assuming a finite coefficient of friction in the cracks, you arrive at this yield criterion:

$$\left[(N_x^s - N_x) - \beta_1 (N_y^s - N_y)\right] \left[(N_y^s - N_y) - \beta_1 (N_x^s - N_x)\right] = (2 \beta_2 N_{xy})^2,$$

which is equation (31) of your paper. Here N_x^s and N_y^s are the required yield forces in the orthotropic reinforcement in the x- and y-directions, and N_x, N_y and N_{xy} are the applied membrane forces with regard to the x, y-system.
The parameters β_1 and β_2 are defined as:

$$\beta_1 = \{\tan (\tfrac{\pi}{4} - \tfrac{\beta}{2})\}^2 \; ; \beta_2 = \tfrac{1}{2} \{\cos (\tfrac{\pi}{4} - \tfrac{\beta}{2})\}^{-2}$$

which is equation (4) of Ref. [68];
where β is the friction angle, i.e. the angle between the cracks and the displacement rate vector.
In the Introductory Paper the definition of β_2 is slightly different, but that must be a misprint.
These expressions are from the paper by Bazant, Tsubaki and Belytschko (Ref. [68]).
Now in the classical approach the yield criterion is simply this:

$$(N_x^s - N_x)(N_y^s - N_y) = N_{xy}^2, \text{ if equal notations are used.}$$

In your paper you state that the slip-free design equals the classical case if we put $\beta = \beta_1 = \beta_2 = 0$. This is obviously not correct.

For one thing, $\beta = 0$ will make neither β_1 nor $\beta_2 = 0$.
No, the fact is that we obtain the classical criterion for

$\beta = \frac{\pi}{2}$, which gives $\beta_1 = 0$ and $\beta_2 = \frac{1}{2}$.

Thus the classical approach is certainly not frictionless; on the contrary, the coefficient of friction is infinite.

Or rather, friction is not an issue at all, because the classical analysis, which is only valid for underreinforced elements, assumes that the collapse cracks form in the sections of least resistance, which means that the deformation rate is always perpendicular to the discontinuity.
Generally the structure will have more cracks in other directions as well, which are formed during earlier stages of the loading history.
But it is assumed that no tangential slip occurs in these, i.e. that friction or shear transfer is unlimited, or at least sufficient to prevent slip.
It is important to note that the tensile strength of concrete is neglected, i.e. no shear can be transferred on any section unless there is a compressive stress delivered by the reinforcement.
This is described by the Coulomb criterion with a zero tension cut-off (see figure 1).

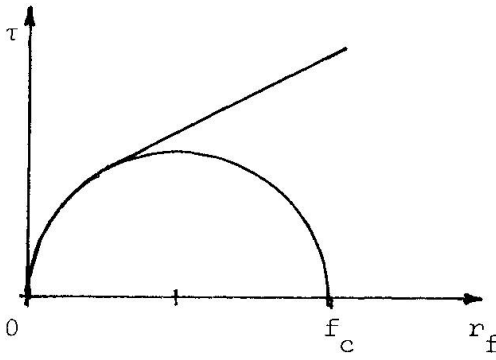

Fig. 1 Modified Coulomb criterion

r_{fy} = compressive strength delivered by reinforcement

Here τ is the shear strength and r_{fy} is the compressive stress, r being the reinforcement ratio.
The slope of the curve may be interpreted as the coefficient of friction, which is infinite at the origin, eventually decreasing to 0,75.
This description is very similar to the classical shear-friction theory, only slightly more sophisticated.
As mentioned, the classical analysis only considered the underreinforced case, where there is always a possibility for the structure to avoid slip in the discontinuities by failing through simple opening of the collapse cracks.
Lately, the analysis has been extended to cases where the failure is constrained by strong reinforcement or for other reasons, in such a way that the optimal failure mechnism involves tangential slip in the discontinuities.
Then this yield criterion is no longer valid and the dissipation is calculated using the modified Coulomb criterion.

To summarize:

The classical limit design does not assume no friction in cracks; on the contrary, it assumes no slip, because it consumes less enery for the structure to let the reinforcement yield, rather than overcome the resistance of the concrete to tangential deformations.
If the reinforcement becomes sufficiently strong, this is no longer true, and tangential slip must be considered.
This is done by the modified Coulomb criterion, which appears to give an adequate description of the shear strength of concrete.

Bazant: Although time does not permit me to deal with your comments in full detail, I wish to summarize at least the following.
Your remarks are useful, but I cannot quite agree with them.
You seem to have a different concept of friction. Apparantly, if the yield surface depends on the mean stress σ, you call that friction.

A proper definition of frictional force, in the context with thermodynamics, is different: it is a force which affects the response, but does no work in the response (see, e.g., Hill and Rice, VMPS, early 1970's, and Bazant, IASS, 1980). Thus, it is the salient feature of friction that it cannot be derived from a work expression by differentiation, i.e., no potential exists. In this sense, the slip-dilatancy model Tsubaki and I developed is a frictional model, which yours is not because you assume normality!

Now, within your point of view, we were well aware that the classical design corresponds to infinite friction coefficient on the crack and we stated so in our first paper (Bazant-Tsubaki, ASCE, Struct.Div. 1979, p.327).

As a consequence of this fact, however, the critical crack (which you curiously call "discontinuity") and actually the only possible crack is that on which there is no slip (no tangential displacement), and since there is no slip there is no shear stress on the crack, i.e. no friction.
So, classical design is a design based on the assumption of no shear stress (no friction) on the critical crack.
Thus I just cannot see how anyone can object to the word "frictionless".
Your arguments are based strictly on the assumption of a plastic yield surface and the type of the yield surface you need to assume to get these results. But that is clearly secondary.

Anyhow, I do not favour predicting the behaviour of concrete on the basis of plasticity, even though plasticity solutions may be adapted (after the fact) to fit reasonably well certain test data for concrete structures.

Prof. Bazant outlined some conceptual problems with applying plasticity to concrete. This discussion can be summarized as follows (see figure).

a. The lack of ductility, i.e. lack of a horizontal plateau in the σ-ε-diagram, means that all points of a postulated collapse surface cannot reach the maximum stress (or any stress value known in advance) simultaneously. So we do not a priori know the stresses at the failure surface at the moment of collapse.

b. The literature on plasticity of concrete strikes us by one difference from the literature on plasticity of metals. In the latter, one always starts with the σ-ε-relation, and being satisfied that it is close enough to ideal plasticity, one uses plasticity to solve a structural problem and compares the calculation results with tests.
In the literature on plasticity of concrete, people also compare the results of the analysis with tests of structures (or adjust them to fit the tests of structures), but suspiciously omit the first stage; they never start by showing the stress-strain relation. If they did, there would be of course no resemblance of ideal plasticity.

Problem of Ductility of Concrete

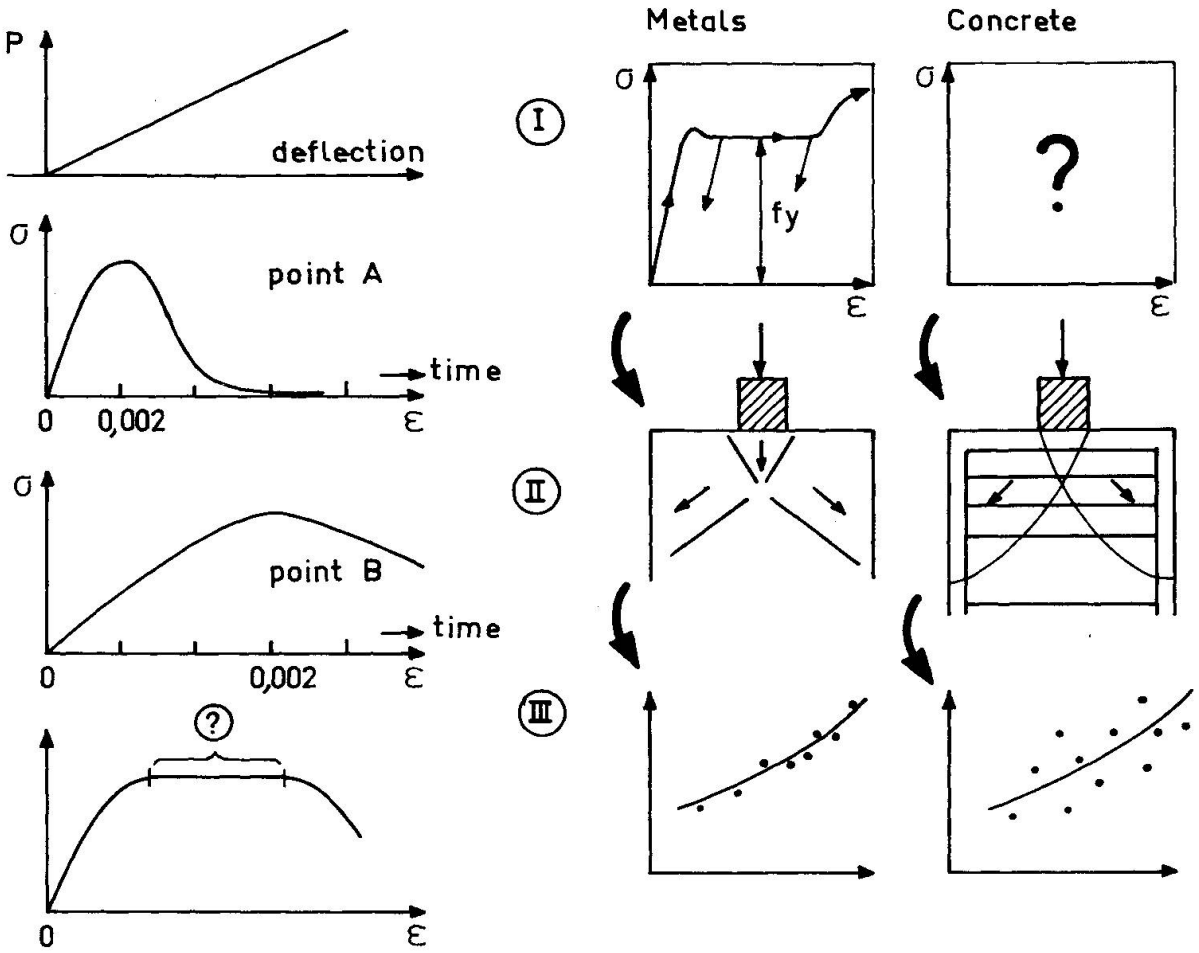

Concrete is not plastic

DISCUSSION

Session 1, part 2: Modelling of Material Behaviour

Introductory Report by Gerstle, U.S.A.

Kotsovos (U.K.): In the report cracked concrete is discussed. In the cracked state however, the plane stress assumption is not valid any more. This should be explained.
On the other hand, simplified methods have to be found for structural design.

Gerstle: Threedimensional approach of cracked concrete is complicated. A simplification for structural design is necessary.

Bazant (U.S.A.): No categorical distinction can be made between bond-slip relevance in microscopic and macroscopic approaches. The bond-slip behaviour is important in both.

Gerstle: I agree with the statement, in principle. However, it would be practical to have criteria to distinguish cases when the bond-slip should be considered from those when it can be neglected. In case of cyclic loading the bond-slip behaviour is to be taken into account in the macro-approach as well as in the microscopic approach.

Schnobrich (U.S.A.): Should Peter's tests be considered as micro- or as macro-tests? There are some doubts with respect to these tests, concerning the edge constraint and strain measurements.

Gerstle: Peter's tests are to be understood as element (macro) tests. Peter's dissertation gives more information on details as mentioned.

Braestrup (Denmark): The reason of putting steel in concrete is to prevent the cracks from opening. Its yielding should not be called premature.

Gerstle: I agree. The term "premature" may be inappropriate in this case; the yielding steel has done the job.

Paper by Gambarova, Italy

Braestrup (Denmark): The paper consideres one crack. To have shear stresses in the plane of that crack the principal stress axes must be different from those corresponding to the stresses that have produced the crack. As a consequence, these further stresses may cause new cracks in different directions: a complicated model should be necessary to describe the different systems of cracks!

Gambarova: The Rough Crack Model, which is considered in this paper, was conceived with the aim of analysing the shear stiffness and the shear strength of primary (preformed) cracks, when further loads are applied, with shear in the plane of the crack. It is completely true that any load combination, not related to the primary cracks, may produce "secondary" cracks in the solid concrete between the "primary" cracks: this fact is going to be introduced in the Rough Crack Model. However, also in the case of principal axes aligned with the crack axes (normal and tangent), the aggregate interlock is exploited, provided that the bars are not symmetric with respect to the axis normal to the crack. The same is true when the principal axes coincide with the axes of the bars.

Bazant (U.S.A.): I agree with Dr. Gambarova. A recent model developed at Northwestern University shows that not only cracks perpendicular to the direction of the maximum principal tensile stress matter. This model involving solely an elastic matrix, plus rough cracks of all directions, gives a complete description, also for plain concrete. A current work is dedicated to the description of different cracks.

Paper by Walraven, The Netherlands

Bazant (U.S.A.): I am surprised that there is, in your opinion, no rubble in the crack. I think that there is some evidence which points the contrary. For example: if it is tried to return the shear displacement to zero and then to close the crack, it will turn out that this is impossible. The same is observed in rock mechanics.

Walraven: After the tests on the specimens with external bars, the specimens were opened, and then only a negligible amount of powder was observed. That was my evidence that the behaviour is principally governed by irreversible deformation of the matrix between the particles, and not by the action of loose aggregate particles, rotating between the crack faces. If it is tried to close the crack after opening, this is indeed not perfectly possible without any normal compressive stress. However, this may also be due to microcracking under the level of the crack faces,resulting in a deformation of these faces.

Kotsovos (U.K.): It is known that on the tip of the crack there are very high stress concentrations, and these stress concentrations are of the order of magnitude equivalent to chemical forces or even physical forces. What would be the contribution of the state of stress on the tip of the crack on the overall strength behaviour?

Walraven: The behaviour at the crack tip was not studied in detail. The model that was developed was meant to be used for finite element analysis, where we distinguish in general between cracked and uncracked elements, so that we do not have to deal with this question. To my opinion the influence of the state of shear at the crack tip on the behaviour of most concrete structures is not very great.

Mehlhorn (F.R.G.): I wonder why the diameter of the aggregate does not influence the relations between stresses and displacements very much.

Walraven: If I compare two mixes, one with a maximum particle diameter of 32 mm and the other of 16 mm, these mixes contain the same total aggregate volume. So actually every large particle is replaced by a number of smaller ones. Apparently these effects compensate each other.

Gambarova(Italy): With reference to your tests with embedded bars, you said that a mechanism based on the information of concrete struts occurs. These struts, which are at an angle to the crack plane, improve the crack shear stiffness. What is in your opinion the nature of these struts? Do they consist of concrete rubble (aggregate particles detached from the crack faces during the loading process) or are they made of solid concrete in between the secondary cracks originating from the bar deformations? Have you noticed any remarkable amount of concrete rubble at the crack interface, after each test?

Walraven: This aspect of the behaviour was most surprising. We knew that tests of Mattock, conducted at the University of Washington D.C., showed inclined cracking at the outside of the specimen. However, the only thing that we saw, was that the crack opening was constant, independent of the reinforcement ratio, which raised the supposition that also here inclined struts had been active. As we did not realize in advance that such a mechanism was possible, we had not made any arrangement to study the behaviour inside the specimen.
A reasonable explanation is that the crack in the direct vicinity of the bars has a smaller width than elsewhere, which will attract stress concentrations and result in internal cracking, attended with solid concrete struts, which are invisible from outside. It is true that after opening of the specimen, after testing, concentrations of rubble were found in cratershaped holes, directly around the bars, but this may have been caused by the opening procedure itself, since a considerable pull-out of the bars is necessary before the specimen halves can be separated.
A definite answer may be found by injecting the cracks during testing with a fluorescent fluid and studying the micro-cracking pattern after the tests.

Paper by Nilsson/Glemberg, Sweden

Braestrup (Denmark): Experiments have shown that brittle failure can occur even when the corresponding stress is zero or even compressive. Can your model take account of such a phenomenon?

Nilsson: It is possible when the tensile strength is greater than or equal to zero, but not in other cases.

Paper by Dieterle/Bachmann, Switzerland

Flesch (F.R.G.): Did you use a constant bond stress in your calculations?

Dieterle: As a first assumption a bond stress is assumed that is constant over the length of the beam. In a second calculation the real bond stress is used, as can be calculated from the paper by Rehm, published by the Deutscher Ausschuss für Stahlbeton. Also the height of the load was considered calculating the real bond stress.

Flesch: My paper is quite in accordance with your results, given in reference [2], e.g. showing the high damping for small amplitudes and a decrease of damping, with increasing amplitudes; further an increase with the percentage of reinforcement, etc.

Paper by Roelfstra/Wittmann, Switzerland

Bazant (U.S.A.): In your model creep recovery is due to the elastic recovery of the aggregate. Does this mean that in cement paste there will be no creep recovery?

Roelfstra: The elastic energy stored in aggregates contributes to the total creep recovery of concrete. Hardened cement paste is far from being a homogeneous material. There are unhydrated clinker particles and weak zones randomly distributed in the microstructure. Therefore even in hardened cement paste locally elastic energy is stored during time-dependent deformation and therefore even in hardened cement paste creep recovery is observed.